Accumulation distribution on Abramov Glacier from GPR measurements



Master thesis

Unit of Geography, Faculty of Sciences, University of Fribourg

Silas Walther
Häuslenmatt
3531 Oberthal

Supervised by Dr. Horst Machguth

Fribourg, 30 October 2018



Abramov winter camp January 2018
Radar equipment with snow pit

Acknowledgement

This master thesis became only possible through the support of numerous people. First of all, I thank Marlene Kronenberg that convinced me in a short meeting in spring 2017 to perform my master thesis in her PHD project and to change to the University of Fribourg. I give sincere thanks to Prof. Dr. Martin Hoelzle and Prof. Dr. Christine Bichsel that enabled this change.

For the field work I express my gratitude to Ruedi and Christine Käser as well as Claudine Frieden for the uncomplicated and fast allowance for three days of acclimatisation at Jungfraujoch. I thank Dr. med. Peter Abbühl and Thomas Ulrich who lent me some very warm clothes for winter camping on Abramov Glacier. I thank Dr. Horst Machguth for all decisions in sometimes externally-influenced difficult situations during field work in January 2018 and Marlene Kronenberg and Dr. Horst Machguth for the organization of the entire field campaign. I also give sincere thanks to Dr. Horst Machguth for the time and advice he gave me during the master thesis. I appreciated these meetings for keeping the aim of my master thesis and staying on the right way after unexpected changes during field work.

Furthermore, I thank Martina Barandun for some hints concerning the old Soviet data, Dr. Karl-Josef Sandmeier for his answer considering his ReflexW-Software, University of Fribourg for its contribution on the excursion costs and Warren Stainbank for helping me starting with van Pelt's mass balance model and all previous work he did during his master thesis setting up the model.

Finally, I thank sincerely the world's best and most fascinated meteorologist Ralph Rickli for the promotion of my meteorological and climatological knowledge by frequent mail newsletters and sigwx.ch since I was 11 years old when he first gave me the opportunity to have a look in his weather office at Meteotest.

Silas Walther

Abstract

In Central Asia, glaciers are especially important during dry continental summers providing melt water. Accordingly, knowledge about glacier mass balance sensitivity to changes in climate is crucial. Abramov Glacier is located between the headwaters of Syr Darya and Amu Darya rivers. It is the only glacier with long-term mass balance observations in Pamir and was monitored from 1967–1999 by Soviet scientists and again since 2011.

In modelling the mass balance, precipitation is a critical input parameter due to measuring uncertainties and extrapolation difficulties. It is common to apply a precipitation correction factor as well as an altitudinal precipitation gradient to distribute precipitation over the glacier area.

This master thesis provides spatially distributed precipitation multiplier (PM) rasters for Abramov Glacier. Thereto, comprehensive ground penetrating radar (GPR) surveys are performed in January 2018. Benefitting from simultaneous density measurements from two firn cores and three snow pits, direct conversion from two-way traveltimes to water equivalents is possible. Water equivalents are extrapolated to the entire glacier by multiple regressions based on the historical snow depth distribution, winter precipitation and two topographical parameters. After normalization, this PM raster replaces the altitudinal precipitation gradient in the mass balance model of *van Pelt et al. (2012)*. Using extensive Soviet measurements, additional monthly PM rasters are generated for assessing the intermonthly comparability.

The PM rasters reduce the number of tuning parameters in the mass balance model. Currently the mass balance model performs slightly worse using the GPR or Soviet PM raster, attaining an R^2 of 0.81 instead of 0.84. This shows that there remain other model parameters to calibrate. Further progress is to achieve performing GPR measurements encompassing the entire glacier and steep slopes and calibrating other model input parameters.

Keywords: *Abramov Glacier, GPR, mass balance modelling, accumulation distribution, precipitation multiplier*

Content

Acknowledgement I

Abstract III

List of abbreviations VIII

List of symbols IX

Figures XI

Tables XV

1 Introduction and research questions 1

1.1 Introduction 1

1.2 Hypothesis and research questions 3

2 Theory 5

2.1 Relevance of glaciers 5

2.1.1 Runoff 5

2.1.2 Sea level 5

2.1.3 Hazards 6

2.2 Valley glaciers: General terms 7

2.3 Glacier adaption to climate change 8

2.4 Glacier mass and energy balance 9

2.4.1 General terms mass balance 9

2.4.2 Mass balance measurement methods 9

2.4.3 Spatial inter- and extrapolation of mass balance 12

2.4.4 Energy balance 13

2.5 Precipitation and its relationship to glacier accumulation 13

2.5.1 Precipitation versus accumulation 13

2.5.2 Precipitation uncertainty 14

2.5.3 Accumulation distribution 15

2.5.4 Extrapolation to the entire glacier: Precipitation multiplier (PM) raster 16

2.6 Ground penetrating radar (GPR) 17

2.6.1 GPR in detail 17

2.6.2 Use of GPR for accumulation measurements 19

3 Research site 21

3.1 Research site 21

3.1.1 Geography 21

3.1.2 Climate 22

3.1.3 Water importance and runoff in Central Asia 24

3.2 Glacier observations in Central Asia ... 26
3.3 Previous work on Abramov Glacier ... 28
3.3.1 Exceptional Soviet Union measurements ... 28
3.3.2 Reanalysis of seasonal mass balances ... 29

4 Data and methods ... 31
4.1 Soviet field data ... 31
4.2 January 2018 field data ... 32
4.2.1 GPR planning ... 32
4.2.2 Processing steps GPR data ... 34
4.2.3 Data GPR surveys ... 34
4.2.4 Data firn cores ... 40
4.2.5 Data snow pits ... 40
4.3 Additional data ... 41
4.3.1 Digital Elevation Model ... 41
4.3.2 Weather reconstruction ... 42
4.4 Relationship between TWT and water equivalent ... 42
4.5 PM rasters ... 44
4.5.1 Multiple linear regression ... 46
4.5.2 Soviet PM rasters ... 46
4.5.3 Soviet January 2018 water equivalent raster ... 49
4.5.4 GPR PM raster ... 49
4.5.5 Validation PM rasters ... 49
4.6 Energy balance–snow model ... 50
4.6.1 Coupled energy balance–snow model *van Pelt et al. (2012)* ... 50
4.6.2 Implementation of PM raster in the coupled energy balance–snow model *van Pelt et al. (2012)* ... 50

5 Results ... 53
5.1 Soviet snow depth distribution rasters ... 53
5.2 PM rasters ... 54
5.2.1 Soviet PM rasters ... 54
5.2.2 GPR PM raster ... 59
5.2.3 Soviet January 2018 raster and validation ... 60
5.2.4 Validation GPR with Soviet PM raster ... 61
5.3 Mass balance model *van Pelt et al. (2012)* ... 62

6 Discussion 65
6.1 GPR Measurements and layer extraction 65
6.1.1 Uncertainties GPR horizon extraction 66
6.2 Uncertainties GPR-derived water equivalents 67
6.3 Parameters Soviet SDD and PM rasters 68
6.4 Water equivalent distribution January 2018 69
6.4.1 Small-scale water equivalent variations between the Soviet January 2018 raster and the GPR trace 70
6.4.2 Water equivalent deviations between the Soviet January 2018 raster and the GPR raster 71
6.5 Slope correction 72
6.6 Representativeness of winter 2017/2018 76
6.7 Mass balance model implementation 77
6.8 Applicability 78
6.8.1 Snow distribution representativeness for other months 78
6.8.2 Snow distribution representativeness for other years 79
6.8.3 Recommendations for other sites 79

7 Conclusion 81
Literature 83
Appendix A: Personal field equipment 93
Appendix B: Soviet snow depth distribution raster parameter calculations 95
Appendix C: TWT to water equivalent 99
Appendix D: Soviet PM raster parameter calculations 102
Appendix E: GPR PM raster parameter calculations 109
Appendix F: Snow depth distribution rasters 112
Appendix G: PM rasters 113
Appendix H: Model constants and settings 118
Appendix I: Model results 124
Appendix J: ERA5 500 hPa 134
Appendix K: R-Scripts 136

List of abbreviations

20CRV2c	20th Century Reanalysis data set version 2c
AAR	Accumulation area ratio
a.s.l.	Above sea level
ASTER	Advanced Spaceborne Thermal Emission and Reflection Radiometer
CAIAG	Central Asian Institute on Geophysical Research
CATCOS	Capacity Building and Twinning for Climate Observing Systems
CNES	Centre National d'Etudes Spatiales (French Space Agency)
DEM	Digital elevation model
ELA	Equilibrium line altitude
FOPD	First order partial derivative
GFZ	German Research Center for Geosciences
GPR	Ground penetrating radar
GRACE	Gravity Recovery and Climate Experiment
ICEsat	Ice, Cloud and Land Elevation Satellite
Lidar	Light detection and ranging
NAO	North Atlantic oscillation
NS	North-South
PM	Precipitation multiplier
ProfCurv	Profile curvature
PSI	Paul Scherrer Institute
R^2	Coefficient of determination
RCP	Representative concentration pathway
SANIGMI	Central Asian Hydrometeorological Institute
SDD	Snow depth distribution
SLE	Sea level equivalent
SOMARS	Simulation of glacier surface mass balance and related subsurface processes
SOPD	Second order partial derivative
SPOT	Satellite Pour l'Observation de la Terre
SRTM	Shuttle Radar Topography Mission
SWE	Snow water equivalent
TWT	Two-way traveltime
w.e.	water equivalent
WGS	World Geodetic System
WGMS	World Glacier Monitoring Service
winterP_m	Accumulated precipitation from October until the end of the corresponding month
WMO	World Meteorological Organisation

List of symbols

Symbol	Description	Unit[1]
α	Intercept of regression	
β_i	Coefficient of parameter p_i	
c	Speed of light in vacuum	300'000'000 m s^{-1}
E	Evapotranspiration	m^3 or mm
ε	Electric permittivity	F m^{-1}
ε'_d	Dielectric permittivity of dry snow	F m^{-1}
$\Delta\varepsilon'_s$	Incremental dielectric permittivity	F m^{-1}
f	Antenna frequency	s^{-1}
λ	Wave length	m
LW_{net}	Net longwave radiation	W m^{-2}
μ	Magnetic permeability	F m^{-1}
m	Month	
n	Number of stake or snow pit measurements	
P	Precipitation	m^3 or mm
p_i	Regression parameter i	
R^2	Coefficient of Determination	
ρ_d	Density of snow	kg m^{-3}
Q_E	Latent heat flux	W m^{-2}
Q_H	Sensible heat flux	W m^{-2}
Q_{melt}	Energy consumed through snow, firn or ice melt	W m^{-2}
Q_P	Heat flux from precipitation	W m^{-2}
Q_{Sub}	Subsurface heat flux	W m^{-2}
σ	Electric conductivity	F m^{-1}
S	Storage	m^3 or mm
SS	Sum of squares	
SW_{net}	Net shortwave radiation	W m^{-2}
u	Electromagnetic wave velocity	m s^{-1}
W	Water content	volumetric proportion
$\bar{X}$	Mean measured snow depth or water equivalent at all measurement locations	m or m w.e.
X_i	Measured snow depth or water equivalent at location i	m or m w.e.
Δx_{max}	Maximal critical measurement spacing	m

[1] F m^{-1} = Farad per meter, derived SI unit. In SI base units: F m^{-1} = kg^{-1} m^{-3} s^4 A^2

$\bar{Y}$	Mean regression-calculated snow depth or water equivalent at all measurement locations	m or m w. e.
Y_i	Regression-calculated snow depth or water equivalent at location i	m or m w. e.

Figures

Figure 1: Relative glacier storage change (dS) contribution to August runoff at different parts of the Rhine river. The numbers in brackets show the glaciation of the catchment. 1977 was a wet summer, 2003 a dry summer (Figure from *Huss (2011)*). 5

Figure 2: Sea level rise contribution and cumulative ice mass loss of glaciers and today's two ice sheets (Figure from *Vaughan et al. 2013*). 6

Figure 3: Accumulation zone of a glacier (from *Paterson 1981*). The soaked zone is also referred to as «wet-snow zone» or «infiltration zone» *(Hoelzle 2015[a]; Oerlemans 2001)*. 8

Figure 4: Snow pit on Abramov Glacier at 4'168 m a.s.l., 30 January 2018. The hole is dug until the previous summer horizon is reached recognizable on its dusty color and hard crust. Using an avalanche probe, a cylindrical tube, a plastic bag and a spring scale, the weight of every roughly 30 cm part is measured and the density calculated. 10

Figure 5: Mean annual precipitation 1961–1990 for three water balance areas and twelve elevation zones from *Schädler and Weingartner (2002)* with unit gradient (grey) from *Kirchhofer and Sevruk (1992)*, represented in *Spreafico und Weingartner (2005)*. 15

Figure 6: Overview of Central Asia with Abramov Glacier location (background shading: Elevation; black dotted grid: Coordinates in degree (World Geodetic System (WGS) 84)). 21

Figure 7: Mass balance gradients of Abramov Glacier in different time periods and hypsometry of the year 2013. Figure from *Barandun et al. (2015)*. 22

Figure 8: Annual mean precipitation of Kyrgyzstan and Central Asia from 1970–2000 (black dotted grid: Coordinates in degree (WGS 84)). 23

Figure 9: Climate diagram Fergana, 1981–2010 (*ClimateCharts (2018)*, data Source: *NOAA (2011*). 23

Figure 10: Water resources of the Aral Sea basin (from *CAWATERinfo (2017)*). 25

Figure 11: Ratio of summer/winter flow (Q) in the Naryn River at Uchkurgan (from *Karimov et al. 2010*). 26

Figure 12: Historical mass balance network on Abramov Glacier (from *Hoelzle et al. 2017*). 29

Figure 13: Number of monthly stake (empty circles) and pit (small filled circles) measurements from 1967–1999. The year indicates the midyear, the color the month Jan (1) to Dec (12). 31

Figure 14: Planned GPR traces with priorities 1 (first priority) to 3 (last priority), planned drill site and planned camp for the field work in January 2018. Background: Soviet map with glacier extent in 1986. 33

Figure 15: Field data overview. Black numbers label the GPR profiles. 2016 snow pits and stakes were measured during the summer campaign of CAIAG and University of Fribourg. Soviet snow pits and stakes were measured year-around from 1967–1999. Background: Soviet map with glacier extent in 1986. 35

Figure 16: Filtered GPR profile 0715 (labelled inFigure 15) without (above) and with (below) equidistant trace interpolation. The numbers shown in the upper profile's abscissa are trace numbers instead of distance (bug in REFLEX software). 36

Figure 17: Filtered GPR profile 0728 (labelled in Figure 15) with equidistant trace interpolation. 37

Figure 18: Filtered GPR profile 0730 (labelled in Figure 15) with equidistant trace interpolation. 38

Figure 19: Filtered GPR profile 0735 (labelled in Figure 15) with equidistant trace interpolation. 38

Figure 20: Filtered GPR profile 0736 (labelled in Figure 15) with equidistant trace interpolation. Entire profile (above) and zoom to the main accumulation area (below). 39

Figure 21: Densities from snow pits January 2018 (density 870 kg m^{-3}: Ice lense). 41

Figure 22: Dependence of electromagnetic wave velocity [m ns^{-1}] (right scale) on snow density [kg m^{-3}] (lower scale) and liquid water content W [volumetric ratio] (left scale) (from Bradford et al. 2009). 43

Figure 23: Relationship between TWT from GPR measurements and water equivalent from two firn cores and three snow pits (details in Appendix C). 44

Figure 24: Methodology for the SDD and PM rasters. Text around lines indicates the input parameters used for the best regressions (compare Chapter 5). Light colored areas represent the observed values used to establish the regression, darker colored areas represent the output that is calculated with the best regressions. Consider that the SDD and PM rasters are normalized (not shown in the figure). (Precip = Precipitation, Sov = Soviet, other abbreviations see p. VI). 45

Figure 25: Soviet SDD rasters December to April [m]. 54

Figure 26: Soviet water equivalent rasters December to April [m w. e.]. 56

Figure 27: Soviet PM rasters December to April [dimensionless]. 57

Figure 28: Average Soviet PM raster of all months from December to April [dimensionless]. 58

Figure 29: Water equivalent raster based on January 2018 GPR measurements [m w. e.]. 59

Figure 30: PM raster based on GPR measurements [dimensionless]. 60

Figure 31: Soviet January 2018 water equivalent raster (background) and difference between Soviet January 2018 and GPR-derived (Figure 29) water equivalents (colored lines) [m w. e.]. 61

Figure 32: Quotient between the GPR PM raster and the mean Soviet PM raster [dimensionless]. 62

Figure 33: Measured versus simulated mass balance for the period 1 November 2013 02:55 until 1 October 2017 02:55. Stainbank's best simulation (blue) is compared with the simulations using the Soviet PM and the same settings (red) as well as with improved parameter settings (green). Details about parameter settings: Appendix H Table 29. 63

Figure 34: Measured versus simulated mass balance for the period 1 November 2013 02:55 until 1 October 2017 02:55. Warren's best simulation (blue) is compared with the simulations using the GPR PM and the same settings (red) as well as with improved parameter settings (green). Details about parameter settings: Appendix H Table 29. 64

Figure 35: Comparison of an extraction of GPR profile 0715 (labelled in Figure 15) with firn core 4391 (right) (Table 4). The abscissa of the core is density in kg m^{-3}. Orange dashed lines mark dust horizons, blue lines or rectangles represent ice lenses. 65

Figure 36: Snow pit 3867 (Figure 15 and Table 5) 26 January 2018. 65

Figure 37: Abramov Glacier from the location of the automatic weather station on 5 August 2017. 66

Figure 38: High accumulation area around drill site 4389 with topography [m] with GPR extract and water equivalent differences between Soviet January 2018 raster and the GPR trace [m w.e.]. 71

Figure 39: GPR PM rasters (normalized water equivalent rasters) without (top) and with (bottom) slope-correction (linear decrease from 100 % for slopes up to 15 ° to 0 % from 55 ° and steeper) [dimensionless]. 74

Figure 40: Measured versus simulated mass balance for the period 1 November 2013 02:55 until 1 October 2017 02:55. Warren's best simulation (blue) is compared with the simulations using the Soviet PM, without (left) and with (right) correction for slopes steeper than 15 °, and the same settings (red) as well as with improved parameter settings (green). Details about parameter settings: Appendix H. 75

Figure 41: Relationship between TWT and water equivalent from two firn cores and three snow pits with altitude. 101

Figure 42: Relationship between TWT, water equivalent and elevation in 3D with regression plain. 101

Figure 43: Normalized Soviet SDD rasters December to April based on Soviet stake data [dimensionless]. 112

Figure 44: Quotients between the monthly Soviet PM rasters and the average Soviet PM raster [dimensionless]. 113

Figure 45: Soviet slope-corrected water equivalent rasters December to April with linear decrease from 100 % up to 15 ° to 0 % above 55 ° [m w.e.]. 114

Figure 46: GPR slope-corrected water equivalent raster with linear decrease from 100 % up to 15 ° to 0 % above 55 ° [m w. e.]. 115

Figure 47: Soviet slope-corrected PM rasters December to April with linear decrease from 100 % at 15 ° to 0 % at 55 ° [dimensionless]. 116

Figure 48 Soviet PM rasters without (top) and with (bottom) slope-correction (linear decrease from 100 % for slopes up to 15 ° to 0 % for slopes of 55 ° and steeper) [dimensionless]. 117

Figure 49: Measured versus simulated mass balance for the period 1 November 2013 02:55 until 1 October 2017 02:55. Warren's best simulation (blue) is compared with the simulations using the Soviet precipitation multiplier and the same settings (red) as well as with improved parameter settings (green). Details about parameter settings: Table 29. 124

Figure 50: Measured versus simulated mass balance for the period 1 November 2013 02:55 until 1 October 2017 02:55. Warren's best simulation (blue) is compared with the simulations using the Soviet precipitation multiplier and the same settings (red) as well as with improved parameter settings (green). Details about parameter settings: Table 29. 125

Figure 51: Measured versus simulated mass balance for the period 1 November 2013 02:55 until 1 October 2017 02:55. Warren's best simulation (blue) is compared with the simulations using the Soviet PM and the same settings (red) as well as with improved parameter settings (green). Details about parameter settings: Table 29. 126

Figure 52: Measured versus simulated mass balance for the period 1 November 2013 02:55 until 1 October 2017 02:55. Warren's best simulation (blue) is compared with the simulations using the Soviet PM and the same settings (red) as well as with improved parameter settings (green). Details about parameter settings: Table 29. 127

Figure 53: Measured versus simulated mass balance for the period 1 November 2013 02:55 until 1 October 2017 02:55. Warren's best simulation (blue) is compared with the simulations using the Soviet PM and the same settings (red) as well as with improved parameter settings (green). Details about parameter settings: Table 29. 128

Figure 54: Measured versus simulated mass balance for the period 1 November 2013 02:55 until 1 October 2017 02:55. Warren's best simulation (blue) is compared with the simulations using the Soviet PM and the same settings (red) as well as with improved parameter settings (green). Details about parameter settings: Table 29. 129

Figure 55: Measured versus simulated mass balance for the period 1 November 2013 02:55 until 1 October 2017 02:55. Warren's best simulation (blue) is compared with the simulations using the GPR PM and the same settings (red) as well as with improved parameter settings (green). Details about parameter settings: Table 29. 130

Figure 56: Measured versus simulated mass balance for the period 1 November 2013 02:55 until 1 October 2017 02:55. Warren's best simulation (blue) is compared with the simulations using the GPR PM and the same settings (red) as well as with improved parameter settings (green). Details about parameter settings: Table 29. 131

Figure 57: Measured versus simulated mass balance for the period 1 November 2013 02:55 until 1 October 2017 02:55. Warren's best simulation (blue) is compared with the simulations using the GPR PM, corrected for slopes steeper than 15 °, and the same settings (red) as well as with improved parameter settings (green). Details parameter settings: Table 29. 132

Figure 58: Measured versus simulated mass balance for the period 1 November 2013 02:55 until 1 October 2017 02:55. Warren's best simulation (blue) is compared with the simulations using the Soviet PM, corrected for slopes steeper than 15 °, and the same settings (red) as well as with improved parameter settings (green). Details parameter settings: Table 29. 133

Tables

Table 1: Precipitation measurement errors after *WMO (2008)*. 14

Table 2: Mass balance changes of selected Central Asian mountain regions from different authors. Values from *Kääb et al. (2015)* given in m a^{-1} are converted to m w.e a^{-1} by factor 0.85 as proposed by *Kääb et al. (2015)*. 28

Table 3: Georeferencing of reference points from the local coordinate system to WGS 84 UMT zone 42 N (x = x coordinate, y = y coordinate). 32

Table 4: Firn cores drilled during the 2018 winter campaign (PSI = Paul Scherrer Institute). 40

Table 5: Snow pits measured during the 2018 winter campaign. 40

Table 6: List of the 54 parameters tested in the multiple regressions for the SDD. 100 denotes 100 m radian environment around each stake. All *FOPD* and *SOPD* are topographical curvature parameters. 47

Table 7: Regression coefficients of the three most important variables for the SDD (abbreviations see p. VI). 53

Table 8: Regression coefficients of the four most important variables for the Soviet water equivalent distribution, whereas m corresponds to the month (abbreviations see p. VI). 55

Table 9: Extracted statistical values (SD = Standard deviation) from monthly PM rasters compared to the average PM raster of all five months (raster in Appendix Figure 44). 58

Table 10: Regression coefficients of the three most important variables for the GPR water equivalent distribution. *Elevation* and *FOPDdyNS* are taken at the GPR measurement point locations while for the *Profile Curvature*, the median of the 100 m radius around the GPR measurement points fitted best (abbreviations see p. VI). 59

Table 11: GPR-measured TWTs from the surface to the previous year's summer horizon, calculated depths (details Section 4.4) and measured depth at the core location 4381 (profiles labelled in Figure 15). 67

Table 12: ERA5 reanalysis of mean temperature, humidity and wind speed/direction at 500 hPa and surface precipitation *(ECMWF 2018)* as well as mean measurements *(italic)* at the GFZ Abramov weather station (*SDSS (2018)*). 2011 OJ = Oct 2011 to Jan 2012, 2011 OA = Oct 2011 to Apr 2012 etc. *Wind speeds at the weather station represent the average of all 10 min maximal wind speeds. 76

Table 13: Best regressions for Soviet December SDD using 3 explaining parameters. 95

Table 14: Best regressions for Soviet January SDD using 3 explaining parameters. 96

Table 15: Best regressions for Soviet February SDD using 3 explaining parameters. 96

Table 16: Best regressions for Soviet February SDD using 4 explaining parameters. 97

Table 17: Best regressions for Soviet March SDD using 3 explaining parameters. 98

Table 18: Best regressions for Soviet April SDD using 3 explaining parameters. 98

Table 19: Best regressions for Soviet December water equivalents using 4 explaining parameters. 102

Table 20: Best regressions for Soviet January water equivalents using 4 explaining parameters. 104

Table 21: Best regressions for Soviet February water equivalents using 4 explaining parameters. 105

Table 22: Best regressions for Soviet February water equivalents using 3 explaining parameters. 106

Table 23: Best regressions for Soviet March water equivalents using 4 explaining parameters. 107

Table 24: Best regressions for Soviet April water equivalents using 4 explaining parameters. 108

Table 25: Best regressions using only every 100th GPR measurement points. 109

Table 26: Best regressions using 1000 randomly chosen GPR measurement points. 109

Table 27: Best regressions for GPR derived water equivalents using 3 explaining topographical parameters. 110

Table 28: Best regressions for GPR derived water equivalents using 4 explaining topographical parameters. 111

Table 29: Changes in model constants and number of simulation. 123

Table 30: ERA5 reanalysis of mean temperature, humidity, wind speeds, calculated wind direction and geopotential at 500 hPa as well as surface precipitation *(ECMWF 2018).* 134

1 Introduction and research questions

1.1 Introduction

Glaciers encompass all perennial surface land ice masses *(Vaughan et al. 2013)* and ice sheets. They form where climatic conditions and topographic parameters allow snow to accumulate over several years, subsequently transforming to firn and finally to ice. Glaciers are sensitive climate indicators, as they directly respond with their mass balances to changes in external conditions (radiation, temperature, precipitation) *(Vaughan et al. 2013)*. On global scale, glaciers represent major contributors to sea level rise and on regional scale, they are important seasonal to long-term hydrologic reservoirs. Glacier meltwater is especially important where summers are dry and glacier-sustained runoff enters dry regions *(Cisneros et al. 2014; Kaser et al. 2010)*.

In Central Asia, glaciers are most important for availability of potable water and water for irrigation. Located far away from any humidity source, Central Asia is dominated by continental climate conditions with considerable precipitation restricted to the Tien Shan and Pamir mountain ranges. Syr Darya sourcing in Kyrgyzstan and Amu Darya sourcing in Tajikistan and Kyrgyzstan flow downstream through the deserts of Turkmenistan and Uzbekistan with annual precipitation of less than 200 mm towards the (former) Aral Sea *(Laity 2008; Fick and Hijmans 2017)*. Runoff from glacier melt especially covers the driest period of the year after snow melt and before the onset of autumn precipitation. In summer, glacier melt contribution to runoff at Amu Darya was estimated reaching 50 % *(Sorg et al. 2012)*.

Beside the operation mode[2] of the reservoirs reaching capacities up to 19.5 km^3 at Toktogul *(Karimov et al. 2010; Bar 2015)*, changes in summer water availability in arid Central Asia have to be assessed. For a projection of the future summer water availability, knowledge about Tien Shan and Pamir glacier evolution is required *(Unger-Shayesteh et al. 2013; Sorg et al. 2014)*.

In recent years, numerous studies have assessed the evolution of Central Asian glaciers in terms of mass balance changes. In Tien Shan, *Gardner et al. (2013)* calculated −0.12 m w.e. a^{-1} and *Baumann (2017)* −0.51 m w.e. a^{-1}. In Pamir, published mass balance changes range from −0.42 m w.e. a^{-1} *(Baumann, 2017)* over −0.41 m w.e. a^{-1} *(Kääb et al. 2015)* and −0.12 m w.e. a^{-1} *(Gardner et al. 2013)* to +0.14 m w.e. a^{-1} *(Gardelle et al. 2013)*. These studies are based on either geodetic (height change) or gravimetric (mass change) remote sensing data from two different time steps (details in Table 2). As measurements of direct mass balance are time and labour intensive, the glaciologi-

[2] Irrigation mode focusing on summer runoff or hydropower generation mode focusing on electricity generation during wintertime.

cal method is not applicable for whole mountain ranges. However, direct mass balance measurements are of vitally importance for model calibration. Therefore, accurate mass balance data on reference glaciers is crucial.

Abramov Glacier is the only Pamir glacier with long-term direct mass balance measurements *(Dyurgerov and Meier 2005; Hoelzle 2017)* and thus it is of special relevance. On Abramov Glacier, extensive mass balance measurements have been performed from 1967–1999 by Soviet researchers living year-round in a research station near the glacier tongue. This data was published by *Pertziger (1996)* and included in the WGMS data base *(WGMS 2015)*. A small amount of the measurements have been resumed in 2011 in the Capacity Building and Twinning for Climate Observing Systems (CATCOS) project by German, Kyrgyz and Swiss researchers *(Barandun et al. 2013; Schöne et al. 2013; MeteoSwiss 2017)*.

Barandun et al. (2015) reanalysed the existing Soviet mass balance data. They created a consistent and homogeneous time series of measured mass balances and calculated seasonal time series of mass balances for the period 1968–2014 using a spatially distributed mass balance model. They tuned the precipitation input in their model using a precipitation correction factor as well as a normalized, dimensionless spatial snow distribution multiplier *(Barandun et al. 2015)*. The latter they derived from inverse-distance interpolation of the point winter balance measurements. With this approach they tried to catch non-altitude dependent small-scale effects of snow distribution, including topographic effects and redistribution processes by wind *(Barandun et al. 2015)*. However, the measurements they used were point mass balance data of eight Soviet snow pit locations. Considering the glacier area of 24 km^2, eight point measurements represent a coarse sampling on which their inverse-distance interpolation was based.

When modelling glaciers, spatial variability of the accumulation distribution remains among the most important uncertainty factors *(Richardson et al. 1997; Hawley et al. 2014; van Pelt et al. 2012; Sold et al. 2015; Sold et al. 2016)*. This arises from uncertainties in precipitation measurements especially during wintertime and in mountaineous environments *(Schädler and Weingartner 2002)* as well as elevational precipitation gradients in combination with snow relocation processes by wind and avalanching *(e.g. Richardson et al. (1997))*. This is where the present study delivers an alternative possibility.

The aim of this study is to perform comprehensive accumulation distribution measurements and therewith to improve the modelled mass balance of Abramov Glacier by decreasing the number of tuning parameters. Therefore, the accumulation distribution is measured by ground penetrating radar (GPR), a fast and non-destructive geophysical technique to investigate the subsurface. GPR surveys are performed in January 2018 covering the orographic right branch and the ablation area of Abramov Glacier, providing spatially high resolution two-way traveltime (TWT) data of the winter 2017/2018 accumulation horizon. Using three snow pits as well as two firn cores per-

formed during the same field campaign in January 2018, direct conversion from TWT to water equivalents (w.e.) is possible.

Benefitting from extensive Soviet stake and snow pit measurements, water equivalents are inter- and extrapolated to the entire glacier using multiple regression. Thereby, precipitation multiplier (PM) rasters are generated representing the accumulation distribution on Abramov Glacier. With these PM rasters, the coupled snow and energy mass balance model of *van Pelt et al. (2012)* is run. The rasters replace the linear altitudinal precipitation gradient with which the model is run up to now *(van Pelt et al. (2012), Warren 2018)*.

1.2 Hypothesis and research questions

As Abramov Glacier is the only Pamir glacier with long-term mass balance measurements, it is of special relevance as reference glacier in these mountains. With the background of required knowledge about changing Pamir glacier meltwater contribution to runoff during dry continental summers and model uncertainties especially arising from challenging accumulation distribution, the following hypothesis and research questions are assessed:

Hypothesis:

High resolution gridded accumulation distribution data gained from winter GPR measurements on Abramov Glacier increase the accuracy of modelled glacier mass balance.

Research questions:

1) Can the winter 2017/2018 accumulation horizons be followed over the entire Abramov Glacier performing GPR, firn core and snow pit measurements?
2) Is it possible to build two independent precipitation multiplier rasters of Abramov Glacier using Soviet data and GPR measurements?
3) Do the precipitation multiplier rasters improve the modelled glacier mass balance of Abramov Glacier?

2 Theory

2.1 Relevance of glaciers

2.1.1 Runoff

Glaciers influence the hydrological regime: In a glacial regime in northern hemisphere, Pardé Coefficient (monthly runoff divided by annual runoff per month) is highest in July and August *(Weingartner and Aschwanden 1992)*. This is due to remarkable contribution of glacier meltwater to total runoff during late summer.

Glacier meltwater contribution to runoff depends principally on the proportion of glaciation at a specific point of the river as well as the amount of input from other sources like precipitation, groundwater or snowmelt *(Huss 2011)*. The proportion of glacier meltwater contribution to runoff is determined by two factors: The amount of glaciation of the catchment as well as the precipitation input whose interannual variabilities can produce variations up to factor 10 (Figure 1). The dryer the summer, the more important glacial meltwater is.

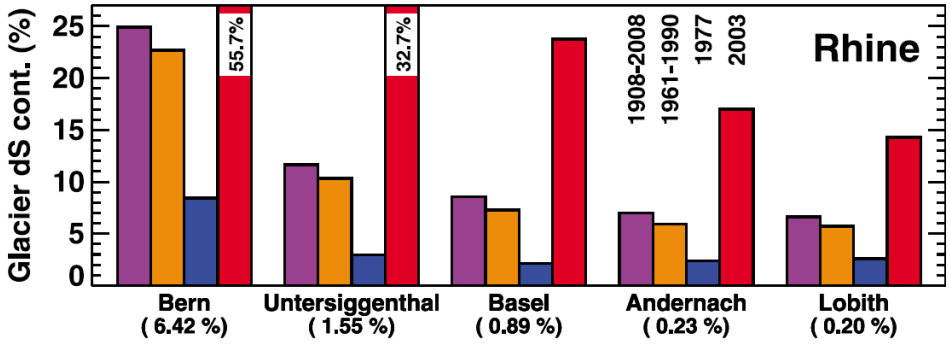


Figure 1: Relative glacier storage change (dS) contribution to August runoff at different parts of the Rhine river. The numbers in brackets show the glaciation of the catchment. 1977 was a wet summer, 2003 a dry summer (Figure from *Huss (2011)*).

Glaciers in the Pamir play a key role for summer runoff generation of the important transboundary Amu Darya and Zeravshan[3] rivers *(Unger-Shayesteh et al. 2013)*. At Amu Darya headwaters, contribution of glacier melt to summer runoff of up to 50 % has been computed *(Sorg et al. 2012)*.

2.1.2 Sea level

On a global scale, glaciers currently are the most important water source contributing to sea level rise (Figure 2). However, their contribution is not to overestimate: Compared to the two ice sheets in Greenland and Antarctica, available water from glacier melt is limited: While all glaciers worldwide contain about 0.4 m sea level water equiv-

[3] A tributary stream to Amu Darya

alent, Greenland ice sheet contains 7.4 m and Antarctic ice sheet 58.3 m *(Vaughan et al. 2013)*. While all Central European glaciers contain 0.3 mm sea level water equivalent, Central Asian's potential contribution to sea level rise was estimated to 16.7 mm *(Vaughan et al. 2013)*.

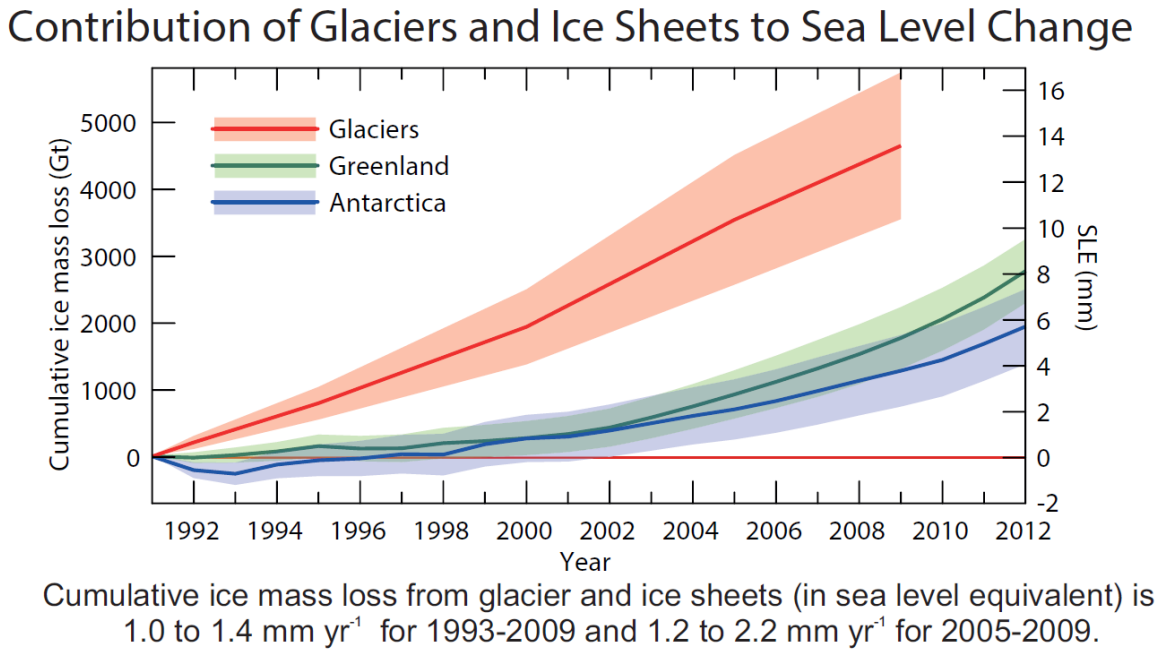


Figure 2: Sea level rise contribution and cumulative ice mass loss of glaciers and today's two ice sheets (Figure from *Vaughan et al. 2013*).

Beside the contribution to sea level rise from melting glaciers and ice sheets, thermal expansion of the sea water occurs. Currently, its amount is comparable to the glacier melt water contribution and is in the range of 0.2 m until 2100 and 0.3 m until 2300 for RCP2.6 respectively 0.3 and 1.2 m for RCP8.5 *(Palmer et al. 2018)*.

2.1.3 Hazards

Glaciers can produce different kinds of hazards. They arise from ice fall or ice slide *(Richardson and Reynolds 2000; Kaser et al. 2003; Walliserbote 2017)*, glacier- or moraine-dammed lake outbursts *(Richardson and Reynolds 2000; Huggel et al. 2002; Le Matin 2018)*, glacier surges *(Richardson and Reynolds 2000)*, glacier fluctuations *(Richardson and Reynolds 2000)* or debris flows *(Kaser et al. 2003)*. Glaciers also can play a key role in cascadeous hazards like the rock fall in the Bondasca valley in summer 2017, where instantaneous glacier liquification produced a debris flow with considerable damage on buildings, furnishing and infrastructure *(AWN 2017)*. Moreover, glaciers can cause catastrophic Lahars when in combination with volcanic activity and produce water resource problems in timescales of climate change *(Richardson and Reynolds 2000)*. As the importance of glaciers for hazards is beyond the primary objective of this study, it is referred to the mentioned literature for further details.

2.2 Valley glaciers: General terms

Valley glaciers are perennial ice and firn masses flowing down a predefined valley with a well defined glacier outline and a distinct glacier tongue *(Cogley et al. 2011)*. They consist of an accumulation and an ablation area, separated by the equilibrium line. The equilibrium line represents all points on the glacier, where the surface mass balance[4] is 0 *(Oerlemans 2001)* and therefore is often referred to as equilibrium line altitude (ELA). At these points, the glacier neither gains nor loses mass in a specific year. The equilibrium line follows more or less the isohypses *(Oerlemans 2001)*. Above the equilibrium line lies the accumulation area with positive mass balances and below the ablation area with negative mass balances. In case a hypothetical glacier is in equilibrium, ablation is balanced by accumulation and therefore the equilibrium line does not change within years. In case of negative mass balance, it rises and vice versa. The equilibrium line of a glacier alters by the interplay of snow accumulation and radiation, while temperature solely is not an adequate indicator *(Oerlemans 2001)*.

Figure 3 represents the internal structure of the accumulation area of a schematic glacier that encompasses all possible facies zones. Above the dry snow line, no melt occurs *(Oerlemans 2001)*. This dry snow zone does not exist on most valley glaciers, as it requires mean annual air temperatures lower than approximately -20 °C *(Hoelzle 2015[a])*. In the percolation zone below, if melt water is formed it percolates, but still refreezes in the same annual layer and hence does not run off. In the cold infiltration zone (upper soaked zone), in years where melt occurs, melt water percolates several annual layers but refreezes. In contrast, in the warm infiltration zone (lower soaked zone) runoff is generated *(Hoelzle 2015[a])* and firn temperature reaches 0 °C. In the Alps the warm infiltration zone is located between 3'000 and 4'000 m a.s.l.

Temperate glaciers do not reach further up than into the warm infiltration zone. Their firn and ice temperature is at melting point or reaches it at least once a year[5]. Cold glaciers experience ice temperatures below melting point throughout the glacier while on polythermal glaciers, vertical temperature profiles measured in summer shows both zones.

[4] More details about mass balance is given in Subsection 2.4.1.

[5] Uppermost firn layers especially in continental climate with low temperatures and low amounts of accumulation can experience considerable cooling during wintertime but reach melting point again during warm season.

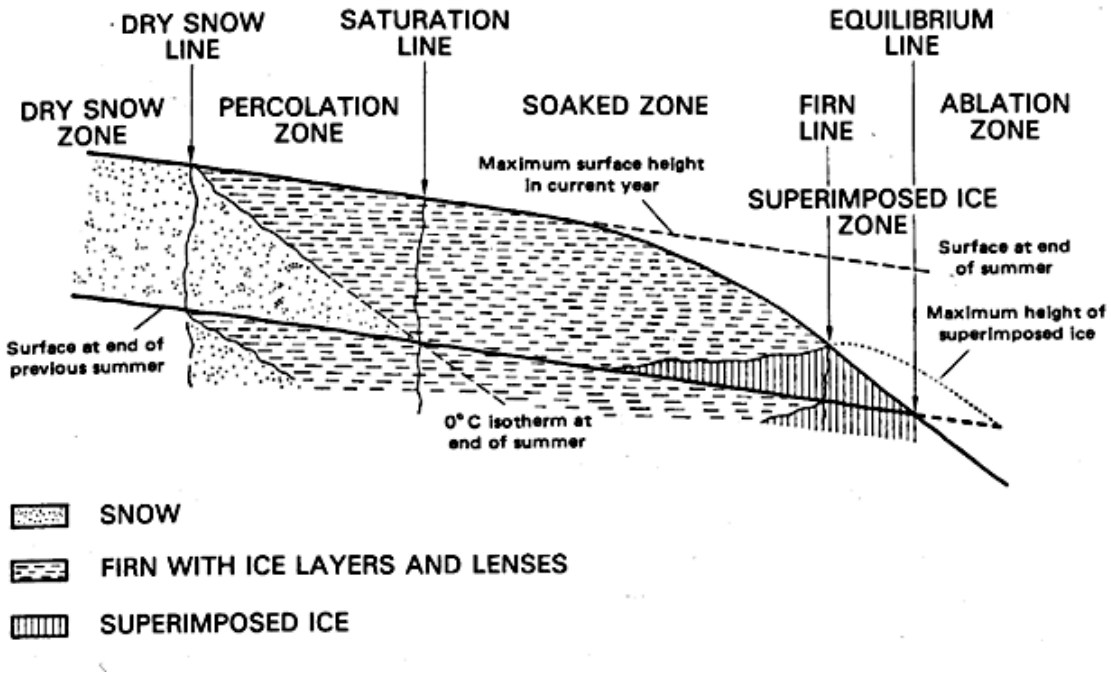


Figure 3: Accumulation zone of a glacier (from *Paterson 1981*). The soaked zone is also referred to as «wet-snow zone» or «infiltration zone» *(Hoelzle 2015[a]; Oerlemans 2001)*.

2.3 Glacier adaption to climate change

Glaciers basically never are in equilibrium. Except from disturbances through cascadeous hazards and surging glaciers[6], glacier changes represent always a reaction to changes in weather or climate *(Johannesson et al. 1989)*. Different reactions can be measured: Changes in mass balance, flow velocity or in size and length *(Paul et al. 2015)*. Glaciers directly respond to changes in energy balance and precipitation input by mass balance (details in the following section) and indirectly with a delay of several years to several decennials by length change.

The most direct response of a glacier to changed weather conditions is observable in mass balances deviations over the entire area of a glacier: More snow is accumulated in case of increased precipitation and more melt is generated under higher energy input. These changes can be measured directly in the annual mass balance of the glacier. However, glacier velocity and glacier length react with a time lag of several up to 100 years (depending on glacier size and amount of perturbation) to changed climatic conditions *(Johannesson et al. 1989)*.

[6] Glaciers that naturally occur a speed-up in regular intervals.

2.4 Glacier mass and energy balance

2.4.1 General terms mass balance

The glacier mass balance is calculated by subtracting the glacier-wide ablation from the glacier-wide accumulation over a certain time period *(Cogley et al. 2011)*. This time period depends on the system chosen: In the fixed-date system, it is the hydrological year[7] and in the stratigraphic system, it is the period between the formation of two successive minima in the sequence of annual cycles *(Cogley et al. 2011)*. The mass balance from these two systems can vary substantially in one year, while for long-term analyses, they convert to be identical. For a good comparability, the glacier mass balance is mostly given in units of meter water equivalent (w.e.).

Traditionally *winter mass balance*, *summer mass balance* and *annual mass balance* are distinguished. The *winter mass balance* ranges from the begin of the accumulation season until the end of the winter snow accumulation and the *summer mass balance* enfolds the entire ablation season while the *annual mass balance* covers the whole hydrological year *(Cogley et al. 2011)*.

Apart from an exact definition of the temporal framework, it is also important to define which parts of a glacier are considered in the mass balance: The *surface mass balance*[8] (or *stake mass balance (van Pelt and Kohler 2015)*) is the sum of accumulation and ablation above the previous year's summer surface *(Cogley et al. 2011)*. The *internal mass balance* contains all mass changes occurring in the interior of a glacier and firn below the previous year's summer surface while the *basal mass balance* comprises all mass changes on the bottom of the glacier (e.g. refreezing) *(Cuffey and Paterson 2010; Cogley et al. 2011)*. Therefore, the total mass balance of a glacier is the sum of surface, internal and basal accumulation and ablation. The correct term for this is *climatic-basal mass balance*. In case the for temperate valley glaciers insignificant basal mass balance is not considered, *climatic mass balance* is the appropriate term *(Cogley et al. 2011)*.

2.4.2 Mass balance measurement methods

There exist various possibilities to measure glacier mass balance. The most popular of them are the direct glaciological method, the geodetic method, the gravimetric method and modelling approaches *(Vaughan et al. 2013)*. However, the applicability of these methods strongly depends on the research question. The different methods are dis-

[7] Hydrological year: Normally reaching from 1 October to 30 September, usually the same as the glaciological year *(Cogley et al. 2011)*. This is a less useful concept for summer and year-round accumulation glaciers.

[8] Mass gain by precipitation, condensation, riming, wind drift and/or avalanching and mass loss by melt, evaporation, sublimation, wind drift and/or avalanching (*van Pelt et al. 2015*, complemented)

cussed in the following subsections with a focus on the methods used later in this study.

2.4.2.1 Glaciological method

The glaciological method (also known as direct method) is based on in-situ measurements of accumulation and ablation on the glacier at two different times. It is performed using snow pits and stakes and sometimes is complemented with depth measurements *(Cogley et al. 2011)*. At snow pit locations, profiles are dug in the end of the accumulation season until the previous summer horizon is reached (Figure 4). Then snow weights are measured in regular intervals using a tube with a known volume and densities are calculated, leading to an estimate of the surface mass balance at the snow pit locations.



Figure 4: Snow pit on Abramov Glacier at 4'168 m a.s.l., 30 January 2018. The hole is dug until the previous summer horizon is reached recognizable on its dusty color and hard crust. Using an avalanche probe, a cylindrical tube, a plastic bag and a spring scale, the weight of every roughly 30 cm part is measured and the density calculated.

Stakes ideally are fixed in the end of the hydrological year in firn or ice and normally are used for ablation measurements but can also be used for accumulation measurements. Additionally, accumulated snow depths can be measured with snow probes or probe poles. In the following, when referring to Soviet measurements, the term stakes is used for ablation as well as accumulation measurements in meter.

Stakes for accumulation measurements are much less time and labour intensive than snow pits. Multiplied with the measured near-surface densities gained from snow pits, the gain or loss in water equivalent yields an estimate of the mass balance at this point *(Kaser et al. 2003)*. To obtain the glacier-wide surface mass balance, all point measurements are inter- and extrapolated to the entire glacier.

The most basic interpolation procedure is built on a regression equation between the elevation and the mass balance, considering the glacier area at each elevation band. Another method is to contour a map *(Kaser et al. 2003)*. Interpolation methods are discussed in detail in Subsection 2.4.3.

Important for the correct understanding of the direct glaciological method is, that it only measures the surface mass balance, neglecting the internal and basal mass balances.

For single years, the glaciological method is considered having the greatest accuracy of all methods *(Kaser et al. 2003)*. The only disadvantage beside the fact that it measures the surface mass balance is, that especially the accumulation measurements with snow pits are time and labour intensive. However, large-scale applicability of GPR is an alternative to this laborious work and is described in detail in Section 2.6.

2.4.2.2 Geodetic method

The geodetic method, sometimes also referred to as cartographic or topographic method, is a method to determine the subsurface mass balance of a glacier or ice sheet by differencing two glacier surface elevation maps from different times *(Cogley et al. 2011)*. These elevation maps may be of different origin like ground-based using theodolites or airborne constructed from stereo images of aerial photographs, from laser scanning (Lidar) *(Kääb et al. 2012; Gardner et al. 2013)* or from satellites like the SRTM, ASTER (both freely available), SPOT5 or Tan-DEM-X digital elevation models (DEMs) with spatial resolutions of <= 90 m for all of them and nearly global coverage *(Paul et al. 2015)*.

The great advantage of the geodetic method is that nowadays it can be used to determine not only local, but region-wide or even world-wide mass balances *(Paul et al. 2015)* as topographic maps already exist since a long time. Furthermore, it is useful to compare geodetic measurements performed over five years or more (depending on the DEM accuracy and the amount of mass balance change of the glacier) with measurements from the direct glaciological method to detect systematic errors *(Andreassen 1999; Zemp et al. 2013; O'Neel et al. 2014)*. However, the following limitations have to be considered: Insufficient surface definition due to the high albedo in the accumulation area can lead to significant errors in the surface elevation and the density of the firn/ice can only be estimated *(Kaser et al. 2003)*.

2.4.2.3 Further methods

The *gravimetric Method* is a remote sensing technique that calculates glacier mass variations from direct measurements of changes in Earth's gravity field *(Cogley et al. 2011)*. Gravimetric remote sensing of glaciers became possible with the Gravity Recovery and Climate Experiment (GRACE). GRACE, launched in 2002, measures the gravity of the Earth using twin satellites following each other on the same orbital track *(Baumann 2017)*. The advantage of this method is to easily cover large areas and that it directly measures the mass. In contrast, due to the spatial resolution of roughly 400 km *(Tapley et al. 2004)*, this method is not suitable for single valley glaciers.

Once a good data base has been established, *index methods* allow an estimation of the mass balance based on some indicators and an empirical relationship to the mass balance *(Hoelzle 2015[b])*. This might be the ELA or the accumulation area ratio (AAR) at the end of the hydrological year *(Hoelzle 2015[b])*. These very simplistic index methods have to be used with caution especially in times of fast climate change, as the glacier hypsometry alters or the index leaves the range unsed to establish the empirical relationship.

Increasing popularity was observed considering mass balance *modelling* approaches. They allow a wide range of possible applicabilities from sub-daily resolution up to climate scenario runs *(Klok and Oerlemans 2002; Jouvet et al. 2011; van Pelt et al. 2012)*. Nevertheless, models need calibration data and hence are dependent on measurements from other methods. Furthermore, as soon as precipitation data is taken from meteorological stations, precipitation models or climate reanalysis, the problematic of precipitation accuracy as outlined in Subsection 2.5.2 has to be investigated carefully.

The *hydrological method* determines the glacier mass balance indirectly by solving the water balance for change in storage (ΔS): $\Delta S = P - E - R$ *(Cogley et al. 2011)*. However, for using the hydrological method reasonably, good input data of evapotranspiration (E), runoff (R) and especially precipitation (P) would be required. The latter usually is of poor quality and error prone. This method only gives information about the entire catchment and the storage change not only includes changes in glacier mass, but also changes of stored water in natural and artificial lakes or reservoirs, in aquifers and in snowpatches. Therefore, this method is rather used in hydrology than in glaciology.

There exist further mass balance measurement methods such as the flux-divergence method, the kinematic-equation method or discharge methods that are not discussed in more detail here *(Cogley et al. 2011)*.

2.4.3 Spatial inter- and extrapolation of mass balance

To inter- and extrapolate point measurements of glacier mass balance to the entire glacier, traditional methods comprise the profile method *(Escher-Vetter et al. 2009)* and the contour line method *(Østrem and Brugmann 1991, Sold et al. 2016)*. The profile method

considers mass balance only depending on elevation while the contour line method is based on expert's opinion considering altitude, exposition and field measurements *(Sold et al. 2016)*. Nowaday's methods also comprise inverse-distance interpolation *(Barandun et al. 2015, Sold et al. 2016)* as well as different modelling approaches that are energy-balance based *(e.g. Escher-Vetter 2009)*.

2.4.4 Energy balance

For modelling glaciers, melt simulation is crucial. To simulate melt physically based, the surface energy budget is used *(Cuffey and Paterson 2010)*. Assuming no horizontal energy fluxes on the ground, the energy fluxes occurring on a glacier surface are the following *(Cuffey and Paterson 2010; van Pelt et al. 2012)*:

$$Q_{melt} = SW_{net} + LW_{net} + Q_H + Q_E + Q_P + Q_{sub}. \qquad (1)$$

Its components are the net shortwave radiation (SW_{net}), the net longwave radiation (LW_{net}), the sensible and latent heat fluxes (Q_H and Q_E), the energy introduced by precipitation (Q_P) as well as the heat flux into the ice (Q_{sub}). The sign conversion is usually positive for fluxes from the atmosphere to the glacier, therefore a negative Q_{melt} represents refreezing. By convention, the latent heat flux in glaciology only refers to the vapor phase transitions (evaporation, sublimation, condensation, deposition) *(Cuffey and Paterson 2010)*.

The energy available for melt is principally determined by three contributors: The sunlight determining the incoming shortwave radiation and the earth's atmospheric heat content influencing the downward longwave radiation as well as the sensible heat transfer. The surface characteristics and temperature are determining the albedo as well as the outgoing longwave radiation *(Cuffey and Paterson 2010)*.

All contributors to the energy balance can be estimated using well-known physical laws and constants. This is widely done and therefore it is referred to the literature for more details about the parameter selections (e.g. *Klok and Oerlemans 2002; Cuffey and Paterson 2010; van Pelt et al. 2012; van Pelt and Kohler 2015*).

2.5 Precipitation and its relationship to glacier accumulation

2.5.1 Precipitation versus accumulation

For modelling glaciers, the accumulation distribution is crucial. It is crucial to see the difference between precipitation distribution and accumulation distribution. Between individual precipitation events and the accumulation distribution after several snowfalls, relocation of snow by avalanching and snow drift occurs. Both of them are not implemented in recent mass balance models *(Klok and Oerlemans 2002; van Pelt et al. 2012; van Pelt and Kohler 2015; Sold et al. 2016)*.

However, this study focuses on the accumulation distribution, already encompassing all kind of snow relocation processes, that can be used as PM to distribute precipitation of single precipitation events all over the glacier.

2.5.2 Precipitation uncertainty

A common known source of uncertainty modelling the mass balance of glaciers represents the precipitation. There arise two major challenges:

First of all, precipitation measurements, especially in mountainous regions, are still prone to huge measurement uncertainties, as indicated by the World Meteorological Organisation (WMO) (Table 1). Therefore, measurement uncertainty of snow can dramatically exceed 50 % *(Østrem and Brugman 1991)*, while for example in Switzerland, a snowfall correction of 35 % at mountainous stations is recommended *(Sevruk 1985)*. However, the uncertainty is large and this correction factor has to be used with caution.

Table 1: Precipitation measurement errors after *WMO (2008)*.

	Source of error	**Uncertainty**
systematic	Deformation of wind field	Rain: 2–10 % Snow: 10–50 %
	Wettening losses internal walls of the collector and emptying	Summer: 2–15 % Winter: 1–8 % Extreme: 15–20 %
	Evaporation from collector	0–4 %
	Splash-in and splash-out	1–2 %
	Blowing and drifting snow	not quantifiable
random	Random errors from instruments and observations	not quantifiable

If the accumulation is measured in form of density measurements of snow, the accuracy of the water equivalent measurement is better (typically less than 5 % error) compared to the accuracy of precipitation measurements. Furthermore, this has the advantage that dislocation of snow by snow drift and avalanching are already included. However, beside the low temporal resolution other problems may arise concerning the choice of representative measurement locations and, if the measurements are performed after melt started, the amount of occurred melt as well as internal accumulation.

Secondly, the precipitation inter- and extrapolation from point measurements to the entire glacier is challenging. *Schädler and Weingartner (2002:190)* recognized this problematic:

> *«Im Gebirge ist die Interpolation des Niederschlages zwischen den Messstationen und noch ausgeprägter die Extrapolation in Höhen ohne Niederschlagsmessung eine Quelle grosser Unsicherheiten und Fehler (...)».*

Up to now, in most mass balance models, precipitation data from weather stations in the vicinity or downscaled from regional climate models is used and inter- and extrapolated to a grid by elevation-dependent multiplication factors *(Klok and Oerlemans 2002; Huss et al. 2008; Reijmer and Hock 2008; van Pelt et al. 2012; van Pelt and Kohler 2015)*.

However, elevation-dependent multiplication factors underlie huge regional variations, as represented in Figure 5. Therefore, this commonly used elevation gradient approach has to be questioned.

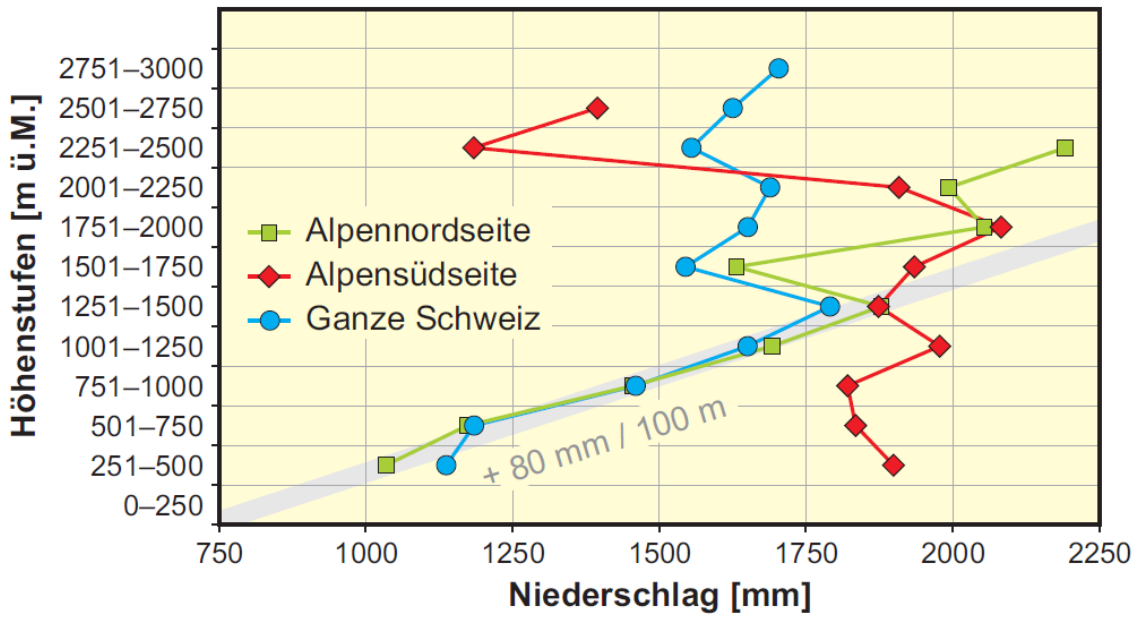


Figure 5: Mean annual precipitation 1961–1990 for three water balance areas and twelve elevation zones from *Schädler and Weingartner (2002)* with unit gradient (grey) from *Kirchhofer and Sevruk (1992)*, represented in *Spreafico und Weingartner (2005)*.

2.5.3 Accumulation distribution

The consensus of a lack in spatially extensive accumulation distribution measurements is evident *(Richardson et al. 1997; Hawley et al. 2014; Sold et al. 2015; Sold et al. 2016)*, as noted by *van Pelt et al. (2012:657)*:

> *«One of the main uncertainties in the model forcing is related to spatial and temporal variability in snow accumulation.»*

Klok and Oerlemans (2002) state that optimizing the snow accumulation parameterization scheme is challenging due to difficulties in estimating the spatial distribution of snow accumulation. Therefore, the quality of accumulation measurements could be increased substantially by combining snow pit point measurements with area-wide measurements of the end-of-winter accumulation, capturing the highly variable accu-

mulation distribution. *Richardson et al. (1997)* point especially on the redistribution of snow by wind having a major influence on the local accumulation pattern. Furthermore, they observed a generally static interannual accumulation pattern, while absolute values experience large variations. *Sold et al. (2016)* conclude that the accumulation pattern is consistent over the years and attach great importance to extensive snow accumulation measurements by GPR being beneficial to mass balance evaluations, even if they are not obtained for the complete study period.

The advantages of the, compared to snow pits, relatively fast and non-destructive area-wide GPR measurements especially in reproducing the spatial variability of snow accumulation are frequently highlighted *(Melvold 2008; Sold et al. 2013; Sold et al. 2015; Sold et al. 2016; Marchenko et al. 2017; Kenzhebaev et al. 2017)*.

2.5.4 Extrapolation to the entire glacier: Precipitation multiplier (PM) raster

Different attempts have been made to get information about the accumulation distribution of snow. These involve snow transport modelling *(Liston and Sturm 1998; Purves et al. 1998; Lehning et al. 2008)* or either correlations or multiple regressions with topographical parameters *(Huss et al. 2009; Schmidt et al. 2009; Farinotti et al. 2010; Sold et al. 2013; McGrath et al. 2018)*.

According to *McGrath et al. (2018)*, the most common method to extrapolate snow water equivalents (SWE) from point measurements to the entire glacier is to relate SWE to a series of explanatory topographical parameters. These topographical parameters are proxies for the physical processes that control the SWE distribution. The processes comprise orographic precipitation gradient and snow drift by prevailing wind direction that are captured by elevation, slope, curvature and aspect *(McGrath et al. 2018)*.

Schmidt et al. (2009) developed a multiple linear regression that describes the snow cover pattern in relation to topographical parameters. They used elevation, slope, aspect and curvature as primary topographical parameters.

Sold et al. (2013) investigated the snow depth distribution (SDD) pattern, derived from Lidar-DEM differencing, with three topographical parameters: They considered slope and curvature as proxies for local variations in snow depth due to preferential deposition and redistribution as well as elevation for the amount of precipitation. They used a DEM in 10 m resolution and 70 m radian environment of each grid cell for the curvature.

As snow redistribution processes are controlled by topographic effects, there is evidence that snow distribution patterns are often consistent over time (e. g. *Elder et al. 1991; Farinotti et al. 2010; McGrath et al. 2018*). Therefore, a PM matrix accounting for the complex patterns of snow redistribution when applied on every precipitation event was already successfully applied *(Jackson 1994; Huss et al. 2009; Farinotti et al. 2010)*.

The requirements for applying a multiple regression to develop a PM raster are a high-resolution DEM as well as spatially dense measurements of snow depths or densities for calibration. For this, GPR represents a unique technique.

2.6 Ground penetrating radar (GPR)

GPR measures the TWT of electromagnetic waves by the interpretation of density differences in the subsurface producing reflections. The advantages of GPR are that a glacier only needs to be visited once in time, its large-scale applicability *(Richardson et al. 1997)*, its fast application and its non-destructiveness *(Marchenko et al. 2017)* as well as the possibility to combine GPR measurements with stake and snow pit measurements. However, this geophysical method can only be used for accumulation measurements, as glacier melt during previous summers is lost for radar measurements. Therefore, GPR does not replace any ablation measurements. The GPR method is described in detail in the following subsections.

2.6.1 GPR in detail

GPR transmits electromagnetic pulses at a certain centre frequency down into the subsurface and detects reflected energy as a function of time and amplitude *(Berthling and Melvold 2008)*. Therefore, a transmitter antenna as well as a receiver antenna are used. Reflections are generated at any boundary where electromagnetic properties of the materials change *(Berthling and Melvold 2008)*. Once the velocity of electromagnetic waves in the material of interest is known, the measured TWT from the transmitter to the layer boundary in the ground and back to the receiver is converted to depth.

The velocity of electromagnetic signals is determined by the electromagnetic properties of the material, namely the electric permittivity (ε), the electric conductivity (σ) and the magnetic permeability (μ), whereof the latter is unimportant in GPR applications *(Berthling and Melvold 2008)*. While the dielectric constant ε'_d (the real part of the electric permittivity) is strongly influenced by the water content of a material, the electric conductivity is determined by the amount of dissolved ions present in the water *(Berthling and Melvold 2008)*. For a more detailed explanation of the electromagnetic principles, the reader is referred to e. g. *Annan (2009)*.

In GPR practical application, the dielectric constant is used, permitting the calculation of the electromagnetic wave velocity. However, the determination of the dielectric constant for materials consisting of several components such as snow (consisting of ice, water and air) is not trivial as outlined in Subsection 4.4.

The most commonly used GPR is the time-domain impulse radar. Beside the transmitter and receiver antenna, it consists of a control unit handling accurate timing and processing as well as a computer display for adjusting the survey parameters, data storage and real-time data display *(Berthling and Melvold 2008)*. The centre frequency and the

bandwidth of a time-domain impulse radar are determined by the antenna characteristics.

For GPR-profiling, three different antenna set-ups are used *(Berthling and Melvold 2008)*: The common offset (fixed space between the two antennas), the common mid-point (where the two antennas are moved away from each other at constant intervals) and the wide-angle reflection and refraction set-up (where one antenna is fixed while the other is moved away). The common mid-point set-up hast the advantage to estimate the travel velocity of the medium and can be used additionally to the common offset mode if this is possible from the antenna construction.

There exist shielded and unshielded antennas. Shielded antennas force the transmitted electromagnetic waves to manly propagate in one direction (in most GPR applications downwards) and therefore prevent undesired reflections from trees, other electrical infrastructure, cellphones etc. *(Annan 2009)*. Shielding however increases the weight of the antenna *(Annan 2009)*.

The choice of the antenna frequency depends on the electromagnetic properties of the ground (signal attenuation) and the research focus. Lower frequencies reduce the resolution while increasing the penetration depth and vice versa *(Berthling and Melvold 2008)*. Details can be found in the manuals of the corresponding GPR devices and analysing the equipment of earlier studies used in similar research environments. As an example, *MALÅ Geosciences AB (2016)* specifies the penetration depth in normal geological environment to 25 m for the 100 MHz antenna and to 2.5 m for the 800 MHz antenna. For measurements of firn layers, frequencies of 400, 500 or 800 MHz are commonly used *(Kohler et al. 1997; Machguth et al. 2006; Sold et al. 2013; Hawley et al. 2014; Marchenko et al. 2017)* and permit penetration to more than 20 m depth.

The antenna can be moved continuously (reducing ground coupling) or stepwise (reducing survey speed) *(Berthling and Melvold 2008)*. The available settings of the device such as time window (how long data is collected after a pulse is sent), sampling interval (frequency of pulses sent), spacing of the measurements and stacking (reflections from how many individual pulses that are summarized) should be done according to the antenna in use, type of movement and subsurface of interest. A rule of thumb considers the maximum critical measurement spacing Δx_{max} as one fourth of the wave length λ *(Berthling and Melvold 2008)* and can be calculated as

$$\Delta x_{max} = \frac{\lambda}{4} = \frac{\mathrm{u}}{4f} \qquad (2)$$

using the electromagnetic wave velocity u and the antenna frequency f.

Henceforeward, focus of subsurface is set on snow.

The resolution of GPR data, limiting the accuracy of recognized TWTs, can be estimated to be half the wavelength *(Sold et al. 2013)*. For 800 MHz and a velocity of 0.2 m ns^{-1}, the resolution[9] is thus 0.0625 m.

2.6.2 Use of GPR for accumulation measurements

The advantage of the use of GPR to improve understanding about the snow accumulation distribution is already known since 20 years, as outlined by *Richardson et al. (1997:20352)*:

> *«Ground-based snow radar soundings provide an excellent method to map spatial variability in snow accumulation.»*

Other advantages using GPR for accumulation measurements are its fast application, that it is sufficient to visit the glacier once, its non-destructiveness *(Marchenko et al. 2017)* and its capabilities to be combined with stake and snow pit measurements. Moreover, it can be used for different snow, firn or glacier depths depending on the antenna frequency chosen and the type of research question. Electromagnetic properties of snow, firn and ice make them well suited for GPR application.

[9] $\lambda = \frac{u}{f} = \frac{200'000'000 \frac{m}{s}}{800'000'000 \frac{1}{s}} = 0.25 \text{ m} \rightarrow \Delta x_{max} = \frac{\text{u}}{4f} = \frac{\lambda}{4} = \frac{0.25 \text{ m}}{4} = 0.0625\ m$

3 Research site

3.1 Research site

3.1.1 Geography

Abramov Glacier is a temperate Central Asian glacier located in the very south of Central Asian Kyrgyzstan (Figure 6). The glacier is situated at the head of the Koksu valley, a side valley of the Alay valley in northwestern Pamir. The mountain range where Abramov Glacier is located is often referred to as Pamir Alay. The Kollektorskiy Range in the north of Abramov Glacier builds the water divide between the Syr Darya watershed in the north and the Amu Darya watershed in the south, the two principal Central Asian rivers (details in Subsection 3.1.3). From Abramov Glacier, water flows into Vakhsh river that represents one of the largest tributaries of Amu Darya.

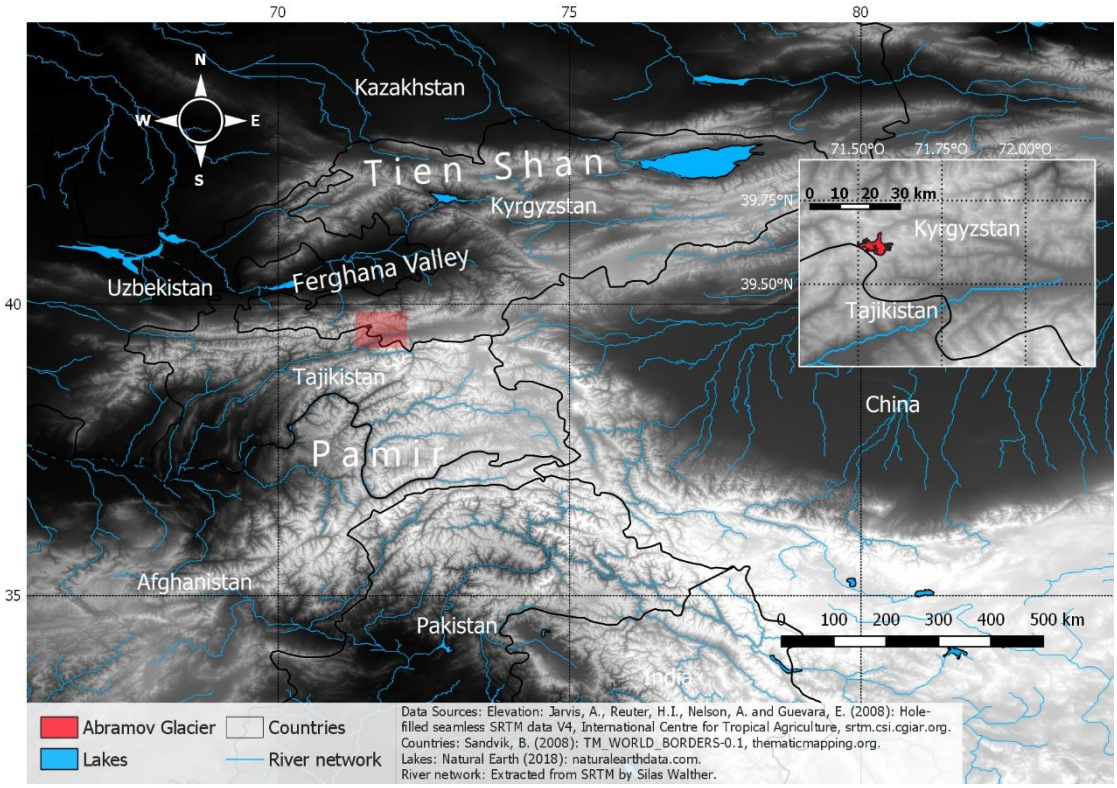


Figure 6: Overview of Central Asia with Abramov Glacier location (background shading: Elevation; black dotted grid: Coordinates in degree (World Geodetic System (WGS) 84)).

In the World Glacier Monitoring Service (WGMS), Abramov Glacier earlier on was located in the Pamir Alay mountains *(WGMS 2013)*, while in the most recent publication, it was changed to Tien Shan *(WGMS 2015)*. However, in most studies Abramov Glacier is considered as a Pamir glacier *(Khromova et al. 2006; Gardelle et al. 2013; Barandun et al. 2015; Kronenberg et al. 2016; Baumann 2017)*. This is relevant, as located in the northwest of Pamir mountain range, Abramov is the only glacier with long-term observations from these mountains *(Gardner et al. 2013; Hoelzle 2017)*. Furthermore,

there are several indications that glacier behaviour in Pamir is difficult to understand and is different from the one in Tien Shan *(Kääb et al. 2015; Baumann 2017)*.

Abramov Glacier has an area of 24 km² and covers an altitudinal range from 3'650 to nearly 5'000 m a.s.l. *(WGMS 2015)*, reaching up into the warm infiltration zone (Section 2.2). Figure 7 presents its hypsometry. Most parts of the glacier are located between 4'100 and 4'400 m a.s.l. with an ELA at 4'250 m a.s.l. in the most recent period.

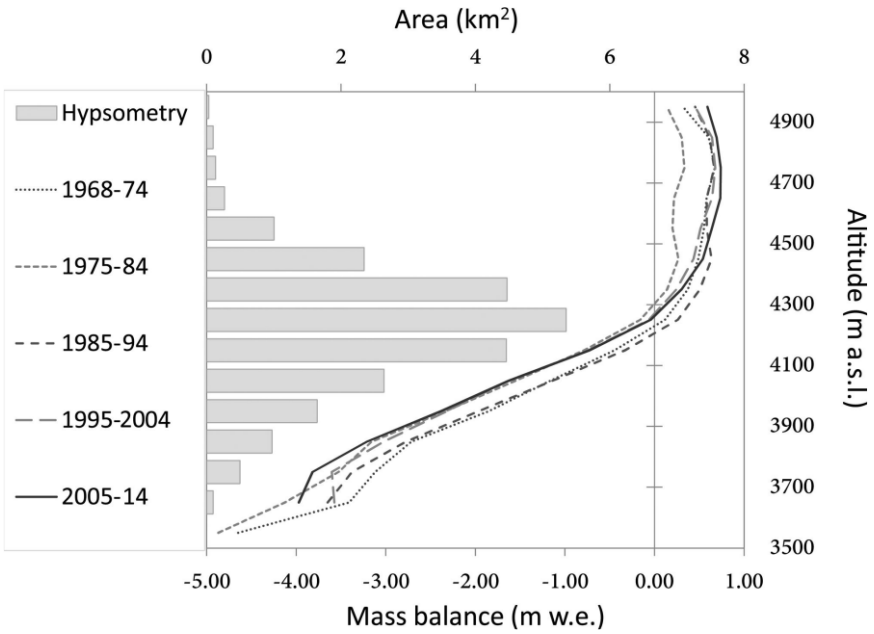


Figure 7: Mass balance gradients of Abramov Glacier in different time periods and hypsometry of the year 2013. Figure from *Barandun et al. (2015)*.

For Abramov Glacier, *Rasmussen (2013)* found a relatively high temperature sensitivity of –0.47 m w.e. K^{-1} and a high correlation between reanalysed positive degree days temperature and interannual variations of glacier-wide summer surface mass balance.

3.1.2 Climate

According to Köppen's climate classification, Tien Shan and Pamir mountains are classified as cold continental with dry, hot summers. The regions around the two mountain ranges are classified as arid steppe cold respectively hot in the Fergana valley *(Peel et al. 2007)*.

Figure 8 shows the annual precipitation in Central Asia. Hyper-arid desert climate is dominating Central Asian's precipitation regime: In Turkmenistan, Uzbekistan and Kazakhstan, annual precipitation is below 200 mm in most parts of the country, what is classified as desert[10] *(Laity 2008)*. In Kyrgyzstan and Tajikistan as water towers of Central Asia, precipitation exceeds 1'000 mm at the western part of the mountain ridges of Tien Shan and Pamir.

[10] Threshold from semiarid to arid at 200 mm a^{-1} *(Laity 2008)*.

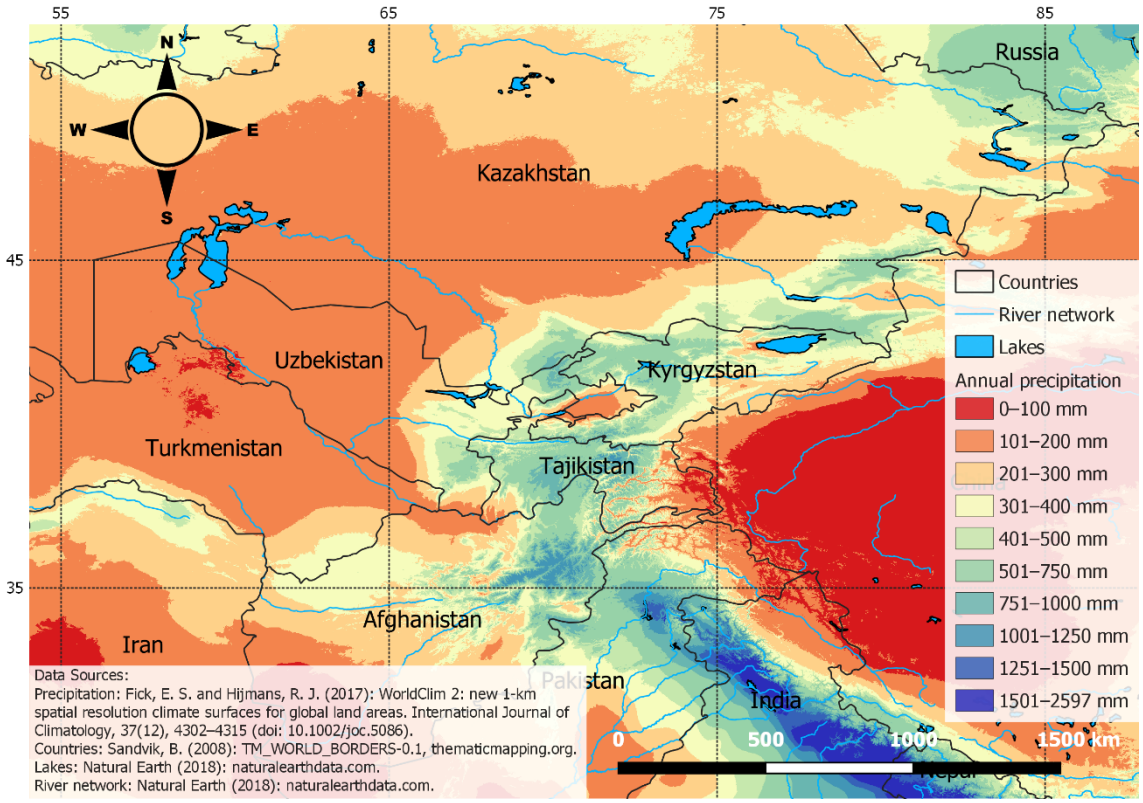


Figure 8: Annual mean precipitation of Kyrgyzstan and Central Asia from 1970–2000 (black dotted grid: Coordinates in degree (WGS 84)).

Concerning the annual cycle, high continental summer temperatures coincide with lowest precipitation during summer, both in Bishkek (north of Kyrgyzstan) as well as in Fergana basin (Figure 9). Total annual precipitation in Fergana amounts to about 200 mm with maximum precipitation during winter and early spring.

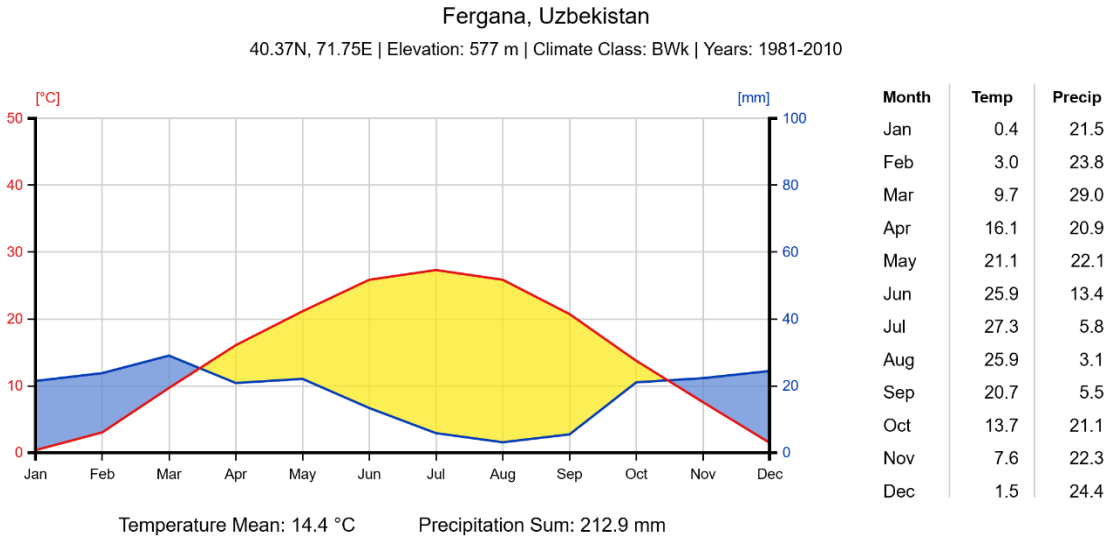


Figure 9: Climate diagram Fergana, 1981–2010 (*ClimateCharts (2018)*, data Source: *NOAA (2011)*.

Aizen et al. (2001) studied large-scale weather patterns and their influence on Central Asian precipitation. Thereafter, a stronger meridional northern hemispheric circulation, associated with low pressure over Europe and the Siberian High shifted eastwards favours annual precipitation increase in Central Asia *(Aizen et al. 2001)*. In contrast, positive North Atlantic oscillation (NAO) phases with corresponding strong zonality effectuate below average Central Asian winter precipitation *(Aizen et al. 2001)*.

According to *Suslov and Akbarov (1973)* and *Glazirin et al. (1993)*, Pamir experiences an important precipitation gradient with 1'900 mm a^{-1} in the west at the border between Kyrgyzstan and Tajikistan and 400 mm a^{-1} in the east. Precipitation maximum in western Pamir occurs during autumn and winter, while in eastern Pamir it is observed in spring and summer.

Located far away from any larger water reservoir, the climate at Abramov Glacier is continental. Despite the considerable ELA of 4'260 m, average annual precipitation measured at 3'837 m a.s.l. is about 750 mm *(Glazirin et al. 1993)* and mean annual air temperature ranges from –6.5 to –8 °C *(Kamnyansky 2001)*. However, the precipitation gradient is extraordinary steep: Near the glacier tongue at 3'600 m a.s.l., mean[11] precipitation from October to May of 340 mm was measured while above 4'200 m a.s.l., 1'800 mm were recorded *(Kislov 1982)*. Winter accumulation was responsible for 80 % of total annual precipitation *(Kislov 1982)*. Interestingly the precipitation gradient is much smaller during summer with 153 mm at 3'600 m a.s.l. and 310 mm above 4'200 m a.s.l. According to extensive accumulation measurements on Abramov Glacier (details in Section 4.1), most accumulation occurs from October to December and again from February to April *(Pertziger 1996)* which is in line with precipitation observations in Fergana shown before.

3.1.3 Water importance and runoff in Central Asia

Central Asian's two principal rivers Syr Darya and Amu Darya, source in Tien Shan respective Pamir mountains (Figure 10) and reach the Aral Sea after having passed Kazakhstans and Uzbekistans deserts *(De Pauw 2008)*.

The natural flow regime of Syr Darya river was characterized by high flow in summer due to snow and ice melt and low flow in winter *(Karimov et al. 2010)*. At the uppermost parts of Syr Darya at Naryn River, glacial influence is especially high during dry summers, resulting in a glacial regime type after *Weingartner and Aschwanden (1992)*.

During Soviet Union period, large reservoirs were built reaching capacities up to 19.5 km^3 (Toktogul)[12]. Huge irrigation systems were established like the Karakum-

[11] Mean between 1968 and roughly 1980

[12] This corresponds exactly to the triple of Lake Thun's volume or 50 times the volume of Lac des Dix, Switzerland's largest artificial reservoir.

Canal at Amu Darya, with 1'350 km the longest irrigation canal on earth *(Bar 2015)*, significantly reducing river inflow into the Aral Sea *(Karimov et al. 2010)*. Focus of reservoir operation was on runoff for summer irrigation rather than energy production, wherefore headwater regions of today's Kyrgyzstan and Tajikistan got fossil energy compensation in winter as well as industrial and agricultural products *(Bar 2015)*.

Self-sufficient energy supply by the republics was not foreseen in Soviet Union. However, Kyrgyzstan and Tajikistan mainly had hydropower plants for independent energy production *(Bar 2015)*. After the breakdown of the Soviet Union in 1991, they shifted operation mode of their reservoirs from irrigation to hydropower generation *(Karimov et al. 2010)*. This shift resulted in an enormous change of seasonal runoff, as shown in Figure 11.

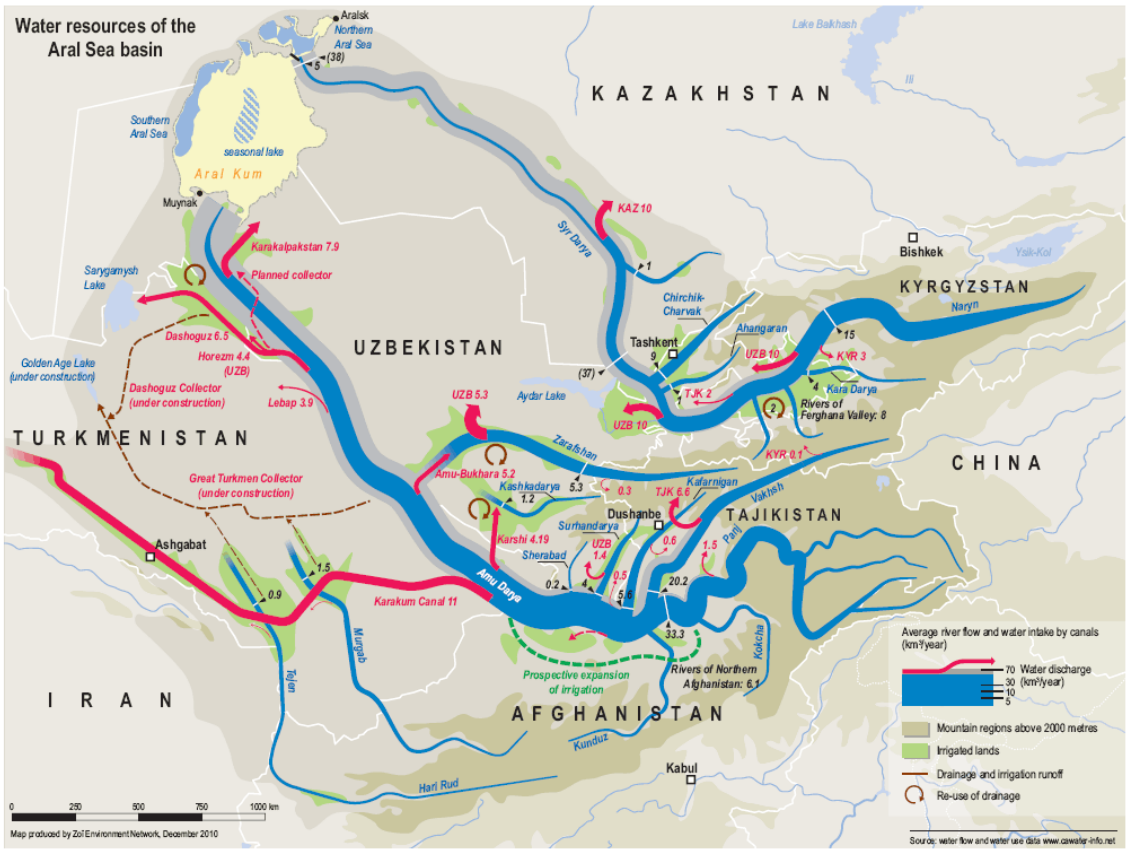


Figure 10: Water resources of the Aral Sea basin (from *CAWATERinfo (2017)*).

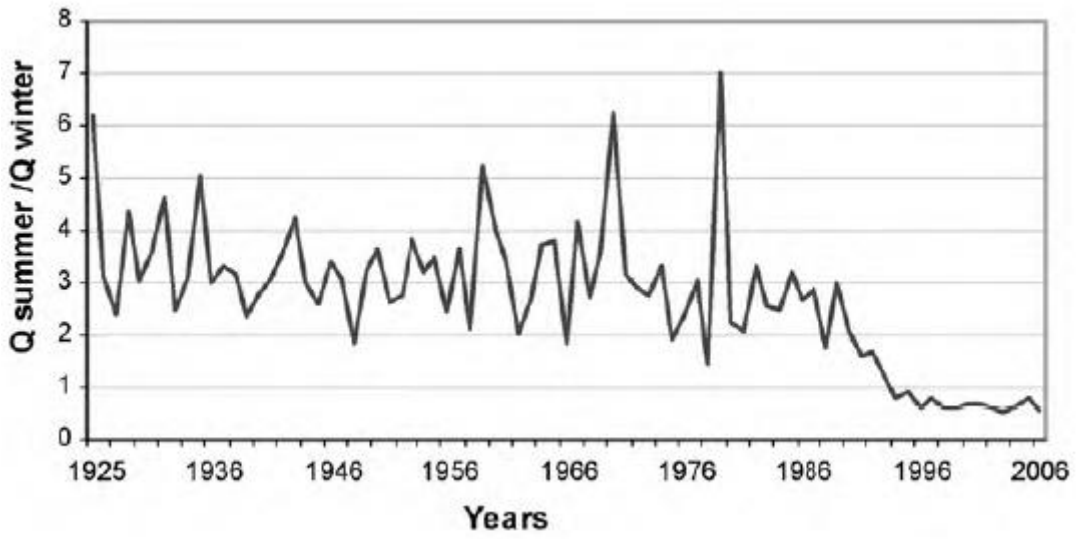


Figure 11: Ratio of summer/winter flow (Q) in the Naryn River at Uchkurgan (from *Karimov et al. 2010*).

With this regime shift, Syr Darya and Amu Darya became platforms of long-lasting conflicts concerning water allocation through artificial regime manipulation as in the hyper-arid Ferghana Valley (Subsection 3.1.2), three million people are living from agriculture based on summer irrigation *(Bar 2015)*. Many attempts and meetings have been made with the aim of solving these water conflicts[13]. Behind is the conviction that the overall hydropower production does not depend on the runoff regime, while such regimes have a strong effect on the irrigated agriculture *(Petrov 2015)*.

Considering the fact that glacial influence to runoff is especially important in dry summers (Subsection 2.1.1) common in Central Asia and that glacier melt amounts to 8 % of total annual runoff of all Central Asian rivers *(Suslov and Akbarov 1973)*, glacier changes have to be seen in this context and accurate glaciological knowledge is important for glacier modelling (e. g. *Siegfried et al. 2012*).

3.2 Glacier observations in Central Asia

In the late 1960s, Soviet Union initiated an extensive glacier-monitoring network for selected glaciers *(Dyurgerov 2002; WGMS 2005)*. In Kyrgyz Tien Shan, long-term[14] measurements were performed on Karabatkak from 1957–1997 and Golubin from 1969–1994 while in Pamir, Abramov with measurements from 1967–1999 is the only glacier with long-term mass balance measurements *(Dyurgerov 2002, WGMS 2015)*.

[13] Possible solutions to the water conflicts: Integrated power system, pumped storage hydropower plants, water pricing, agreement accepting by all actors, increased water use efficiency and water banking *(Heltzer 2003; Gracheva et al. 2009; Karimov et al. 2010; Bar 2015; Petrov 2015)*.

[14] In this study, long-term is used for at least 20 years of measurements.

After the collapse of the Soviet Union in 1991, most glacier-monitoring programmes were abandoned *(Barandun et al. 2015; Hoelzle et al. 2017)*. Representing a glaciated area of remarkable 62'500 km², in entire Central Asia, only two long-term mass balance programmes at Tuyuksu and Urumqi Glacier, located in the Kazakh and Chinese Tien Shan, have not been interrupted *(WGMS 2015)*. Apart this data scarcity, uncertainty arises in Pamir due to the heterogeneous behaviour of individual glaciers *(Kääb et al. 2015)* resulting from different climates described in Subsection 3.1.2. Therefore, Central Asian glaciers are greatly under-represented in the global databases *(Unger-Shayesteh et al. 2013; WGMS 2015)*.

Recently, five Soviet mass balance measurement series have been resumed *(Hoelzle et al. 2017)*. This is the case for Abramov, Golubin, Batysh Sook, Glacier No. 354 and Barkrak Middle (the latter three only experienced short measurement intervals during Soviet time *(Hoelzle et al. 2017)*). Abramov Glacier with its 24 km² is by far the largest of these glaciers *(WGMS 2015)*. Moreover, it is the only glacier with available long-term direct mass balance measurement in western Pamir *(Dyurgerov and Meier 2005; Hoelzle 2017)*, where in situ mass balance measurements are especially rare *(Baumann 2017)*. Therefore, history of mass balance measurements at Abramov Glacier is assessed in detail in the following section.

Glacier mass balance changes of Tien Shan and Pamir were estimated by several studies using different methods (Table 2). However, comparability is limited as the study regions vary. For lucidity, this is not a complete list of all studies[15].

[15] For example *Farinotti et al. (2015)* gave values in Gt a^{-1} without mentioning the corresponding area.

Table 2: Mass balance changes of selected Central Asian mountain regions from different authors. Values from *Kääb et al. (2015)* given in m a^{-1} are converted to m w.e a^{-1} by factor 0.85 as proposed by *Kääb et al. (2015)*.

Region (glaciated area) ***Author***	**Period**	**Method (details Section 2.4)**	**Mass balance change (m w.e. a^{-1}) and uncertainty**
Tien Shan (14'500 km²) *Gardner et al. (2013)*	2003–2009	Geodetic (ICEsat and SRTM)	–0.12 ± 0.24 (± 2σ)
Tien Shan (12'530 km²) *Baumann (2017)*	2004–2012	Gravimetric (GRACE)	unfiltered -0.51 ± 0.25 filtered -0.15 ± 0.08 (± 1σ)
Pamir and Hissar Alay (16'900 km²) *Gardner et al. (2013)*	2003–2009	Geodetic (ICEsat and SRTM)	–0.12 ± 0.24 (± 2σ)
Pamir (9'369 km²) *Gardelle et al. (2013)*	1999–2011	Geodetic (SPOT5 and SRTM)	+0.14 ± 0.14 (± 1σ)
Pamir (6'500 km²) *Kääb et al. (2015)*	2003–2008	Geodetic (ICEsat and SRTM)	–0.41 ± 0.12 (± 1σ)
Pamir (14'290 km²) *Baumann (2017)*	2004–2012	Gravimetric (GRACE)	unfiltered -0.42 ± 0.47 filtered -0.12 ± 0.13 (± 1σ)
All High Mountain Asia (120'200 km²) *Gardner et al. (2013)*	2003–2009	Geodetic (ICEsat and SRTM)	–0.24 ± 0.11 (± 2σ)
All High Mountain Asia (80'500 km²) *Kääb et al. (2015)*	2003–2008	Geodetic (ICEsat and SRTM)	–0.31 ± 0.09 (± 1σ)

The positive mass balance estimations by *Gardelle et al. (2013)* for the Pamir mountain range have to be used with care due to uncertainties in SRTM C-band penetration depth *(Gardelle et al. 2013; Kääb et al. 2015)*.

Although nowadays modelling of glacier mass balance over entire regions is popular, high resolution local data is required for model calibration *(Rasmussen 2013; Barandun et al. 2015; Sold et al. 2015; WGMS 2015; Baumann 2017)*.

3.3 Previous work on Abramov Glacier

3.3.1 Exceptional Soviet Union measurements

At Abramov Glacier, a research station was built in 1967 by the Central Asian Hydrometeorological Institute (SANIGMI) *(Hoelzle et al. 2017)*. This station was manned year-round. Spatially dense mass balance measurements were performed on monthly temporal resolution at nine snow pits and 165 stakes represented in Figure 12 from October 1967 to July 1999 with a data gap from October 1968 to February 1969 *(Pertziger 1996 and personal communication)*. Furthermore, daily meteorological observations were

performed at the scientific station located above the right side moraine of the glacier tongue at 3'837 m a.s.l.

In summer 1999, the scientific station has been destroyed by a group of armed men. With the station, research equipment was lost and the measurement network abandoned *(Hoelzle et al. 2017)*.

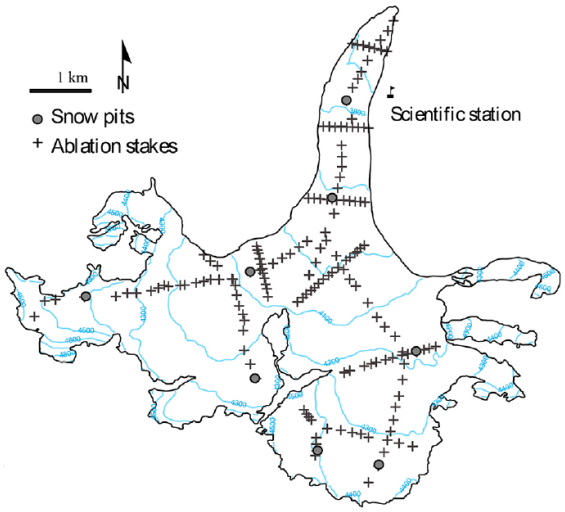


Figure 12: Historical mass balance network on Abramov Glacier (from *Hoelzle et al. 2017*).

A small amount of these spatially and temporally extraordinary dense Soviet measurements were resumed by the University of Fribourg in 2011 *(Barandun et al. 2015)* thanks to the CATCOS Project, funded by the Swiss Agency for Development and Cooperation *(MeteoSwiss 2017)*. Since then, 16 ablation stakes as well as three to four snow pits are measured once a year in collaboration with the Central Asian Institute on Geophysical Research (CAIAG) *(Barandun et al. 2015)*. Furthermore, in August 2011 a new and fully automated meteorological station was installed by the German Research Center for Geosciences (GFZ) and CAIAG, on the right side above the glacier tongue at an altitude of 4'100 m a.s.l. *(Schöne et al. 2013)*.

3.3.2 Reanalysis of seasonal mass balances

The exceptional Soviet measurements from Abramov Glacier were used in several studies *(Kamnyansky 2001; Dyurgerov 2002; WGMS 2005; Barandun et al. 2015)* and represent the starting point of the study of *Barandun et al. (2015)*. They calculated seasonal mass balances from 1968–2014 and filled the data gap from 1999–2011 using a spatially distributed surface mass balance model in 20 m resolution. To run the model initially developed by *Huss et al. (2009)* they used snow accumulation input at any location as following: They multiplied the precipitation data from the weather station with a correction factor accounting for systematic measurement errors (precipitation underestimation, station dislocation) and a spatial snow distribution raster *(Barandun et al. 2015)*. The precipitation correction factor was calibrated with winter point mass balance

measurements *(Barandun et al. 2015)*. The snow distribution raster was derived from inverse-distance interpolation of the point winter balance measurements of the years 1971–1994 with sufficient measurements, normalized over the entire glacier area. They assumed the spatial accumulation variability to be similar for years without measurements. For further calibration, snow line observations from satellite imagery and terrestrial camera images were used.

They also performed some GPR traces with an 800 MHz antenna in the vicinity of the snow pits and tried to extract accumulation rates and to compare them with modelled point mass balance data *(Barandun et al. 2015)*. However, their major drawback was not having any reference data such as firn cores to ensure that the high-density layers registered truly corresponded to summer surfaces and that all summer horizons were present *(Barandun et al. 2015)*.

4 Data and methods

4.1 Soviet field data

As described in detail in Subsection 3.3.1 extensive stake and snow pit measurements were performed on Abramov Glacier from 1967–1999 by Soviet researchers living all year round in a research station near the glacier tongue. Beside daily meteorological measurements, at most of the nine snow pit locations mass balance measurements have been performed every month. At the 168 stake locations, snow depth or ablation measurements have been performed every month. Figure 13 shows the numbers of monthly stake and snow pit measurements. Therefore, the largest amount of measurements were performed between 1969 and 1998.

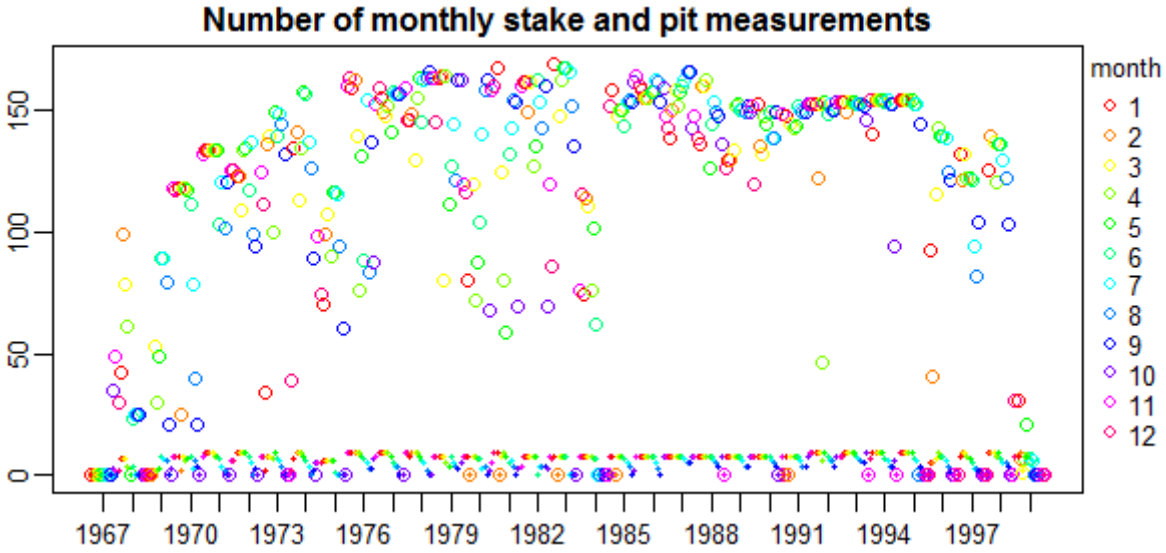


Figure 13: Number of monthly stake (empty circles) and pit (small filled circles) measurements from 1967–1999. The year indicates the midyear, the color the month Jan (1) to Dec (12).

Soviet snow pit, stake and precipitation measurements from 1968–1998 are used here. Only eight of the nine snow pits are used as one snow pit was not measured throughout the entire Soviet measurement period as it was located on the glacier tongue and got lost due to glacier melt.

For using the Soviet field data, a transformation from the local coordinate system with unknown reference points (in which all the coordinates of the Soviet stakes and snow pits are given) to the global projected coordinate system WGS 84 UTM zone 42 N (EPSG 32642) is performed. Therefore, a spatial adjustment of the vector points is done in ArcGIS, based on six reference points with knowledge of both coordinates thanks to exact measurements in summer 2014 (Table 3).

Table 3: Georeferencing of reference points from the local coordinate system to WGS 84 UMT zone 42 N (x = x coordinate, y = y coordinate).

Point Number	Soviet x	Soviet y	WGS 84 UTM 42 N x	WGS 84 UTM 42 N y
1M3	47884	44755	719073	4386985
1M4	50663	45474	721828	4387781
1M10	50000	50000	721042	4392283
1M17	50033	47215	721151	4389501
1M18	47518	48609	718443	4390844
3M1a	51120	49902	722160	4392215

From Soviet meteorological measurements *(Pertziger 1996)*, precipitation data is used in daily resolution and aggregated to monthly or supramonthly sums.

4.2 January 2018 field data

From 20 January 2018 until 2 February 2018, a group of eight researchers spent 14 days in a winter camp on Abramov Glacier at 4'100 m a. s. l. to drill firn cores. Within this field campaign, GPR measurements were performed and snow pits dug. The planned and collected data are presented in the following subsections, focusing on its relevance for this study.

4.2.1 GPR planning

For the GPR survey, it was planned to cover most parts of the accumulation area with as regular radar profile lines as possible. As *Sold et al. (2016)* made good experience with a 500 m spacing of the linear helicopter borne GPR profiles on Findelengletscher (13 km²), this would have been the optimal case also on Abramov Glacier. However, as the survey on Abramov Glacier was planned to be executed walking with skis on the glacier pulling a radar sledge instead of air borne, intensively crevassed zones were planned to omit for safety reasons and due to difficult interpretation of the reflected radar signals *(Petrakov et al. 2014)*.

The different traces planned were given priorities (Figure 14) accounting for the unknown field work progress depending on the weather conditions (possibility of fog, storms and avalanche risk), discharge rate of the radar's batteries at roughly –20 °C and state of health of the researchers. The most important traces should cover the principal branches of the glacier in zigzag, producing numerous intersection points. Second priority was given to smaller tributary streams and third priority to steep slopes (if snow conditions allowed access), to a finer mesh with more intersection points as well as to the ablation area.

For reducing the risk to fall into crevasses during GPR survey, crevasses were mapped using Pléiades images with 0.5 m resolution from autumn 2015 (details see Section

4.3.1). The criteria small versus big was based on the risk for snow mobiles, initially planned to use for the firn core measurements during the same campaign, to fall into the crevasse.

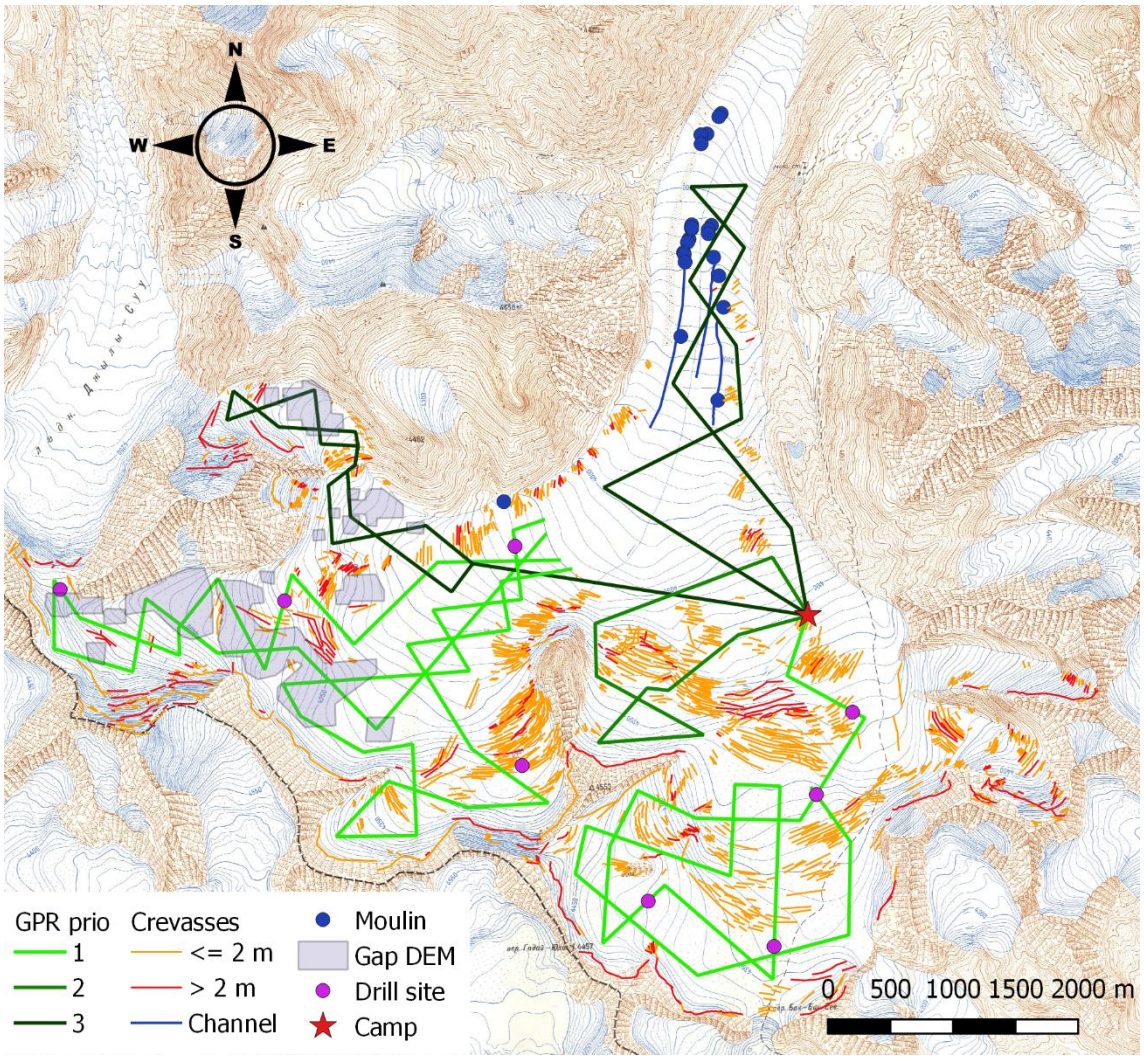


Figure 14: Planned GPR traces with priorities 1 (first priority) to 3 (last priority), planned drill site and planned camp for the field work in January 2018. Background: Soviet map with glacier extent in 1986.

For GPR measurements, the MALÅ ProEx GPR system with an 800 MHz shielded antenna was used. The parameter settings of the GPR were taken as following: The antenna was used at a time interval of 0.5 s, a sampling frequency of 8'123 MHz, 8 stacks and the maximum possible time window at this sampling frequency of 245.3 ns. Maximum penetration depth that could be recorded by the MALÅ ProEx device with the 800 MHz antenna, above settings and an assumed average travel speed of the electromagnetic waves of 0.200 m ns^{-1} is 24 m. For the trace in the ablation area, a sampling frequency of 13'000 MHz was used, resulting in an increased spatial resolution but a bisection of the penetration depth.

To allow trace location, the MALÅ ProEx GPR-own GPS sensor was used as well as an additional external Garmin 64s GPS.

To estimate radar accuracy, the intersections of radar survey lines are used as it was done by *Petrakov et al. (2014)*. Therewith, accuracy of the registered traveltimes for specific horizons is assessed.

4.2.2 Processing steps GPR data

For processing the registered GPR traces, ReflexW software from Sandmeier Scientific Software (Karlsruhe, Germany) is used. For one profile, the GPS connection did not work and therefore, the external Garmin GPS data is used. Afterwards, several processing steps (following *Machguth et al. (2006)* and *Sold et al. (2013)*) are executed with the aim to remove noise and to account for the signal attenuation with depth. The following processing steps are performed: Bandpassfrequency filter (lower cut-off 500 MHz and higher cut-off 1'200 MHz), phase follower and static correction to get the first reflection, background removal to avoid horizontal noise lines, a linear and exponential gain function[16] to improve visibility of the horizons and trace interpolation to 0.5 m to achieve equidistant traces. Then several processed radar profiles are combined where necessary.

The individual layers are marked by hand and exported as a table, containing the TWTs as well as the coordinates and trace numbers. These tables are postprocessed in R to account for missing traces or traces with double pickings (Appendix K Pick_korrektur.R).

Uncertainties of the manual picking of the annual horizons are estimated picking three times the same horizon and calculating deviations from mean (Appendix K Pick_Ungenauigkeiten.R).

4.2.3 Data GPR surveys

Figure 15 shows the GPR profiles that have been recorded during field work in January 2018. Compared to the planned profile lines from Figure 14, a slight reduction in line density on the orographic right branch of Abramov Glacier occurred. On the left branch, no GPR trace could be recorded due to instable weather conditions: After two clear days in the beginning needed for acclimatisation, weather worsened and acceptable visibility was present only in the ablation area and on the orographic left branch on three more days during our two-week stay on Abramov Glacier. Nevertheless, more data from the ablation area was measured than expected: Thanks to the considerable amount of winter precipitation fallen until January 2018, snow depth in the ablation

[16] Linear gain: 0.1 or 0.15; exponent: 0.1, 0.2 or 0.25

area was already high enough for accumulation distribution measurements by GPR and visibility was better in these lower parts of Abramov Glacier.

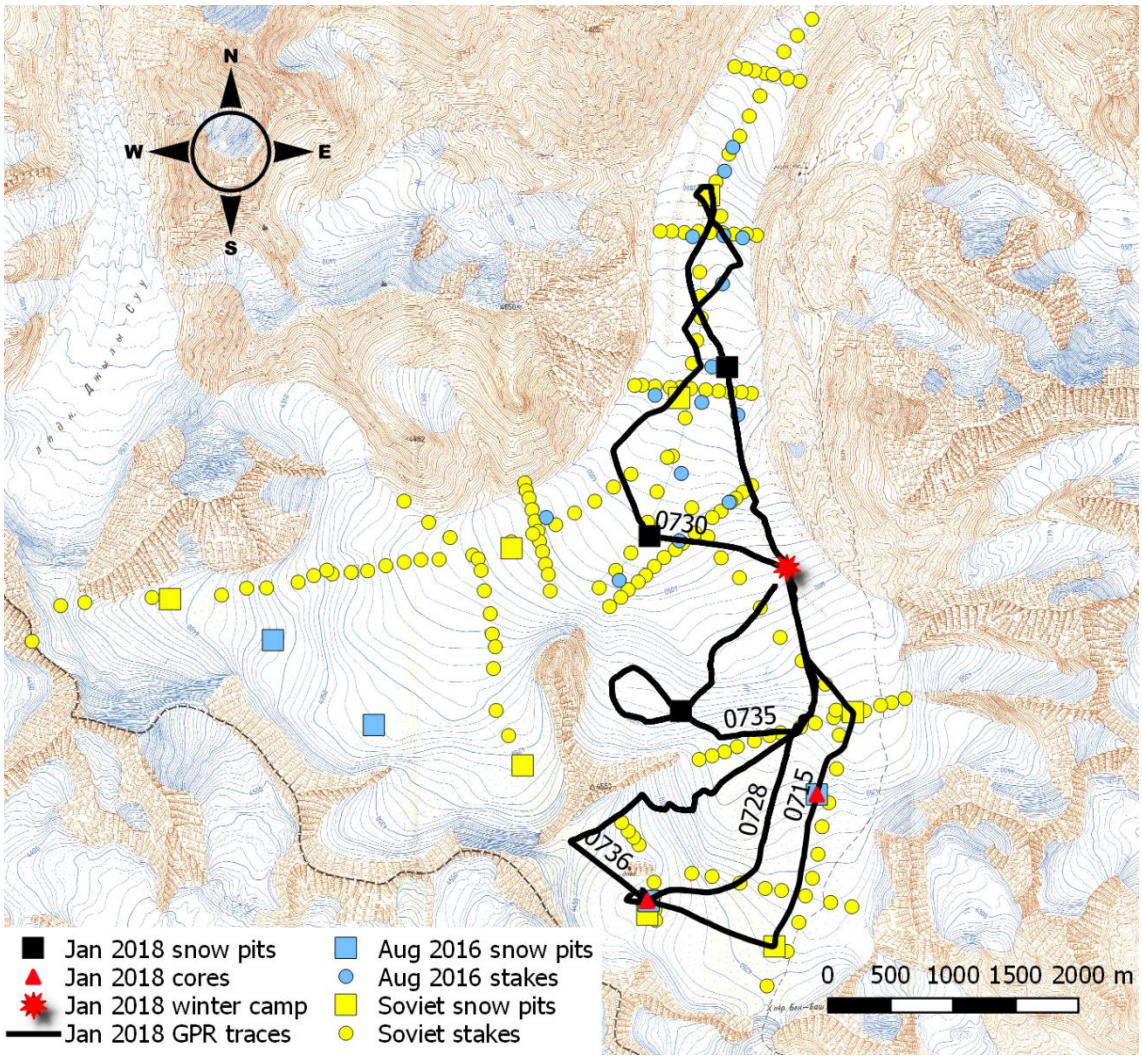


Figure 15: Field data overview. Black numbers label the GPR profiles. 2016 snow pits and stakes were measured during the summer campaign of CAIAG and University of Fribourg. Soviet snow pits and stakes were measured year-around from 1967–1999. Background: Soviet map with glacier extent in 1986.

Henceforth, the profiles are labelled with their numbers from Figure 15.

Although GPR measurements look like lines, in reality these are point data measured in regular time intervals. With the settings described above (Subsection 4.2.1), in total 50'521 recorded point measurements were performed on the traces shown in Figure 15 and used for the analysis.

Figure 16 shows the GPR profile 0715. For this profile, equidistance generation was more complicated than for the other profiles as the GPR-own GPS did not work. Therefore, GPS data was taken from the supplementary Garmin GPS. For all two combination pairs of the GPR profile and the GPS coordinates where exact location was

known[17], coordinates were interpolated for the more numerous GPR points using one GPS coordinate per minute and linear interpolation in between (Appendix K 0715_Verortung.R).

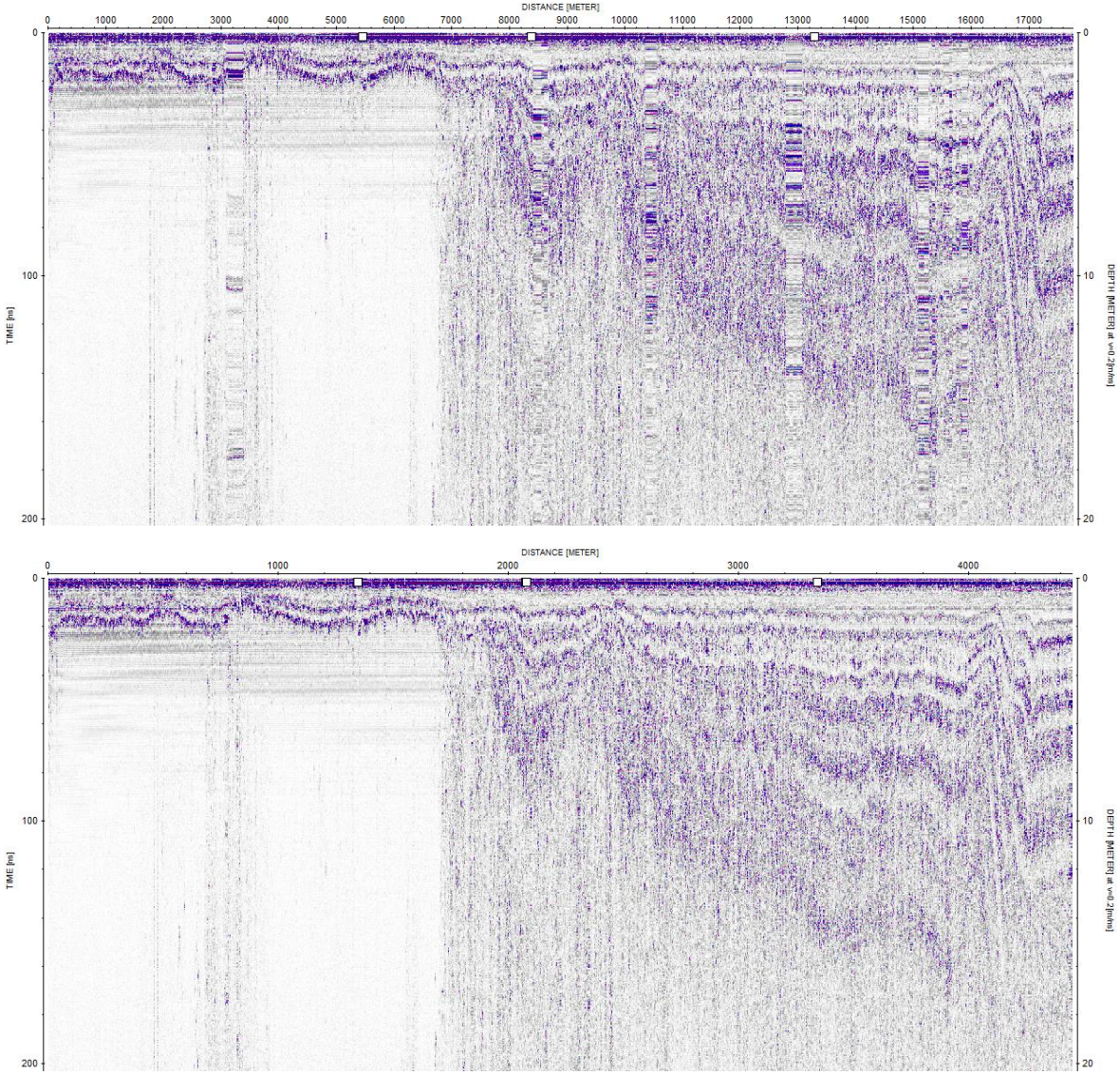


Figure 16: Filtered GPR profile 0715 (labelled inFigure 15) without (above) and with (below) equidistant trace interpolation. The numbers shown in the upper profile's abscissa are trace numbers instead of distance (bug in REFLEX software).

With the trace interpolation performed in REFLEX, each GPR reflection covers 0.5 m of distance. Figure 16 shows two reflection horizons throughout the profile and several additional reflection horizons after one third of the profile. This is where perennial accumulation area begins.

[17] This is the case for the three measurement sites that were marked in GPR when passing and ten positions where stops of more than one minute occurred (as these stops are visible in both the GPR as well as the GPS data).

For all other profiles, equidistant generation was a fast last step in GPR processing as GPS data was measured and added automatically to all traces. In most profiles, changes from equidistant conversion are not huge. Exceptions are the profiles that include some descents where speed was higher on some parts of the profile.

Figure 17 shows the profile 0728 measured on the way down to the camp. Clearly distinguishable are several horizons down to the middle of the profile as well as the noisy zone from 500 to 900 m.

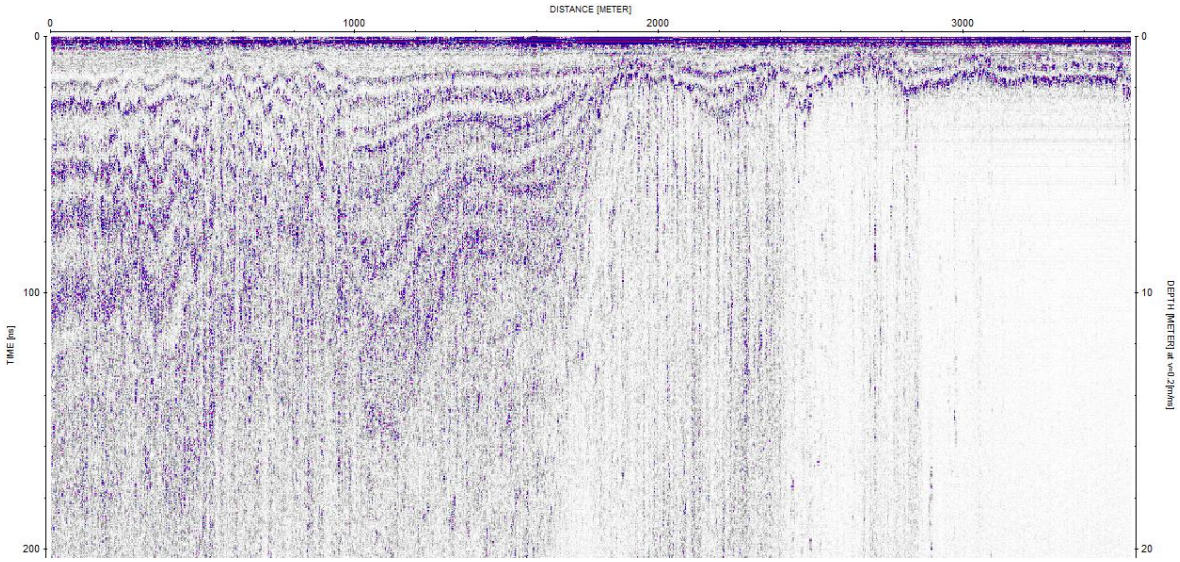


Figure 17: Filtered GPR profile 0728 (labelled in Figure 15) with equidistant trace interpolation.

Profile 0730 in Figure 18 covers the ablation area only while in profile 0735 in Figure 19 some perennial parts exist. Figure 19 on its main part covers a glacier plateau at about 4'150 m of elevation, being bordered in the south and west by very steep slopes reaching up to 4'550 m a.s.l. and producing regular avalanches that reach the flat plateau.

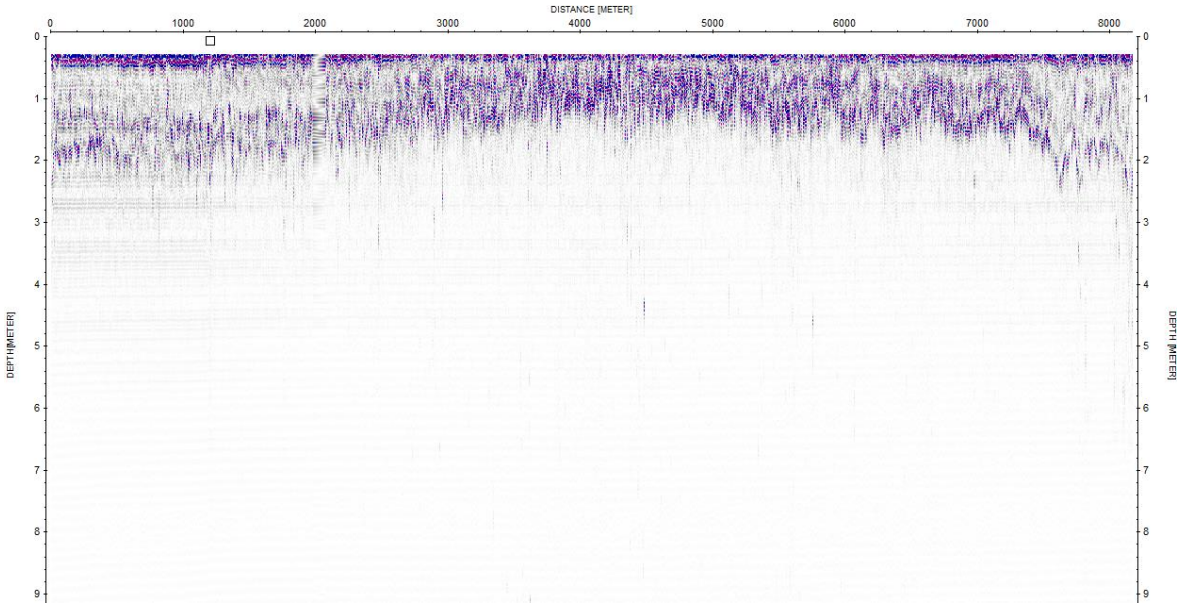


Figure 18: Filtered GPR profile 0730 (labelled in Figure 15) with equidistant trace interpolation.

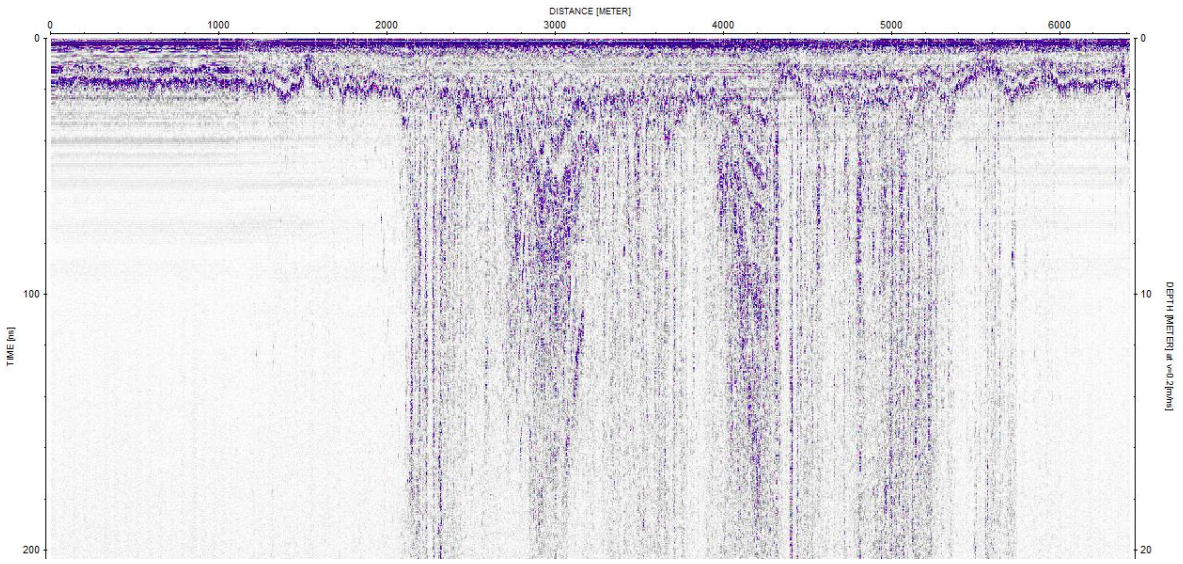


Figure 19: Filtered GPR profile 0735 (labelled in Figure 15) with equidistant trace interpolation.

Profile 0736 in Figure 20 covers the steepest slope up to the uppermost drill site passing the northerly branch of the nunatak. With 18 °, this is the steepest slope measured during the field survey in January 2018. It includes some crevassed zones as well as a part of reduced horizontal resolution due to higher speed when descending.

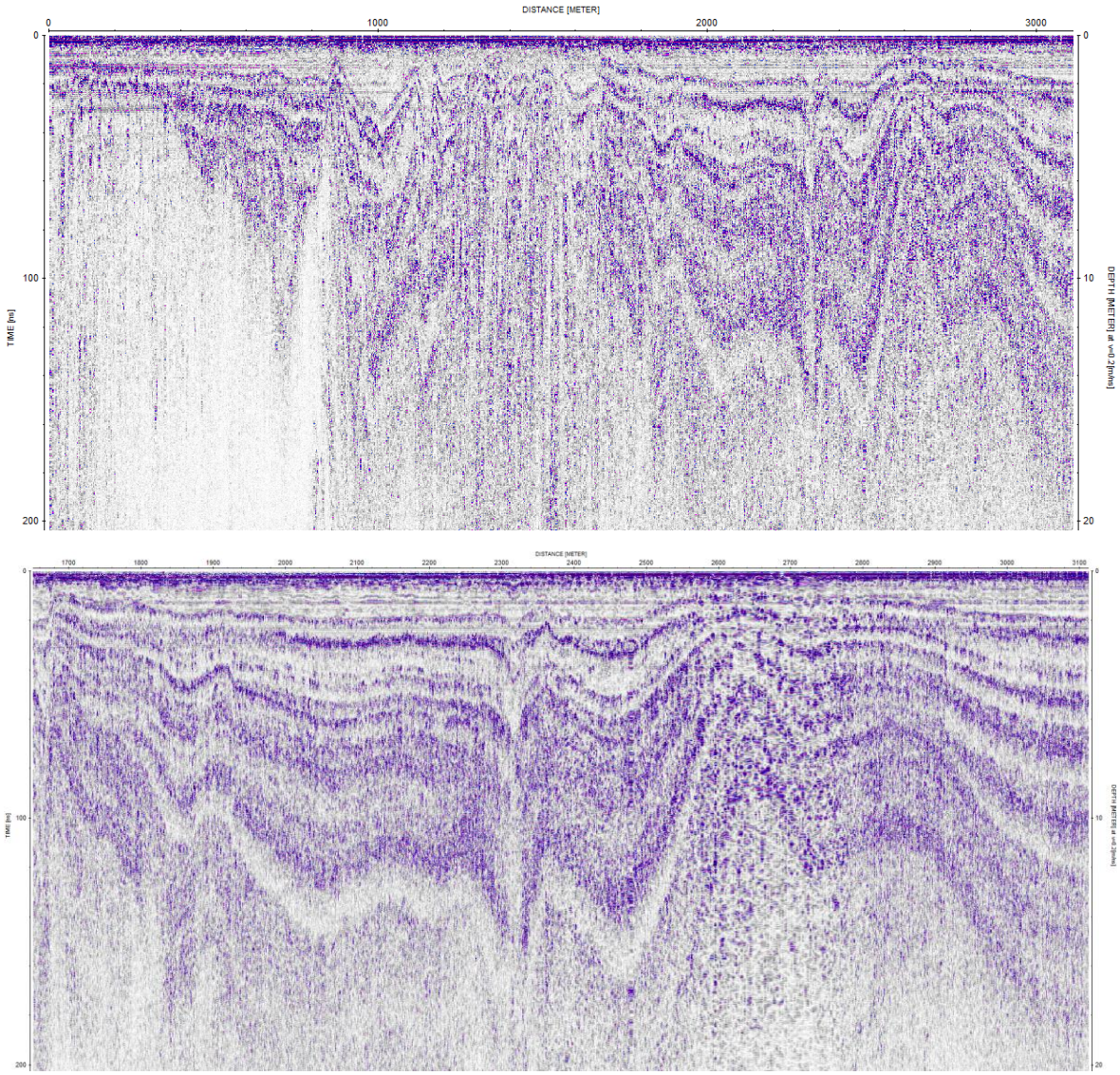


Figure 20: Filtered GPR profile 0736 (labelled in Figure 15) with equidistant trace interpolation. Entire profile (above) and zoom to the main accumulation area (below).

4.2.4 Data firn cores

During the same field campaign, three firn cores were drilled by other researchers (Table 4 and Figure 15). Two of the firn cores were drilled at the plateau on the upper-most part of Abramov Glacier. Only the data of the core directly analysed in the field is used. A third core was drilled half-way down to the camp at 4'240 m a. s. l. Densities from the two firn cores measured in the field are used in this study.

Table 4: Firn cores drilled during the 2018 winter campaign (PSI = Paul Scherrer Institute).

Core	Elevation	Depth	Measurement	Resolution	Data
4381	4'381 m	17.0 m	Field	0.20 m	Depth, density, stratigraphy
4381_2	4'381 m	17.0 m	PSI laboratory	0.09 m	Depth, density, stratigraphy, chemical analyses
4240	4'240 m	12.1 m	Field	0.20 m	Depth, density, stratigraphy

Firn temperature measurements carried out at the upper coring site indicated frozen firn to about 10 m depth.

4.2.5 Data snow pits

As drilling firn cores is time and labour intensive, snow pits were dug at any GPR trace not passing at a firn core location (Table 5 and Figure 15). They provide depth and density information of the current winter layer in 30 cm intervals and allow water equivalent calculation (Figure 21). Ice lenses' depths are registered separately and their densities set to 870 kg m^{-3}.

Table 5: Snow pits measured during the 2018 winter campaign.

Pit	Elevation	Depth	Resolution	Data
4168	4'168 m	2.5 m	0.30 m	Depth, density
3971	3'971 m	1.6 m	0.30 m	Depth, density
3867	3'867 m	1.3 m	0.30 m	Depth, density

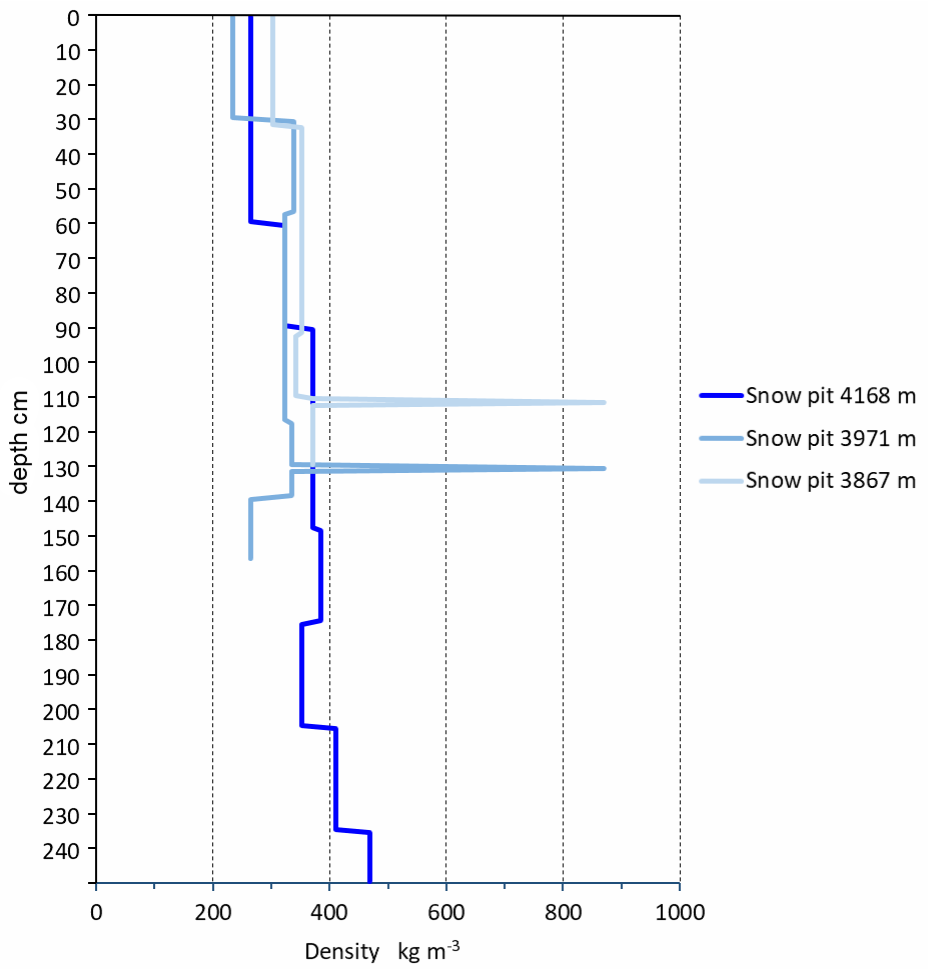


Figure 21: Densities from snow pits January 2018 (density 870 kg m^{-3}: Ice lense).

In the following, the firn cores and snow pits are labelled according to their elevation.

4.3 Additional data

4.3.1 Digital Elevation Model

For the establishment of accumulation distribution relationships with topographical parameters, a gapless digital elevation model (DEM) is required. In this study, a 4 m resolution DEM is used, constructed by Etienne Berthier at *Centre national d'études spatiales – French Space Agency (CNES)* with Pléiades stereo images of 0.5 m resolution from autumn 2015. This DEM is aggregated to 20 m resolution. However, it contains several gaps on the orographic left branch of Abramov Glacier amounting to 8 % of the glacier area. For this purpose, the SRTM DEM with 90 m resolution *(Jarvis et al. 2008)* is projected from geodetic WGS 84 into the projected WGS 84 UTM zone 42 N coordinate system and upsampled to 20 m resolution using bilinear interpolation. The gaps in the Pléiades DEM are filled using the upsampled SRTM DEM.

The above described gap-filling approach is used because the discrepancies between these two DEMs exceed one meter only in very steep mountain slopes and in the abla-

tion area, where the SRTM contains 10 to 15 m higher elevations[18]. Both of these constraints are not relevant for the use in this research as gaps only occur in rather flat parts of the accumulation area with slopes < 10 °, where none of these constraints are relevant. Further, the two DEMs are not used to calculate absolute elevation differences where accuracy of the DEMs would be critical.

4.3.2 Weather reconstruction

For the regressions, in addition to the topographical parameters, three weather reconstruction parameters from the 20th Century Reanalysis data set version 2c (20CRV2c) are used (*Compo et al. 2011; NOAA/OAR/ESRL PSD 2018).* 20CRV2c is a six-hourly four dimensional global atmospheric dataset from 1851–2014 in a spatial resolution of 2 °. From this dataset, *humidity*, *wind speed* and *wind direction* all at the 600 hPa level are extracted for the pixel reaching from 38 to 40 ° N and 71 to 73 ° E in monthly resolution, providing information about the monthly average circulation.

To assess the representativeness of the present winter, measurements at the weather station from 2011 to 2018 are complemented by average winter circulation at Abramov Glacier of the same time period. As data is required until April 2018, 20CRV2c cannot be used for this step. Therefore, ERA5 reanalysis of *temperature*, *humidity*, *wind speed* and *wind direction* is used at the available 500 hPa level from October 2011 to April 2014 for 38 to 40 °N and 71 to 73 ° W *(ECMWF 2018)*.

4.4 Relationship between TWT and water equivalent

In this study, GPR measures TWTs of electromagnetic waves through snow and firn and back to the radar. To calculate the distance travelled, the electromagnetic wave velocity has to be known. However, to obtain the electromagnetic wave velocity, the dielectric permittivity is required, depending itself on the density of snow or firn and the water content *(Frolov and Macheret 1999; Sold et al. 2015)*.

Kotlyakov and Macheret (2017) explained the relationship between the electromagnetic wave velocity and the density of snow, firn and ice. It ranges for dry snow from 0.279 m ns^{-1} for a density of 100 kg m^{-3} over 0.227 m ns^{-1} for 400 kg m^{-3} to 0.179 m ns^{-1} for 700 kg m^{-3}: The higher the snow density for a given water content is, the lower the electromagnetic wave velocity will be and similarly, the electromagnetic wave velocity decreases with increasing water content. These relations are shown in Figure 22.

[18] SRTM was produced in the year 2000 while Pléiades was produced in 2015 and therefore, glacier melt occurred in between especially visible in the ablation area when subtracting the two DEMs.

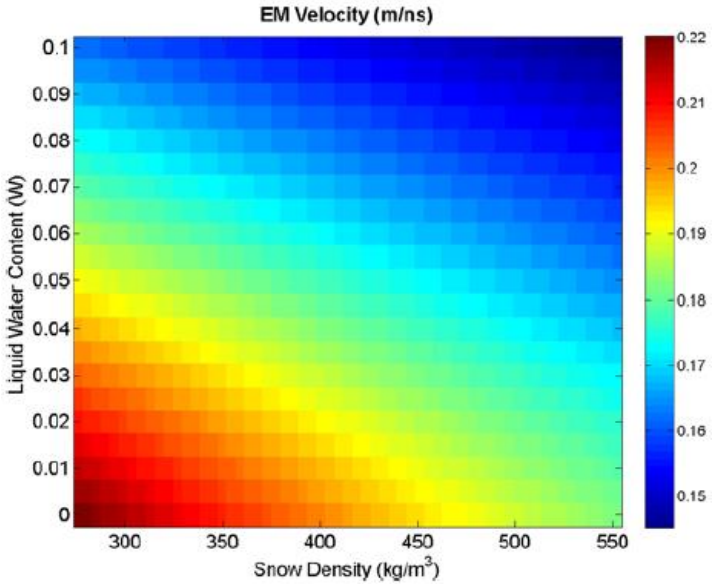


Figure 22: Dependence of electromagnetic wave velocity [m ns^{-1}] (right scale) on snow density [kg m^{-3}] (lower scale) and liquid water content W [volumetric ratio] (left scale) (from Bradford et al. 2009).

Theoretically it is possible to account for the influence of water content on the electromagnetic wave velocity by adding the incremental dielectric permittivity due to water volumetric content $\Delta\varepsilon'_s$ to the dielectric permittivity of dry snow ε'_d *(Frolov and Macheret 1999)*. $\Delta\varepsilon'_s$ could be calculated using the water content W as

$$\Delta\varepsilon'_s = 16.7\,W + 42.5\,W^2. \qquad (3)$$

In case snow is wet and liquid water content considerable, it is recommended to measure the dielectric constant of snow in the field *(Østrem and Brugman 1991)*. As snow temperatures in continental winter on Abramov Glacier were well below the freezing point, water content was not measured and dry snow with 0 % liquid water content is assumed *(Techel and Pielmeier 2011; Fierz et al. 2009)*.

The January 2018 GPR measurements on Abramov Glacier benefit from layer thickness and density measurements by boreholes and snow pits. This allows to directly solve the equations for the velocity, not requiring any other indirect method[19] proposed by *Bradford et al. (2009)*.

Using the density of snow ρ_d, ε'_d is calculated as proposed by *Frolov and Macheret (1999)* with

$$\varepsilon'_d = (1 + 0.857\,\rho_d)^2. \qquad (4)$$

[19] Like common-midpoint, moveout analysis of diffraction hyperbolas or reflection tomography (*Bradford et al. (2009)*).

With this dielectric permittivity, the electromagnetic wave velocity u is calculated using the speed of light in vacuum c = 300'000'000 m s^{-1} as following *(Hawley et al. 2014)*:

$$u = c\,(\varepsilon'_d)^{-0.5}. \qquad (5)$$

To directly transform the measured TWTs into water equivalents, several steps are required. First, velocity profiles are calculated using the density profiles from the five intersections of the GPR traces with the firn cores and snow pits. Therefore, Formula 5 is used. These velocity profiles are then applied as a 2D-model in ReflexW on the GPR profile sections around the firn core and snow pit sites to perform a time-depth conversion (details in Appendix C). Therewith, the following direct relationship between TWT and water equivalent is established (Figure 23):

$$Water\ equivalent = 0.0274\ TWT^{1.1352}. \qquad (6)$$

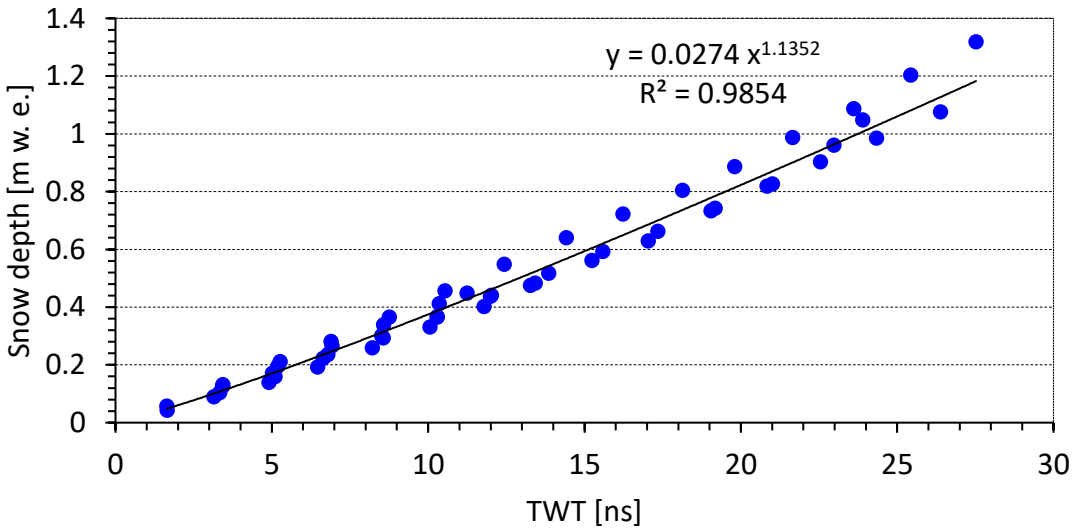


Figure 23: Relationship between TWT from GPR measurements and water equivalent from two firn cores[20] and three snow pits (details in Appendix C).

This relationship then is applied on all GPR measurements to directly convert them from TWTs to water equivalents.

4.5 PM rasters

With the final aim to better represent the accumulation distribution, two independent PM rasters are generated. An overview of the methodology developed is given in Fig-

[20] The firn core data in Figure 23 is restricted to 1.4 m w.e. as interest to establish the relationship is on the current winter's accumulation horizon.

ure 24. Using the extensive Soviet snow pit and stake archive, in a first step monthly Soviet SDD rasters are calculated for the five months from December to April (Subsection 4.5.2.1) by multiple linear regressions (Subsection 4.5.1) similar to *Sold et al. (2013).* They are then transformed to monthly Soviet PM rasters (Subsection 4.5.2.2). Using the Soviet January PM regression and winter precipitation from October 2017 to January 2018, the Soviet January 2018 water equivalent raster is established (Subsection 4.5.3). The second and independent PM raster is calculated based on the GPR data from January 2018 (Subsection 4.5.4).

It is important to understand that the PM rasters, when multiplied with a precipitation event, will represent the accumulation distribution rather than the precipitation distribution and therefore incorporate mass relocations by avalanches or snow drift.

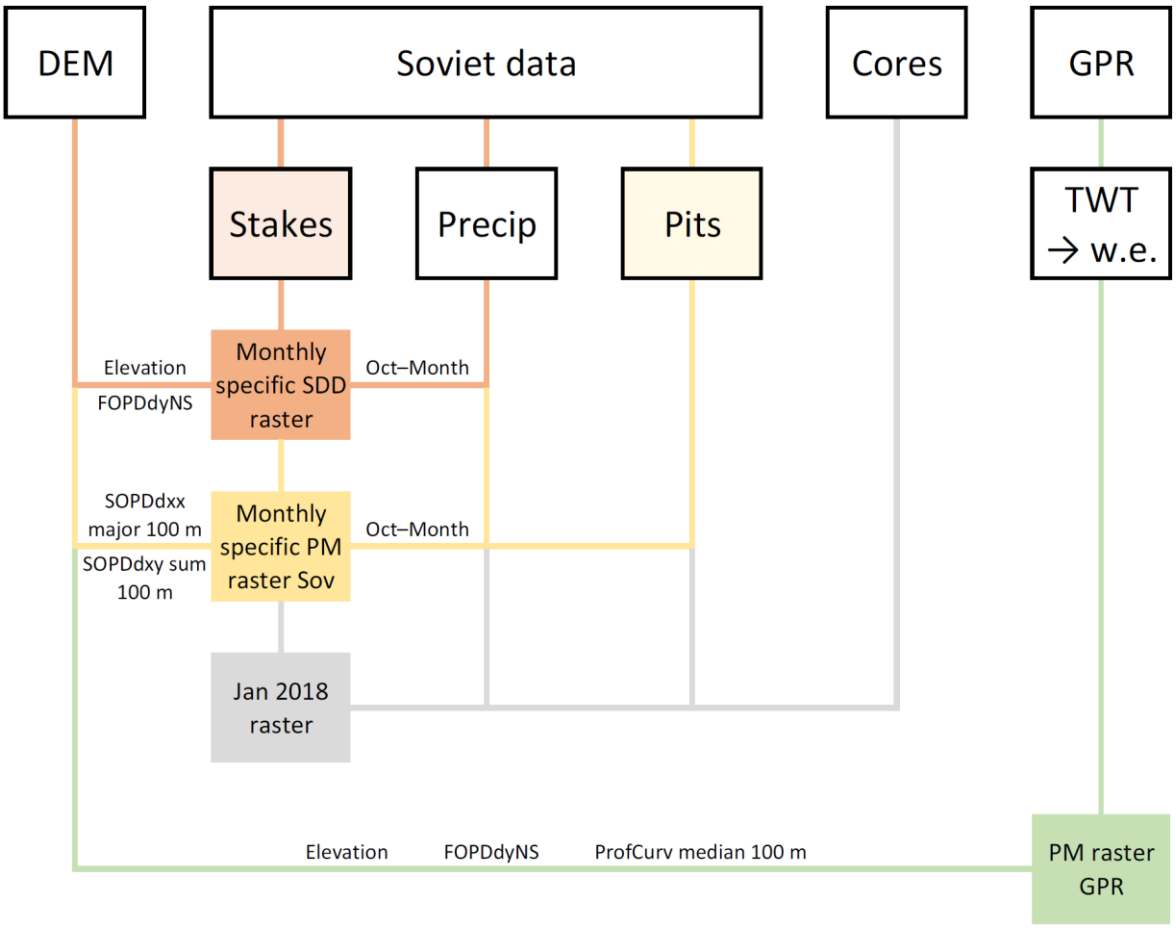


Figure 24: Methodology for the SDD and PM rasters. Text around lines indicates the input parameters used for the best regressions (compare Chapter 5). Light colored areas represent the observed values used to establish the regression, darker colored areas represent the output that is calculated with the best regressions. Consider that the SDD and PM rasters are normalized (not shown in the figure). (Precip = Precipitation, Sov = Soviet, other abbreviations see p. VI).

For the monthly specific SDD rasters, precipitation, altitude and one topographical parameter serve as input. For the monthly specific PM rasters, precipitation, two topographical parameters and the monthly specific SDD rasters serve as inputs. The detailed steps are described in the following subsections.

4.5.1 Multiple linear regression

For the SDD as well as PM rasters, multiple linear regressions are used to extract the most important parameters for simulating the snow depth or snow water equivalent respectively out of a set of 50 possible explaining parameters (Table 6).

The multiple linear regression is in the form

$$Y\,(m,p) = \alpha + \beta_1 p_1 + \beta_2 p_2 + \ldots + \beta_n p_n + \xi \qquad (7)$$

with Y representing the snow depth (SDD raster) or water equivalent (PM raster) for month m, α the intercept, β_i the coefficient of parameter p_i and ξ the residual (e.g. *Schmidt et al. 2009; Hedderich and Sachs 2012*) whereas the intercept and the coefficients change within m. The parameter selection changes between Soviet SDD, Soviet PM and GPR PM rasters.

To determine how many parameters should be used and where the information of an additional parameter is not worth including it, the coefficient of determination R^2 is calculated using the sums of squares (SS) by

$$R^2 = \frac{SS_{xy}{}^2}{SS_{xx}\ SS_{yy}} = \frac{\left(\sum_{i=1}^{n}(X_i - \bar{X})(Y_i - \bar{Y})\right)^2}{\sum_{i=1}^{n}(X_i - \bar{X})^2\ \sum_{i=1}^{n}(Y_i - \bar{Y})^2} = [0,1] \qquad (8)$$

with n stake locations, the measured snow depth X_i at stake location i, the mean measured snow depth $\bar{X}$, the regression-calculated snow depth Y_i at stake location i and the mean regression-calculated snow depth $\bar{Y}$ (e.g. *Hedderich and Sachs 2012; Dümbgen 2013*). The coefficient of determination is equivalent to the square of the Pearson correlation coefficient and expresses how much variability of the dependent variable (snow depth or water equivalent) is accounted for by the regression. An R^2 of close to 1 therefore would nearly perfectly represent the dependent variable by the independent variables.

4.5.2 Soviet PM rasters

To generate a PM raster, water equivalent information from as many points as possible is desirable. However, only the snow pit locations allow a conversion from depth to water equivalent. As multiple regressions showed that snow depth is the most important parameter influencing the water content, SDD rasters are generated first (Subsection 4.5.2.1), serving as one input to the PM rasters (Subsection 4.5.2.2). This allows

to consider all Soviet stake measurements and therefore considerably enlarges the sample size.

4.5.2.1 Soviet snow depth distribution raster

The Soviet snow depth measurements described in Subsection 4.1 are analysed for every month from December to April: Multiple regressions are established describing the snow depth measured with a selection of three out of a set of ten topographical parameters at the Soviet stake locations as well as 36 parameters of their 100 m radian environment, accumulated winter precipitation from October until the end of the corresponding month and three weather reconstruction parameters (total 54 parameters). The topographical parameters are extracted in QGIS from the gap-filled DEM and contain *elevation, slope, aspect, profile curvature, tangential curvature, first order partial derivative (FOPD)dyNS*[21]*, FOPDdxEW, second order partial derivative (SOPD)dyy, SOPDdxy* and *SOPDdxx*. Precipitation data is taken from Soviet measurements and accumulated from October until the end of the corresponding month m (*winterP_m*). The three weather reconstruction parameters *humidity, wind speed* and *wind direction* from 20CRV2c are described in Subsection 4.3.2. A complete list of the parameters examined is given in Table 6.

Table 6: List of the 54 parameters tested in the multiple regressions for the SDD. 100 denotes 100 m radian environment around each stake. All *FOPD* and *SOPD* are topographical curvature parameters.

Elevation	*Slope100 sum*	*FOPDdyNS100 sum*
Slope	*Slope100 mean*	*FOPDdyNS100 mean*
Aspect	*Slope100 median*	*FOPDdyNS100 median*
Tangential curvature	*Slope100 mode*	*FOPDdyNS100 mode*
Profile curvature	*Aspect100 sum*	*SOPDdxx100 sum*
FOPDdxEW	*Aspect100 mean*	*SOPDdxx100 mean*
FOPDdyNS	*Aspect100 median*	*SOPDdxx100 median*
SOPDdxx	*Aspect100 mode*	*SOPDdxx100 mode*
SOPDdxy	*Tangential curvature100 sum*	*SOPDdxy100 sum*
SOPDdyy	*Tangential curvature100 mean*	*SOPDdxy100 mean*
winterP_Dec	*Tangential curvature100 median*	*SOPDdxy100 median*
winterP_Jan	*Tangential curvature100 mode*	*SOPDdxy100 mode*
winterP_Feb	*Profile curvature100 sum*	*SOPDdyy100 sum*
winterP_Mrz	*Profile curvature100 mean*	*SOPDdyy100 mean*
winterP_Apr	*Profile curvature100 median*	*SOPDdyy100 median*
20CRV2c humidity 600 hPa	*Profile curvature100 mode*	*SOPDdyy100 mode*
20CRV2c wind speed 600 hPa	*FOPDdxEW100 sum*	
20CRV2c wind dir 600 hPa	*FOPDdxEW100 mean*	
	FOPDdxEW100 median	
	FOPDdxEW100 mode	

[21] NS as well as WE give the direction of these two coordinate-parallel topographical parameters.

For the selection of the most important variables, multiple linear regressions as described in Subsection 4.5.1 are calculated for all possible parameter combinations using two, three and four parameters. Independent of the winter or spring month chosen, the inclusion of a forth explaining variable only increased the R^2 by 0.005. Therefore, the best three parameters p_1, p_2 and p_3 are chosen.

Using the monthly relations, SDD rasters of the entire Abramov Glacier are calculated for every month. These rasters are then normalized dividing the snow depth at every 20 m pixel by the average of all snow depths on the glacier of that month.

The exact dates of the stake measurements vary within every month and year. Therefore, always the end of the month was taken as cut-off date. This is a simplification that is taken intentionally. To establish the regressions, it would be possible to use the exact winter precipitation until the corresponding day and to include the exact day of the stake measurements. But later on, when calculating the SDD raster, 151 daily instead of 5 monthly rasters would be needed to calculate.

4.5.2.2 Soviet PM raster

For the PM rasters, the parameters from Table 6 are used at all Soviet snow pit locations or its 100 m radian environments with five additional parameters: The values extracted from the SDD rasters of the corresponding months (*SDD_Dec, SDD_Jan, SDD_Feb, SDD_Mrz* and *SDD_Apr*). Therewith, the best regressions are searched within these 59 parameters.

Furthermore, the inclusion of all topographical data of an environment of 200, 300 and 400 m around the snow pits (*slope200 sum, slope200 mean, slope200 median* and *slope200 mode* etc.) was analysed. The inclusion of topographical parameters of > 100 m radian environment around the snow pits only increased the stability index by 0.005 while the inclusion of a forth topographical parameter lead to an increase of 0.05. Therefore, four explaining parameters p_1, p_2, p_3 and p_4 are incorporated but the topographical parameters > 100 m are not considered in the range of possible parameters.

With the four best regression parameters, the water equivalent rasters are calculated. These water equivalent rasters are then normalized to finally obtain the PM rasters. For normalization of every raster from December to April, each pixel of the monthly water equivalent raster is divided through the average of all pixels of the same raster. This step is necessary as for the precipitation multiplication in the mass balance model, it is not the water equivalent at every point on the glacier that is of interest but rather its distribution (the proportion relative to average).

For the Soviet PM rasters, a total of 1'069 Soviet water equivalent measurements of the months December to April of 31 years were used to establish the regressions.

4.5.3 Soviet January 2018 water equivalent raster

Based on the best regression for the Soviet January water equivalent raster (Table 8), a specific water equivalent raster is calculated for January 2018. Therefore, *SDD_Jan* as well as the two topographical parameters *SOPDdxx100 mode* and *SOPDdxy100 sum* together with the winter precipitation *winterP_Jan* are taken as explaining parameters. However, winter precipitation was not measured any more in winter 2017/2018 as it was done during Soviet period.

To account for this, the average Soviet precipitation from October to January is multiplied by the quotient of the snow water equivalent at core 4381 with P (winter precipitation from October to the end of January of the next year) as following:

$$P_{2017} = P_{mean\ Soviet} \frac{w.e._{Jan\ 2018\ core\ 4381}}{w.e._{mean\ Soviet\ pit\ 4381}} = 245.9\ mm\ \frac{1076\ mm}{760.9\ mm} = 347.7\ mm \quad (9)$$

Using this constructed precipitation input from October 2017 to January 2018 and the best parameters for the Soviet January water equivalent raster, the Soviet January 2018 water equivalent raster is calculated.

4.5.4 GPR PM raster

With the GPR measurements a PM raster independent to the Soviet raster is calculated. Therefore, the measured TWTs are transformed to water equivalents using Function 9 described in Section 4.4. The regression is calculated based on the parameters given in Table 6 and *SDD_Jan*. With three parameters, the R^2 only decreases by 0.004 compared to the best regression with four parameters, therefore only three parameters p_1, p_2 and p_3 are used (details in Appendix E).

To test the stability of the parameter selection, other runs are performed selecting only every 100th GPR point or a random choice of 1'000 GPR points. In both simulations, the best regression consists of the same three parameters (Appendix E Table 25 and Table 26).

The water equivalent raster is calculated using the best regression from Table 10. This raster is normalized to finally get the GPR PM raster.

4.5.5 Validation PM rasters

4.5.5.1 Validation of the January 2018 water equivalent raster

The January 2018 raster described in Subsection 4.5.3 is compared directly to all GPR point measurements. Therefore, the measured TWTs at all 50'521 GPR points are transferred to water equivalents using Formula 6 described in Section 4.4. Afterwards, every GPR point water equivalent is subtracted from the January 2018 water equivalent. This allows to directly compare the water equivalents of both independent variants.

4.5.5.2 *Validation of the GPR PM raster*

To validate the normalized GPR PM raster, it is divided by the mean Soviet PM raster. These two rasters share only the original DEM as common input. Therefore, these two rasters are considered being independent.

4.6 Energy balance–snow model

The accumulation distribution results of this study finally are used with the coupled energy balance–snow model recently refined by *van Pelt et al. (2012)*.

4.6.1 Coupled energy balance–snow model *van Pelt et al. (2012)*

Klok and Oerlemans (2002) developed a two dimensional mass balance model that is based on the surface energy balance of a glacier (Subsection 2.4.4). Their aim was to calculate mass balance without using meteorological data directly influenced by the glacier boundary layer. Instead they used several synoptic weather stations located in the vicinity of the glacier to shape the model. The weather stations located on the glacier as well as snow temperatures and density profiles were used to evaluate the model results *(Klok and Oerlemans 2002)*. They concluded that optimizing the snow-accumulation parameterization scheme is challenging due to difficulties in estimating the spatial distribution of snow accumulation *(Klok and Oerlemans 2002)*.

Van Pelt et al. (2012) coupled *Klok and Oerlemans (2002)*'s energy balance model with the snow model SOMARS (Simulation Of glacier surface Mass balance And Related Subsurface processes) from *Greuell and Konzelmann (1994)*. This allowed them to handle meltwater production at the surface as input for the snow model simulating storage and refreezing of this percolating water in subsurface layers as well as using the subsurface heat flux, depending on vertical temperature and density profiles, as input for the surface energy budget *(van Pelt et al. 2012)*. However, they still used a precipitation gradient to distribute precipitation over the entire glacier.

This is where the present study delivers an alternative possibility, described in the following subsection. The model of *van Pelt et al. (2012)* recently has already been applied on Abramov Glacier by Warren Stainbank in his master thesis (Stainbank 2018).

4.6.2 Implementation of PM raster in the coupled energy balance–snow model *van Pelt et al. (2012)*

In the coupled energy balance–snow model of *van Pelt et al. (2012)*, up to now, precipitation input from reanalysis data is multiplied by a precipitation correction factor and distributed over the glacier by an altitudinal precipitation gradient. The Soviet and GPR PM rasters are implemented in the model to reduce the uncertainty in snow accumulation variability.

To test performance of the model using one of the two PM rasters, three variants are calculated: The PM raster with neither precipitation correction nor precipitation gradient, the PM raster with precipitation correction but without precipitation gradient and the PM raster with precipitation correction and with precipitation gradient. In case the model is already well calibrated concerning all other parameters[22] and the PM raster performs satisfactory, no precipitation gradient correction should be required any more as this is included in the PM raster. However, a precipitation correction still may be necessary. Therefore, focus is set on the second variant using the PM raster with a precipitation correction factor but without a precipitation gradient correction.

Details about the changes in model structure compared to *van Pelt et al. (2012)* are given in Appendix H.

[22] Details about the model parameters see *van Pelt et al. (2012)* or Appendix H.

5 Results

5.1 Soviet snow depth distribution rasters

The best three parameters explaining the SDD are *elevation*, the curvature parameter *FOPDdyNS* as well as *winterP_m*. This parameter selection lead to the best SDD in every month (details considering the parameter combination performance of the regressions in Appendix B). Their monthly-specific regression coefficients are given in Table 7.

Table 7: Regression coefficients of the three most important variables for the SDD (abbreviations see p. VI).

Month	**Intercept**	***Elevation***	***FOPDdyNS***	***winterP_m***	**R^2**
Dec	-7.97	0.00208	0.4237	0.00491	0.67
Jan	-9.09	0.00237	0.2860	0.00457	0.69
Feb	-10.47	0.00280	0.4938	0.00363	0.68
Mrz	-12.87	0.00340	0.5925	0.00402	0.70
Apr	-16.38	0.00422	0.8866	0.00406	0.62

Using the best three explaining parameters out of the set of 54 parameters introduced in Table 6, the spatial SDD rasters are calculated for every winter month (Figure 25). The snow depth increases throughout the winter and early spring. Snow depth reaches around 4 m on the plateau where the two firn cores were drilled. Especially high values are observed on highest elevations on the uppermost part of the orographic left branch and on the southern edges of glacier branches.

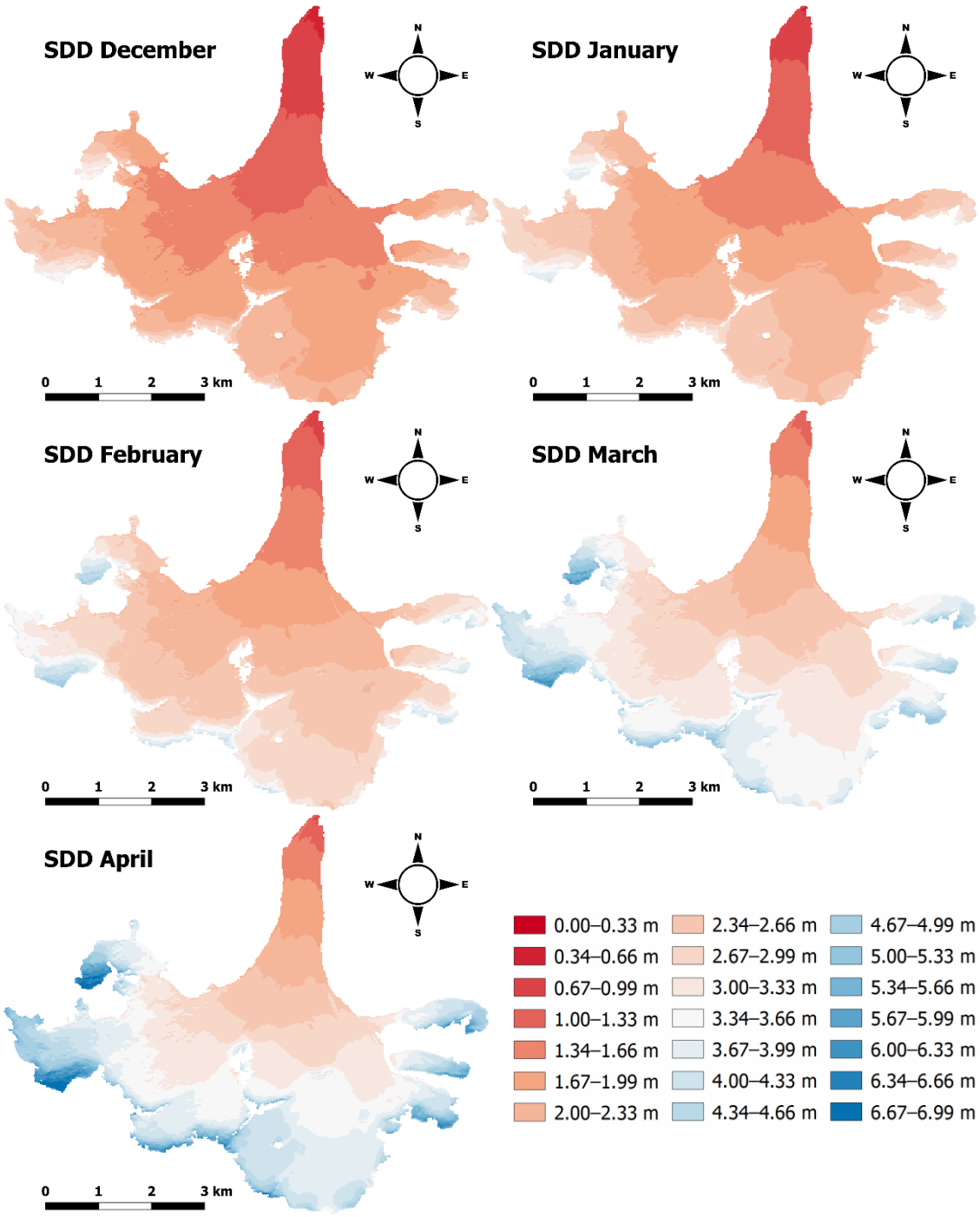


Figure 25: Soviet SDD rasters December to April [m].

The normalized versions of these rasters (Appendix F Figure 43) serve as one input to the Soviet PM rasters.

5.2 PM rasters

5.2.1 Soviet PM rasters

For the PM rasters, three of the four explanatory parameters remain the same throughout all months: The monthly specific value from the SDD raster *SDD_m*, the curvature

parameter *SOPDdxx100 mode* of the 100 m environment around the snow pit location and *winterP_m*. The topographical parameter *SOPDdxy100 sum* as forth variable remains under the best 10 of the calculated 487'635 regressions except in December, whereas the stability index decreases by 0.015 compared to the best parameter choice when using this forth parameter. Nevertheless, the inclusion of this parameter leads to an increase of the stability index by 0.02 compared to the use of only three parameters. For simplicity, the same topographical parameters are used for every month as only in December this setting is not among the best ones (details considering the parameter combination performance of the regressions in Appendix D).

The best parameters selection with the corresponding coefficients is given in (Table 8). These are the monthly-specific normalized SDD rasters (Subsection 4.5.2.1) *SDD_m*, the two topographical curvature parameters *SOPDdxx* and *SOPDdxy* as well as *winterP_m*. With these four best explaining parameters out of the set of 59 possible explaining parameters (Subsection 4.5.2.2), the water equivalent rasters are calculated.

Table 8: Regression coefficients of the four most important variables for the Soviet water equivalent distribution, whereas m corresponds to the month (abbreviations see p. VI).

Month m	**Intercept**	***SDD_m***	***SOPDdxx 100 mode***	***SOPDdxy 100 sum***	***winterP_m***	**R^2**
Dec	-0.3548	0.4947	-40.02	3.5750	0.00197	0.70
Jan	-0.4570	0.6171	-54.60	4.6727	0.00201	0.80
Feb	-0.4983	0.7470	-72.29	6.0678	0.00184	0.79
Mrz	-0.7717	1.0940	-82.03	6.9504	0.00185	0.82
Apr	-0.8822	1.2515	-97.19	8.8361	0.00192	0.84

To generate the Soviet PM rasters first the water equivalent distribution rasters are required. Figure 26 shows the corresponding water equivalent distribution rasters. The water equivalent increase from December to April is evident, reaching in the confluence region of the two branches from 0.4 m w.e. in December to 1.0 m w.e. in April. Highest values are atteined at highest elevations in southern parts of the accumulation area with water equivalents up to 3.00 m w.e.

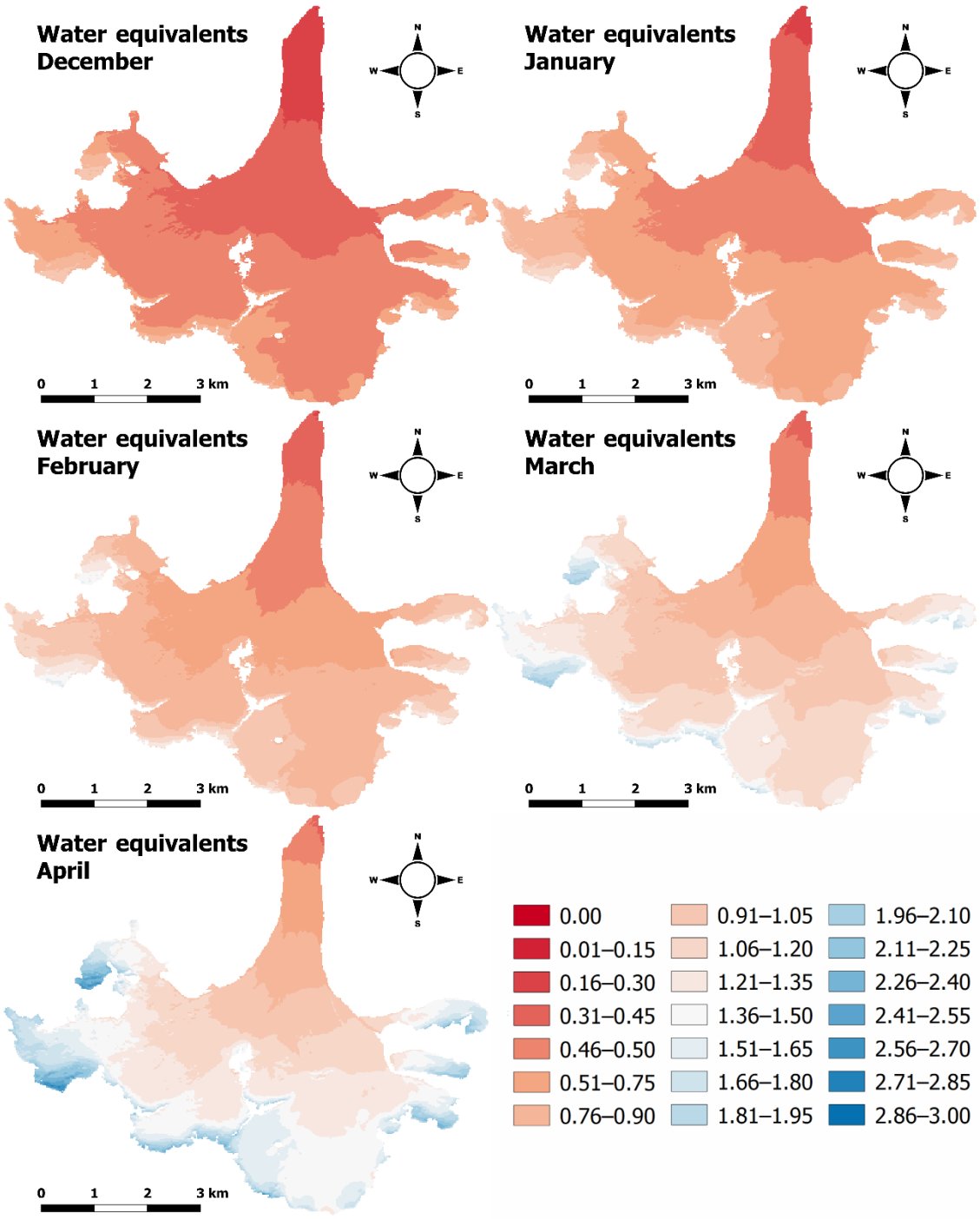


Figure 26: Soviet water equivalent rasters December to April [m w.e.].

The final product required for modelling of Abramov Glacier are the PM rasters. They are generated in a second step by normalizing the water equivalent rasters from Figure 26. Figure 27 shows the resulting PM rasters.

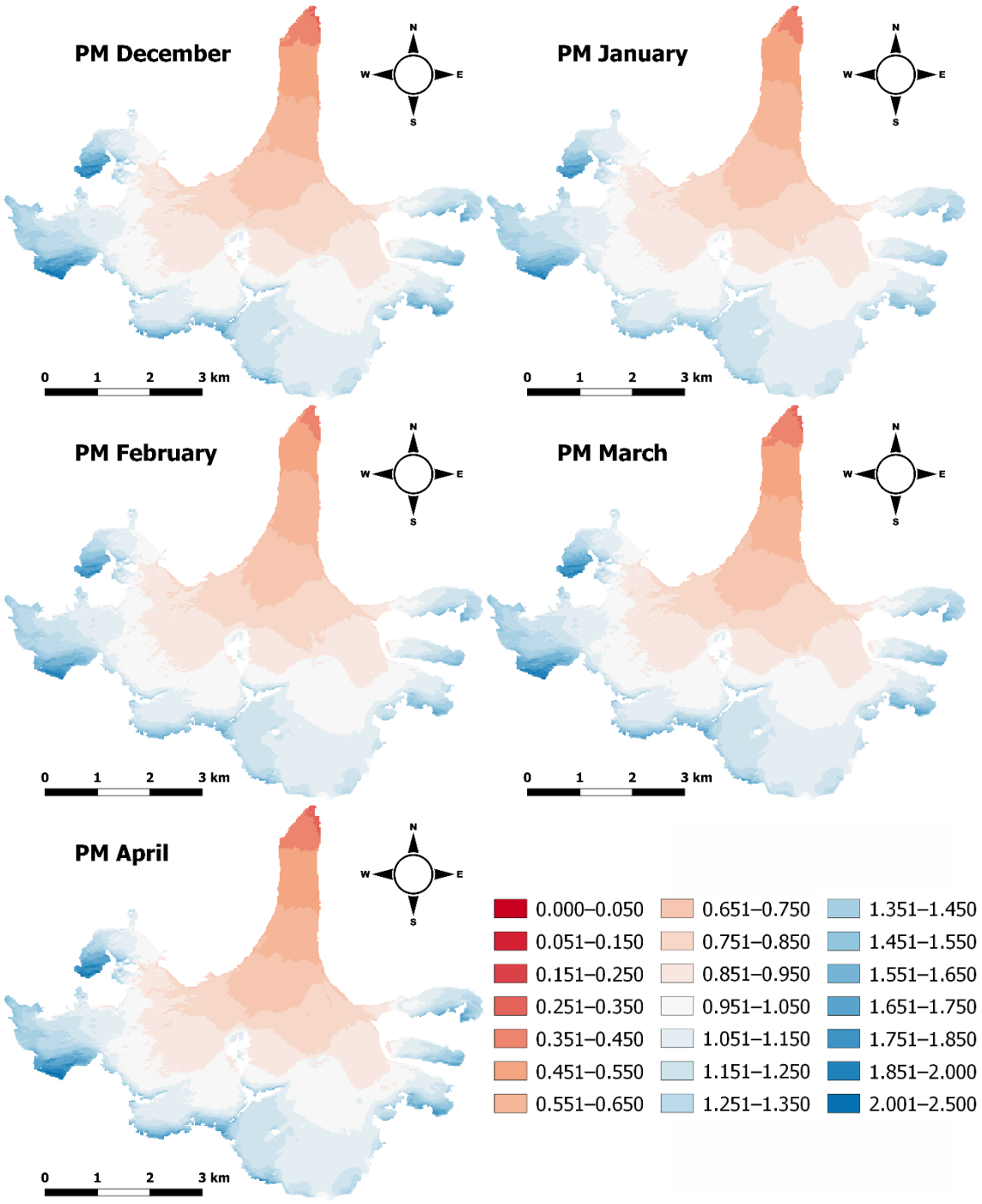


Figure 27: Soviet PM rasters December to April [dimensionless].

The differences between the various months are much less pronounced in the PM rasters than in the water equivalent rasters. To assess these differences in more detail, the PM raster for each month is divided through the average between all months (rasters in Appendix G Figure 44). The resulting statistics are presented in Table 9.

The mean pixel deviation from the average PM raster of all months from December to April is less than ± 0.005. Most individual pixel values lie between 0.98 and 1.02 of the average raster, as the standard deviation varies between 0.006 for March and 0.019 for

February. The extreme values for one single pixel are 0.87 in April and 1.13 in February.

Table 9: Extracted statistical values (SD = Standard deviation) from monthly PM rasters compared to the average PM raster of all five months (raster in Appendix Figure 44).

Month	Mean	SD	Max	Min
Dec	0.998	0.009	1.05	0.95
Jan	1.003	0.017	1.11	0.89
Feb	1.004	0.019	1.13	0.96
Mrz	0.999	0.006	1.01	0.96
Apr	0.996	0.019	1.08	0.87

This homogeneity between the different PM rasters allows a simplification for the mass balance model without losing accuracy. Therefore, one single PM raster is calculated by averaging all five monthly rasters (Figure 28). This raster is then used in the model as a monthly-independent precipitation multiplicator.

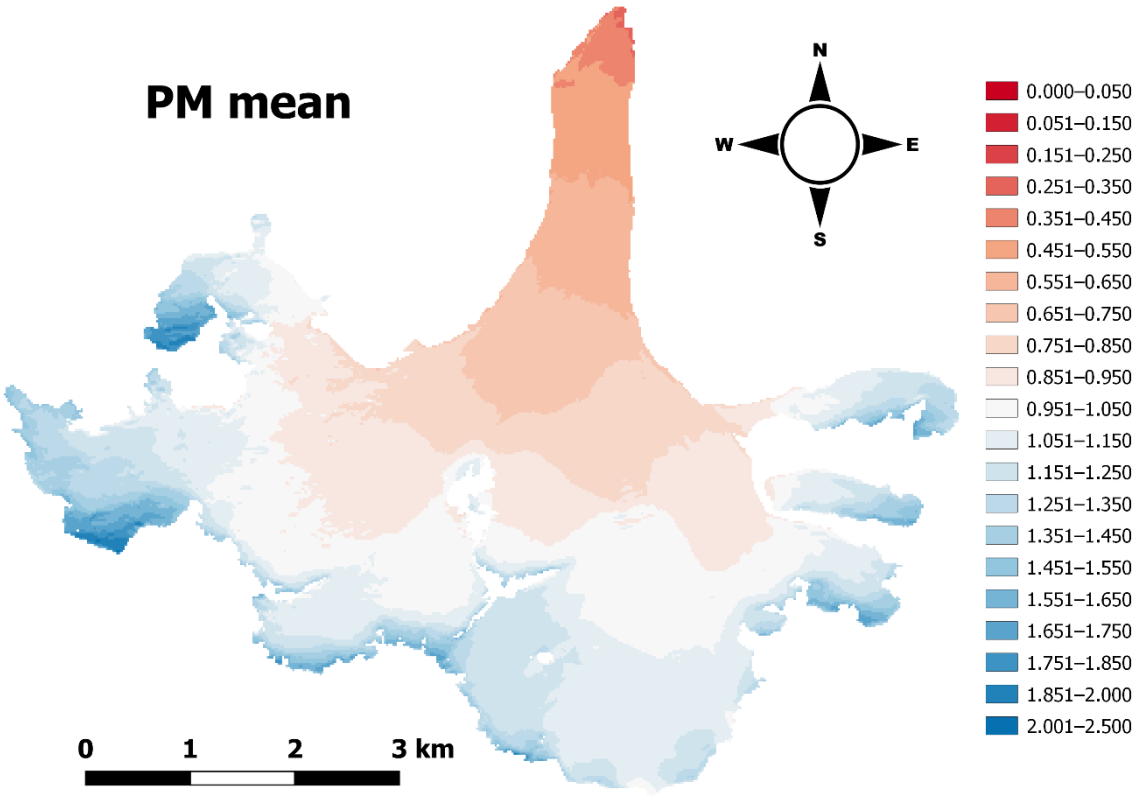


Figure 28: Average Soviet PM raster of all months from December to April [dimensionless].

5.2.2 GPR PM raster

The best regression for the GPR water equivalent raster is reached with *elevation* and the two topographical parameters *FOPDdyNS* as well as the *profile curvature100 median* (Table 10).

Table 10: Regression coefficients of the three most important variables for the GPR water equivalent distribution. *Elevation* and *FOPDdyNS* are taken at the GPR measurement point locations while for the *Profile Curvature*, the median of the 100 m radius around the GPR measurement points fitted best (abbreviations see p. VI).

	Intercept	***Elevation***	***FOPDdyNS***	***Profile curvature 100 median***	**R^2**
3 Parameter	-4.9455	0.0014	1.2080	-90.95	0.75

To test the stability of the parameter selection, other runs are performed selecting only every 100th GPR point or a random choice of 1'000 GPR points. In both simulations, the best regression consists of the same three parameters (Appendix E Table 25 and Table 26).

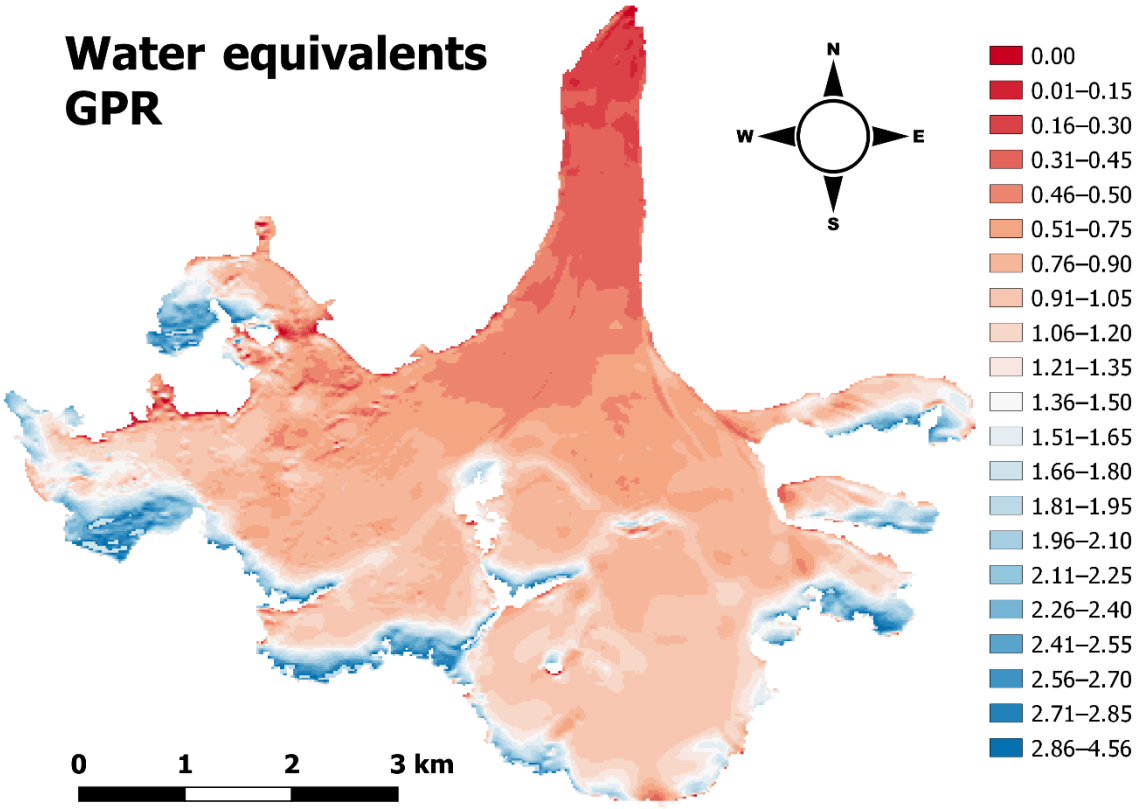


Figure 29: Water equivalent raster based on January 2018 GPR measurements [m w. e.].

Figure 29 shows the water equivalent distribution based on GPR measurements. Clearly visible is the increasing water content with elevation and steep slopes.

The normalized version of this raster, Figure 30, represents the GPR PM raster that is independent of all Soviet data. What is evident is the high range of values from 0 to 4.56. Highest values are observed at all steep northerly oriented slopes.

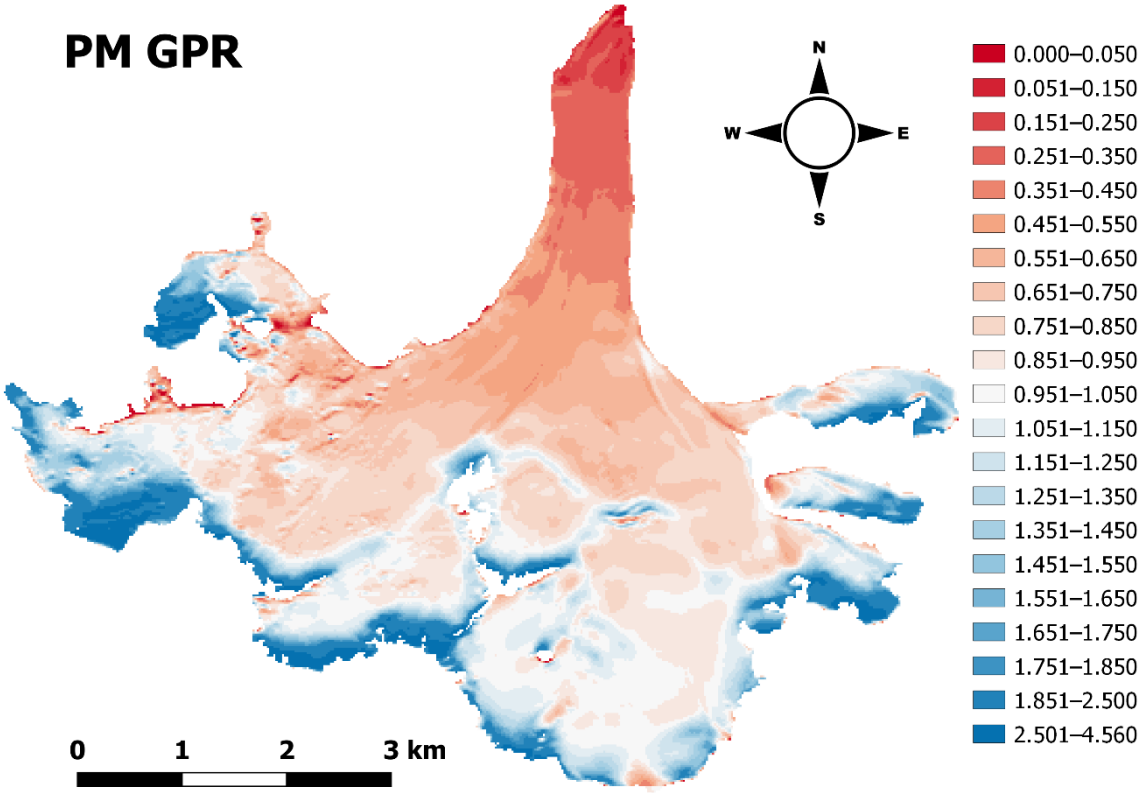


Figure 30: PM raster based on GPR measurements [dimensionless].

The very high values at all steep slopes lead to PM factors < 1 on most parts of Abramov Glacier.

5.2.3 Soviet January 2018 raster and validation

Figure 31 shows the Soviet data based January 2018 water equivalent raster and its comparison to the water equivalents derived from GPR measurements (previous sub-section).

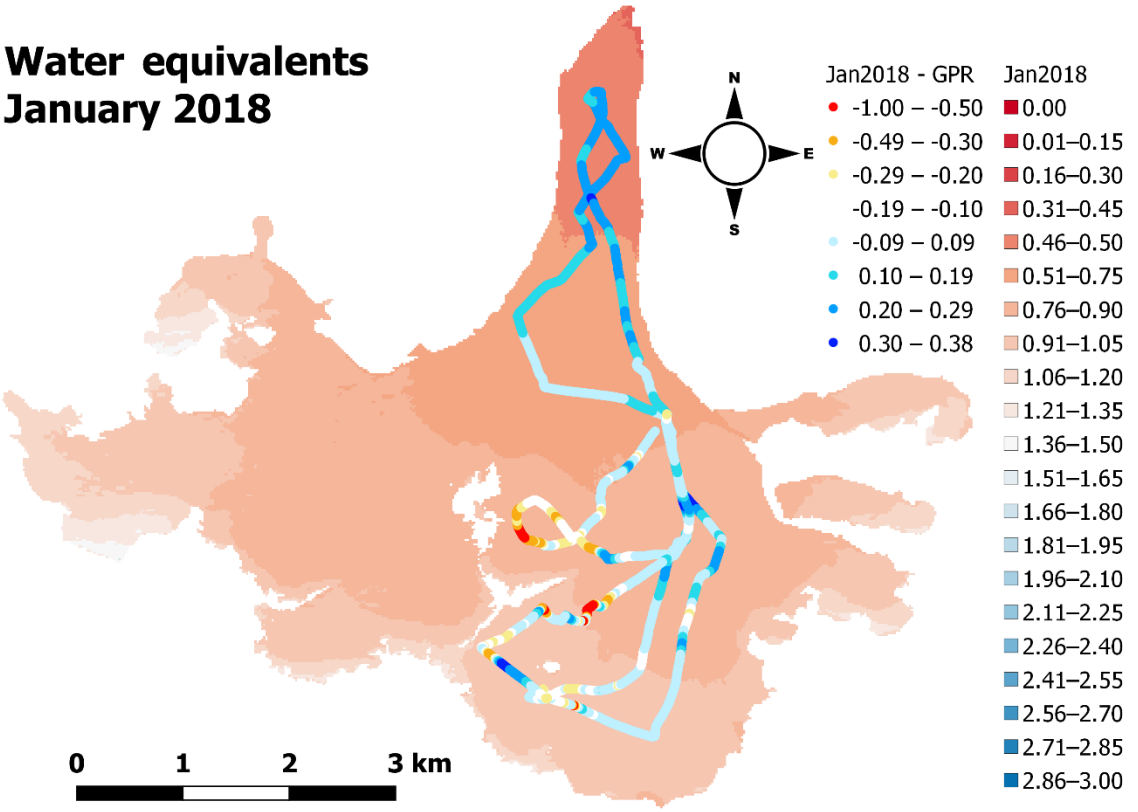


Figure 31: Soviet January 2018 water equivalent raster (background) and difference between Soviet January 2018 and GPR-derived (Figure 29) water equivalents (colored lines) [m w.e.].

What is peculiar on Figure 31 are the mostly positive water equivalent differences in the ablation area. This means that in the ablation area the regression-based water equivalents are systematic 0.1 to 0.3 m w.e. higher than the GPR derived water equivalents. In contrast, there exist some zones where GPR-extracted water equivalents exceed the regression-based water equivalents by 0.5 up to 1 m w.e. These zones are mainly located either on steeper slopes (southern red dots) or in an avalanche-prone region (northern red dots).

Another feature is observable at the westernmost GPR trace: Negative differences of 0.4 m w.e. turn into positive differences of 0.35 m w.e. only 170 m further downslope. In the GPR profile, this is observable as a bisection of the GPR traveltimes, although the topographical parameters do not change remarkably on this rather homogeneous area near firn core 4381.

Considering all 50'051 comparison points, the mean difference between the regression and the GPR derived water equivalents is 0.03 m with a standard deviation of 0.18 m w.e.

5.2.4 Validation GPR with Soviet PM raster

As the Soviet and the GPR PM raster only share the elevation as common input, independent comparison of the two is possible. Figure 32 shows the quotient between the

GPR PM raster and the mean Soviet PM raster. In most parts of the glacier, the Soviet PM factors are higher than the GPR PM factors. Only in steep northerly oriented slopes, GPR multiplication factors are higher than the Soviet ones.

Therefore, the influence of elevation and slope (indirectly through the 100 m median radius profile curvature) is more pronounced in the GPR PM raster than in the Soviet one.

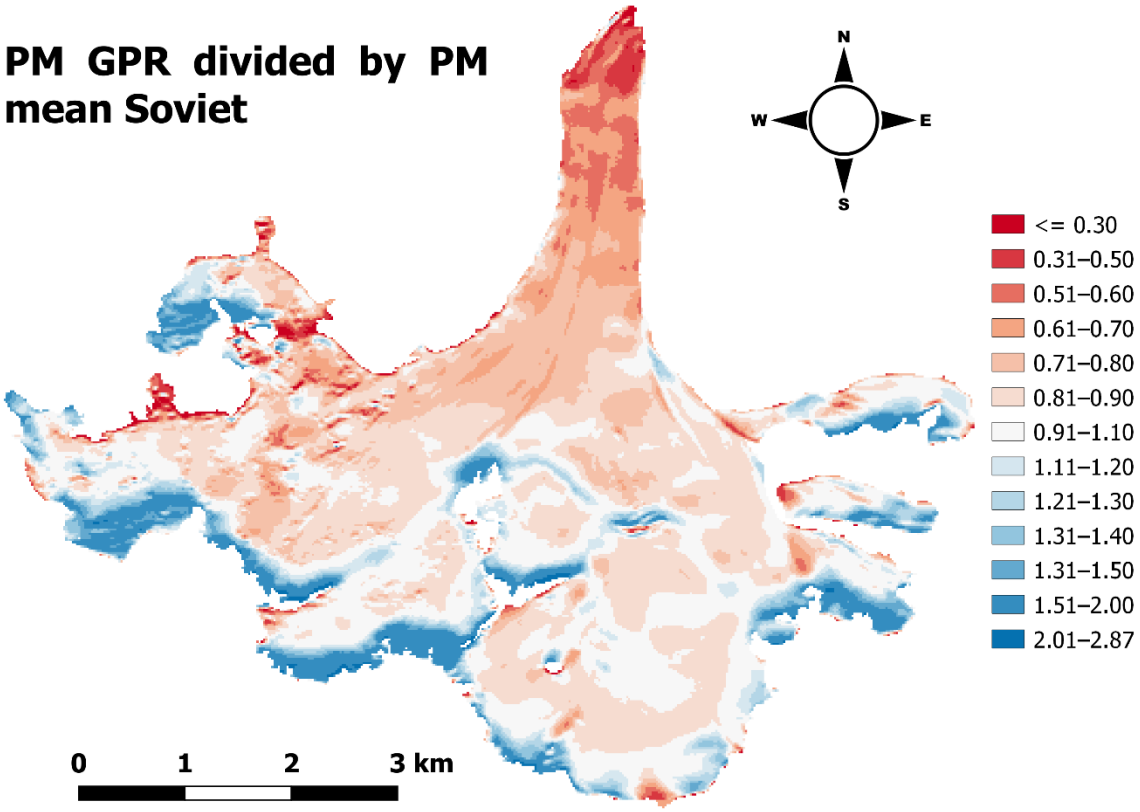


Figure 32: Quotient between the GPR PM raster and the mean Soviet PM raster [dimensionless].

5.3 Mass balance model *van Pelt et al. (2012)*

The mass balance model of van *Pelt et al. (2012)* has previously been used with reanalysis precipitation as precipitation input, distributing it over the glacier by a precipitation correction factor of 2.2 and a linear altitudinal correction factor gradient of 0.00313 (dimensionless).

Using the GPR and the Soviet raster, around 50 runs are performed with new spin-ups of the model and replacing the altitudinal gradient by the PM raster. The only other constants that have been changed for some simulations are the ice albedo (0.25 or 0.20) and the temperature lapse rate (from -0.005 Km^{-1} to -0.0078 Km^{-1}) (details about the parameter settings in Appendix H Table 29, all model runs in Appendix I).

Figure 33 shows the effect of the mean Soviet PM raster on the performance of the mass balance simulations before (red) and after calibration (green) in comparison with the best simulation without PM raster (blue). Precipitation correction leads to a vertical displacement of the regression line while either a change in precipitation gradient or in the temperature lapse rate change the slope. The best calibrated Soviet PM run is achieved using a precipitation correction factor of 1.356 and a temperature lapse rate of -0.0075 Km^{-1}.

Therefore, only calibrating the precipitation correction factor and the precipitation gradient does not improve the model when using the Soviet PM raster.

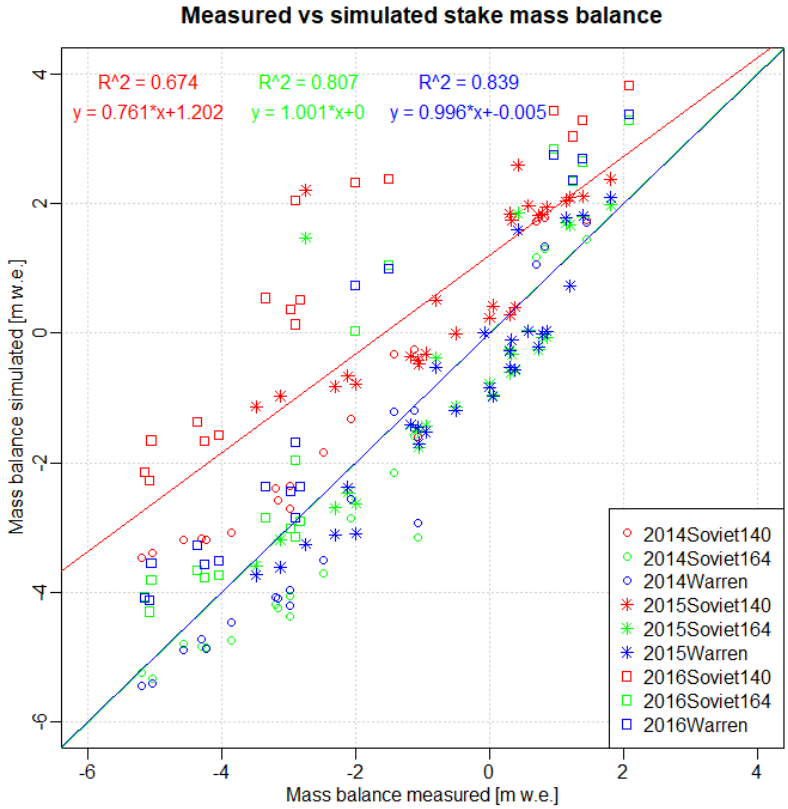


Figure 33: Measured versus simulated mass balance for the period 1 November 2013 02:55 until 1 October 2017 02:55. Stainbank's best simulation (blue) is compared with the simulations using the Soviet PM and the same settings (red) as well as with improved parameter settings (green). Details about parameter settings: Appendix H Table 29.

The same was done using the GPR PM raster (Figure 34). The best regression was found using a precipitation correction factor of 1.44 and a temperature lapse rate of -0.0072 Km^{-1}. The coefficient of determination achieves 0.81 in contrast to 0.84 without PM raster.

The differences whether the GPR or the Soviet PM raster is used are of minor influence: In both cases, the model performs worse than in the simple old model version that distributed the reanalysed precipitation input over the glacier by a precipitation gradient.

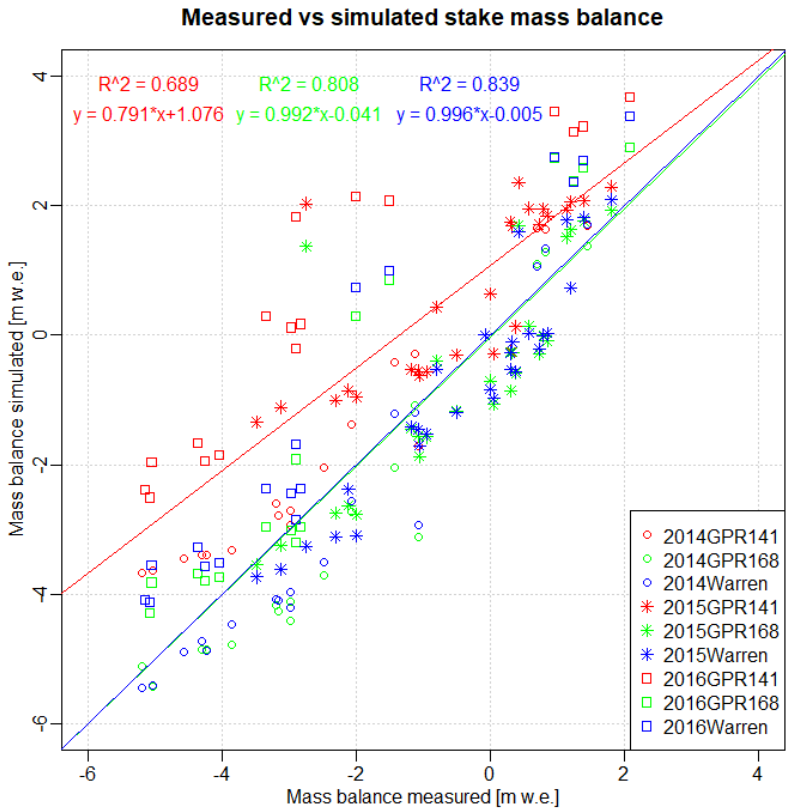


Figure 34: Measured versus simulated mass balance for the period 1 November 2013 02:55 until 1 October 2017 02:55. Warren's best simulation (blue) is compared with the simulations using the GPR PM and the same settings (red) as well as with improved parameter settings (green). Details about parameter settings: Appendix H Table 29.

The same is true for the deviation between individual years: It is independent on the applied PM raster: In 2014 and 2015, no obvious shift is observable as too positive as well as too negative mass balance simulations occur. In contrast, in 2016 mass balance at most stakes is simulated 0.5 to 2 m w.e. higher than measured. In the accumulation area, simulated mass balance is always too positive, independent on the year.

6 Discussion

6.1 GPR Measurements and layer extraction

Thanks to the negative January 2018 firn temperatures down to 10 m and corresponding negligible liquid water content, up to ten horizons are distinguishable with the chosen 800 MHz antenna. GPR primarily reacts to changes in density. However, density changes may not necessarily occur from annual layer boundaries as ice lenses are frequent. From the contemporaneous drill of firn cores at two locations of the GPR profiles, direct comparison is possible (Figure 35). Most annual layer boundaries are located where a dust layer coincides with an ice lense.

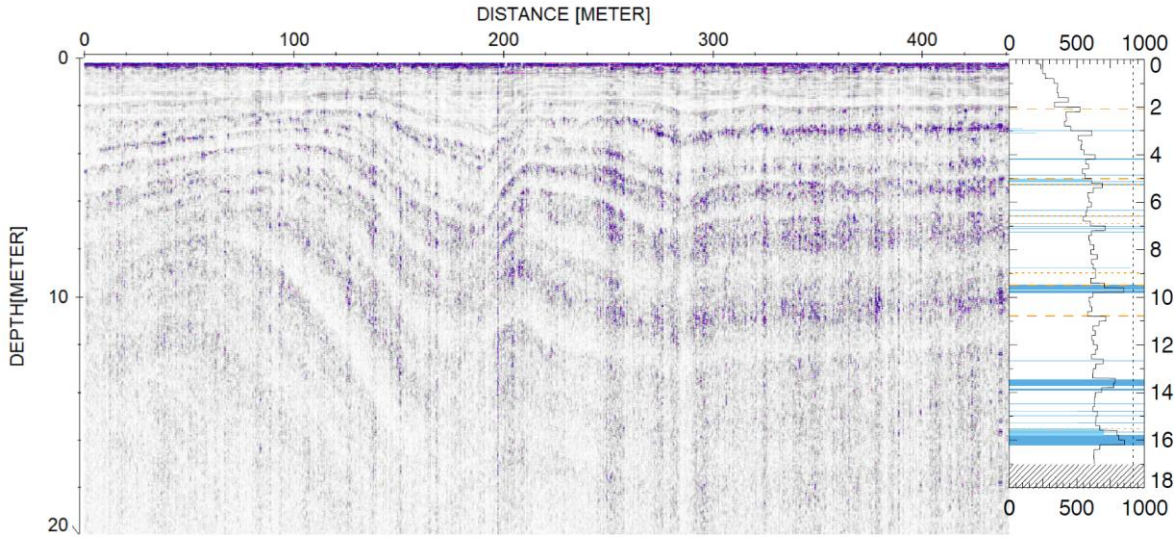


Figure 35: Comparison of an extraction of GPR profile 0715 (labelled in Figure 15) with firn core 4391 (right) (Table 4). The abscissa of the core is density in kg m^{-3}. Orange dashed lines mark dust horizons, blue lines or rectangles represent ice lenses.



Figure 36: Snow pit 3867 (Figure 15 and Table 5) 26 January 2018.

In this study, only the uppermost current winter's accumulation was of interest. Hence for correct layer determination and water equivalent calculation, beside the firn cores also observations from three additional snow pits were used. The snow pits show a dust layer several decimetres above a hard ice layer (Figure 34). The dust occurs in combination with a small crust, below which constructive metamorphism took place due to a very high temperature gradient in autumn favouring water vapor transport in the snow cover and constructing typical faceted crystals with low internal cohesion («sugar snow»). This is in line with what is known from webcam images: An early snowfall event in September was followed by two months without remarkable additional snowfall

before larger amounts of snowfall occurred in December and January. In the GPR profiles, the uppermost reflection horizon is the dust layer. The previous summer surface is visible in all GPR profiles at the bottom of the second reflection horizon

With these observations in the field, it is evident that the first thin reflection horizon in the GPR profiles is induced by the longer precipitation-free period after early snowfall in September, leading to a thin ice crust. This observation is confirmed by all profiles, as the two reflecting horizons are present in the accumulation and ablation area (Figure 16, Figure 17, Figure 18, Figure 19, Figure 20): As Abramov Glacier was snow free in August 2017 up to an elevation of 4'100 m a.s.l. (Figure 37), it is not possible that the lower layer could be an older perennial layer.



Figure 37: Abramov Glacier from the location of the automatic weather station on 5 August 2017.

6.1.1 Uncertainties GPR horizon extraction

Uncertainties in manual picking depend on the thickness of the horizon: For the last summer horizon, the standard deviation is 0.59 ns for a mean TWT of 20.35 ns. This corresponds to an uncertainty of ± 2.9 %. However, if this layer would be thicker (assuming that, by the end of the accumulation season, the previous year's summer horizon would reach the depth at which the penultimate summer horizon was during field survey in January), the standard deviation would be 0.53 ns at a mean TWT of 48.6 ns, decreasing the uncertainty to ± 1.08 %.

At the drill site at 4'381 m a.s.l., five different GPR profiles intersect. The variations of the TWTs within the different profiles and the corresponding depths are shown in Table 11. The measured reference depth from core 4381 was determined at the upper edge of the 20 cm core part where the density jumps from 455 kg m^{-3} (typical for old snow) to 611 kg m^{-3} (more typical for firn; *Cuffey and Paterson 2010*). Measured TWTs from surface to the previous summer horizon vary by 3.1 ns, corresponding to depth differences of 0.15 m.

Table 11: GPR-measured TWTs from the surface to the previous year's summer horizon, calculated depths (details Section 4.4) and measured depth at the core location 4381 (profiles labelled in Figure 15).

	TWT [ns]	Depth [m] calculated	Depth [m] measured
Profile 0715	24.7	1.04	
Profile 0723	25.8	1.10	
Profile 0726	25.0	1.06	
Profile 0728	27.8	1.19	
Profile 0736	27.1	1.16	
Core 4381			1.08

These uncertainties arise from the GPR data processing: As there is some noise, the first reflection does not correspond to the snow surface. Therefore, a zero static correction was applied using a phase follower. This phase follower sometimes turns either to the upper or lower edge of the phase.

The uncertainties from horizon picking combined with the static correction for the first reflection explain the ranges of the five different GPR measurements observed at core 4381 in Table 11. The absolute error in static correction and in layer picking are independent on the depth of the horizon of interest. The relative uncertainties however decrease with increasing depth. These uncertainties would have less impact when performing GPR measurements towards the end of the accumulation season in March/April. By then, in an average winter, the accumulated snow thickness may double compared to end of January as is known from Soviet snow pit measurements and the precipitation regime.

6.2 Uncertainties GPR-derived water equivalents

Considering the variability of electromagnetic wave velocity (Section 4.4), the conversion from measured TWTs to water equivalents is challenging. Knowledge about liquid water contents as well as snow densities in different depths is required (Figure 22). In this study, the snow was assumed being dry. Is this assumption justified?

In an other study that performed GPR measurements on Findelengletscher in April, the snowpack was assumed being dry *(Sold et al. 2013)*, although mentioning the uncertainty of a possible liquid water content up to 5 % *(Sold et al. 2013; Sold et al. 2016)* what would reduce the electromagnetic wave velocity by 20 % (Figure 23). However, this is different on Abramov Glacier, as it was frozen to about 10 m depth, far below the current accumulation horizon. For frozen snow, liquid water content is negligible *(Fierz et al. 2009; Techel and Pielmeier 2011)*.

Therefore, the second difficulty for attaining water equivalents from measured TWTs arises from changing snow densities. Thanks to the availability of two firn cores and three snow pits that were covered by GPR traces, this study benefits from direct comparison of TWTs and water equivalents. This is a very important benefit as with the R^2 of 0.99 (Figure 23), deviations from TWT to water equivalent conversion by Formula 6 are restricted to a minimum. It was observed that density increase with depth is higher at lower altitudes. As this lowers the travel speed, measured TWT will be higher than for a less dense layer of the same depth at higher altitude and likewise the calculated water equivalent, compensating for the effect of reduced travel speed at lower altitudes.

For these two reasons, water equivalents calculated here can be considered as being very accurate. Another more advanced option would be the application of an iterative densification model *(e.g. Reeh 2008)*.

6.3 Parameters Soviet SDD and PM rasters

The Soviet SDD rasters benefit from 30 years of monthly Soviet stake measurements at 165 stakes. The stakes comprise a wide range of various terrain characteristics (elevations, slopes, curvatures, expositions). These dense measurements are the reason why Soviet SDD rasters were calculated first rather than directly calculating Soviet PM rasters using the snow pits.

The inclusion of the Soviet precipitation measurements as one explaining variable allows to use all stake data as snow depth is always scaled by the variable *WinterP_m*. Thanks to this abundant data base, the Soviet SDD rasters based on this data can be considered as accurate for most parts of the glacier.

Via these Soviet SDD rasters, also the Soviet PM rasters benefit from the spatially dense stake measurements as *SDD_m* represents one of the four independent variables to calculate the water equivalent distribution.

Water equivalents of the Soviet PM rasters were better represented by a 4th parameter than including topographical statistical values from up to 400 m radian environment of each pixel. This is obvious as topographical gradients over a distance of 400 m can be large, where for example mountain ridges were passed on some parts of Abramov Glacier. Furthermore, the 100 m used are in line with the study of *Sturm and Benson (2004)* that showed major influence of 100 m radius topography on the snow distribution, depending on the DEM resolution.

One important parameter was not included in both the Soviet SDD and PM raster parameter set: This is the local wind direction. Satellite pictures from Abramov Glacier show features of snow drift especially near some of the passes. These signatures of wind transport are observable over hundreds of meters. However, the inclusion of a

high-resolution wind model that estimates the snow relocation is beyond the scope of the present work but has been tried before *(Purves et al. 1998; Lehning et al. 2008)*.

The best parameter selections for the Soviet SDD rasters *(elevation, one curvature parameter, winterP_m;* Table 7*)*, Soviet PM rasters *(SDD_m, two curvature parameters, winterP_m;* Table 8*)* and the GPR raster (*elevation, one curvature parameter, winterP_m;* Table 10) are in line with *McGrath et al. (2018)*. They investigated interannual snow accumulation variability on two glaciers and found elevation, snow drift potential[23] and curvature being the most important parameters explaining the water equivalent distribution. The wind direction was also included in this study but did not appear among the best regressions for the SDD or water equivalent distribution.

The simplification applied when producing monthly SDD and PM rasters instead of daily ones is appropriate: It was shown that even the distribution between normalized rasters for different months experiences only minor changes (Subsection 5.2.1, Table 9). Thereby this simplification does not introduce mentionable uncertainty.

6.4 Water equivalent distribution January 2018

To transform the mean Soviet PM raster to a January 2018 raster comparable to the GPR data from January 2018, the water equivalent measured at firn core 4381 was used (Subsection 4.5.3, Formula 9) to estimate the winter 2017/2018 precipitation required as regression input. Today precipitation is still measured but on a different place and with other devices than in Soviet times. Therefore, the uncertainties were assumed being even higher if today's precipitation would have been used.

Nevertheless, the independence between the Soviet and the GPR water equivalent raster and therefore also the PM raster is still given as the precipitation value only changes the amount of water equivalent but does not change its distribution at all. Indeed the question is to assess whether it is satisfactory to only use one single location for the precipitation adaptation to the winter 2017/2018. This becomes an even more important drawback when being aware of the highly variable accumulation distribution (Figure 38) combined with some incertitude concerning the exact locations of Soviet measurements, as during Soviet times, an unknown local coordinate system was used which is difficult to tie to present-day global coordinate systems. However, thanks to comparisons with Soviet photographs, there is now certitude that the snow pit during Soviet measurements corresponds well with the winter 2018 firn core location 4381. Moreover, as there is evidence that the accumulation distribution pattern is nearly constant

[23] *McGrath et al. (2018)* calculated the snow drift potential by the modal daily wind direction from October to May for wind speeds exceeding 5 m s^{-1}.

within different years (e.g. *McGrath et al. 2018*), one single location adequately represents the amount of snow for the entire glacier.

It is important to keep in mind that the PM rasters already include all kind of mass relocations after the snow has deposited. They do not represent the exact amount of precipitation that falls on every part of the glacier during a precipitation event but rather the distribution of this precipitation after relocation by wind drift and avalanching. Therefore, the PM rasters are destined to be used as PMs in glacier mass balance models that do not account for any surface mass transports.

Some of the features in the orographic left parts of Abramov Glacier are artificially induced by the DEM: As the high resolution Pléiades DEM from 2015 contained some data gaps in the orographic left region of Abramov Glacier, it was filled using SRTM. However, the SRTM was generated in the year 2000 and glacier elevation has changed substantially in the 15 years in between the two DEMs. The major change occurred in the ablation area with up to 30 m lower elevations measured by Pléiades. In the gap-spiked region of interest on the upper orographic left branch, no explicit difference is detectable: Differences reach from –10 to +10 m. Therefore, it was not possible to add a certain vertical offset to the SRTM DEM before filling the gaps.

The Soviet and GPR derived water equivalents were compared in Figure 31. Their behaviour is discussed in the following two subsections.

6.4.1 Small-scale water equivalent variations between the Soviet January 2018 raster and the GPR trace

In the uppermost, rather flat part of Abramov Glacier that has been measured by GPR, there remain remarkable variations in water equivalent differences on small spatial scales of less than 200 m. The topography at this plateau of Abramov Glacier is rather regular without major changes in exposure nor slope as it can be seen from the contour lines in Figure 38.

The water equivalents from the regression approach therefore do not experience much change while the GPR measurements show strong variations on spatial scales in the order of 100 m. We assume that these small scale variations are wind induced and strongly influenced by the ridge in the west. This ridge culminates at an elevation of 4'700 m a.s.l. and probably leads to a jet effect at the southern pass through canalisation, resulting in higher wind speed and less snow deposition. Behind the highest peak and the ridge, lee effects favour snow deposition.

However, these spatially variable wind induced effects are difficult to assess by topographical parameters and therefore only assumptions can be undertaken. Strong spatial variabilitiy of snow distribution has been observed before *(Richardson et al. 1997; Machguth et al. 2006)*. According to the literature, crucial for a good reproduction of

snow-transport in a model is the simulated wind field *(Liston and Sturm 1998; Purves et al. 1998; Lehning et al. 2008)*.

These impressive variations in Figure 38 are a good example why the accumulation distribution of snow introduces large uncertainties in modelling of glacier mass balances. The question is open whether such small-scale variations ever can be simulated accordingly by wind models. Figure 38 rather shows how useful GPR measurements can be in providing information about the accumulation distribution as wind-induced effects are well and directly represented in GPR measurement.

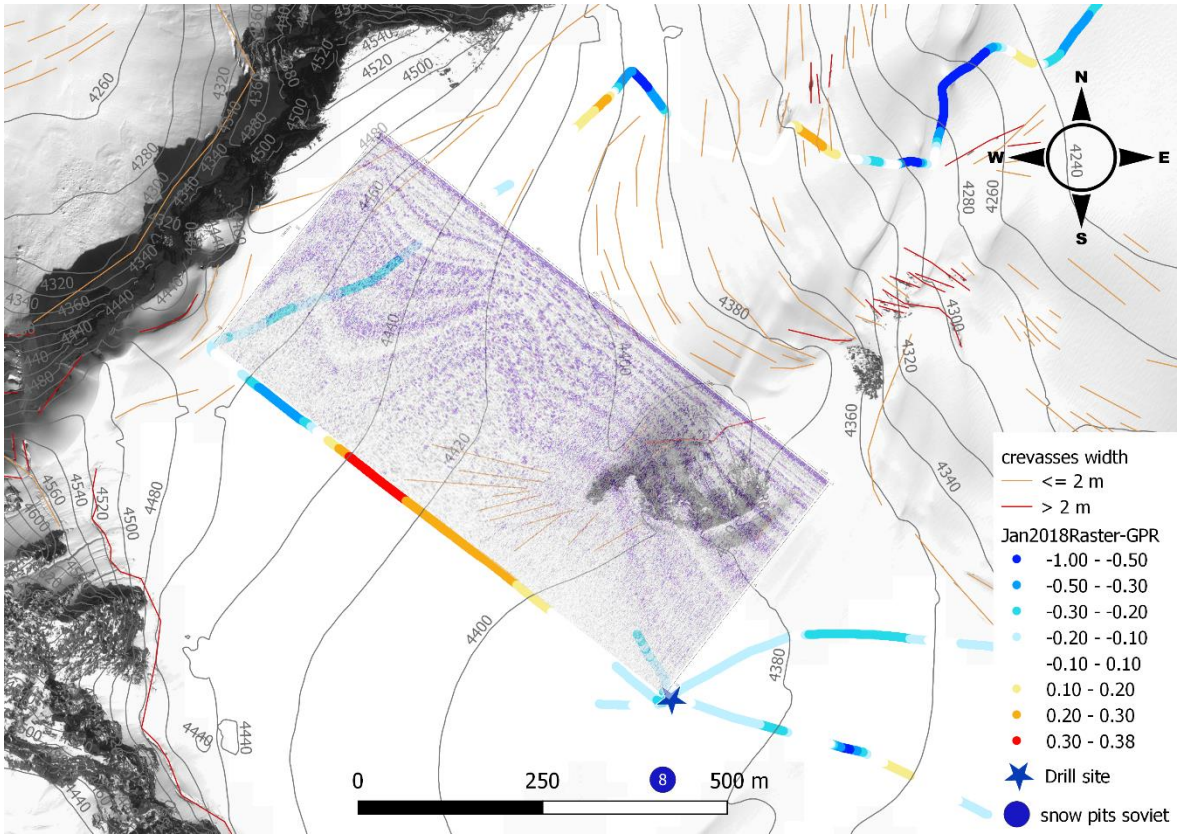


Figure 38: High accumulation area around drill site 4389 with topography [m] with GPR extract and water equivalent differences between Soviet January 2018 raster and the GPR trace [m w.e.].

Over all intersections of the GPR-derived water equivalents at the GPR traces with the regression-based Soviet water equivalents, difference only is about 0.03 m w.e. Considering the absolute independence of the two data sets, this can be considered as a remarkably good concordance.

6.4.2 Water equivalent deviations between the Soviet January 2018 raster and the GPR raster

As it was shown in Figure 32, regression-based GPR water equivalents especially in the ablation area are substantially lower than the regression-based Soviet water equivalents. An explanation therefore may be that in autumn 2017, some important precipita-

tion events did not occur on the entire glacier in form of snow. The same effect would arise from warm temperatures after the first considerable snowfall event, leading to pronounced melt in the ablation area of Abramov Glacier. From observations in the snow pits, the latter explanation seems to be more probable: Especially in the ablation area, the autumn snow layer contains many dust particles. This indicates a longer period without new snowfall probably combined with some melt.

The most likely explanation for the high deviations between the Soviet and GPR water equivalents is the spatial distribution of the source data: While for model calibration, the Soviet raster considers eight snow pits distributed over the entire glaciers, the GPR raster considers 50'521 point measurements but only on the orographic right part. Therefore, it could be possible that under similar topographical conditions, accumulation is considerably higher on the orographic left part. Qualitatively this is what has been observed during the winter campaign when the orographic left part was much cloudier with earlier onset and longer duration of precipitation. This behaviour had already been noted by *Kislov (1982)*. Therefore, the incorporation of orographic left data only in the Soviet data base could explain the shift of around 10 % between the Soviet and the GPR raster.

The differences when comparing the GPR-derived raster with the Soviet January 2018 raster may furthermore arise from the parameter choice and limitations in measurements: Only one short slope exceeding 15 ° was measured by GPR, reaching a maximum of 18 °. This slope was probably a lee slope not very representative for the entire glacier. Very steep slopes will hardly have three times higher accumulations than flat areas, as snow is more and more relocated by avalanching once 30 ° are exceeded *(SLF 2018)*. The influence of elevation and slope on the water equivalent distribution of the GPR raster is too pronounced. When normalizing the GPR water equivalent raster to attain the GPR PM raster, the unreasonably high values at slopes steeper than 15 ° remarkably decrease the PM values on the flat parts of the glacier.

Therefore, the GPR raster has to be used with caution. However, when extrapolated on the entire glacier, also the Soviet January 2018 raster has to be used with caution as slopes steeper than 15 ° likewise were not measured by snow pits and stakes.

6.5 Slope correction

Considering the Soviet SDD, water equivalent and PM rasters in Figure 25, Figure 26 and Figure 27, highest values were calculated in the steepest uppermost parts of glacier branches up to 4'950 m a.s.l. These values are subject to large uncertainties. The SDD raster is based on a regression with elevation being one of three explaining variables. However, the regression is calculated using Soviet snow depth measurements located at maximum at 4'550 m a.s.l. In high altitudes above 4'550 m a.s.l as well as slopes

above 15 °, no snow depths were measured. Therefore, the regression corresponds to an extrapolation in these parts of the glacier with corresponding high uncertainties.

The Soviet SDD rasters could be improved when limiting snow depth in steep terrain. From observation and literature it is known that snow cover decreases with increasing slope *(Blöschl and Kirnbauer 1992; Farinotti et al. 2010)*. *Blöschl and Kirnbauer (1992)* concluded that slopes steeper than 60 ° are virtually never snow covered. They found that snow cover increases with elevation but decreases with increasing slope. *Farinotti et al. (2010)* pointed out that the threshold slope where no snow is deposited depends on the resolution of the DEM grid. For 25 m resolution, they gave a threshold value of 55 ° and for 100 m resolution 45 °.

Considering these findings, parameter choices for the Soviet and GPR water equivalent raster in this study have to be questioned. In the prevailing PM rasters, water equivalents do not decrease with increasing slope. Instead they rather increase due to increasing altitude and curvature, reaching highest values in steep high-altitude slopes. Therefore, the Soviet SDD rasters (and with it the Soviet water equivalent and PM rasters depending on them) could be improved applying a linear relation that reduces regression-calculated snow depths linearly from 100 % for slopes from 0 ° to a certain threshold slope to 0 % for slopes above 55 °.

This threshold slope is determined as 15 ° due to several reasons: As 99.9 % of all GPR measurements and all Soviet measurements were performed on flater areas of Abramov Glacier, slopes above 15 ° are clearly underrepresented in the measurements used to calibrate the regressions. Therefore, applying the regressions to slopes steeper than this threshold corresponds to extrapolation into unknown terrain. Moreover, the lower limit of 15 ° is in line with findings from *Blöschl and Kirnbauer (1992)*.

Alternatively, a simpler regression using only elevation and slope was used by other authors *(Farinotti et al. 2010; Elder et al. 1991)*. However, this would not lead to success here due to the lack of data for slopes above 15 °.

To improve plausibility of the PM rasters, the produced Soviet and GPR water equivalent rasters are refined using a linear decrease reaching from 100 % of the calculated water equivalent values for slopes from 0 to 15 ° to 0 % for slopes steeper than 55 °. Figure 39 compares the two GPR rasters (Soviet rasters Appendix G Figure 48).

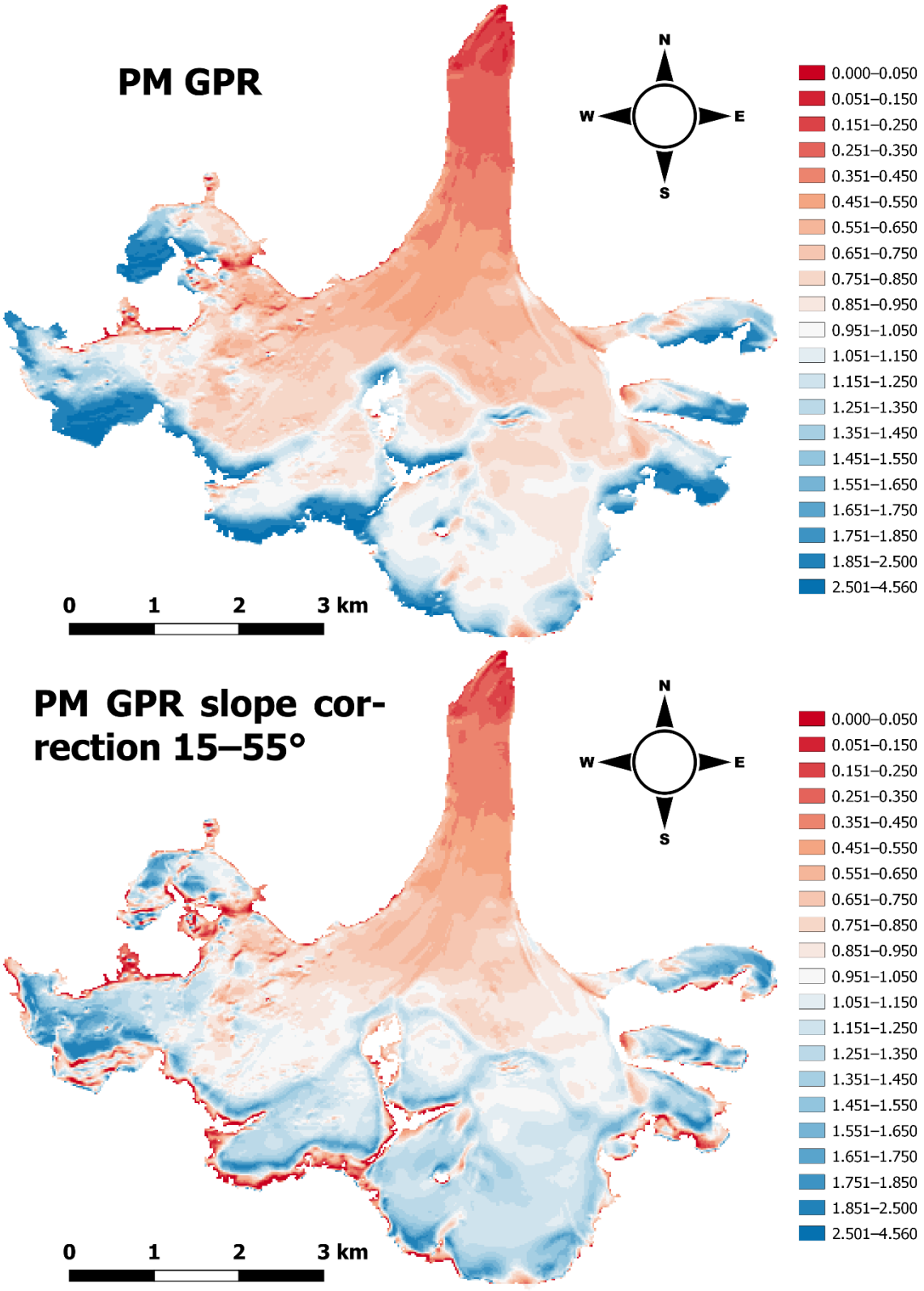


Figure 39: GPR PM rasters (normalized water equivalent rasters) without (top) and with (bottom) slope-correction (linear decrease from 100 % for slopes up to 15 ° to 0 % from 55 ° and steeper) [dimensionless].

Remarkable changes occur: Instead of a pronounced increase, water equivalents are decreased at steep slopes above 15 °, especially visible at the southern edges of

Abramov Glacier. Therewith, domination of the steep slopes over the entire glacier disappears. As average water equivalent becomes smaller, PM values increase on the main parts of the glacier: PM values on the plateau around the uppermost drill site reach area-wide factor 1.5 while the glacier tongue receives around one forth of average glacier precipitation. Therefore, the slope correction leads to more realistic PM values.

The model is spun-up and calibrated again using this slope-corrected PM raster changing the constants for precipitation correction, albedo and temperature gradient. Figure 40 compares the model run with the initial PM raster and with the slope-corrected one. Surprisingly, changes are marginal. Due to the above described increase of PM value over most parts of the glacier in the slope-corrected raster, precipitation correction value is lower (1.17) in this model run (number 208 in the right part of Figure 40) than in the first version (model run number 164 in the left part of Figure 40). Nevertheless, the model does not perform much better with this more realistic PM input.

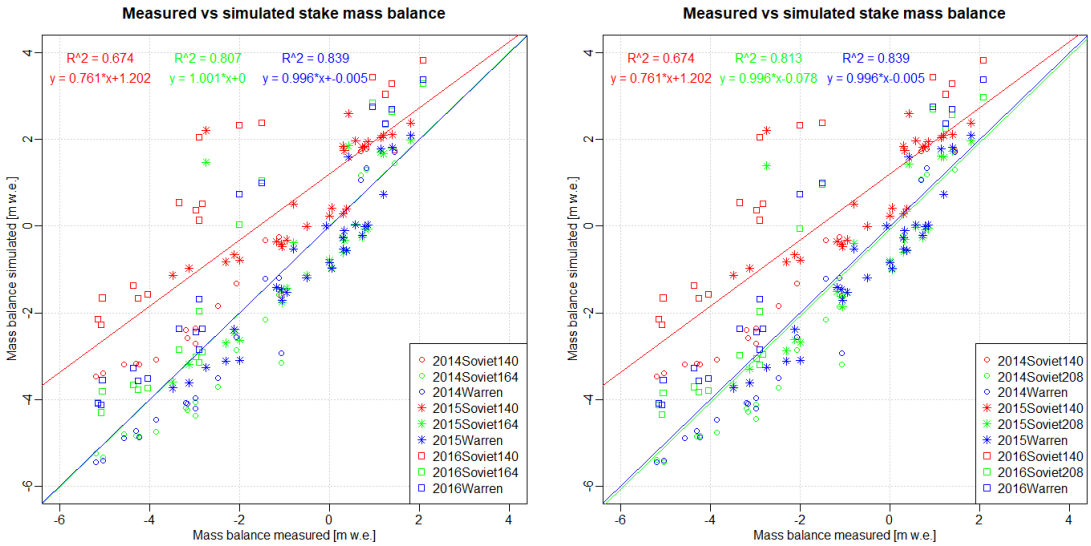


Figure 40: Measured versus simulated mass balance for the period 1 November 2013 02:55 until 1 October 2017 02:55. Warren's best simulation (blue) is compared with the simulations using the Soviet PM, without (left) and with (right) correction for slopes steeper than 15 °, and the same settings (red) as well as with improved parameter settings (green). Details about parameter settings: Appendix H.

The mass balance model cannot be further improved by precipitation correction, independent whether a precipitation correction factor, a gradient, one of the PM rasters or a combination of them is used. Therefore, it is to assume that other constants in the mass balance model or an interplay between them need to be changed in order to optimize the deviation between calculated and measured mass balance at the stake locations. Further information would be gained by specifically analysing the locations with extreme deviations.

6.6 Representativeness of winter 2017/2018

The snow accumulation distribution pattern is assumed to stay more or less constant over the years because most redistribution processes are controlled by topographic effects *(Farinotti et al. 2010; Sold et al. 2016, McGrath et al. 2018)*. Changes in the accumulation distribution pattern and hence the PM raster could be induced primarily by anomalies of humidity advection in the middle troposphere and wind strengths at the glacier.

For an estimation of the representativeness of the winter 2017/2018 circulation, Table 12 compares ERA5 reanalysis data as well as measurements at the GFZ weather station beside Abramov Glacier (Table 12, *italic*) to the six previous winters.

The winter 2017/2018 was among the warmest winters both in free atmosphere and at the weather station. However, humidity, wind speeds and wind directions in 500 hPa as proxies for middle-tropospheric humidity advection are comparable to the earlier winters.

Table 12: ERA5 reanalysis of mean temperature, humidity and wind speed/direction at 500 hPa and surface precipitation *(ECMWF 2018)* as well as mean measurements *(italic)* at the GFZ Abramov weather station (*SDSS (2018)*). 2011 OJ = Oct 2011 to Jan 2012, 2011 OA = Oct 2011 to Apr 2012 etc. *Wind speeds at the weather station represent the average of all 10 min maximal wind speeds.

Time period	Temp °C	*Temp °C*	Wind speed m/s	*Wind speed * m/s*	Wind dir. °	Humidity %	Precipitation mm
2011 OJ	−22.5	*−11.9*	12.7	*5.2*	239	72	347
2011 OA	−21.0	*−12.9*	11.2	*5.1*	240	71	579
2012 OJ	−21.7	*−14.3*	9.2	*4.4*	250	60	186
2012 OA	−21.0	*−11.8*	9.3	*4.3*	243	62	386
2013 OJ	−21.1	*NA*	10.0	*NA*	241	59	162
2013 OA	−21.5	*NA*	10.1	*NA*	240	62	388
2014 OJ	−21.6	*−10.5*	11.4	*4.8*	241	66	262
2014 OA	−20.9	*−10.4*	11.1	*4.7*	242	66	515
2015 OJ	−20.4	*−9.4*	11.4	*4.8*	244	64	252
2015 OA	−19.9	*−9.3*	9.9	*4.3*	242	62	411
2016 OJ	−21.2	*−10.4*	13.2	*5.2*	242	68	363
2016 OA	−21.2	*−11.0*	12.3	*5.3*	243	67	691
2017 OJ	−21.2	*−9.7*	10.8	*4.6*	243	63	193
2017 OA	−20.5	*−9.8*	10.9	*4.9*	244	63	439

This is in contrast with what was observed by the research team. Based on Soviet precipitation measurements *(Kislov 1982)*, drier conditions were expected than they observed during their field survey in January 2018. However, reanalysis data shows that precipitation from October 2017 to January 2018 was below average of the last seven winters. By only considering January ERA5 reanalysis precipitation, January 2018 got

66 mm while average January precipitation amounts to 59 mm and 84 mm were recorded in the precedent January (details in Appendix J Table 30).

Therefore, winter 2017/2018 as well as January 2018 are representative for nowadays winters on Abramov Glacier. The GPR accumulation distribution measurements likewise are representative, as snow amounts and relocation processes by wind are within the range observed during the last winters.

6.7 Mass balance model implementation

Van Pelt et al. (2012) concluded similar to *Klok and Oerlemans (2002)* that one of the main uncertainties in the model forcing remains in the variability of snow accumulation. Through the implementation of a PM raster in the mass balance model, uncertainties from snow accumulation variability are reduced. As outlined in Section 4.6.2 and visible e. g. from Figure 33 (blue symbols), the modelled mass balances at the stake locations still show considerable deviations from the measurements: In the accumulation area, simulated mass balances always are too positive, independent on the year, while in the ablation area in 2015 they are too negative and in 2016 too positive. Using the Soviet or the GPR PM raster therefore did not further improve the agreement between measured and modelled mass balances at the stake locations. Being aware of the mentioned reduced uncertainty in snow accumulation variability by the PM rasters, this indicates that the mass balance is more sensitive than expected to other model input parameters than precipitation and temperature lapse rate.

Modelled mass balances experience melt processes. These processes are reproduced in the coupled snow and energy balance model of *van Pelt et al. (2012)* by summarizing all surface energy fluxes. Therefore, it is imaginable that even if the model represents well the accumulation distribution during winter thanks to one of the two PM rasters, deviations arise from assumptions in the melt simulation. These errors might occur from uncertainties in snow, firn or ice albedo, from meteorological input *(van Pelt et al. 2012)* or from other model input parameters (compare Appendix H).

Another possibility could be errors in summer measurements used for the calibration of the model: Using a snow probe in the field, it is not evident to recognize the previous year's summer horizon. If in this case, an ice lens is considered as a summer horizon, the measurement error easily exceeds 25 %. This might be the case for some snow probe measurements in the year 2016 where deviation is especially high, comparable to observations made by *Machguth et al. (2006)* on a Swiss glacier. However, it is nearly impossible to retrospectively exclude such measurement errors.

6.8 Applicability

The database of Soviet glacier measurements on Abramov Glacier is unique in terms of stake, snow pit and precipitation measurements. Benefitting from the results of the monthly Soviet PM rasters, this allows to recommend a method for accumulation distribution measurements that is fast and applicable on most other glaciers where no similar long-term, spatially dense network exists.

Considering the absence of precipitation measurements on most other sites not benefiting from long-term in situ measurements, there exist alternative possibilities: Numerous climate reconstructions are available world-wide *(Potter et al. 2018)*. In the Swiss Alps, with the Rhires, spatially high-resolution precipitation maps from ground-based precipitation measurements combined with weather radar measurements are available *(MeteoSwiss 2016)* and similar products might exist elsewhere. As precipitation measurements in mountainous regions are highly error-prone, the quality of such reconstructed precipitation data is not a priori worse than from in situ rain gauges. Precipitation correction is necessary either way. Therefore, it might be possible to replace Soviet precipitation data by another precipitation product.

Replacing the mass balance measurements on the glacier by another data product is more difficult. The contrary of the German saying «Wer misst misst Mist» is true: Snow water equivalents that have not been measured before the onset of the melt season are lost forever and snow depth changes thereby likewise. Nevertheless, good coverage of the accumulation distribution on the glacier is desired when modelling the mass balance of a glacier. That is where an interesting solution for other glaciers exists: Spatially distributed snow pit and eventually snow depth measurements are to combine with GPR measurements.

To assess the corresponding loss of confidence compared to this study, two constraints arise: Can the PM regression calibrated in one month adequately represent the one of another month? Can the PM of one year adequately represent the one of another year? These two constraints are assessed in the following two subsections.

6.8.1 Snow distribution representativeness for other months

Thanks to the comparison of the PM rasters based on Soviet snow pit and stake data in Table 9, we now know that the accumulation distribution pattern hardly experiences any changes throughout the winter. The average differences in intermonthly PM factors on every pixel of the glacier amount to less than 0.5 %, corresponding to a standard deviation of less than 2 %.

As seen from the monthly Soviet water equivalent and PM rasters in Figure 26 and Figure 27, water equivalents considerably increase within the winter while the PM factors nearly don't change at all. This shows that snow water equivalents increase proportionally all over the glacier from December to April. The relative distribution over

the glacier stays more or less constant, independent on whether the winter just began or accumulation occurred during the entire winter. This temporal consistency in precipitation distribution can be very useful for further studies and for modelling: In regions where weather patterns do not change significantly throughout the winter, measured accumulation distribution can be applied to the entire winter independent in which month the field survey is performed.

6.8.2 Snow distribution representativeness for other years

As melt processes lie in between and GPR measurements were only performed in one winter, it was not possible to directly measure the snow accumulation distribution of several years during this study. However, this concern was assessed by numerous other studies:

Richardson et al. (1997) pointed out that the redistribution of snow by wind has a major influence on the local accumulation pattern and observed a stable interannual accumulation pattern, while absolute values experienced large variations. *Sturm and Benson (2004)* analysed snow distribution patterns on different spatial and temporal scales. They observed that the influence of microtopography of less than 100 m is absent in perennial snow cover, leading to more homogeneity. Another new study from *McGrath et al. (2018)* investigated this interannual snow accumulation variability on two glaciers by extensive GPR survey. They found the spatial pattern of snow accumulation to be temporally stable within different years.

Therefore, there is increasing confidence that SDD and accordingly also the PM patterns are consistent over time as they are controlled by topographical effects that do not change significantly within different years.

6.8.3 Recommendations for other sites

GPR provides a fast and spatially distributed overview about the snow accumulation distribution.

The GPR PM raster allows to simulate the measured mass balances using the mass balance model of *van Pelt et al. (2012)* with an R^2 of 0.83. Therefore, the GPR-based PM raster performs similar like the Soviet data based one. The GPR PM raster is supposed to perform even better when below recommendations are implemented in future research:

The GPR and snow pit measurements in optimal case are performed towards the end of the accumulation season before the onset of melt. This reduces errors from layer picking and static correction, as they absolutely stay the same while relatively decreasing with increasing snow depth. Moreover, it allows including a maximum of different

weather types[24] (wind and humidity advection from different directions) that altered the snow cover and therefore reduces influence of weekly meteorological circulation abnormalities. According to the Soviet PM rasters (Table 9 and Appendix G Figure 44), March seems to be the most appropriate month on Abramov Glacier. Furthermore, it is beneficial to perform GPR measurements on topographically different parts of the glacier (altitude, slope, exposition, curvature) as well as some steeper slopes.

Snow density measurements of the current winter's accumulation are a prerequisite to convert measured TWTs to water equivalents. These density measurements should be distributed over the entire glacier and be covered by GPR traces. They allow to establish a relationship that directly converts TWT empirically based to water equivalents (Figure 23). Five such density measurements in snow pits already provide sufficient[25] data to establish a function for direct conversion of the measured TWTs to water equivalents. These snow pits merely should be performed the same day where the GPR traces passe the locations and the different GPR traces temporally should be performed close together during dry weather to prevent new snow accumulation in between.

Therefore, it is possible to get a representative water equivalent distribution of a glacier in a few days of work using GPR and density measurements. When normalized this accumulation distribution can then be used as a PM raster.

Challenging however may remain the weather conditions during the field survey, the physics of the researcher at cold temperatures and high altitude as well as measuring devices' behaviour under challenging meteorological conditions.

[24] Typical meteorological blocking situations remain for the order of two to four weeks. Therefore, the more months are included in the accumulation season, the smaller is the possibility to get biases through one long blocking situation.

[25] $R^2 = 0.99$ (Figure 23)

7 Conclusion

The spatially highly variable accumulation distribution is one of the main uncertainties in modelling glacier mass balance. Hence, this study aimed at creating two PM rasters on the example of Abramov Glacier, providing spatially high resolution accumulation distribution data. Up to now, precipitation from reanalysis was distributed over the glacier using an altitudinal precipitation gradient combined with a precipitation correction factor. To assess the accumulation distribution in a more detailed manner, GPR measurements were performed on Abramov Glacier in January 2018. Using a shielded 800 MHz antenna and benefiting from frozen uppermost snow and firn layers, up to ten horizons were distinguishable in the accumulation area. Focus was set on the current winter's accumulation. This horizon can be followed in all GPR measurements reaching from 3'800 to 4'500 m a. s. l.

Independent of the field data of the winter campaign, monthly PM rasters in 20 m resolution were generated using multiple regressions with Soviet snow pit measurements as dependent variable and the following four explaining variables: Snow depth distribution from Soviet stake measurements, accumulated winter precipitation and two topographical parameters of the 100 m radian environment of each pixel. As the snow water equivalents increase proportionally all over the glacier, it was observed that the accumulation distribution does not change during the winter. Therefore, an average Soviet PM raster was extracted from the five monthly rasters.

Two firn cores and three snow pits performed during the same winter campaign were used to establish a function for direct conversion of the TWTs to water equivalents. As increasing liquid water content as well as increasing densities both decrease the travel speed of GPR electromagnetic waves, this conversion function reduces uncertainties by omitting the conversion of the measured GPR TWTs to snow depths. Therefore, using the GPR point measurements, a GPR PM raster was generated by a multiple regression with elevation and two topographical parameters as explaining variables.

Both PM rasters show realistic values in areas where either Soviet or GPR measurement have been performed. PM factors generally increase with elevation. However, the rasters are not useful at steep slopes, as no calibration data is available and extrapolation occurs. To avoid unrealistic extrapolation, the PM factors were reduced linearly from 100 % for slopes up to 15 ° to 0 % for slopes of 55 ° or steeper. This lead to more realistic results with PM factors reaching from 0.25 at the glacier tongue to 1.5 at the plateaus of the accumulation area.

Both rasters were then implemented in the mass balance model of *van Pelt et al. (2012)* where each precipitation event was multiplied by the raster instead of using an elevation-dependent gradient. The model was calibrated adapting the precipitation correction factor, the temperature lapse rate and/or the ice albedo and run for the time period

November 2013 to October 2017. The simulated mass balances were compared at each location where mass balance had been measured. Regardless of whether the multiplication raster based on GPR or Soviet measurements is used, the model currently does not perform better than with the earlier altitudinal precipitation gradient. However, this study assumes that the GPR raster performance could be improved when performing snow accumulation measurements also on the orographic left branch and especially in steeper, currently underrepresented parts of the glacier. Once this is achieved, the distributed precipitation input in the model is to consider as fixed and consequently other model parameters have to be changed to increase model performance

Regardless of the remaining constraints, it is highly recommended to reuse GPR in combination with snow pit measurements, DEM and multiple regression to refine precipitation distribution in mass balance models. Measurement and processing errors can be reduced performing the GPR field survey towards the end of the accumulation season, when accumulated snow cover is high and melting has not yet started, benefitting from a maximum amount of different weather types that altered the snow cover. Additionally, five density measurements are recommended to perform simultaneously on different locations of the glacier, allowing the establishment of an empirical function that directly converts the measured TWTs to water equivalents. To extrapolate the water equivalents from GPR traces to the entire glacier, a multiple regression is to establish using the GPR derived water equivalents as dependent variable and three topographical parameters from a gap-less DEM as explaining variables. After normalization and eventually corrections for steep slopes, the raster can be used to distribute precipitation over the entire glacier and therewith to replace an altitudinal gradient.

Literature

Andreassen, L. M. (1999): Comparing traditional mass balance measurements with long-term volume change extracted from topographical maps: a case study of storbreen glacier in jotunheimen, norway, for the period 1940–1997. *Geografiska Annaler*, 81(4), 467–476 (doi: 10.1111/1468-0459.00076).

Annan, A. P. (2009): Electromagnetic principles of Ground Penetrating Radar. In: Jol, H. M. (eds.): *Ground Penetrating Radar theory and applications.* Amsterdam, Elsevier, 524 pp.

Aizen, E. M., Aizen, V. B., Melack, J. M., Nakamura, T. and Ohta, T. (2001): Precipitation and atmospheric circulation patterns at mid-latitudes of Asia. *International Journal of Climatology*, 21, 535–556 (doi: 10.1002/joc.626).

AWN (Amt für Wald und Naturgefahren) (2017): *Kurzbericht der Expertengruppe zu den Ereignissen Cengalo/Bondo für die Medienkonferenz.* Amt für Wald und Naturgefahren, Kanton Graubünden.

Bar, J. (2015): *Wasserproblematik im Kontext regionaler Stabilitätsrisiken. Eine vergleichende Analyse der Ressourcennutzung am Amu Darya/Syr Darya und Tigris/Euphrat*. Wiesbaden, Springer Fachmedien, 483 pp.

Barandun, M., Huss, M., Sold, L., Farinotti, D., Azisov, E., Salzmann, N., Usubaliev, R., Merkushkin, A. and Hoelzle, M. (2015): Re-analysis of seasonal mass balance at Abramov glacier 1968-2014. *Journal of glaciology*, 61(230), 1103–1117 (doi: 10.3189/2015JoG14J239).

Baumann, S. (2017): Comparison of glacier mass balance data in the Tien Shan and Pamir, Central Asia. *Arctic, Antarctic, and Alpine Research*, 49(1), 133–146 (doi: 10.1657/AAAR0015-076).

Berghold, F., Gieseler, U. and Schaffert, W. (2015): *Handbuch der Trekking- und Höhenmedizin. Praxis der Höhenanpassung – Therapie der Höhenkrankheit.* Kaprun, Internationale Lehrgänge für Alpin- und Höhenmedizin GmbH, 117 pp.

Berthling, I. and Melvold, K. (2008): Ground-penetrating Radar. In: Hauck, C. and Kneisel, C. (eds.): *Applied Geophysics in Periglacial Environments*. Cambridge, Cambridge University Press, 240 pp.

Blöschl, G. and Kirnbauer, R. (1992): An analysis of snow cover patterns in a small Alpine catchment. *Hydrological Processes*, 6(1), 99–109 (doi: 10.1002/hyp.3360060109).

Bradford, J. H., Harper, J. T. and Brown, J. (2009): Complex dielectric permittivity measurements from ground-penetrating radar data to estimate snow liquid water content in the pendular regime. *Water Resources Research*, 45(8), 1–12 (doi: 10.1029/2008WR007341).

CAWATERinfo (2017): *Infographic Aral Sea Basin: Water Resources.* «http://www.cawater-info.net/infographic/index_e.htm» [visit: 29.09.2017].

Cisneros, J., Oki, T., Arnell, N. W., Benito, G., Cogley, J. G., Döll, P., Jiang, T. and Mwakalila, S. S. (2014): Freshwater resources. In: Field, C. B., Barros, V. R., Dokken, D. J., Mach, K. J., Mastrandrea, M. D., Bilir, T. E., Chatterjee, M., Ebi, K. L., Estrada, Y. O., Genova, T. C., Girma, B., Kissel, E. S., Levy, A. N., MacCracken, S., Mastrandrea, P. S. and White, L. L. (eds.): *Climate Change 2014: Impacts, Adaptation, and Vulnerability. Part A: Global and Sectoral Aspects. Contribution of Working Group II to the Fifth Assessment Report of the Intergovernmental Panel on Climate Change.* Cambridge, Cambridge University Press, 229–269.

ClimateCharts (2018): *ClimateCharts.net.* Technische Universität Dresden. «https://climatecharts.net/» [visit: 25.10.2018].

Cogley, J. G., Hock, R., Rasmussen, L. A., Arendt, A. A., Bauder, A., Braithwaite, R. J., Jansson, P., Kaser, G., Möller, M., Nicholson, L. and Zemp, M. (2011): *Glossary of Glacier Mass Balance and Related Terms.* IHP-VII Technical Documents in Hydrology No. 86, IACS Contribution No. 2, Paris, UNESCO-International Hydrological Programme, 114 pp.

Compo, G. P., Whitaker, J. S., Sardeshmukh, P. D., Matsui, N., Allan, R. J., Yin, X., Gleason, B. E., Vose, R. S., Rutledge, G., Bessemoulin, P., Brönnimann, S., Brunet, M., Croutha-mel, R. I., Grant, A. N., Groisman, P. Y., Jones, P. D., Kruk, M. C., Kruger, A. C., Mars-hall, G. J., Maugeri, M., Mok, H.Y., Nordli, Ø., Ross, T. F., Trigo, R. M., Wang, X. L., Woodruff, S. D. and Worley, S. J. (2011): The Twentieth Century Reanalysis Project. *Quarterly Journal of the Royal Meteorological Society*, 137(654), 1–28 (doi: 10.1002/qj.776).

Cuffey, K. M. and Paterson, W. S. B. (2010): *The Physics of Glaciers.* Oxford, Butterworth-Heinemann (Elsevier), 704 pp.

De Pauw, E. (2008): *ICARDA Regional GIS Datasets for Central Asia: Explanatory Notes.* GIS Unit Technical Bulletin. Aleppo, International Center for Agricultural Research in the Dry Areas (ICARDA).

Dukhovny, V. and Stulina, G. (2011): Water and Food Security in Central Asia. In: Madramootoo, C. and Dukhovny, V. (eds.): *Water and Food Security in Central Asia*. Dordrecht, Springer Netherlands, 1–23.

Dümbgen, L. (2013): *Statistik für Naturwissenschaften. Für Studierende der Biologie, Biochemie, Chemie, Pharmazie, Geographie und Erdwissenschaften*. Frühjahrssemester 2013, Universität Bern, Bern.

Dyurgerov, M. B., Liu, C., Mikhalenko, V. N. and Xie, Z. (1995): *Oledeneniye Tyan-Shanya [Tien Shan Glaciers]*, Moscow, VINITI [in Russian].

Dyurgerov, M. B. (2002): Glacier Mass Balance and Regime: Data of Measurements and Analysis. Occasional Paper 55. *Institute of Arctic and Alpine Research (INSTAAR)*, University of Colorado, Boulder, 273 pp.

Dyurgerov, M. B. and Meier, M. F. (2005): Glaciers and the changing Earth system: A 2004 snapshot. Occasional Paper 58. *Institute of Arctic and Alpine Research (INSTAAR)*, University of Colorado, Boulder, 117 pp.

ECMWF (2018): ERA5. Generated using Copernicus Climate Change Service Information. «https://www.ecmwf.int/en/forecasts/datasets/archive-datasets/reanalysis-datasets/era5» visit [23.10.2018].

Elder, K., Dozier, J. and Michaelsen, J. (1991): Snow Accumulation and Distribution in an Alpine Watershed. *Water Resources Research*, 27(7), 1541–1552 (doi: 10.1029/91WR00506).

Escher-Vetter, H., Kuhn, M. and Weber, M. (2009): Four decades of winter mass balance of Vernagtferner and Hintereisferner, Austria: methodology and results. *Annals of Glaciology*, 50(50), 87–95 (doi: 10.3189/172756409787769672).

Farinotti, D., Magnusson, J., Huss, M. and Bauder, A. (2010): Snow accumulation distribution inferred from time-lapse photography and simple modelling. *Hydrological Processes*, 24(15), 2087–2097 (doi: 10.1002/hyp.7629).

Farinotti, D., Longuevergne, L., Moholdt, G., Duethmann, D., Mölg, T., Bolch, T., Vorogushyn, S. and Güntner, A. (2015): Substantial glacier mass loss in the Tien Shan over the past 50 years. *Nature Geoscience*, 8(9), 716–722 (doi: 10.1038/NGEO2513).

Fick, E. S. and Hijmans, R. J. (2017): WorldClim 2: new 1-km spatial resolution climate surfaces for global land areas. *International Journal of Climatology*, 37(12), 4302–4315 (doi: 10.1002/joc.5086).

Fierz, C., Armstrong, R. L., Durand, Y., Etchevers, P., Greene, E., McClung, D. M., Nishimura, K., Satyawali, P. K. and Sokratov, S. A. (2009): *The International Classification for Seasonal Snow on the Ground.* IHP-VII Technical Documents in Hydrology, 83, IACS Contribution 1, Paris, UNESCO-IHP, 80 pp.

Frolov, A. D. and Macheret, Y. Y. (1999): On dielectric properties of dry and wet snow. *Hydrological Processes*, 13(12–13), 1755–1760 (doi: 10.1002/(SICI)1099-1085(199909)13:12/13<1755::AID-HYP854>3.0.CO;2-T).

Gardelle, J., Berthier, E., Arnaud, Y. and Kääb, A. (2013): Region-wide glacier mass balances over the Pamir-Karakoram-Himalaya during 1999–2011. *The Cryosphere*, 7, 1263–1286 (doi: 10.5194/tc-7-1263-2013).

Gardner, A. S., Moholdt, G., Cogley, G., Wouters, B., Arendt, A. A., Wahr, J., Berthier, E., Hock, R., Pfeffer, W. T., Kaser, G., Ligtenberg, S. R. M., Bolch, T., Sharp, M. J., Hagen, J. O., van den Broeke, M. R. and Paul, F. (2013): Supplementary Materials for A Reconciled Estimate of Glacier Contributions to Sea-Level Rise: 2003 to 2009. *Science*, 340(6134), 1–40 (doi: 10.1126/science.1234532).

Glazirin, G., Kamnyansky, G., and Pertziger, F. (1993): *Regime of Abramov Glacier*. Gidrometeoizat, Hydrometeo Publishing, Leningrad, Russia, 228 pp. [in Russian].

Gracheva, I., Karimov, A., Turral, H. and Miryusupov, F. (2009): An assessment of the potential and impacts of winter water banking in the Sokh aquifer, Central Asia. *Hydrogeology Journal*, 17(6), 1471–1482.

Greuel, W. and Konzelmann, T. (1994): Numerical modelling of the energy balance and the englacial temperature of the Greenland Ice Sheet. Calculations for the ETH-Camp location (West Greenland, 1155 m asl). *Global Planet Change*, 9(1–2), 91–114 (doi: 10.1016/0921-8181(94)90010-8).

Hawley, R. L., Courville, Z. R., Kehrl, L. M., Lutz, E. R., Osterberg, E. C., Overly, T. B. and Wong, G. J. (2014): Recent accumulation variability in northwest Greenland from ground-penetrating radar and shallow cores along the Greenland Inland Traverse. *Journal of Glaciology*, 60(220), 375–382 (doi: 10.318972014JoG13J141).

Hedderichs, J. and Sachs, L. (2012): *Angewandte Statistik. Methodensammlung mit R.* Springer, Heidelberg, 881 pp.

Helfricht, K., Kuhn, M., Keuschnig, M. and Heilig, A. (2014): Lidar snow cover studies on glaciers in the Ötztal Alps (Austria): comparison with snow depths calculated from GPR measurements. *The Cryosphere*, 8, 41–57 (doi: 10.5194/tc-8-41-2014).

Heltzer, G. (2003): Stalemate in the Aral Sea Basin: Will Kyrgyzstan's New Water Law Bring the Downstream Nations Back to the Multilateral Bargaining Table? *The Georgetown International Environmental Law Review*, 15, 291–319.

Hoelzle, M. (2015[a]): *Einführung in die Kryosphäre.* GG.0253, Gletscher 1 [13.10.2015], University of Fribourg: Unit of Geography.

Hoelzle, M. (2015[b]): *Einführung in die Kryosphäre.* GG.0253, Gletscher 2 [20.10.2015], University of Fribourg: Unit of Geography.

Hoelzle, M. (2017): Presentation on the Cryospheric Climate Services for Improved Adaptation (CICADA) project. *Pre-lunch Seminar* [03.10.2017 12:30 h]. University of Fribourg: Unit of Geography.

Hoelzle, M., Azisov, E., Barandun, M., Huss, M., Farinotti, D., Gafurov, A., Hagg, W., Kenzhebaev, R., Kronenberg, M., Machguth, H., Merkushkin, A., Moldobekov, B., Petrov, M., Saks, T., Salzmann, N., Schöne, T., Tarasov, Y., Usubaliev, R., Vorogushyn, S., Yakovlev, A. and Zemp, M. (2017): Re-establishing glacier monitoring in Kyrgyzstan and Uzbekistan, Central Asia. Geoscientific Instrumentation Methods and Data Systems, 6, 397–418 (doi: 10.5194/gi-6-397-2017).

Huggel, C., Kääb, A., Haeberli, W., Teysseire, P. and Paul, F. (2002): Remote sensing based assessment of hazards from glacier lake outbursts: a case study in the Swiss Alps. *Canadian Geotechnical Journal*, 39, 316–330 (doi: 10.1139/t01-099).

Huss, M. (2011): Present and future contribution of glacier storage change to runoff from macroscale drainage basins in Europe. *Water Resources Research*, 47(7), 1–13, (doi: 10.1029/2010WR010299).

Huss, M., Bauder, A. and Funk, M. (2009): Homogenization of long-term mass-balance time series. *Annals of Glaciology*, 50(50), 198–206 (doi:10.3189/172756409787769627).

ICWC (2017): *International Commission for Water Coordination of Central Asia.* «http://www.icwc-aral.uz/bwosyr.htm» [visit: 29.04.2017].

Jackson, T. (1994): *A spatially distributed snowmelt-driven hydrologic model applied to Upper Sheep Creek*. PhD thesis, Utah State University, Logan.

Jarvis, A., Reuter, H.I., Nelson, A. and Guevara, E. (2008): Hole-filled seamless SRTM data V4. *International Centre for Tropical Agriculture (CIAT)*, «http://srtm.csi.cgiar.org» [visit: 05.10.2017].

Johannesson, T., Raymond, C. and Waddington, E. (1989): Time-scale for adjustment of glaciers to changes in mass balance. *Journal of Glaciology*, 35(121), 355–369 (doi: 10.3189/S002214300000928X).

Jouvet, G., Huss, J., Funk, M. and Blatter, H. (2011): Modelling the retreat of Grosser Aletschgletscher, Switzerland, in a changing climate. *Journal of Glaciology*, 57(206), 1033–1045 (doi: 10.3189/002214311798843359).

Kääb, A., Treichler, D., Nutz, C. and Berthier, E. (2015): Brief Communication: Contending estimates of 2003–2008 glacier mass balance over the Pamir-Karakoram-Himalaya. *The cryosphere*, 9, 557–564 (doi: 10.5194/tc-9-557-2015).

Kamnyansky, G. (2001): Abramov Glacier mass-balance observations resume (1967–1998). *Proc. SANIGMI*, 161(242), 122–131.

Karimov, A., Smakhtin, V., Mavlonov, A. and Gracheva, I. (2010): Water 'banking' in Fergana valley aquifers–A solution to water allocation in the Syrdarya river basin? *Agricultural Water Management*, 97(10), 1461–1468 (doi: 10.1016/j.agwat.2010.04.011).

Kaser, G. , Fountain, A. and Jansson, P. (2003): A manual for monitoring the mass balance of mountain glaciers with particular attention to low latitude characteristics. UNESCO International Hydrological Programme, Technical Documents in Hydrology, 59, 107 pp.

Kenzhebaev, R., Barandun, M., Kronenberg, M., Chen, Y., Usubaliev, R. and Hoelzle, M. (2017): Mass balance observations and reconstruction for Batysh Sook Glacier, Tien Shan, from 2004 to 2016. *Cold Regions Science and Technology*, 135, 76–89 (doi: 10.1016/j.coldregions.2016.12.007).

Khromova, T. E., Osipova, G. B., Tsvetkov, D. G., Dyurgerov, M. B. and Barry, R. G. (2006): Changes in glacier extent in the eastern Pamir, Central Asia, determined from historical data and ASTER imagery. *Remote Sensing of Environment*, 102(1–2), 24–32 (doi: 10.1016/j.rse.2006.01.019).

Kirchhofer, W. and Sevruk, B. (1992): Mittlere jährliche korrigierte Niederschlagshöhen 1951-1980. In: Bundesamt für Umwelt BAFU (ed.): *Hydrologischer Atlas der Schweiz, Tafel 2.2*. Wabern-Bern, Bundesamt für Landestopographie.

Kislov (1982): ФОРМИРОВАНИЕ И РЕЖИМ ФИРНОВО-ЛЕДДЯНОЙ ТОЛЩИ ГОРНОГО ЛЕДНИКА. СРЕДНЕАЭИАТСКИЙ РЕГИОНАЛЬНЪЫЙ НАУЧНО-ИССЛЕДОВАТЕЛЬСКИЙ ИНСТИТУТ, Ташкент, 214 pp. [in Russian].

Klok, E. J. and Oerlemans, J. (2002): Model study of the spatial distribution of the energy and mass balance of Morteratschgletscher, Switzerland. *Journal of Glaciology*, 48(163), 505–518 (doi: 10.3189/172756502781831133).

Kohler, J., Moore, J, Kennett, M., Engeset, R. and Elvehøy, H. (1997): Using ground-penetrating radar to image previous years' summer surfaces for mass-balance measurements. *Annals of Glaciology*, 24, 355–360 (doi: 10.1017/S0260305500012441).

Kotlyakov, V.M., Macheret, Yu.Ya., Sosnovsky, A.V. and Glazovsky, A.F. (2017): Speed of radio wave propagation in dry and wet snow. *Lëd i Sneg*, 57(1), 45–56 (doi: 10.15356/2076-6734-2017-1-45-56) [in Russian].

Kovacs, A., Gow, A., and Morey, R. M. (1993): A Reassessment of the In-Situ Dielectric Constant of Polar Firn. *CREEL Report*, 93(26), 1–26.

Kronenberg, M., Barandun, M., Hoelzle, M., Huss, M., Farinotti, D., Azisov, E., Usubaliev, R., Gafurov, A., Petrakov, D. and Kääb, A. (2016): Mass-balance reconstruction for Glacier No. 354, Tien Shan, from 2003 to 2014. *Annals of Glaciology*, 57(71), 92–102 (doi: 10.3189/2016AoG71A032).

Laity, J. (2008): *Desert and desert environments*. Oxford, Wiley-Blackwell.

Lehning, M., Löwe, H., Ryser, M. and Raderschall, N. (2008): Inhomogeneous precipitation distribution and snow transport in steep terrain. *Water Resources Research*, 44(7), 1–19 (doi: 10.1029/2007WR006545).

Le Matin (2018): Glacier de la Plaine Morte : Le lac des Faverges s'est vidé. «https://www.lematin.ch/suisse/Le-lac-des-Faverges-s-est-vide/story/20193814» [visit: 02.08.2018].

Liston, G. E. and Sturm, M. (1998): A snow-transport model for complex terrain. *Journal of Glaciology*, 44(148), 498–516 (doi: 10.1017/S0022143000002021).

Machguth, H., Eisen, O., Paul, F. and Hoelzle, M. (2006): Strong spatial variability of snow accumulation observed with helicopter-borne GPR on two adjacent Alpine glaciers. *Geophysical Research Letters*, 33(13), 1–5 (doi: 10.1029/2006GL026576).

MALÅ Geosciences AB (2016): *ProEx–Professional Explorer Control Unit.* Operating Manual v. 2.0, 19-001030, Malå, 61 pp.

Marchenko, S., Pohjola, V. A., Pettersson, R., van Pelt, W. J. J., Vega, C. P., Machguth, H., Bøggild, C. E. and Isaksson, E. (2017): A plot-scale study of firn stratigraphy at Lomonosovfonna, Svalbard, using ice cores, borehole video and GPR surveys in 2012–2014. *Journal of Glaciology*, 63(237), 67–78 (doi: 10.1017/jog.2016.118).

McGrath, D., Sass, L., O'Neel, S., McNeil, C., Candela, S. G., Baker, E. H. and Marshall, H.-P. (2018): Interannual snow accumulation variability on glaciers derived from repeat, spatially extensive ground-penetrating radar surveys. *The Cryosphere Discussion*, in review, 1–43 (doi: 10.5194/tc-2018-126).

Melvold, K. (2008): Snow measurements using GPR: example from Amundsenisen, Svalbard. In: Hauck, C. and Kneisel, C. (eds.): *Applied Geophysics in Periglacial Environments*. Cambridge, Cambridge University Press, 240 pp.

MeteoSwiss (2016): *Monthly and Yearly Precipitation: RhiresM and RhiresY. Documentation of MeteoSwiss Grid-Data Products.* «http://www.meteoschweiz.admin.ch/content/dam/meteoswiss/de/Ungebundene-Seiten/Produkte/doc/ProdDoc_RhiresM.pdf» [visit: 04.06.2018].

MeteoSwiss (2017): *CATCOS.* «https://www.meteoswiss.admin.ch/home/research-and-cooperation/projects.subpage.html/en/data/projects/2011/catcos.html» [visit: 29.06.2018].

NOAA (2011): Global Historical Climatology Network-Monthly (GHCN-M). «https://www.ncdc.noaa.gov/ghcnm/» [visit: 25.05.2018].

NOAA/OAR/ESRL PSD (2018): *NOAA-CIRES Twentieth Century Reanalysis (V2c): Summary.* Boulder, Colorado, «https://www.esrl.noaa.gov/psd/data/gridded/data.20thC_Rean V2c.html» [visit: 29.05.2018].

Oerlemans, J. (2001): *Glaciers and climate change*. Lisse, Balkema Publishers, 148 pp.

O'Neel, S., Hood, E., Arendt, A. and Sass, L. (2014): Assessing streamflow sensitivity to variations in glacier mass balance. *Climate Change*, 123(2), 329–341 (doi: 10.1007/s10584-013-1042-7).

Østrem, G. and Brugman, M. (1991): Glacier mass-balance measurements. Manual for field and office work. *NHRI Science Report*, 4, Saskatchewan, Canada, National Hydrology Research Institute, 224 pp.

Palmer, M. D. , Harris, G. R. and Gregory, J. M. (2018): Extending CMIP5 projections of global mean temperature change and sea level rise due to thermal expansion using a physically-based emulator. *Environmental Research Letters*, in press (doi: 10.1088/1748-9326/aad2e).

Paterson, W. S. B. (1981): *The physics of glaciers.* New York, Pergamon Press, 380 pp.

Paul, F., Bolch, T., Kääb, A., Nagler, T., Nutz, C., Scharrer, K., Shepherd, A., Strozzi, T., Ticconi, F., Bhambri, R., Berthier, E., Bevan, S., Gourmelen, N., Heid, T., Jeong, S., Kunz, M., Lauknes, T. R., Luckman, A., Boncori, J. P. M., Moholdt, G., Muir, A., Neelmeijer, J., Rankl, M., Van Looy, J. and Van Niel, T. (2015): The glaciers climate change initiative: Methods for creating

glacier area, elevation change and velocity products. *Remote Sensing of Environment*, 162, 408–426 (doi: 10.1016/j.rse.2013.07.043).

Peel, M. C., Finlayson, B. L. and McMahon, T. A. (2007): Updated world map of the Köppen-Geiger climate classification. *Hydrology and Earth System Sciences*, 11(5), 1633–1644 (doi: 10.1029/2006GL028098).

Petrakov, D. A., Lavrientiev, I. I., Kovalenko, N. V. and Usubaliev, R. A. (2014): Ice thickness, volume and current changes of the Sary-Tor Glacier area (AK-Shyirak Massif, Inner Tian (sic.) Shan). *Earth's cryosphere*, 18(3), 83–91 (doi: 10.1016/j.gloplacha.2012.07.010).

Petrov, G. N. (2015): Water Apportioning and Runoff Regulation in the Joint Use of Water – Power Resources of Transboundary Rivers in Central Asia. *Water Resources*, 42(2), 269–274 (doi: 10.1134/S0097807815020116).

Pertziger, F. (1996): *Abramov Glacier data reference book: climate, runoff, mass balance.* Central Asian Research Hydrometeorological Institute, Tashkent.

Potter, G. L., Carriere, L., Hertz, J., Bosilovich, M., Duffy, D., Lee, T. and Williams, D. N. (2018): Enabling Reanalysis Research Using the Collaborative Reanalysis Technical Environment (CREATE). *Bulletin of the American Meteorological Society*, 99(5), 677–687 (doi: 10.1175/BAMS-D-17-0174.1).

Rasmussen, L. A. (2013): Meteorological controls on glacier mass balance in High Asia. *Annals of Glaciology*, 54(63), 352–359 (doi: 10.3189/2013AoG63A353).

Reeh, N. (2008): A nonsteady-state firn-densification model for the percolation zone of a glacier. *Journal of Geophysical Research*, 113(3), 1–13 (doi: 10.1029/2007JF000746).

Reijmer, C. and Hock, R. (2008): Internal accumulation on Storglaciaren, Sweden, in a multi-layer snow model coupled to a distributed energy-and mass-balance model. *Journal of Glaciology*, 54(184), 61–72 (doi: 10.3189/002214308784409161).

Richardson, C., Aarholt, E., Hamran, S.-E., Holmlund, P. and Isaksson, E. (1997): Spatial distribution of snow in western Dronning Maud Land, East Antarctica, mapped by a ground-based snow radar. *Journal of Geophysical Research*, 102(20), 343–353 (doi: 10.1029/97JB01441).

Richardson, S. D. and Reynolds, J. M. (2000): An overview of glacial hazards in the Himalayas. *Quaternary International,* 65, 31–47 (doi: 10.1016/S1040-6182(99)00035-X).

Schädler, B. und Weingartner, R. (2002): Ein detaillierter hydro*logischer* Blick auf die Wasserressourcen der Schweiz. *Wasser Energie Luft*, 94(7–8), 189–197.

Schmidt, S., Weber, B. and Winiger, M. (2009): Analyses of snow disappearance in an alpine valley from micro- to meso-scale (Loetschental, Switzerland). *Hydrological Processes*, 23(7), 1041–1051 (doi: 10.1002/hyp.7205).

Schneider, T. and Jansson, P. (2004): Internal accumulation in firn and its significance for the mass balance of Storglaciaren, Sweden. *Journal of Glaciology*, 50(168), 25–34 (doi: 10.3189/172756504781830277).

Schöne, T., Zech, C., Unger-Shayesteh, K., Rudenko, V., Thoss, H., Wetzel, H.-U., and Zubovich, A. (2013): A new permanent multiparameter monitoring network in Central Asian high mountains – from measurements to data bases. *Geoscientific Instrumentation, Methods and Data Systems*, 2(1), 97–111 (doi: 10.5194/gi-2-97-2013).

Schwarb, M., Frei, C., Schär, C., Daly, C. (2001): Mittlere jährliche Niederschlagshöhen im europäischen Alpenraum 1971-1990. In: Bundesamt für Umwelt BAFU (ed.): *Hydrologischer Atlas der Schweiz, Tafel 2.6*. Wabern-Bern, Bundesamt für Landestopographie.

SDSS (2018): *Sensor Data Storage System (SDSS).* «http://sdss.caiag.kg/sdss/index.php?&page=measure_page» [visit: 16.07.2018].

Sevruk, B. (1985): Systematischer Niederschlagsmessfehler in der Schweiz. In: Sevruk, B. (eds.): *Der Niederschlag in der Schweiz.* Beiträge zur Geologie der Schweiz–Hydrologie, 31, 65–75, Bern.

Siegfried, T., Bernauer, T., Guiennet, R., Sellars, S., Robertson, A., Mankin, J., Bauer-Gottwein, P., and Yakovlev, A.: Will climate change exacerbate water stress in Central Asia? *Climatic Change*, 112(3–4), 881–899 (doi: 10.1007/s10584-011-0253-z).

SLF (2018): *Lawinenbildende Faktoren*. «https://www.slf.ch/de/lawinen/lawinenkunde-und-praevention/lawinenbildende-faktoren.html» [visit: 12.06.2018].

Spreafico, M. and Weingartner, R. (2005): *Hydrologie der Schweiz. Ausgewählte Aspekte und Resultate*. Berichte des BWG, Serie Wasser, 7, Bern, Bundesamt für Wasser und Geologie BWG.

Sold, L., Huss, M., Hoelzle, M., Andereggen, H., Joerg, P. C. and Zemp, M. (2013): Methodological approaches to infer end-of-winter snow distribution on alpine glaciers. *Journal of Glaciology*, 59(218), 1047–1059 (doi: 10.3189/*2013JoG13J015)*.

Sold, L., Huss, M., Eichler, A., Schwikowski, M. and Hoelzle, M. (2015): Unlocking annual firn layer water equivalents from ground-penetrating radar data on an Alpine glacier. *The cryosphere*, 9, 1075–1087 (doi:10.5194/tc-9-1075-2015).

Sold, L., Huss, M., Machguth, H., Joerg, P. C., Vieli, G. L., Linsbauer, A., Salzmann, N., Zemp, M. and Hoelzle, M. (2016): Mass Balance Re-analysis of Findelengletscher, Switzerland; Benefits from Extensive Snow Accumulation Measurements. *Frontiers in Earth Science*, 4(18), 1–16 (doi: 10.3389/feart.2016.00018).

Sorg, A., Bolch, T., Stoffel, M., Solomina, O. and Beniston, M. (2012): Climate change impacts on glaciers and runoff in Tien Shan (Central Asia). *Nature climate change*, 2(1592), 725–731 (doi: 10.1038/NCLIMATE1592).

Sorg A, Huss, M., Rohrer, M. and Stoffel, M. (2014): The days of plenty might soon be over in glacierized Central Asian catchments. *Environmental Research Letters*, 9(10), 1–8 (doi: 10.1088/1748-9326/9/10/104018).

Sorokin, A. (2011): Scenarios of Future Development in the Aral Sea Basin. In: Madramootoo, C. and Dukhovny, V. (eds.): *Water and Food Security in Central Asia*, Dordrecht, Springer Netherlands, 121–130.

Sturm, M. and Benson, C. (2004): Scales of spatial heterogeneity for perennial and seasonal snow layers. *Annals of Glaciology*, 38, 253–260 (doi: 10.3189/172756404781815112).

Suslov, V. and Akbarov, A. (1973): Hydrological regime of glaciers in the Alay Range, Central Asia. In: *Symposium on the Hydrology of Glaciers*, Cambridge, vol. 95, 235–238.

Tapley, B. D., Bettadpur, S., Ries, J. C., Thompson, P. F. and Watkins, M. M. (2004): GRACE Measurements of Mass Variability in the Earth System. *Science*, 305(5683), 503–506 (doi: 10.1126/science.1099192).

Techel, F. and Pielmeier, C. (2011): Point observations of liquid water content in wet snow–investigating methodical, spatial and temporal aspects. *The Cryosphere*, 5, 405–418 (doi: 10.5194/tc-5-405-2011).

Unger-Shayesteh, K., Vorogushyn, S., Farinotti, D., Gafurov, A., Duethmann, D., Mandychev, A. and Merz, B. (2013): What do we know about past changes in the water cycle of Central Asian headwaters? A review. *Global and Planetary Change*, 110, 4–25 (doi: 10.1016/j.gloplacha.2013.02.004).

Van Pelt, W. J. J., Oerlemans, J., Reijmer, C. H., Pohjola, V. A., Pettersson, R. and van Angelen, J. H. (2012): Simulating melt, runoff and refreezing on Nordenskiöldbreen, Svalbard, using a coupled snow and energy balance model. *The Cryosphere*, 6, 641–659 (doi: 10.5194/tc-6-641-2012).

Van Pelt, W. J. J. and Kohler, J. (2015): Modelling the long-term mass balance and firn evolution of glaciers around Kongsfjorden, Svalbard. *Journal of Glaciology*, 61(228), 731–744 (doi: 10.3189/2015JoG14J223).

Vaughan, D. G., Comiso, J. C., Allison, I., Carrasco, J., Kaser, G., Kwok, R., Mote, P., Murray, T., Paul, F., Ren, J., Rignot, E., Solomina, O., Steffen, K. and Zhang, T. (2013): Observations: Cryosphere. In: Stocker, T. F., Qin, D., Plattner, G. - K., Tignor, M., Allen, S. K., Boschung, J., Nauels, A., Xia, Y., Bex, V. and Midgley, P. M. (eds.): *Climate Change 2013: The Physical Science Basis.* Contribution of Working Group I to the Fifth Assessment Report of the Intergovernmental Panel on Climate Change. Cambridge, Cambridge University Press, 317–382.

Walliserbote (2017): *Gefahr am Triftgletscher gebannt. Evakuierte Personen kehren in ihre Häuser zurück.* «http://www.1815.ch/news/wallis/aktuell/gletscherabsturz-bedroht-saas-grund/» [visit: 05.07.2018].

Stainbank (2018): *Simulation of Abramov Glacier energy balance and firn properties.* Master thesis, University of Fribourg, Fribourg.

Weingartner, R. and Aschwanden, H. (1992): Abflussregimes als Grundlage zur Abschätzung von Mittelwerten des Abflusses. In: Bundesamt für Umwelt BAFU (ed.): *Hydrologischer Atlas der Schweiz, Tafel 5.2*. Wabern-Bern, Bundesamt für Landestopographie.

WGMS (2005): *Fluctuations of Glaciers 1995–2000 (Volume VIII)*. Haeberli, W., Zemp, M., Frauenfelder, R., Hoelzle, M. and Kääb, A. (eds.): IUGG(CCS) / UNEP / UNESCO. Zürich, World Glacier Monitoring Service, 288 pp.

WGMS (2009): *Glacier Mass Balance Bulletin No. 10 (2006–2007)*. Haeberli, W., Gärtner-Roer, I., Hoelzle, M., Paul, F., Zemp, M. I. (eds.): ICSU (WDS) / IUGG (IACS) / UNEP / UNESCO / WMO. Zürich, World Glacier Monitoring Service, 96 pp.

WGMS (2013): *Glacier Mass Balance Bulletin No. 12 (2010–2012)*: Zemp, M., Nussbaumer, S. U., Naegeli, K., Gärtner-Roer, I., Paul, F., Hoelzle, M. and Haeberli, W. (eds.): ICSU (WDS) / IUGG (IACS) / UNEP / UNESCO / WMO. Zürich, World Glacier Monitoring Service, 106 pp.

WGMS (2015): *Global Glacier Change Bulletin No. 1 (2012–2013)*. Zemp, M., Gärtner-Roer, I., Nussbaumer, S.U., Hüsler, F., Machguth, H., Mölg, N., Paul F. and Hoelzle, M. (eds.): ICSU(WDS) / IUGG(IACS) / UNEP / UNESCO / WMO. Zürich, World Glacier Monitoring Service, 230 pp.

WMO (2008): *Guide to Meteorological Instruments and Methods of Observation. WMO-No. 8*. Geneva, World Meteorological Organisation, 681 pp.

Zemp, M., Thibert, E., Huss, M., Stumm, D. and Denby, C. R.: Reanalysing glacier mass balance measurement series. *The Cryosphere*, 7(4), 1227–1245 (doi: 10.5194/tc-7-1227-2013).

Appendix A: Personal field equipment

Recommended personal equipment for fieldwork and camping at temperatures between -10 and -25 °C (Horst Machguth and Marlene Kronenberg, University of Fribourg). Considering the challenges of high altitude, it is recommended to carefully study the medical book of Berghold et al. (2015): Handbuch der Trekking- und Höhenmedizin.

Mountaineering equipment
- warm mountain boots
- touring skis with skins and ski boots and poles
- avalanche beacon, shovel, probe
- climbing harness with at least three carbines
- prusik ropes, ice screws, crevasse rescue kit
- ice axe
- crampons
- backpack for day trips on the glacier (about 40 - 50 l volume)
- ski helmet (not mandatory, only if you want to bring one)

Personal equipment
- very warm winter boots (comfort zone down to -40°C or lower)
- down jacket (as warm as possible)
- Gore Tex jacket or similar
- warm Gore Tex pants or similar
- several fleece jackets (or wool)
- several pairs of warm woolly (e.g. IceBreaker) underwear (underpants, t-shirts, long sleeves)
- several pairs of warm woolly socks
- vapour barrier socks (if you do not have them, you can also use plastic bags - we will bring them)
- normal touring pants (maybe two pairs)
- dark sun glasses
- skiing goggles
- sun screen
- lip balm
- seat pad (not mandatory, only if you want to bring one)
- several pairs of gloves (fleece, woolly, thick down mittens)
- hats (woolly, more than one if possible)
- balaclava (=face mask)
- warm scarf or buff
- personal medication

Camping gear

- head lamp
- toilet set
- pocket knife
- Thermos bottle (about 1l volume)
- tent (not mandatory, only if you have a very sturdy personal tent you want to use - we will also bring some sleeping tents)
- very warm sleeping bag (down to -20 °C)
- warm sleeping bag (down to -5°C, two of them if you want to combine them)
- liner (silk or cotton, for inside the sleeping bag)
- foam sleeping pad
- inflatable sleeping pad (e.g. Thermarest, Exped down)
- little portable gas stove (not mandatory, only if you have one)

Appendix B: Soviet snow depth distribution raster parameter calculations

Table 13: Best regressions for Soviet December SDD using 3 explaining parameters.

results_auto2_BestRegressionsSDD_NS_Dec.csv - Editor

Datei Bearbeiten Format Ansicht ?

"R.2"	"Terrainparameterchoice"
0.670923975316012	"Tiefe ~ Z_m + FOPDdyNS + WinterNS_Dez , data=tab"
0.668384158288227	"Tiefe ~ Z_m + FOPDdxEW_1 + WinterNS_Dez , data=tab"
0.669674715901011	"Tiefe ~ Z_m + FOPDdxEW_2 + WinterNS_Dez , data=tab"
0.670944573716715	"Tiefe ~ Z_m + FOPDdyNS_s + WinterNS_Dez , data=tab"
0.670961747073189	"Tiefe ~ Z_m + FOPDdyNS_m + WinterNS_Dez , data=tab"
0.671210662782773	"Tiefe ~ Z_m + FOPDdyNS_1 + WinterNS_Dez , data=tab"
0.671507504620557	"Tiefe ~ Z_m + FOPDdyNS_2 + WinterNS_Dez , data=tab"
0.669461716102244	"Tiefe ~ Z_m + ProfCurv_1 + WinterNS_Dez , data=tab"
0.668295201800229	"Tiefe ~ Z_m + slope_majo + WinterNS_Dez , data=tab"
0.668159240080456	"Tiefe ~ Z_m + SOPDdxx__1 + WinterNS_Dez , data=tab"
0.668398017326059	"Tiefe ~ Z_m + SOPDdyy__1 + WinterNS_Dez , data=tab"
0.668823173450676	"Tiefe ~ Z_m + TangCurv_1 + WinterNS_Dez , data=tab"

"Intercept"	"a_V1"	"b_V2"	"c_V3"
-7.96809023033413	0.00207643219419636	0.423665398073532	0.00491361738436368
-7.69875105284935	0.00201422401363656	0.231157669857967	0.00491164896332099
-7.62079927717723	0.0019968505657838	0.267251554074892	0.00491593317044305
-8.01673137871691	0.00208585699112716	0.00712005156123276	0.00491425495916378
-8.01924495879536	0.00208644901117452	0.561608054572854	0.00491437720291179
-8.01590375581	0.00208528683446878	0.57788671401257	0.00491306646552034
-7.98325475819137	0.00208166485920464	0.38350961495194	0.00491860078423343
-7.90302013265776	0.00206650496742656	-75.3576059098685	0.00491399268136354
-7.72794396253144	0.00203041714849039	-0.00455461215326248	0.00491533535164738
-7.77235341545113	0.00203465376984065	-26.5054995879768	0.00491130444605247
-7.80827028479611	0.00204309473691551	-47.5823730202414	0.00491357985059895
-7.69470561340866	0.00201593590809792	-55.8450839768619	0.00491409298271379

Table 14: Best regressions for Soviet January SDD using 3 explaining parameters.

results_auto2_BestRegressionsSDD_NS_Jan.csv - Editor

Datei Bearbeiten Format Ansicht ?

"R.2"	"Terrainparameterchoice"
0.688270047406966	"Tiefe ~ Z_m + FOPDdyNS + WinterNS_Jan , data=tab"
0.686057851176584	"Tiefe ~ Z_m + FOPDdxEW_2 + WinterNS_Jan , data=tab"
0.687437189605718	"Tiefe ~ Z_m + FOPDdyNS_s + WinterNS_Jan , data=tab"
0.687459651281207	"Tiefe ~ Z_m + FOPDdyNS_m + WinterNS_Jan , data=tab"
0.688076987629127	"Tiefe ~ Z_m + FOPDdyNS_1 + WinterNS_Jan , data=tab"
0.688765092831289	"Tiefe ~ Z_m + FOPDdyNS_2 + WinterNS_Jan , data=tab"
0.686778652221973	"Tiefe ~ Z_m + ProfCurv_1 + WinterNS_Jan , data=tab"
0.686453896312188	"Tiefe ~ Z_m + SOPDdyy__1 + WinterNS_Jan , data=tab"
0.68719900790229	"Tiefe ~ Z_m + TangCurv_1 + WinterNS_Jan , data=tab"

"Intercept"	"a_V1"	"b_V2"	"c_V3"
-9.08946631484375	0.00237325207682504	0.508125118722574	0.00456613099252266
-8.69135261176676	0.00228246002860574	0.286045744288949	0.00456520988171872
-9.1144313571813	0.00237739852420384	0.00769564922321161	0.00456609442227669
-9.11745151829713	0.00237810612358991	0.607433153097403	0.00456620991499786
-9.13108861474	0.00238059252878421	0.654181778407293	0.00456591945969086
-9.09804231107553	0.00237743868789581	0.446243864543983	0.00456983932321461
-8.97725712880058	0.0023532983840156	-95.6987937616768	0.00456313096679324
-8.88771954543645	0.00233095785583633	-78.8260207422065	0.00456492994180271
-8.70383075191802	0.00228736749329488	-88.7098287823447	0.0045605286991975

Table 15: Best regressions for Soviet February SDD using 3 explaining parameters.

results_auto2_BestRegressionsSDD_NS_Feb.csv - Editor

Datei Bearbeiten Format Ansicht ?

"R.2"	"Terrainparameterchoice"
0.68184503328115	"Tiefe ~ Z_m + FOPDdyNS + WinterNS_Feb , data=tab"
0.681286178944198	"Tiefe ~ Z_m + FOPDdyNS_s + WinterNS_Feb , data=tab"
0.681309369918896	"Tiefe ~ Z_m + FOPDdyNS_m + WinterNS_Feb , data=tab"
0.681669260374137	"Tiefe ~ Z_m + FOPDdyNS_1 + WinterNS_Feb , data=tab"
0.682951173546899	"Tiefe ~ Z_m + FOPDdyNS_2 + WinterNS_Feb , data=tab"
0.681627631363396	"Tiefe ~ Z_m + ProfCurv_1 + WinterNS_Feb , data=tab"
0.681120487710109	"Tiefe ~ Z_m + slope_majo + WinterNS_Feb , data=tab"
0.68130242263774	"Tiefe ~ Z_m + SOPDdyy__1 + WinterNS_Feb , data=tab"
0.683036189751226	"Tiefe ~ Z_m + TangCurv_1 + WinterNS_Feb , data=tab"

"Intercept"	"a_V1"	"b_V2"	"c_V3"
-10.4699453380174	0.0027981134419111	0.493758909657342	0.003628576066537
-10.4967429001599	0.00280287136242786	0.00734272790975719	0.00362978401857469
-10.4998368956014	0.00280358074571119	0.58067879644012	0.00362985614162473
-10.5081879832659	0.00280489451856044	0.621171846673148	0.00362916232534848
-10.5061831002054	0.00280814961812132	0.47995210981936	0.00363593370415512
-10.4166191195135	0.00279198767626922	-103.720971486129	0.00363406543869288
-10.1674702498024	0.00274433211829791	-0.00858129132311971	0.00362754272111748
-10.3276401470222	0.00277013395959279	-85.3752009985831	0.00363251734294858
-10.0868001174674	0.00271243389365241	-111.329428016795	0.00363266031723088

Table 16: Best regressions for Soviet February SDD using 4 explaining parameters.

results_auto2_BestRegressionsSDD4Param_NS_Feb.csv - Editor

Datei Bearbeiten Format Ansicht ?

"R.2"	"Terrainparameterchoice"
0.686170511508804	"Tiefe ~ Z_m + FOPDdyNS + SOPDdyy__1 + WinterNS_Feb , data=tab"
0.686202251283718	"Tiefe ~ Z_m + FOPDdyNS + TangCurv_1 + WinterNS_Feb , data=tab"
0.685636375188712	"Tiefe ~ Z_m + FOPDdyNS_s + SOPDdyy__1 + WinterNS_Feb , data=tab"
0.686047160556229	"Tiefe ~ Z_m + FOPDdyNS_s + TangCurv_1 + WinterNS_Feb , data=tab"
0.6856656322095	"Tiefe ~ Z_m + FOPDdyNS_m + SOPDdyy__1 + WinterNS_Feb , data=tab"
0.686046487403157	"Tiefe ~ Z_m + FOPDdyNS_m + TangCurv_1 + WinterNS_Feb , data=tab"
0.685580083820697	"Tiefe ~ Z_m + FOPDdyNS_1 + SOPDdyy__1 + WinterNS_Feb , data=tab"
0.685901903800795	"Tiefe ~ Z_m + FOPDdyNS_1 + TangCurv_1 + WinterNS_Feb , data=tab"
0.685785618144451	"Tiefe ~ Z_m + FOPDdyNS_2 + ProfCurv_1 + WinterNS_Feb , data=tab"
0.685282589980797	"Tiefe ~ Z_m + FOPDdyNS_2 + SOPDdyy_su + WinterNS_Feb , data=tab"
0.685311668782946	"Tiefe ~ Z_m + FOPDdyNS_2 + SOPDdyy_me + WinterNS_Feb , data=tab"
0.687179389910835	"Tiefe ~ Z_m + FOPDdyNS_2 + SOPDdyy__1 + WinterNS_Feb , data=tab"
0.687272457154581	"Tiefe ~ Z_m + FOPDdyNS_2 + TangCurv_1 + WinterNS_Feb , data=tab"
0.685720572448698	"Tiefe ~ Z_m + slope_majo + TangCurv_1 + WinterNS_Feb , data=tab"

"Intercept"	"a_V1"	"b_V2"	"c_V3"	"d_V4"
-10.6366039692798	0.00283681415291785	0.641682219876778	-115.285026803294	0.00363548112111218
-10.3058704936685	0.00275908151502978	0.501821770516714	-112.644531235679	0.00363369501428042
-10.6881069458132	0.00284651883102727	0.0100167354565663	-116.308203361082	0.00363724967252335
-10.3452123715972	0.00276622466306812	0.0080678506154079	-118.03890829568	0.00363534572664626
-10.6919490663629	0.00284740946858193	0.791106132105326	-116.380865237301	0.00363734822463844
-10.3477509733444	0.00276683719795123	0.634868397265613	-117.714370841881	0.0036353981024561
-10.6658969946138	0.00284117009356188	0.772030248401305	-108.5830842987	0.00363577062800003
-10.3419173550272	0.00276545910665965	0.618566307391174	-111.012831804385	0.00363418519916596
-10.6695116734248	0.00284818737661719	0.479154692046545	-103.468371738618	0.0036423530023944
-10.5032037251971	0.00280416589778987	0.57939247484005	-0.621141664467172	0.00364249774894156
-10.5024108189994	0.00280394309037562	0.580374035704365	-49.2624564416861	0.0036425303321106
-10.6597501608671	0.00284448909462254	0.582289021670718	-112.972158232875	0.00364419195286988
-10.3412189666527	0.0027689630222546	0.483657008528549	-112.171778941363	0.00364107976897707
-9.98888548165427	0.00270286272691056	-0.00920097884979738	-115.883926077855	0.00363278742367668

Table 17: Best regressions for Soviet March SDD using 3 explaining parameters.

results_auto2_BestRegressionsSDD_NS_Mrz.csv - Editor

Datei Bearbeiten Format Ansicht ?

"R.2"	"Terrainparameterchoice"
0.697460314845368	"Tiefe ~ Z_m + FOPDdyNS + WinterNS_Mrz , data=tab"
0.697087040674677	"Tiefe ~ Z_m + FOPDdyNS_1 + WinterNS_Mrz , data=tab"
0.6980156396504	"Tiefe ~ Z_m + FOPDdyNS_2 + WinterNS_Mrz , data=tab"
0.698131860548355	"Tiefe ~ Z_m + ProfCurv_1 + WinterNS_Mrz , data=tab"
0.697438368434956	"Tiefe ~ Z_m + SOPDdyy__1 + WinterNS_Mrz , data=tab"
0.698018529909183	"Tiefe ~ Z_m + TangCurv_1 + WinterNS_Mrz , data=tab"

"Intercept"	"a_V1"	"b_V2"	"c_V3"
-12.8701908257578	0.00339987508432611	0.592504529051625	0.00401889582880267
-12.9055970255698	0.00340563957317204	0.723441312219808	0.00402089396974497
-12.8885041451752	0.00340636988098951	0.531334054598016	0.0040240463034962
-12.8432082713499	0.00340105962171708	-139.419519489746	0.00402896669123716
-12.7071739795448	0.00336793809505876	-111.289036301249	0.00402534133394133
-12.438633122177	0.00330384114013787	-121.217492824433	0.00402180462703709

Table 18: Best regressions for Soviet April SDD using 3 explaining parameters.

results_auto2_BestRegressionsSDD_NS_Apr.csv - Editor

Datei Bearbeiten Format Ansicht ?

"R.2"	"Terrainparameterchoice"
0.615129684731978	"Tiefe ~ Z_m + Slope + WinterNS_Apr , data=tab"
0.617730781772016	"Tiefe ~ Z_m + FOPDdyNS + WinterNS_Apr , data=tab"
0.615333013880915	"Tiefe ~ Z_m + FOPDdxEW_1 + WinterNS_Apr , data=tab"
0.61558645933262	"Tiefe ~ Z_m + FOPDdxEW_2 + WinterNS_Apr , data=tab"
0.6167560034321	"Tiefe ~ Z_m + FOPDdyNS_s + WinterNS_Apr , data=tab"
0.616766540161682	"Tiefe ~ Z_m + FOPDdyNS_m + WinterNS_Apr , data=tab"
0.616873841696105	"Tiefe ~ Z_m + FOPDdyNS_1 + WinterNS_Apr , data=tab"
0.617362590430891	"Tiefe ~ Z_m + FOPDdyNS_2 + WinterNS_Apr , data=tab"
0.615030088103103	"Tiefe ~ Z_m + ProfCurv_s + WinterNS_Apr , data=tab"
0.615040970648936	"Tiefe ~ Z_m + ProfCurv_m + WinterNS_Apr , data=tab"
0.615487221439765	"Tiefe ~ Z_m + ProfCurv_1 + WinterNS_Apr , data=tab"
0.61515943897787	"Tiefe ~ Z_m + slope_majo + WinterNS_Apr , data=tab"
0.615311608965193	"Tiefe ~ Z_m + SOPDdyy__1 + WinterNS_Apr , data=tab"
0.616352159455383	"Tiefe ~ Z_m + TangCurv_1 + WinterNS_Apr , data=tab"

"Intercept"	"a_V1"	"b_V2"	"c_V3"
-15.8914163172847	0.00412994202224416	-0.0103488995111137	0.00406892662616292
-16.379261567612	0.00422118242083993	0.886639257168723	0.00405557085381453
-15.7833456910321	0.00408085047171032	0.569107579080352	0.00406822715462244
-15.7084333291036	0.0040672087721678	0.469922086710098	0.00406828467368144
-16.4114136735766	0.0042255646764077	0.013101217781635	0.00405935505866751
-16.4157991785707	0.00422662817787304	1.03244171618794	0.00405928991677359
-16.4090471547382	0.00422462685944623	1.05194294165448	0.00405748219655348
-16.3464256481231	0.00421771510996605	0.70882135243299	0.00405647633445617
-16.1429189124863	0.00417151661818675	-0.728458629098491	0.00407082845647961
-16.1433488561575	0.00417162525606683	-57.1516485217193	0.00407083006779799
-16.1607522471237	0.00417864308565	-135.153080640302	0.00407027463328651
-15.8373528268456	0.00411692624094008	-0.0113104080791184	0.00406582017159385
-16.0388981321712	0.0041482759663063	-114.639328789363	0.00407301261376873
-15.756068756825	0.00408106365186368	-140.677792572178	0.00407149117710093

Appendix C: TWT to water equivalent

TWT [ns]	m w.e.	Höhe [m.ü.M.]	Tiefe [m]	real effective dielectric constant (nach Kovacs et al. 1995:246)[26]
1.657	0.043	4381	0.2	1.542
3.149	0.09	4381	0.4	1.393
4.908	0.139	4381	0.6	1.503
6.462	0.193	4381	0.8	1.466
8.221	0.259	4381	1	1.519
10.062	0.331	4381	1.2	1.580
11.789	0.402	4381	1.4	1.593
13.276	0.475	4381	1.6	1.547
15.244	0.562	4381	1.8	1.612
17.038	0.629	4381	2	1.631
19.05	0.734	4381	2.2	1.685
20.843	0.819	4381	2.4	1.695
22.549	0.903	4381	2.6	1.690
24.343	0.985	4381	2.8	1.698
26.385	1.076	4381	3	1.738
28.484	1.198	4381	3.2	1.780
30.278	1.3	4381	3.4	1.782
32.377	1.408	4381	3.6	1.817
34.171	1.514	4381	3.8	1.817
36.139	1.624	4381	4	1.834
38.195	1.751	4381	4.2	1.858
40.248	1.865	4381	4.4	1.880
42.173	1.982	4381	4.6	1.889
44.098	2.09	4381	4.8	1.896
46.153	2.203	4381	5	1.914
48.122	2.324	4381	5.2	1.924
50.134	2.462	4381	5.4	1.937
52.332	2.587	4381	5.6	1.962
54.433	2.703	4381	5.8	1.979
56.506	2.821	4381	6	1.993
1.643	0.057	4240	0.2	1.516
3.44	0.132	4240	0.4	1.662
5.269	0.211	4240	0.6	1.733
6.899	0.281	4240	0.8	1.671
8.756	0.366	4240	1	1.723
10.538	0.456	4240	1.2	1.733
12.433	0.549	4240	1.4	1.772
14.419	0.64	4240	1.6	1.825
16.238	0.723	4240	1.8	1.829

[26] Formula for first value (line 5, row A=TWT, row D=Tiefe): =(A5*10^-9*299792458/(2*D5))^2

18.134	0.804	4240	2	1.847
19.801	0.887	4240	2.2	1.820
21.659	0.987	4240	2.4	1.830
23.618	1.087	4240	2.6	1.854
25.437	1.204	4240	2.8	1.854
27.522	1.319	4240	3	1.891
29.607	1.446	4240	3.2	1.923
31.73	1.573	4240	3.4	1.957
33.829	1.715	4240	3.6	1.984
35.952	1.835	4240	3.8	2.011
37.847	1.946	4240	4	2.012
39.894	2.065	4240	4.2	2.027
41.862	2.192	4240	4.4	2.034
44.023	2.331	4240	4.6	2.058
46.221	2.475	4240	4.8	2.083
48.382	2.61	4240	5	2.104
50.429	2.749	4240	5.2	2.113
52.581	2.885	4240	5.4	2.130
54.893	3.067	4240	5.6	2.159
57.167	3.232	4240	5.8	2.183
59.541	3.388	4240	6	2.213
	0.047	3971	0.2	
3.329	0.104	3971	0.4	1.556
5.026	0.172	3971	0.6	1.577
6.797	0.236	3971	0.8	1.622
8.51	0.301	3971	1	1.627
10.28	0.366	3971	1.2	1.649
11.994	0.438	3971	1.4	1.649
13.425	0.483	3971	1.57	1.643
	0.061	3867	0.2	
3.424	0.125	3867	0.4	1.646
5.199	0.196	3867	0.6	1.687
6.932	0.266	3867	0.8	1.687
8.58	0.339	3867	1	1.654
10.356	0.412	3867	1.2	1.673
11.243	0.449	3867	1.3	1.681
	0.053	4168	0.2	
	0.106	4168	0.4	
5.1	0.159	4168	0.6	1.623
6.639	0.223	4168	0.8	1.547
8.564	0.293	4168	1	1.648
10.296	0.367	4168	1.2	1.654
12.028	0.441	4168	1.4	1.658
13.856	0.517	4168	1.6	1.685
15.588	0.593	4168	1.8	1.685
17.353	0.663	4168	2	1.691
19.182	0.742	4168	2.2	1.708
21.01	0.827	4168	2.4	1.722

22.982	0.961	4168	2.6	1.756
23.896	1.048	4168	2.7	1.760

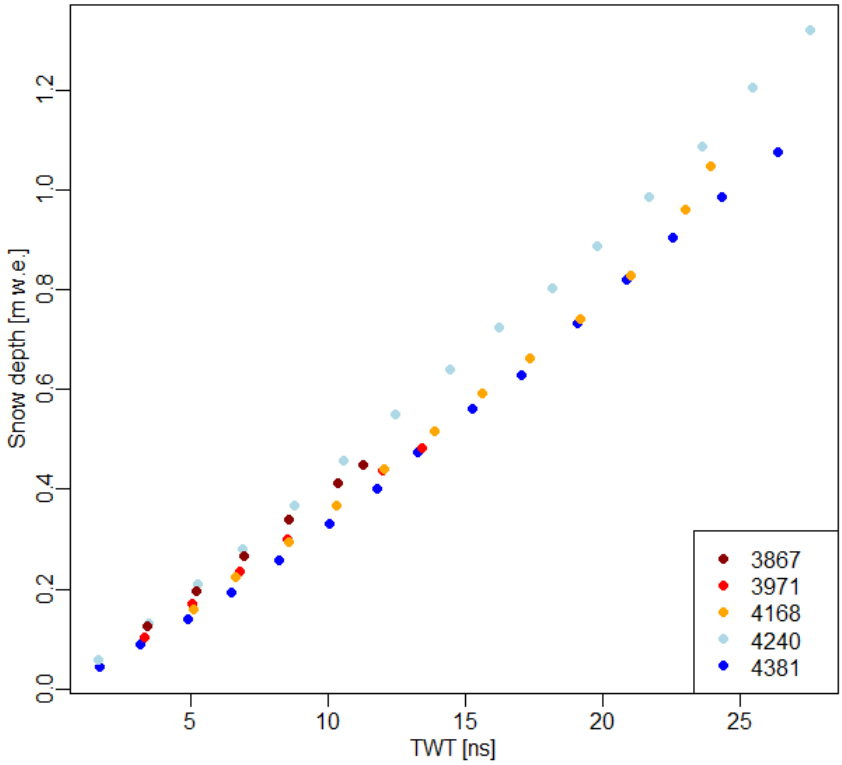


Figure 41: Relationship between TWT and water equivalent from two firn cores and three snow pits with altitude.

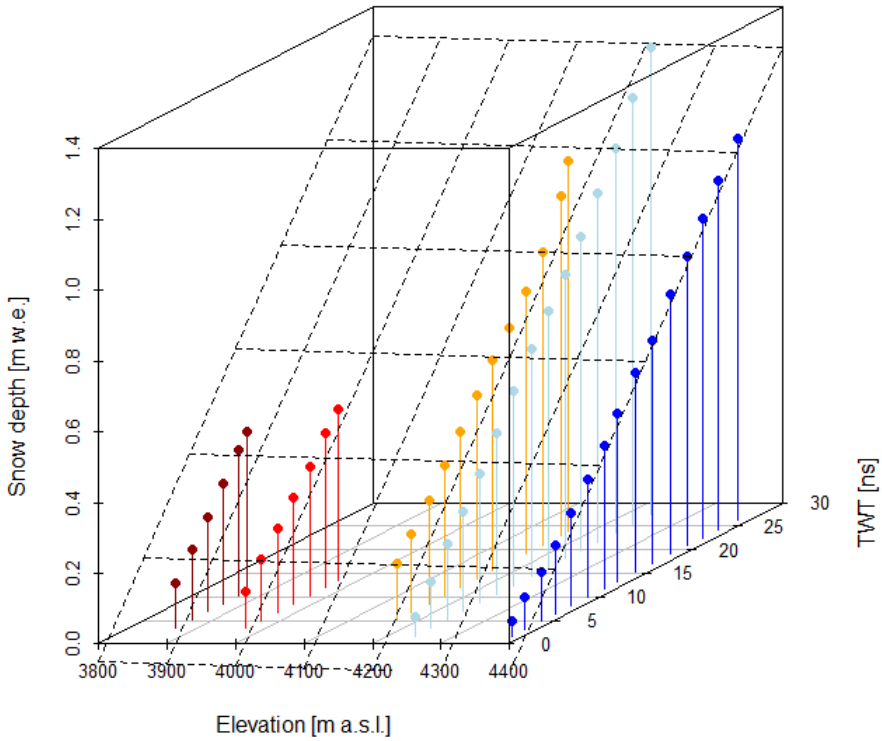


Figure 42: Relationship between TWT, water equivalent and elevation in 3D with regression plain.

Appendix D: Soviet PM raster parameter calculations

Table 19: Best regressions for Soviet December water equivalents using 4 explaining parameters.

results_auto2_BestRegressions4Param_Dez.csv - Editor

Datei Bearbeiten Format Ansicht ?

"R.2"	"Terrainparameterchoice"
0.71422064040299	"we ~ SDD_Dec + X100m_ProfCurv_2 + WinterNS_Dez + WinterNS_Jan , data=tab"
0.710939196687366	"we ~ SDD_Dec + X100m_ProfCurv_2 + WinterNS_Dez + WinterNS_Feb , data=tab"
0.715909529584548	"we ~ SDD_Dec + X100m_SOPDdxx_ma + WinterNS_Dez + WinterNS_Jan , data=tab"
0.712915661227306	"we ~ SDD_Dec + X100m_SOPDdxx_ma + WinterNS_Dez + WinterNS_Feb , data=tab"
0.710805318956375	"we ~ SDD_Dec + X100m_TangCurv_2 + WinterNS_Dez + WinterNS_Jan , data=tab"
0.713658320096823	"we ~ SDD_Jan + X100m_ProfCurv_2 + WinterNS_Dez + WinterNS_Jan , data=tab"
0.710383607446211	"we ~ SDD_Jan + X100m_ProfCurv_2 + WinterNS_Dez + WinterNS_Feb , data=tab"
0.715050772964307	"we ~ SDD_Jan + X100m_SOPDdxx_ma + WinterNS_Dez + WinterNS_Jan , data=tab"
0.71206739043317	"we ~ SDD_Jan + X100m_SOPDdxx_ma + WinterNS_Dez + WinterNS_Feb , data=tab"
0.710246279242826	"we ~ SDD_Jan + X100m_TangCurv_2 + WinterNS_Dez + WinterNS_Jan , data=tab"
0.714037407084687	"we ~ SDD_Feb + X100m_ProfCurv_2 + WinterNS_Dez + WinterNS_Jan , data=tab"
0.710758124672683	"we ~ SDD_Feb + X100m_ProfCurv_2 + WinterNS_Dez + WinterNS_Feb , data=tab"
0.715630183963729	"we ~ SDD_Feb + X100m_SOPDdxx_ma + WinterNS_Dez + WinterNS_Jan , data=tab"
0.712639709498932	"we ~ SDD_Feb + X100m_SOPDdxx_ma + WinterNS_Dez + WinterNS_Feb , data=tab"
0.710625144692746	"we ~ SDD_Feb + X100m_TangCurv_2 + WinterNS_Dez + WinterNS_Jan , data=tab"
0.714022795171606	"we ~ SDD_Mrz + X100m_ProfCurv_2 + WinterNS_Dez + WinterNS_Jan , data=tab"
0.710743691068058	"we ~ SDD_Mrz + X100m_ProfCurv_2 + WinterNS_Dez + WinterNS_Feb , data=tab"
0.715607700561416	"we ~ SDD_Mrz + X100m_SOPDdxx_ma + WinterNS_Dez + WinterNS_Jan , data=tab"
0.71261750470571	"we ~ SDD_Mrz + X100m_SOPDdxx_ma + WinterNS_Dez + WinterNS_Feb , data=tab"
0.710610442413914	"we ~ SDD_Mrz + X100m_TangCurv_2 + WinterNS_Dez + WinterNS_Jan , data=tab"
0.714262382753761	"we ~ SDD_Apr + X100m_ProfCurv_2 + WinterNS_Dez + WinterNS_Jan , data=tab"
0.71098044216635	"we ~ SDD_Apr + X100m_ProfCurv_2 + WinterNS_Dez + WinterNS_Feb , data=tab"
0.715973463879919	"we ~ SDD_Apr + X100m_SOPDdxx_ma + WinterNS_Dez + WinterNS_Jan , data=tab"
0.712978813490176	"we ~ SDD_Apr + X100m_SOPDdxx_ma + WinterNS_Dez + WinterNS_Feb , data=tab"
0.710846197646643	"we ~ SDD_Apr + X100m_TangCurv_2 + WinterNS_Dez + WinterNS_Jan , data=tab"
0.71404412221236	"we ~ SDD_mean + X100m_ProfCurv_2 + WinterNS_Dez + WinterNS_Jan , data=tab"
0.710764759146714	"we ~ SDD_mean + X100m_ProfCurv_2 + WinterNS_Dez + WinterNS_Feb , data=tab"
0.715640446165184	"we ~ SDD_mean + X100m_SOPDdxx_ma + WinterNS_Dez + WinterNS_Jan , data=tab"
0.712649842645328	"we ~ SDD_mean + X100m_SOPDdxx_ma + WinterNS_Dez + WinterNS_Feb , data=tab"
0.710631763131829	"we ~ SDD_mean + X100m_TangCurv_2 + WinterNS_Dez + WinterNS_Jan , data=tab"
0.71166129539304	"we ~ Hoehe + X100m_ProfCurv_2 + WinterNS_Dez + WinterNS_Jan , data=tab"
0.714076598749001	"we ~ Hoehe + X100m_SOPDdxx_ma + WinterNS_Dez + WinterNS_Jan , data=tab"
0.711080209986597	"we ~ Hoehe + X100m_SOPDdxx_ma + WinterNS_Dez + WinterNS_Feb , data=tab"
0.710501474093945	"we ~ Hoehe + X100m_TangCurv_2 + WinterNS_Dez + WinterNS_Jan , data=tab"
0.7175150343933	"we ~ FOPDdxEW + X100m_slope_majo + WinterNS_Dez + WinterNS_Jan , data=tab"
0.71470051407777	"we ~ FOPDdxEW + X100m_slope_majo + WinterNS_Dez + WinterNS_Feb , data=tab"
0.718369503250194	"we ~ X100m_FOPDdxEW_s + X100m_slope_majo + WinterNS_Dez + WinterNS_Jan , data=tab"
0.715514900076364	"we ~ X100m_FOPDdxEW_s + X100m_slope_majo + WinterNS_Dez + WinterNS_Feb , data=tab"
0.710067550544246	"we ~ X100m_FOPDdxEW_s + X100m_slope_majo + WinterNS_Dez + WinterNS_Apr , data=tab"
0.719262766537174	"we ~ X100m_FOPDdxEW_m + X100m_slope_majo + WinterNS_Dez + WinterNS_Jan , data=tab"
0.716384112319862	"we ~ X100m_FOPDdxEW_m + X100m_slope_majo + WinterNS_Dez + WinterNS_Feb , data=tab"
0.710941903252035	"we ~ X100m_FOPDdxEW_m + X100m_slope_majo + WinterNS_Dez + WinterNS_Apr , data=tab"
0.721096453445422	"we ~ X100m_FOPDdxEW_1 + X100m_slope_majo + WinterNS_Dez + WinterNS_Jan , data=tab"
0.718194406802097	"we ~ X100m_FOPDdxEW_1 + X100m_slope_majo + WinterNS_Dez + WinterNS_Feb , data=tab"
0.712800044016374	"we ~ X100m_FOPDdxEW_1 + X100m_slope_majo + WinterNS_Dez + WinterNS_Apr , data=tab"
0.711979910106181	"we ~ X100m_FOPDdxEW_2 + X100m_slope_majo + WinterNS_Dez + WinterNS_Jan , data=tab"
0.723943616826846	"we ~ X100m_ProfCurv_1 + X100m_slope_majo + WinterNS_Dez + WinterNS_Jan , data=tab"
0.72064471480276	"we ~ X100m_ProfCurv_1 + X100m_slope_majo + WinterNS_Dez + WinterNS_Feb , data=tab"
0.715710124574526	"we ~ X100m_ProfCurv_1 + X100m_slope_majo + WinterNS_Dez + WinterNS_Apr , data=tab"
0.712872901496737	"we ~ X100m_ProfCurv_2 + X100m_TangCurv_1 + WinterNS_Dez + WinterNS_Jan , data=tab"

"Intercept"	"a_V1"	"b_V2"	"c_V3"	"d_V4"
-0.163028524676689	0.391789301224244	-75.4329671464319	0.00202723078153253	-0.000523064437877727
-0.144119912479788	0.388204743489047	-75.8169546598743	0.00200931662166832	-0.000470038225445467
-0.205086941466429	0.461462915028593	-30.6490530932184	0.00203630434861455	-0.00052074315143945
-0.185666670389476	0.457973947152651	-30.8764605406104	0.0020186985202715	-0.000470169388093627
-0.21890581026099	0.471776300873462	-30.0826751541107	0.00204744282661341	-0.000517331358120724
-0.162761603112768	0.385682362259715	-76.4624119698769	0.00202743761304288	-0.000523146800533358
-0.14382748545976	0.382145342530282	-76.8382275755536	0.0020095260208396	-0.000470177583048415
-0.205594235648079	0.455630729268757	-31.0515489890934	0.00203680071620753	-0.000520804530289596
-0.186137779116044	0.452181945707228	-31.2761375626187	0.00201920020249027	-0.000470319741219306
-0.219755080990777	0.465992250034442	-30.5875906921903	0.00204801148751826	-0.000517351676768667
-0.175805644498876	0.402610117670231	-75.7755494923692	0.0020273023349549	-0.000523092917667074
-0.156770851207661	0.398923648862148	-76.1568236475055	0.00200938890377099	-0.000470085001502507
-0.220424679509329	0.474679735312811	-30.7830665329429	0.0020364720030461	-0.000520764841572703
-0.200877789921158	0.471089480518046	-31.0095361852609	0.0020188678023814	-0.000470219868604688
-0.234695172748099	0.485346418053521	-30.2510798825879	0.00204763436054044	-0.00051733919254859
-0.189000564821353	0.415655947843783	-75.8029392956352	0.0020273061856308	-0.000523095102377596
-0.169844207933118	0.411849800662258	-76.1839943179203	0.00200939283815914	-0.000470088696371363
-0.23600572343063	0.490099658039057	-30.7937697741366	0.00203648324814662	-0.000520766456997588
-0.216340127450301	0.486392670558529	-31.0201641316554	0.00201887920400631	-0.000470223848556468
-0.250635223482162	0.501117722963379	-30.2644811291507	0.0020476475081123	-0.000517339703514271
-0.150093145336849	0.379314392127277	-75.3535898966564	0.00202721375007636	-0.000523057599630856
-0.131304978727224	0.375844585282392	-75.7382084248074	0.00200929943291466	-0.000470027181059405
-0.189791630298461	0.446666918363811	-30.6180418021531	0.00203626500937292	-0.000520737863007228
-0.170489447705558	0.44329010477002	-30.8456665635278	0.00201865881722561	-0.000470157466534973
-0.203244635401292	0.45663746451109	-30.0436207488006	0.00204739802301313	-0.000517329294937032
-0.167730226400807	0.394611717086264	-75.76234294896	0.00202729892701499	-0.000523091795068818
-0.148769719298943	0.390998586992227	-76.1437229651492	0.00200938547638194	-0.000470083196309056
-0.210893048681004	0.465231895864835	-30.7778466701087	0.00203646482373154	-0.000520763977573668
-0.191418651789059	0.461713143005267	-31.0043532835983	0.0020188605679172	-0.000470217909953189
-0.224945275904527	0.475684128624206	-30.2445742388338	0.00204762618676973	-0.00051733887197194
-1.7137154919697	0.000455094475434682	-76.6037935847463	0.00202811968655425	-0.000523317386936045
-2.04714094048779	0.000539853356417666	-31.2434340394857	0.00203743944515177	-0.000521115986143129
-2.01354884063175	0.000535716282094257	-31.4685485684667	0.00201981287716635	-0.000470517173865224
-2.10653187369072	0.000552857886870306	-31.0556323000348	0.00204848580470633	-0.000517682330899135
0.683533567947752	1.10784342220278	-0.113439605208235	0.00202101984805393	-0.000522200490155844
0.699864759702979	1.10225326834762	-0.113238355561856	0.00200379803809671	-0.000473158379931359
0.725534881959585	0.0166769321108019	-0.127070864407717	0.00201103114219792	-0.000524159615327806
0.741661967758642	0.0165883455390737	-0.126796243604768	0.00199377474235209	-0.000474760690145923
0.750745673237787	0.0165066029372156	-0.126177426151878	0.00199574556852669	-0.000324435391283045
0.725239237240194	1.28360238876588	-0.126822452548884	0.00201198839285686	-0.000524135466142819
0.741305373325588	1.27663608792109	-0.126547471026397	0.00199470241902458	-0.000474531685889477
0.750388761460538	1.27048301819555	-0.125931645587657	0.00199666849652031	-0.000324279619175926
0.703846084343615	1.2983535749032	-0.120442022258064	0.00201386669960073	-0.000524659508494907
0.720001630628008	1.29126239278129	-0.120201151976874	0.00199653542909735	-0.000474853930486557
0.729372615339681	1.28567479295596	-0.11961881324743	0.00199856991472263	-0.000324898372036967
0.765245405380457	0.917099594598925	-0.127036201975264	0.00199671431282624	-0.000525412535902396
0.753013250910799	-332.250717404114	-0.116412243900563	0.00203429237602807	-0.000522293562841627
0.767657516412744	-329.561560921001	-0.116183492813094	0.00201642014727407	-0.000469092325503666
0.777956491884039	-329.300798266228	-0.115634995911273	0.0020188771294838	-0.000323372240208097
0.173520764249997	-116.345958654927	-182.815057499026	0.00203059034708203	-0.000527005079803698

Table 20: Best regressions for Soviet January water equivalents using 4 explaining parameters.

results_auto2_BestRegressions4Param_Jan.csv - Editor

Datei Bearbeiten Format Ansicht ?

"R.2"	"Terrainparameterchoice"
0.798766207685682	"we ~ SDD_Dec + X100m_SOPDdxx_ma + X100m_SOPDdxy_su + WinterNS_Jan , data=tab"
0.798670488430971	"we ~ SDD_Dec + X100m_SOPDdxx_ma + X100m_SOPDdxy_me + WinterNS_Jan , data=tab"
0.797153771746958	"we ~ SDD_Dec + X100m_SOPDdxx_ma + X100m_SOPDdxy__1 + WinterNS_Jan , data=tab"
0.798901078677797	"we ~ SDD_Jan + X100m_SOPDdxx_ma + X100m_SOPDdxy_su + WinterNS_Jan , data=tab"
0.798805582676626	"we ~ SDD_Jan + X100m_SOPDdxx_ma + X100m_SOPDdxy_me + WinterNS_Jan , data=tab"
0.797442365997924	"we ~ SDD_Jan + X100m_SOPDdxx_ma + X100m_SOPDdxy__1 + WinterNS_Jan , data=tab"
0.798819538430787	"we ~ SDD_Feb + X100m_SOPDdxx_ma + X100m_SOPDdxy_su + WinterNS_Jan , data=tab"
0.798723847358441	"we ~ SDD_Feb + X100m_SOPDdxx_ma + X100m_SOPDdxy_me + WinterNS_Jan , data=tab"
0.797256219022034	"we ~ SDD_Feb + X100m_SOPDdxx_ma + X100m_SOPDdxy__1 + WinterNS_Jan , data=tab"
0.798823174821842	"we ~ SDD_Mrz + X100m_SOPDdxx_ma + X100m_SOPDdxy_su + WinterNS_Jan , data=tab"
0.798727470290028	"we ~ SDD_Mrz + X100m_SOPDdxx_ma + X100m_SOPDdxy_me + WinterNS_Jan , data=tab"
0.797263805763923	"we ~ SDD_Mrz + X100m_SOPDdxx_ma + X100m_SOPDdxy__1 + WinterNS_Jan , data=tab"
0.798752476329384	"we ~ SDD_Apr + X100m_SOPDdxx_ma + X100m_SOPDdxy_su + WinterNS_Jan , data=tab"
0.798656746974303	"we ~ SDD_Apr + X100m_SOPDdxx_ma + X100m_SOPDdxy_me + WinterNS_Jan , data=tab"
0.797128957875554	"we ~ SDD_Apr + X100m_SOPDdxx_ma + X100m_SOPDdxy__1 + WinterNS_Jan , data=tab"
0.798817517814841	"we ~ SDD_mean + X100m_SOPDdxx_ma + X100m_SOPDdxy_su + WinterNS_Jan , data=tab"
0.798721807241652	"we ~ SDD_mean + X100m_SOPDdxx_ma + X100m_SOPDdxy_me + WinterNS_Jan , data=tab"
0.797252358065316	"we ~ SDD_mean + X100m_SOPDdxx_ma + X100m_SOPDdxy__1 + WinterNS_Jan , data=tab"
0.798703304364296	"we ~ Hoehe + X100m_SOPDdxx_ma + X100m_SOPDdxy_su + WinterNS_Jan , data=tab"
0.798606469457985	"we ~ Hoehe + X100m_SOPDdxx_ma + X100m_SOPDdxy_me + WinterNS_Jan , data=tab"
0.797488701512918	"we ~ Hoehe + X100m_SOPDdxx_ma + X100m_SOPDdxy__1 + WinterNS_Jan , data=tab"

"Intercept"	"a_V1"	"b_V2"	"c_V3"	"d_V4"
-0.453759667180307	0.622134597113558	-53.880727780642	4.57131444371003	0.00201358152147112
-0.451667452278316	0.620120884510216	-54.0295749821523	351.012351272093	0.00201370110372208
-0.394645041513476	0.577095673142951	-52.5946548599516	407.237636857719	0.00201045335597061
-0.456973739045068	0.617097581351751	-54.6032736411856	4.67273168706141	0.00201411278267312
-0.45483158591962	0.615063810320083	-54.7546217353992	358.822897159663	0.00201423253334361
-0.396505345701134	0.57178797678564	-53.3028854479626	418.624516288959	0.00201080346797499
-0.475306303444471	0.640928626676611	-54.1212971394435	4.60519775708862	0.0020137569529626
-0.473130721994743	0.638841402091591	-54.2709795057037	353.621559084514	0.00201387661070485
-0.414248509899396	0.594304938286315	-52.8303947399569	411.027652848036	0.00201056909449106
-0.496417130387594	0.66183013035764	-54.1407410141194	4.60798564873949	0.00201377003245027
-0.494171595787661	0.65967370484933	-54.2904876385603	353.836046628459	0.00201388970516736
-0.433791393842399	0.613666692417223	-52.8494205713437	411.337470544183	0.00201057741074091
-0.432952206887344	0.601974303076002	-53.8250363224621	4.5634364113259	0.00201354092041542
-0.43093029604806	0.600028592248512	-53.9736857085713	350.405619678089	0.00201366048545247
-0.375429898113122	0.558444317884322	-52.5400911136401	406.358757238811	0.00201042651846546
-0.46240594128618	0.628137383217989	-54.1122530342367	4.60403391363623	0.00201374997886636
-0.46027278114028	0.626092184342203	-54.2619034689879	353.531724226868	0.00201386964215364
-0.402299402804347	0.582451407011718	-52.8215411041868	410.895597933772	0.00201056430158066
-2.96154215057826	0.000733605136325035	-54.9830466081583	4.74494375156796	0.00201516974957472
-2.95097663382209	0.000731147947550473	-55.1361454721933	364.364466796227	0.00201528793226503
-2.71528642632731	0.000679402189316529	-53.7181473022081	428.42032629842	0.00201163657126224

Table 21: Best regressions for Soviet February water equivalents using 4 explaining parameters.

results_auto2_BestRegressions4Param_Feb.csv - Editor

Datei Bearbeiten Format Ansicht ?

"R.2"	"Terrainparameterchoice"
0.79209154262078	"we ~ SDD_Dec + Ausrichtung + X100m_ProfCurv_2 + WinterNS_Feb , data=tab"
0.791836842565154	"we ~ SDD_Dec + X100m_aspect_med + X100m_ProfCurv_2 + WinterNS_Feb , data=tab"
0.792737552760974	"we ~ SDD_Dec + X100m_SOPDdxx_ma + X100m_SOPDdxy_su + WinterNS_Feb , data=tab"
0.792520679689497	"we ~ SDD_Dec + X100m_SOPDdxx_ma + X100m_SOPDdxy_me + WinterNS_Feb , data=tab"
0.794377139873632	"we ~ SDD_Dec + X100m_SOPDdxx_ma + X100m_SOPDdxy__1 + WinterNS_Feb , data=tab"
0.792405603981064	"we ~ SDD_Jan + Ausrichtung + X100m_ProfCurv_2 + WinterNS_Feb , data=tab"
0.790294935450612	"we ~ SDD_Jan + X100m_aspect_sum + X100m_ProfCurv_2 + WinterNS_Feb , data=tab"
0.790199675174019	"we ~ SDD_Jan + X100m_aspect_mea + X100m_ProfCurv_2 + WinterNS_Feb , data=tab"
0.792191218436623	"we ~ SDD_Jan + X100m_aspect_med + X100m_ProfCurv_2 + WinterNS_Feb , data=tab"
0.79237264984944	"we ~ SDD_Jan + X100m_SOPDdxx_ma + X100m_SOPDdxy_su + WinterNS_Feb , data=tab"
0.792155300666739	"we ~ SDD_Jan + X100m_SOPDdxx_ma + X100m_SOPDdxy_me + WinterNS_Feb , data=tab"
0.794326866271107	"we ~ SDD_Jan + X100m_SOPDdxx_ma + X100m_SOPDdxy__1 + WinterNS_Feb , data=tab"
0.792203073166355	"we ~ SDD_Feb + Ausrichtung + X100m_ProfCurv_2 + WinterNS_Feb , data=tab"
0.790040505106851	"we ~ SDD_Feb + X100m_aspect_sum + X100m_ProfCurv_2 + WinterNS_Feb , data=tab"
0.79196175076591	"we ~ SDD_Feb + X100m_aspect_med + X100m_ProfCurv_2 + WinterNS_Feb , data=tab"
0.79262446326951	"we ~ SDD_Feb + X100m_SOPDdxx_ma + X100m_SOPDdxy_su + WinterNS_Feb , data=tab"
0.792407374242941	"we ~ SDD_Feb + X100m_SOPDdxx_ma + X100m_SOPDdxy_me + WinterNS_Feb , data=tab"
0.794366457394006	"we ~ SDD_Feb + X100m_SOPDdxx_ma + X100m_SOPDdxy__1 + WinterNS_Feb , data=tab"
0.792210934551108	"we ~ SDD_Mrz + Ausrichtung + X100m_ProfCurv_2 + WinterNS_Feb , data=tab"
0.790050175262089	"we ~ SDD_Mrz + X100m_aspect_sum + X100m_ProfCurv_2 + WinterNS_Feb , data=tab"
0.791970678332854	"we ~ SDD_Mrz + X100m_aspect_med + X100m_ProfCurv_2 + WinterNS_Feb , data=tab"
0.792615567641572	"we ~ SDD_Mrz + X100m_SOPDdxx_ma + X100m_SOPDdxy_su + WinterNS_Feb , data=tab"
0.792398439857583	"we ~ SDD_Mrz + X100m_SOPDdxx_ma + X100m_SOPDdxy_me + WinterNS_Feb , data=tab"
0.794365751983457	"we ~ SDD_Mrz + X100m_SOPDdxx_ma + X100m_SOPDdxy__1 + WinterNS_Feb , data=tab"
0.792064319873719	"we ~ SDD_Apr + Ausrichtung + X100m_ProfCurv_2 + WinterNS_Feb , data=tab"
0.791806496976814	"we ~ SDD_Apr + X100m_aspect_med + X100m_ProfCurv_2 + WinterNS_Feb , data=tab"
0.792762529830376	"we ~ SDD_Apr + X100m_SOPDdxx_ma + X100m_SOPDdxy_su + WinterNS_Feb , data=tab"
0.792545703597921	"we ~ SDD_Apr + X100m_SOPDdxx_ma + X100m_SOPDdxy_me + WinterNS_Feb , data=tab"
0.794378706106659	"we ~ SDD_Apr + X100m_SOPDdxx_ma + X100m_SOPDdxy__1 + WinterNS_Feb , data=tab"
0.792198603289858	"we ~ SDD_mean + Ausrichtung + X100m_ProfCurv_2 + WinterNS_Feb , data=tab"
0.790034955782312	"we ~ SDD_mean + X100m_aspect_sum + X100m_ProfCurv_2 + WinterNS_Feb , data=tab"
0.791956790346509	"we ~ SDD_mean + X100m_aspect_med + X100m_ProfCurv_2 + WinterNS_Feb , data=tab"
0.792628926142722	"we ~ SDD_mean + X100m_SOPDdxx_ma + X100m_SOPDdxy_su + WinterNS_Feb , data=tab"
0.792411821599905	"we ~ SDD_mean + X100m_SOPDdxx_ma + X100m_SOPDdxy_me + WinterNS_Feb , data=tab"
0.794367136228024	"we ~ SDD_mean + X100m_SOPDdxx_ma + X100m_SOPDdxy__1 + WinterNS_Feb , data=tab"
0.792430681514663	"we ~ Hoehe + Ausrichtung + X100m_ProfCurv_2 + WinterNS_Feb , data=tab"
0.790215302670552	"we ~ Hoehe + X100m_aspect_sum + X100m_ProfCurv_2 + WinterNS_Feb , data=tab"
0.790039555677055	"we ~ Hoehe + X100m_aspect_mea + X100m_ProfCurv_2 + WinterNS_Feb , data=tab"
0.79219143278065	"we ~ Hoehe + X100m_aspect_med + X100m_ProfCurv_2 + WinterNS_Feb , data=tab"
0.790963739731922	"we ~ Hoehe + X100m_SOPDdxx_ma + X100m_SOPDdxy_su + WinterNS_Feb , data=tab"
0.790747314607469	"we ~ Hoehe + X100m_SOPDdxx_ma + X100m_SOPDdxy_me + WinterNS_Feb , data=tab"
0.793404838404705	"we ~ Hoehe + X100m_SOPDdxx_ma + X100m_SOPDdxy__1 + WinterNS_Feb , data=tab"

"Intercept"	"a_V1"	"b_V2"	"c_V3"	"d_V4"
-0.43065083909152	0.734992904665782	-0.000622860035562444	-129.506356638294	0.00183963428276889
-0.439024580851599	0.744765353933747	-0.000638022375758931	-130.928822063513	0.0018397978662337
-0.495396142113289	0.753965928274762	-71.415738037575	5.95396645336765	0.00183893014793892
-0.492531067141342	0.751172476068105	-71.5646945031035	455.84156933139	0.00183912410726502
-0.417316112092016	0.695499519550562	-71.2335991801431	585.648558373854	0.00183774454789097
-0.433460889118027	0.729653010516663	-0.00063571677420627	-130.964769820294	0.00183925341304846
-0.445536775193813	0.747087493700089	-8.91870999475809e-06	-129.147611887733	0.0018393827590674
-0.447374211633217	0.749436870905874	-0.000688135283718712	-129.275916824497	0.00183930126188146
-0.442155910578778	0.739769650028313	-0.000651945943010035	-132.427667841427	0.00183940867792689
-0.498266190237119	0.747017015804231	-72.2930574840913	6.06781243592481	0.00183866437671706
-0.495340851816639	0.744201943909123	-72.4447458424512	464.611328841989	0.00183886224639438
-0.41883672638853	0.688546324643309	-72.1041378531493	599.355068743582	0.0018374251424465
-0.455783770069832	0.757413242493581	-0.00062716986698237	-129.989669973336	0.00183950655967182
-0.468010984250721	0.774826144143203	-8.77871440641401e-06	-128.192409451892	0.00183965369811435
-0.464590295372107	0.767627205747829	-0.000642687959428322	-131.425566308945	0.00183966741541038
-0.521158441350411	0.776449992258152	-71.7080327026975	5.99202986129662	0.00183884021685902
-0.518180789854572	0.773556722882047	-71.8579024533052	458.77331535342	0.00183903548887877
-0.440694941893761	0.716046291461842	-71.5235418595961	590.212700590651	0.00183763710395706
-0.480703422275054	0.782126215961229	-0.000627504901302429	-130.02875242416	0.00183949656667023
-0.493518638811051	0.800133694724879	-8.78416352246681e-06	-128.230788944604	0.00183964304629863
-0.48985416110125	0.792685156097293	-0.000643051006017472	-131.46570425421	0.00183965720323251
-0.546705854940073	0.801748281946507	-71.7316381432511	5.99518079166833	0.00183883306297889
-0.543631486910968	0.7987592673024	-71.8815775454187	459.015740205006	0.0018390284466648
-0.464222374680482	0.739359622310218	-71.5468881033773	590.58587797342	0.00183762854069895
-0.406147027307324	0.711127526974921	-0.000621856883856093	-129.394687842007	0.00183966435358355
-0.414174248532667	0.720551342767294	-0.000636936352335401	-130.814050248114	0.00183982857147764
-0.470256597672424	0.729597563846914	-71.3480426113328	5.94511290555021	0.00183895146043452
-0.467488372548387	0.726897976982032	-71.4967822050702	455.159552298888	0.00183914511504941
-0.394213216232607	0.673063828429374	-71.1664558304126	584.589765418802	0.00183776985357016
-0.440550113392014	0.742288475947349	-0.000627009962111787	-129.970816574452	0.00183951148575759
-0.4524199617184	0.759340568772159	-8.77607633068515e-06	-128.173955146961	0.0018396589738528
-0.449147688714719	0.752293320019479	-0.000642514947592069	-131.406195017929	0.0018396724445465
-0.505543737450531	0.760965239370981	-71.697042343914	5.99073485412571	0.00183884361291302
-0.502624785255916	0.758130155486432	-71.8468771675663	458.673296355489	0.00183903884308741
-0.426307779340506	0.701772208590829	-71.5126379414168	590.053720139143	0.00183764112397731
-3.45157885407561	0.000882638178270321	-0.00067442130585331	-129.79481945248	0.00183879041641686
-3.54159413583331	0.000905220814269246	-9.49473263323078e-06	-127.862328851715	0.00183890480717711
-3.5519790957071	0.000907752684822269	-0.000731779050875957	-128.024717441076	0.00183882779662823
-3.50492526598213	0.000895553182725502	-0.000692184645058269	-131.339272345287	0.00183894955062269
-3.51996630580478	0.000885736623928387	-72.7514853828483	6.12937183741987	0.00183825385486182
-3.50546193225104	0.00088235347662855	-72.9054693150763	469.358136633701	0.00183845527119887
-3.20338387475128	0.000816383614394214	-72.6506936840351	610.750484716839	0.0018369533736871

Table 22: Best regressions for Soviet February water equivalents using 3 explaining parameters.

results_auto2_BestRegressions_Feb_ohneMaj.csv - Editor

Datei Bearbeiten Format Ansicht ?

"R.2"	"Terrainparameterchoice"
0.736324322656568	"we ~ SDD_Dec + SOPDdyy + WinterNS_Feb , data=tab"
0.734559161911462	"we ~ SDD_Jan + SOPDdyy + WinterNS_Feb , data=tab"
0.735755892484175	"we ~ SDD_Feb + SOPDdyy + WinterNS_Feb , data=tab"
0.735707461262066	"we ~ SDD_Mrz + SOPDdyy + WinterNS_Feb , data=tab"
0.736453332989846	"we ~ SDD_Apr + SOPDdyy + WinterNS_Feb , data=tab"
0.735776948995452	"we ~ SDD_mean + SOPDdyy + WinterNS_Feb , data=tab"
0.733638694771874	"we ~ Hoehe + SOPDdyy + WinterNS_Feb , data=tab"
0.73528038883314	"we ~ ProfCurv + X100m_SOPDdxx__1 + WinterNS_Feb , data=tab"
0.748752483612638	"we ~ X100m_FOPDdxEW_s + X100m_FOPDdxEW_1 + WinterNS_Feb , data=tab"

"Intercept"	"a_V1"	"b_V2"	"c_V3"
-0.782558462919679	1.06859854933066	200.977374431062	0.00184799391938711
-0.790263440600945	1.06235089266221	204.835563951987	0.0018477620209368
-0.820332780103838	1.10172128911014	202.275025842456	0.00184791230642088
-0.856677643833521	1.13771250118493	202.37466061887	0.00184790678595184
-0.746654243177599	1.03378763697053	200.675486497811	0.00184801379381571
-0.798124742081971	1.07969726903611	202.224367325818	0.00184791559338777
-5.11799564870217	0.00126673997158832	209.051534140858	0.00184674674794148
0.226136464508771	569.614609093445	-784.487672518048	0.0018397071920907
0.351644263661909	-0.420785833397572	33.9403313465311	0.00185183299445575

Table 23: Best regressions for Soviet March water equivalents using 4 explaining parameters.

results_auto2_BestRegressions4Param_Mrz.csv - Editor

Datei Bearbeiten Format Ansicht ?

"R.2"	"Terrainparameterchoice"
0.822904478744504	"we ~ SDD_Dec + X100m_SOPDdxx_ma + X100m_SOPDdxy_su + WinterNS_Mrz , data=tab"
0.822706270205797	"we ~ SDD_Dec + X100m_SOPDdxx_ma + X100m_SOPDdxy_me + WinterNS_Mrz , data=tab"
0.823826723631291	"we ~ SDD_Dec + X100m_SOPDdxx_ma + X100m_SOPDdxy__1 + WinterNS_Mrz , data=tab"
0.822461938511735	"we ~ SDD_Jan + Ausrichtung + X100m_ProfCurv_2 + WinterNS_Mrz , data=tab"
0.822388861195855	"we ~ SDD_Jan + X100m_aspect_med + X100m_ProfCurv_2 + WinterNS_Mrz , data=tab"
0.822746820765339	"we ~ SDD_Jan + X100m_SOPDdxx_ma + X100m_SOPDdxy_su + WinterNS_Mrz , data=tab"
0.822547629964007	"we ~ SDD_Jan + X100m_SOPDdxx_ma + X100m_SOPDdxy_me + WinterNS_Mrz , data=tab"
0.823997199907375	"we ~ SDD_Jan + X100m_SOPDdxx_ma + X100m_SOPDdxy__1 + WinterNS_Mrz , data=tab"
0.822136701347583	"we ~ SDD_Feb + Ausrichtung + X100m_ProfCurv_2 + WinterNS_Mrz , data=tab"
0.822035626928044	"we ~ SDD_Feb + X100m_aspect_med + X100m_ProfCurv_2 + WinterNS_Mrz , data=tab"
0.822863991890585	"we ~ SDD_Feb + X100m_SOPDdxx_ma + X100m_SOPDdxy_su + WinterNS_Mrz , data=tab"
0.822665387085233	"we ~ SDD_Feb + X100m_SOPDdxx_ma + X100m_SOPDdxy_me + WinterNS_Mrz , data=tab"
0.823892462876873	"we ~ SDD_Feb + X100m_SOPDdxx_ma + X100m_SOPDdxy__1 + WinterNS_Mrz , data=tab"
0.822149280752091	"we ~ SDD_Mrz + Ausrichtung + X100m_ProfCurv_2 + WinterNS_Mrz , data=tab"
0.822049306375012	"we ~ SDD_Mrz + X100m_aspect_med + X100m_ProfCurv_2 + WinterNS_Mrz , data=tab"
0.822860433331425	"we ~ SDD_Mrz + X100m_SOPDdxx_ma + X100m_SOPDdxy_su + WinterNS_Mrz , data=tab"
0.822661773642094	"we ~ SDD_Mrz + X100m_SOPDdxx_ma + X100m_SOPDdxy_me + WinterNS_Mrz , data=tab"
0.823897434065323	"we ~ SDD_Mrz + X100m_SOPDdxx_ma + X100m_SOPDdxy__1 + WinterNS_Mrz , data=tab"
0.822912070105737	"we ~ SDD_Apr + X100m_SOPDdxx_ma + X100m_SOPDdxy_su + WinterNS_Mrz , data=tab"
0.822713949735906	"we ~ SDD_Apr + X100m_SOPDdxx_ma + X100m_SOPDdxy_me + WinterNS_Mrz , data=tab"
0.823810118048392	"we ~ SDD_Apr + X100m_SOPDdxx_ma + X100m_SOPDdxy__1 + WinterNS_Mrz , data=tab"
0.822129625940373	"we ~ SDD_mean + Ausrichtung + X100m_ProfCurv_2 + WinterNS_Mrz , data=tab"
0.822028042254496	"we ~ SDD_mean + X100m_aspect_med + X100m_ProfCurv_2 + WinterNS_Mrz , data=tab"
0.82286572880352	"we ~ SDD_mean + X100m_SOPDdxx_ma + X100m_SOPDdxy_su + WinterNS_Mrz , data=tab"
0.822667111804198	"we ~ SDD_mean + X100m_SOPDdxx_ma + X100m_SOPDdxy_me + WinterNS_Mrz , data=tab"
0.823890268949549	"we ~ SDD_mean + X100m_SOPDdxx_ma + X100m_SOPDdxy__1 + WinterNS_Mrz , data=tab"
0.823213691742792	"we ~ Hoehe + Ausrichtung + X100m_ProfCurv_2 + WinterNS_Mrz , data=tab"
0.823131651985065	"we ~ Hoehe + X100m_aspect_med + X100m_ProfCurv_2 + WinterNS_Mrz , data=tab"
0.822578435314553	"we ~ Hoehe + X100m_SOPDdxx_ma + X100m_SOPDdxy_su + WinterNS_Mrz , data=tab"
0.822374981005829	"we ~ Hoehe + X100m_SOPDdxx_ma + X100m_SOPDdxy_me + WinterNS_Mrz , data=tab"
0.824271610453616	"we ~ Hoehe + X100m_SOPDdxx_ma + X100m_SOPDdxy__1 + WinterNS_Mrz , data=tab"
0.822835790648499	"we ~ TangCurv + X100m_FOPDdxEW_s + X100m_FOPDdxEW_1 + WinterNS_Mrz , data=tab"

"Intercept"	"a_V1"	"b_V2"	"c_V3"	"d_V4"
-0.701528995576645	1.02855541662334	-81.6001659086419	6.89156492474405	0.00185500722311573
-0.698265134981035	1.02532836293751	-81.7832219436156	527.831037053585	0.00185529423531096
-0.611493558211686	0.96139449163843	-81.0516966110577	667.765239268648	0.00185299882980879
-0.613328819407814	0.957452369591999	-0.000626349601849478	-156.703870214196	0.00185840287241437
-0.621885885913619	0.967569844640937	-0.000643242810063035	-158.165198391328	0.00185841269272311
-0.705906884336734	1.01974595045717	-82.7874710737272	7.05419684738345	0.00185444425525478
-0.702560929263793	1.01648082239282	-82.97487784524	540.35493965124	0.00185473843014161
-0.613864690342072	0.952233346585018	-82.2375526583248	686.899594133774	0.00185238778710184
-0.642467478041974	0.993635431070962	-0.000614908919487755	-155.452004463249	0.00185870580823017
-0.651082660733615	1.00377428160829	-0.000630910371283537	-156.879658428025	0.00185871860506075
-0.736835617073876	1.059460357242	-81.9955581440267	6.94590059560711	0.0018548197584042
-0.733437397617925	1.05611343999949	-82.1800671749733	532.014832055483	0.00185510916123771
-0.643905837032508	0.989953163472059	-81.4465151980691	674.13457904275	0.00185279530701626
-0.675165728023858	1.02606571685762	-0.000615357237726822	-155.502222101547	0.00185869476618978
-0.684124831585048	1.03655015201514	-0.000631393784415063	-156.931192372006	0.0018587074575538
-0.771707958968718	1.09399785478145	-82.0275210141967	6.95038122574851	0.00185480579892449
-0.768197496489959	1.09053980000267	-82.2121418574268	532.35950720688	0.00185509539728048
-0.676440813841547	1.02219650293331	-81.478353710784	674.654907253052	0.00185277998251924
-0.667199625529081	0.995261484173943	-81.5086197529765	6.87893026614326	0.00185505110037269
-0.664048578654264	0.992143859037388	-81.6913318656759	526.858055985361	0.00185533755747303
-0.579538289834035	0.930347130500178	-80.9602907913394	666.287876897004	0.00185304641218654
-0.622479947815674	0.973788829271877	-0.000614694790303554	-155.427827072134	0.0018587121080876
-0.630886731769944	0.983718678228493	-0.000630679776551033	-156.854838764999	0.00185872496739824
-0.715523625003006	1.03832278568285	-81.980692635803	6.94403909306088	0.00185482736086848
-0.712193451828958	1.03504333030594	-82.165146010792	531.871147171886	0.00185511668106197
-0.624011760123462	0.970212884851438	-81.4316748515506	673.912294278447	0.00185280341955952
-4.58196374905227	0.00116030298435168	-0.000678460187465373	-154.96552112417	0.00185739318810447
-4.63640780377678	0.0011735223334226	-0.000697358863375234	-156.538506528536	0.00185739051770002
-4.84637639007946	0.00121297803205694	-83.3480820358405	7.16830756489945	0.0018530837932182
-4.82947639464031	0.00120902455302525	-83.5379049629168	549.091112056344	0.00185338660399603
-4.47811832529759	0.00113235537393508	-82.8762569662895	703.383998120061	0.0018510297740575
0.40082227588897	170.047198186774	-0.7662033655077	61.8773265809733	0.00184567798390825

Table 24: Best regressions for Soviet April water equivalents using 4 explaining parameters.

results_auto2_BestRegressions4Param_Apr.csv - Editor

Datei Bearbeiten Format Ansicht ?

"R.2"	"Terrainparameterchoice"
0.838735178367888	"we ~ SDD_Dec + X100m_SOPDdxx_ma + X100m_SOPDdxy_su + WinterNS_Apr , data=tab"
0.838581094756935	"we ~ SDD_Dec + X100m_SOPDdxx_ma + X100m_SOPDdxy_me + WinterNS_Apr , data=tab"
0.838230021270894	"we ~ SDD_Dec + X100m_SOPDdxx_ma + X100m_SOPDdxy__1 + WinterNS_Apr , data=tab"
0.838650181667194	"we ~ SDD_Jan + X100m_SOPDdxx_ma + X100m_SOPDdxy_su + WinterNS_Apr , data=tab"
0.838496430889399	"we ~ SDD_Jan + X100m_SOPDdxx_ma + X100m_SOPDdxy_me + WinterNS_Apr , data=tab"
0.838428260142158	"we ~ SDD_Jan + X100m_SOPDdxx_ma + X100m_SOPDdxy__1 + WinterNS_Apr , data=tab"
0.838719345765424	"we ~ SDD_Feb + X100m_SOPDdxx_ma + X100m_SOPDdxy_su + WinterNS_Apr , data=tab"
0.83856530055301	"we ~ SDD_Feb + X100m_SOPDdxx_ma + X100m_SOPDdxy_me + WinterNS_Apr , data=tab"
0.838305369169962	"we ~ SDD_Feb + X100m_SOPDdxx_ma + X100m_SOPDdxy__1 + WinterNS_Apr , data=tab"
0.838717518287465	"we ~ SDD_Mrz + X100m_SOPDdxx_ma + X100m_SOPDdxy_su + WinterNS_Apr , data=tab"
0.83856345224479	"we ~ SDD_Mrz + X100m_SOPDdxx_ma + X100m_SOPDdxy_me + WinterNS_Apr , data=tab"
0.838310886667892	"we ~ SDD_Mrz + X100m_SOPDdxx_ma + X100m_SOPDdxy__1 + WinterNS_Apr , data=tab"
0.838736966027839	"we ~ SDD_Apr + X100m_SOPDdxx_ma + X100m_SOPDdxy_su + WinterNS_Apr , data=tab"
0.838582869363232	"we ~ SDD_Apr + X100m_SOPDdxx_ma + X100m_SOPDdxy_me + WinterNS_Apr , data=tab"
0.83821112169766	"we ~ SDD_Apr + X100m_SOPDdxx_ma + X100m_SOPDdxy__1 + WinterNS_Apr , data=tab"
0.838720069086995	"we ~ SDD_mean + X100m_SOPDdxx_ma + X100m_SOPDdxy_su + WinterNS_Apr , data=tab"
0.83856599500818	"we ~ SDD_mean + X100m_SOPDdxx_ma + X100m_SOPDdxy_me + WinterNS_Apr , data=tab"
0.838302710470715	"we ~ SDD_mean + X100m_SOPDdxx_ma + X100m_SOPDdxy__1 + WinterNS_Apr , data=tab"
0.83821231521515	"we ~ Hoehe + X100m_SOPDdxx_ma + X100m_SOPDdxy_su + WinterNS_Apr , data=tab"
0.838057974280872	"we ~ Hoehe + X100m_SOPDdxx_ma + X100m_SOPDdxy_me + WinterNS_Apr , data=tab"
0.83838342186121	"we ~ Hoehe + X100m_SOPDdxx_ma + X100m_SOPDdxy__1 + WinterNS_Apr , data=tab"

"Intercept"	"a_V1"	"b_V2"	"c_V3"	"d_V4"
-0.925404703486482	1.29343024039123	-97.304275680983	8.85296776299502	0.00191516660687179
-0.921284754817448	1.28940193737596	-97.5806104693417	679.089673577005	0.0019153431821002
-0.811305739691044	1.20807830576018	-95.601085927235	824.444577127185	0.0019131522971475
-0.931376294711948	1.28257030562015	-98.8311083339483	9.06979695432239	0.00191504670113384
-0.927149766475789	1.27849210730382	-99.1135146448125	695.789708840219	0.0019152276198853
-0.814506687259749	1.19656253458177	-97.1084621654474	848.999135886148	0.00191296726098087
-0.969959013694611	1.33236744566179	-97.8127510066982	8.92539077650343	0.00191512604308177
-0.965669960594238	1.32818870177915	-98.091114442384	684.667090555504	0.00191530407124535
-0.852106832870629	1.24396206359317	-96.1030181323319	832.618864347741	0.00191309011378119
-1.01382610615246	1.37580692680775	-97.8538151613289	8.93134096544776	0.0019151238856033
-1.00939680475474	1.37148936150843	-98.1323347261176	685.124903514115	0.00191530203056643
-0.892995081634159	1.28447789708259	-96.1434799709804	833.286021839368	0.00191308612428002
-0.882200020462779	1.25154663658581	-97.1865321058561	8.83612566102643	0.00191517628559792
-0.878221206128973	1.24765511175921	-97.4623872537609	677.792476027868	0.00191535252271268
-0.771134478485415	1.16906536046189	-95.4848653713654	822.548133523259	0.00191316697008914
-0.943151216495594	1.30578204651355	-97.7936307433094	8.92289206830664	0.0019151281902344
-0.938947174198435	1.30168756422176	-98.0719165315838	684.474219307956	0.00191530616703684
-0.827105240618242	1.21915652232689	-96.0841548510014	832.332975357331	0.0019130929750049
-6.14091931037809	0.00152583498576045	-99.6366702839591	9.22509959353948	0.00191517676177895
-6.11978124090011	0.00152090226440908	-99.9239110802802	707.732198733576	0.00191536013630721
-5.6704491378432	0.00142272626729511	-97.9878350627915	869.830070764999	0.00191302073642317

Appendix E: GPR PM raster parameter calculations

Table 25: Best regressions using only every 100th GPR measurement points.

results_auto_3Param_gap100_BestRegressions.csv - Editor

Datei Bearbeiten Format Ansicht ?

"R.2"	"Terrainparameterchoice"
0.742306636767257	"we_GPR ~ z_m + FOPDdyNS + ProfCurv_s , data=tot"
0.74252474500627	"we_GPR ~ z_m + FOPDdyNS + ProfCurv_m , data=tot"
0.749970222736466	"we_GPR ~ z_m + FOPDdyNS + ProfCurv_1 , data=tot"
0.740809724472306	"we_GPR ~ z_m + FOPDdyNS + SOPDdyy_ma , data=tot"
0.740460588786849	"we_GPR ~ z_m + FOPDdyNS_m + ProfCurv_1 , data=tot"
0.74481763565205	"we_GPR ~ z_m + FOPDdyNS_1 + ProfCurv_1 , data=tot"

"Intercept"	"a_V1"	"b_V2"	"c_V3"
-4.96390297209371	0.00136611194904564	1.20405314713587	-0.852548904710888
-4.96390132008651	0.00136612548250244	1.20393563251037	-66.8815987407105
-4.96299331680164	0.00136518584538194	1.24049471965285	-100.856560171895
-4.93987728556821	0.00135860277888774	1.17264791856691	-23.2310054133292
-4.94924293207276	0.00136165950264133	1.2406305983237	-101.388581457389
-5.00761280251588	0.00137502161363147	1.29672026736751	-101.520007343281

Table 26: Best regressions using 1000 randomly chosen GPR measurement points.

results_auto_3Param_npoints1000_BestRegressions.csv - Editor

Datei Bearbeiten Format Ansicht ?

"R.2"	"Terrainparameterchoice"
0.752692399516322	"we_GPR ~ z_m + FOPDdyNS + ProfCurv_s , data=tot"
0.752690245266423	"we_GPR ~ z_m + FOPDdyNS + ProfCurv_m , data=tot"
0.75521467985639	"we_GPR ~ z_m + FOPDdyNS + ProfCurv_1 , data=tot"
0.75074866729102	"we_GPR ~ z_m + FOPDdyNS_1 + ProfCurv_s , data=tot"
0.750741486196118	"we_GPR ~ z_m + FOPDdyNS_1 + ProfCurv_m , data=tot"
0.752832566396873	"we_GPR ~ z_m + FOPDdyNS_1 + ProfCurv_1 , data=tot"

"Intercept"	"a_V1"	"b_V2"	"c_V3"
-4.71815139801052	0.00130613340762267	1.15625480798237	-0.80367011976568
-4.71796458304	0.00130608302765056	1.15651815789448	-62.1371606439393
-4.71991157474205	0.00130621287328042	1.17411189396371	-79.3934711154335
-4.78931269000702	0.00132215817259949	1.24077619006459	-0.84724287695557
-4.78910164937612	0.00132210212905768	1.24101987929819	-65.4887029554344
-4.7893034924087	0.00132185432496532	1.25512670892335	-81.0735492539624

Table 27: Best regressions for GPR derived water equivalents using 3 explaining topographical parameters.

results_auto_3Param_BestRegressions.csv - Editor

Datei Bearbeiten Format Ansicht ?

"R.2"	"Terrainparameterchoice"
0.737993028194375	"we_GPR ~ z_m + SOPDdyy + FOPDdyNS , data=tot"
0.736741781983455	"we_GPR ~ z_m + ProfCurv + FOPDdyNS , data=tot"
0.736347161417433	"we_GPR ~ z_m + FOPDdyNS + FOPDdyNS_s , data=tot"
0.736296212164559	"we_GPR ~ z_m + FOPDdyNS + FOPDdyNS_m , data=tot"
0.737625527077617	"we_GPR ~ z_m + FOPDdyNS + FOPDdyNS_2 , data=tot"
0.74083631774249	"we_GPR ~ z_m + FOPDdyNS + ProfCurv_s , data=tot"
0.740907092908727	"we_GPR ~ z_m + FOPDdyNS + ProfCurv_m , data=tot"
0.746099097681423	"we_GPR ~ z_m + FOPDdyNS + ProfCurv_1 , data=tot"
0.736249699884738	"we_GPR ~ z_m + FOPDdyNS + ProfCurv_2 , data=tot"
0.736069110526886	"we_GPR ~ z_m + FOPDdyNS + SOPDdxx_ma , data=tot"
0.738866727872597	"we_GPR ~ z_m + FOPDdyNS + SOPDdyy_su , data=tot"
0.738849376010517	"we_GPR ~ z_m + FOPDdyNS + SOPDdyy_me , data=tot"
0.738320415986772	"we_GPR ~ z_m + FOPDdyNS + SOPDdyy__1 , data=tot"
0.73801584510559	"we_GPR ~ z_m + FOPDdyNS + SOPDdyy_ma , data=tot"
0.736616664865749	"we_GPR ~ z_m + FOPDdyNS + TangCurv_2 , data=tot"
0.737166734773052	"we_GPR ~ z_m + FOPDdyNS_s + ProfCurv_1 , data=tot"
0.737400466380582	"we_GPR ~ z_m + FOPDdyNS_m + ProfCurv_1 , data=tot"
0.737221370864151	"we_GPR ~ z_m + FOPDdyNS_1 + ProfCurv_s , data=tot"
0.737289942434295	"we_GPR ~ z_m + FOPDdyNS_1 + ProfCurv_m , data=tot"
0.741619005718372	"we_GPR ~ z_m + FOPDdyNS_1 + ProfCurv_1 , data=tot"

"Intercept"	"a_V1"	"b_V2"	"c_V3"
-5.01895287068708	0.00137883390454609	-30.0033384589768	1.21405129568578
-4.97243336244036	0.0013678639631645	-20.1928403294257	1.1834549582827
-4.88558125418028	0.00134926776703179	2.20494236380459	-0.014999733453738
-4.886358776515	0.00134945655917353	2.20950177892972	-1.16191860310524
-4.8774197040141	0.00134486293655942	1.68273947211892	-0.590689792568173
-4.94510258240294	0.00136185596640135	1.17504129077076	-0.787820868092185
-4.94513546073741	0.00136186360792331	1.17523693232007	-61.1568377047365
-4.94553258921467	0.00136138793502067	1.20795018411688	-90.9472759976933
-4.93937540694156	0.00135937828700976	1.15032481225637	-9.48801700495157
-4.96050105245479	0.00136474195909981	1.13378687376863	-6.10284721265217
-4.99942689599069	0.00137412974699572	1.22187081545808	-0.763213517752552
-4.99946211098787	0.00137414006870712	1.22182049863784	-58.8011126097219
-5.00516530636658	0.00137518776793136	1.24098654876569	-59.2179500957096
-4.91750212647113	0.00135363560911536	1.16222142565292	-17.0636368680778
-4.96536532190732	0.00136562471345679	1.13823250805405	-8.34366068496139
-4.93532428727586	0.00135888871243411	0.0156055502637429	-90.7419266292461
-4.93642983575796	0.00135910481990734	1.20713522320221	-90.8765522773285
-4.99852754744018	0.00137382138646962	1.23832608990867	-0.841197851406718
-4.99856455512097	0.00137382999249842	1.23851656315375	-65.253577902971
-4.99581327871938	0.00137267898462742	1.26463655090188	-91.4698513809169

Table 28: Best regressions for GPR derived water equivalents using 4 explaining topographical parameters.

results_auto_4Param_BestRegressions.csv - Editor

Datei Bearbeiten Format Ansicht ?

"R.2"	"Terrainparameterchoice"
0.750176249933866	"we_GPR ~ z_m + FOPDdyNS + FOPDdxEW + FOPDdxEW_s , data=tot"
0.750586402818859	"we_GPR ~ z_m + FOPDdyNS + FOPDdxEW + FOPDdxEW_m , data=tot"
0.748044193697987	"we_GPR ~ z_m + FOPDdyNS + FOPDdxEW_m + ProfCurv_1 , data=tot"
0.748451089247125	"we_GPR ~ z_m + FOPDdyNS + FOPDdyNS_s + ProfCurv_1 , data=tot"
0.748379498283422	"we_GPR ~ z_m + FOPDdyNS + FOPDdyNS_m + ProfCurv_1 , data=tot"
0.750042425238767	"we_GPR ~ z_m + FOPDdyNS + FOPDdyNS_2 + ProfCurv_1 , data=tot"
0.749545324467609	"we_GPR ~ z_m + FOPDdyNS + ProfCurv_1 + SOPDdxx__1 , data=tot"
0.749669973120998	"we_GPR ~ z_m + FOPDdyNS + ProfCurv_1 + TangCurv_1 , data=tot"
0.748279532972311	"we_GPR ~ z_m + FOPDdyNS + ProfCurv_1 + TangCurv_2 , data=tot"

"Intercept"	"a_V1"	"b_V2"	"c_V3"	"d_V4"
-4.83586754128328	0.00133290197849286	1.20321419559496	-1.34316618921572	0.0200826957206964
-4.83362049768224	0.00133233703117527	1.20317026503896	-1.35914473765269	1.56704057780674
-4.87027620578529	0.00134144784141023	1.24429329444264	0.182562940162108	-90.664666398653
-4.886815821137	0.00134899949597805	2.17168261613302	-0.0138209283095751	-89.4645354846803
-4.88788804818076	0.00134924884049804	2.16995795932072	-1.0640977378705	-89.3963332248694
-4.87456950231774	0.00134376211343178	1.725237604484	-0.58268945073216	-90.5524358912453
-5.0645854250088	0.00138843550592857	1.28684269489683	-122.514810229557	43.5191335061978
-5.02616127713911	0.00137963354091149	1.25412290579861	-106.190250877417	45.5090728097049
-4.95923136513196	0.00136388301749911	1.18945435325461	-88.0183493613948	-7.08295941868787

Appendix F: Snow depth distribution rasters

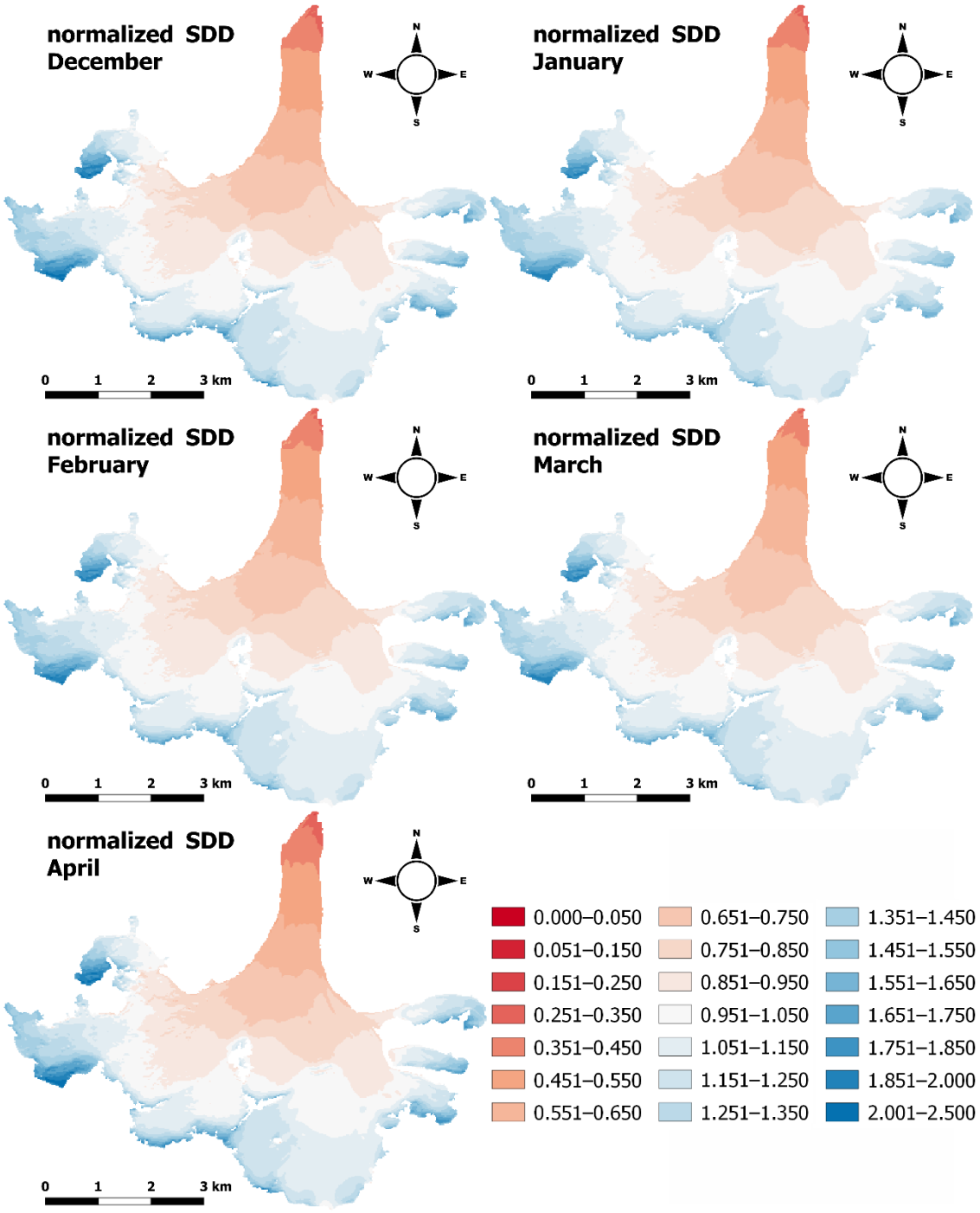


Figure 43: Normalized Soviet SDD rasters December to April based on Soviet stake data [dimensionless].

Appendix G: PM rasters

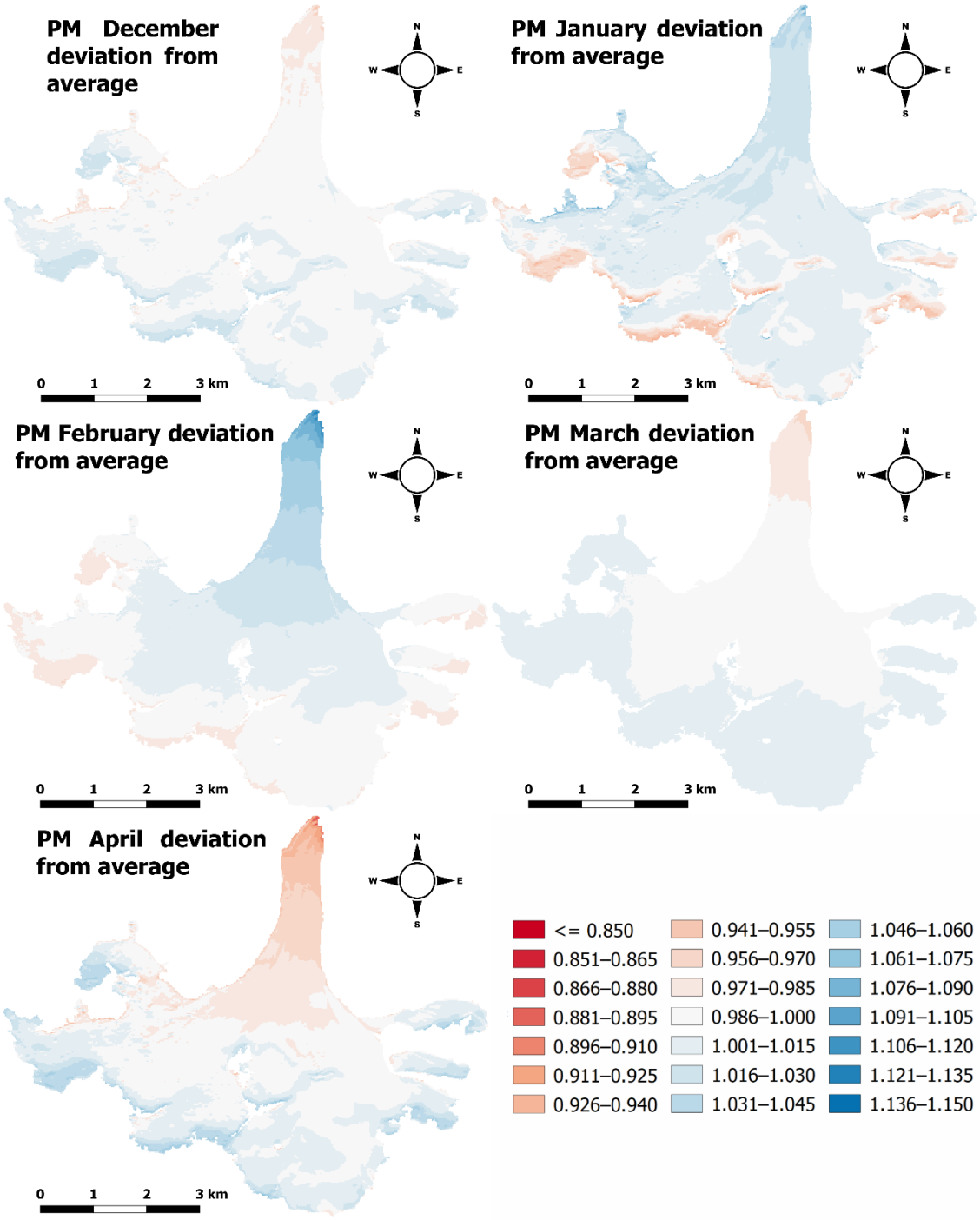


Figure 44: Quotients between the monthly Soviet PM rasters and the average Soviet PM raster [dimensionless].

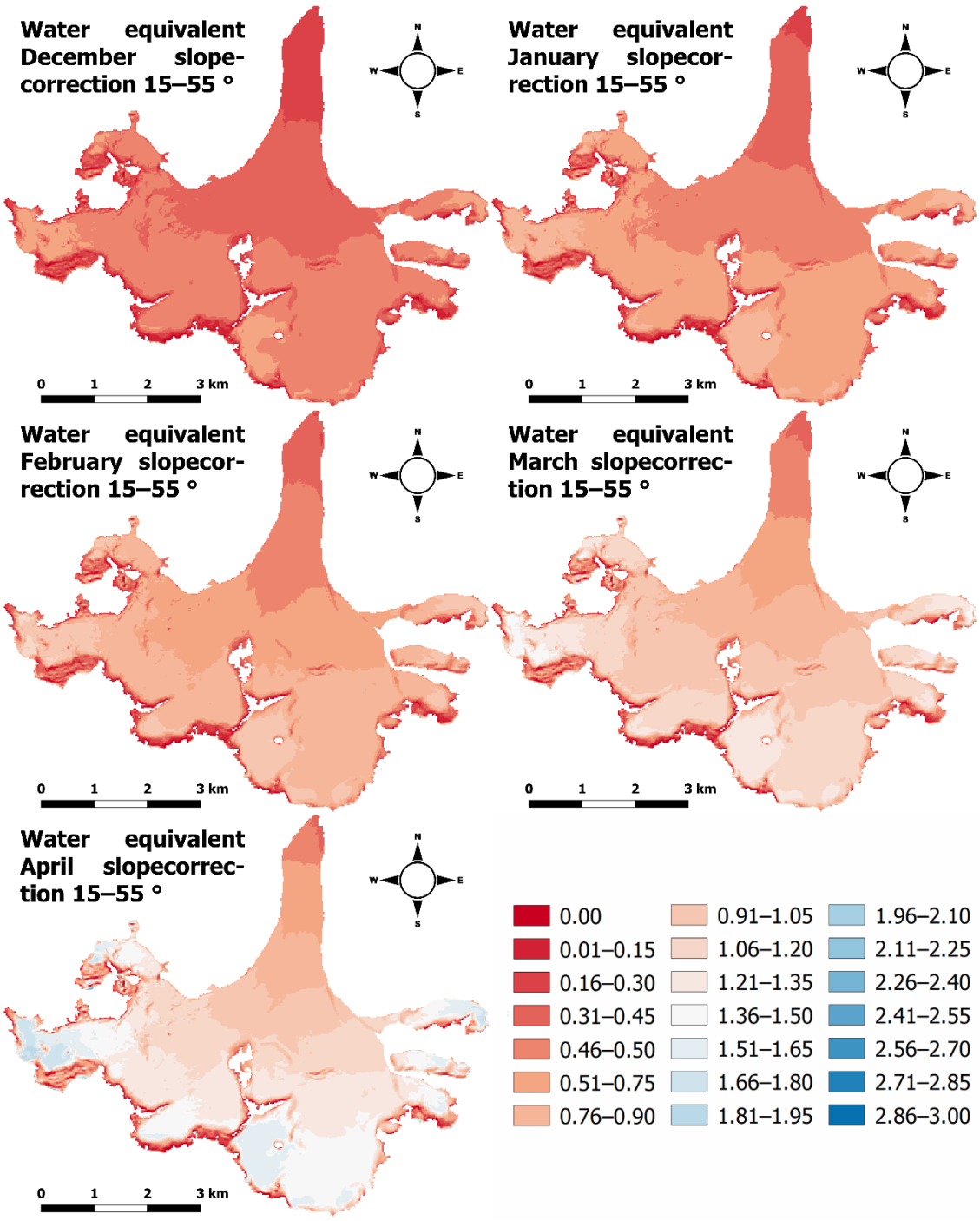


Figure 45: Soviet slope-corrected water equivalent rasters December to April with linear decrease from 100 % up to 15 ° to 0 % above 55 ° [m w. e.].

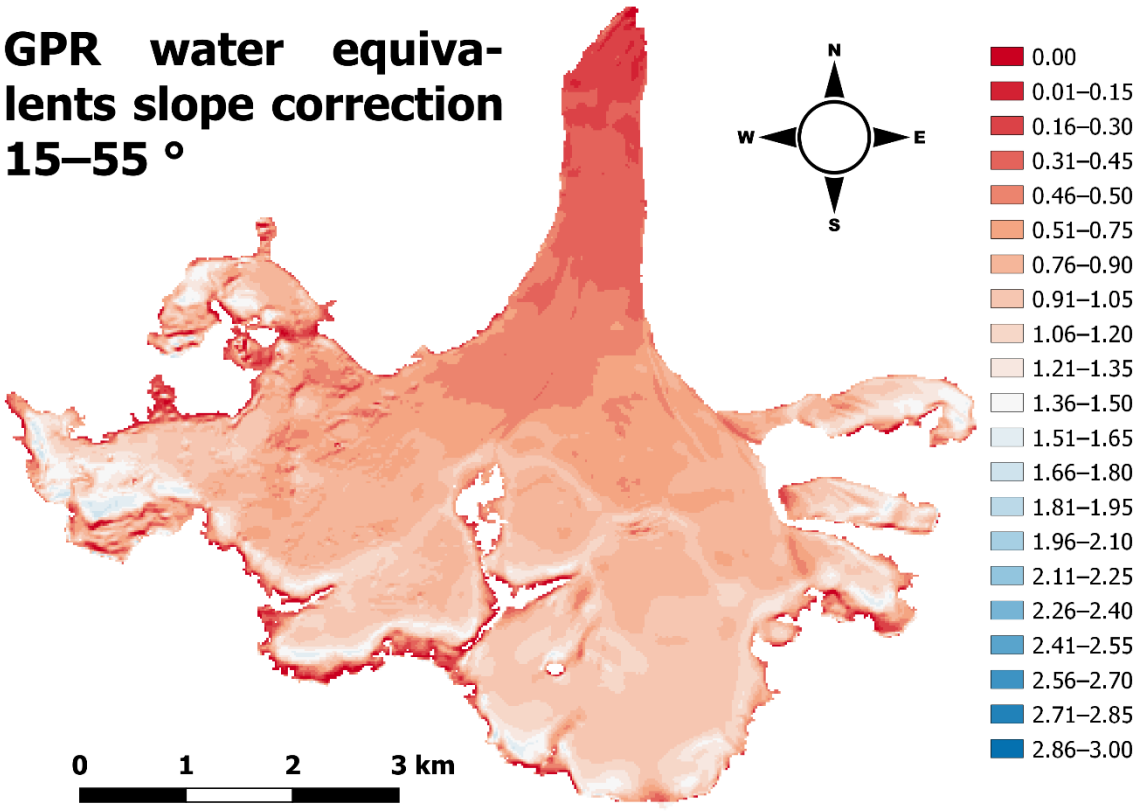


Figure 46: GPR slope-corrected water equivalent raster with linear decrease from 100 % up to 15 ° to 0 % above 55 ° [m w. e.].

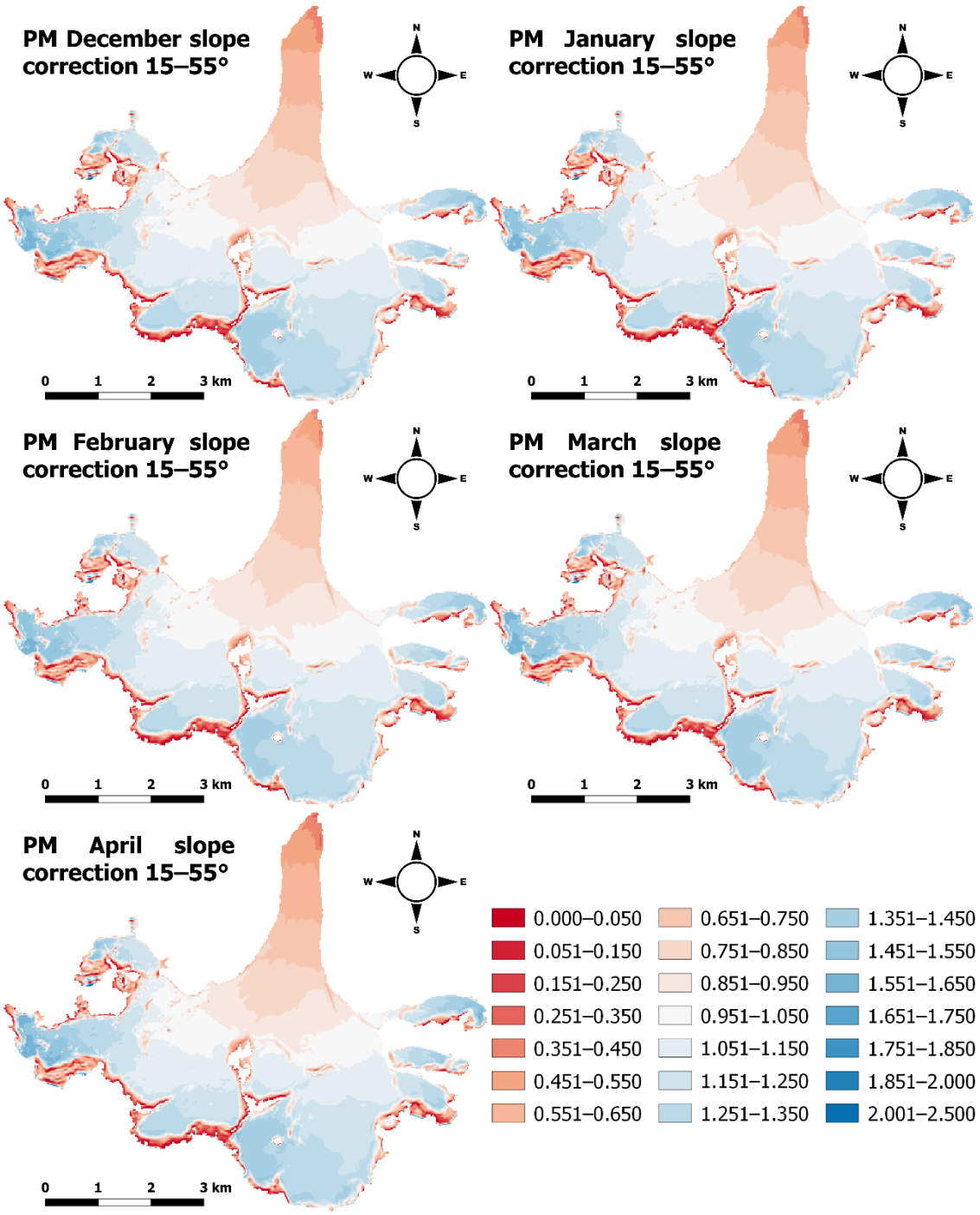


Figure 47: Soviet slope-corrected PM rasters December to April with linear decrease from 100 % at 15 ° to 0 % at 55 ° [dimensionless].

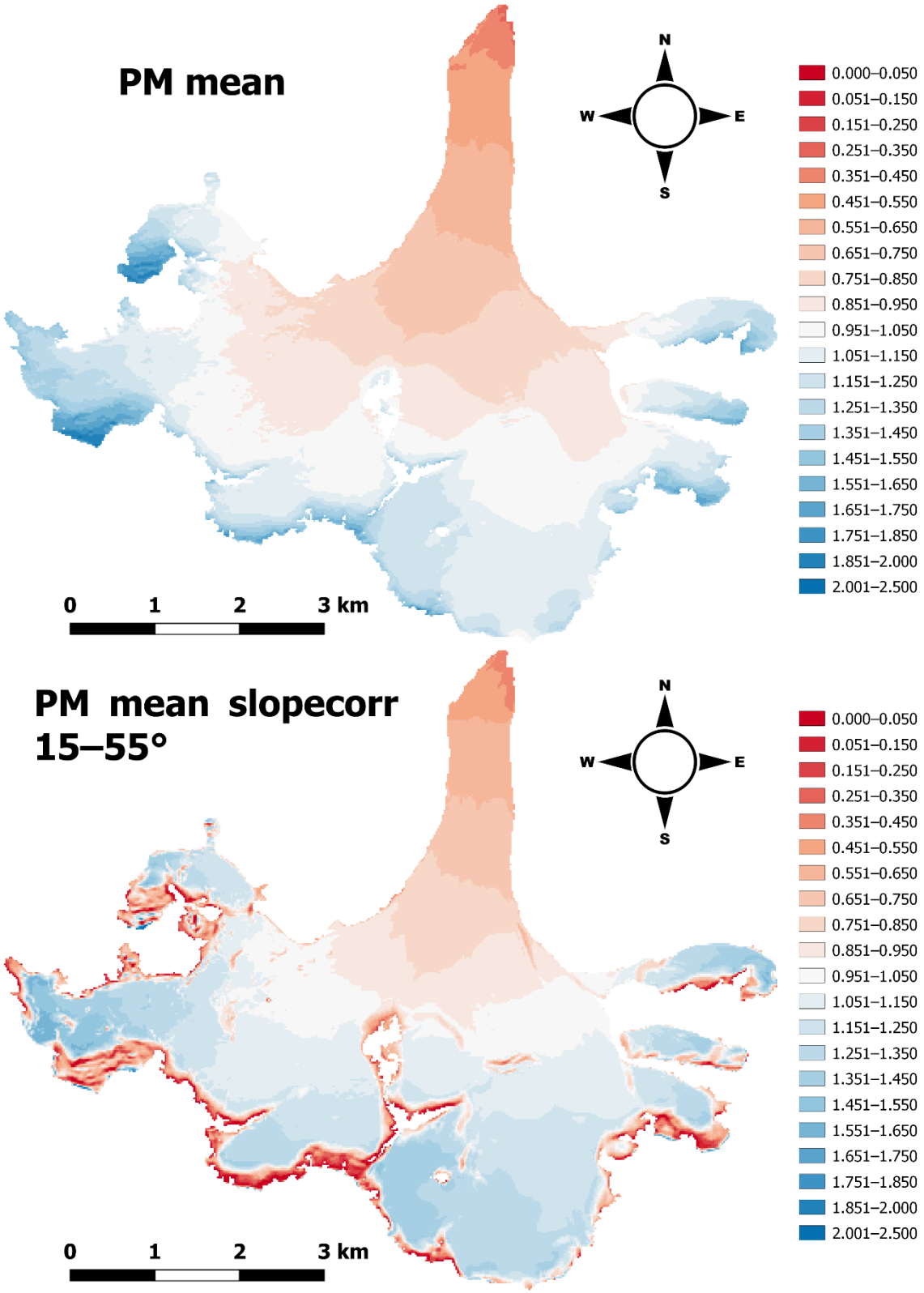


Figure 48 Soviet PM rasters without (top) and with (bottom) slope-correction (linear decrease from 100 % for slopes up to 15 ° to 0 % for slopes of 55 ° and steeper) [dimensionless].

Appendix H: Model constants and settings

Model files were developed by van Pelt et al. (2012) and changed by Horst Machguth and Warren Stainbank. In the following, only (partial) model files are given that have been changed during the prevailing thesis.

func_init_constants.m

```
%%%%%%%%%%%%%%%%%%%%%%%%%%%%%%%%%%%%%%%%%%%%%%%%%%%%%%%%%%%%%%%%%%%%%%%%%%%%%%%%
%%% Model constants
%%%%%%%%%%%%%%%%%%%%%%%%%%%%%%%%%%%%%%%%%%%%%%%%%%%%%%%%%%%%%%%%%%%%%%%%%%%%%%%%

function [C] = func_init_constants()

C.metstat_elev = 4120;      % meteorological station elevation
C.prec_grad = 0.00313;      % precipitation gradient
C.temp_grad = -0.005;       % initially -0.005; not change due to dependencies
C.prec_corr = 1.17;         % precipitation correction factor

C.alb_fresh = 0.835;        % albedo fresh snow
C.alb_firn = 0.55;          % albedo firn
C.alb_ice = 0.25;           % albedo ice
C.tstar = 21.9;             % albedo characteristic timescale (days)
C.dstar = 11.0;             % albedo characteristic depth (mm w.e.)
C.b = 0.447;                % constant in LWin formulation
C.ecl = 0.990;              % constant in LWin formulation
C.p = 2;                    % exponent in LWin formulation
C.boltz = 5.67d-8;          % Stefan-Boltzmann constant (W m-2 K-4)
C.VP0 = 610.5;              % vapor pressure at 0 degrees C
C.Cp = 1005.7;              % specific heat of dry air (J kg-1 K-1)
C.Cw = 4187.0;              % specific heat of water (J kg-1 K-1)
C.Ls = 2.83d6;              % latent heat of sublimation/riming (J kg-1)
C.Lm = 0.33d6;              % latent heat of melting/fusion (J kg-1)
C.Lv = 2.5d6;               % latent heat of evaporation/condensation (J kg-1)
C.Rv = 462.0;               % specific gas constant water vapor (J kg-1 K-1)
C.Rd = 287.0;               % specific gas constant dry air (J kg-1 K-1
C.eps = 0.622;              % C.Rd/C.Rv
C.dTacc = 0.01;             % threshold dT in solving the energy balance equation (K)
C.Pref = 1015d2;            % reference air pressure (Pa)
%C.Pref = 58286.88;          % reference air pressure (Pa)
C.Dfreshsnow = 350.0;       % density of fresh snow (kg m-3)
C.Dice = 900.0;             % density of ice (kg m-3)
C.Dwater = 1000.0;          % density of water (kg m-3)
C.rainsnowT = 274.65;       % temperature of snow to rain transition (K)
C.g = 9.81;                 % gravitational acceleration (m s-2)
C.Ec = 60000;               % gravitational densification factor
C.Eg = 42400;               % gravitational densification factor
C.rd = 8.314;               % universal gas constant (J mol-1 K-1)
C.lambda = 2.18;            % optical thickness empirical constant
C.k_aer = 0.97;             % aerosol transmissivity exponent
C.k_turb = 0.0004;          % turbulent flux coefficient
C.turb = 0.0028;            % background turbulent exchange coefficient
C.Pr = 5;                   % Prandtl number in SHF/LHF formulation
C.T0 = 273.15;              % melting temperature ice
C.Pthres = 1.1d-8;          % threshold precipitation to reset time since last snowfall
(m w.e. s-1)
C.Trunoff = 0.001;          % slush runoff time-scale (days)
C.geothermal_flux = 0.04;   % geothermal heat flux

C.soil_density = 1000.0;    % soil density (no functionality)
C.soil_albedo = 0.15;       % soil albedo
C.soil_Kfrozen = 2.50;      % soil conductivity (frozen)
C.soil_Kthawed = 1.45;      % soil conductivity (thawed)
C.soil_Cfrozen = 1.95d6;    % soil specific heat capacity (frozen)
C.soil_Cthawed = 2.45d6;    % soil specific heat capacity (thawed)
C.soil_THwmin = 0.05;       % soil minimum water content
C.soil_THwmax = 0.30;       % soil maximum water content
C.soil_delta = 0.17;        % soil freezing parameter (deg C)

end
```

func_init_prams.m

```
%%%%%%%%%%%%%%%%%%%%%%%%%%%%%%%%%%%%%%%%%%%%%%%%%%%%%%%%%%%%%%%%%%%%%%%%
%%% Model parameters
%%%%%%%%%%%%%%%%%%%%%%%%%%%%%%%%%%%%%%%%%%%%%%%%%%%%%%%%%%%%%%%%%%%%%%%%

function [grid, time, io] = func_init_params()
clearvars;

%% time parameters
% time.ts = '01-Jan-2007 02:55';                                        % date start run
% time.te = '31-Oct-2013 23:55';                                        % date end run
time.ts = '01-Nov-2013 02:55';                                          % date start run
time.te = '01-Oct-2017 02:55';                                          % date end run
time.ti = '01-Jan-1985 02:55';                                          % date start
climate record
time.dt = 0.125;                                                        % timestep
(days)
time.tn = round((datenum(time.te)-datenum(time.ts))/time.dt+1);         % number of
time-steps

%% grid parameters
grid.dx = 100;                                                          % horizontal
grid spacing (m) %SW: 100 oder 50 (Meter)
grid.utmzone = 42;                                                      % UTM zone
grid.max_subZ = 0.1;                                                    % maximum layer
thickness (m)
grid.nl = 100;                                                          % number of ver-
tical layers
grid.doubledepth = 1;                                                   % double verti-
cal layer depth at layer nr defined in grid.split (1=yes, 0=no)
grid.split = [40;60;80];                                                % vertical layer
nr at which layer depth doubles

%% Stake reading comparison
time.stake_hour = '14:55';                                              % set time of
day to record measurement

%% input/output parameters
io.homedir = 'D:/Studium/Master/MA/Auswertung_Modell_WardVanPelt/MATLAB/EBM_abra';
% home directory
io.rebootdir = [io.homedir '/reboot/'];                                 % reboot direc-
tory
io.outdir = [io.homedir '/output/'];                                    % output direc-
tory

io.gridfile = [io.homedir '/grid/grid100m_slopekorr.mat'];              % grid file con-
taining DEM + mask,
% Precipitation Multiplier: grid50m or grid100m or grid100m_slopekorr; if
grid100m_slopekorr: io.PM=0 and io.PM_slopekorr=1
io.PM = 0;                                                              % if a Precipi-
tation Multiplier raster (line above) and
                                                                        % loadclimate
line 29 is chosen: 1 else 0
io.PM_slopekorr = 1;                                                    % (1=yes, 0=no),
if io.PM_slopekorr = 1, io.PM needs to be 0!!!
io.PM_prec_grad = 0;                                                    % PM raster AND
precipitation gradient+prec. correction factor (1=yes, 0=no)
io.climfile = [io.homedir '/climate/climate.mat'];                      % climate input
file
io.stakefile = [io.homedir '/stake/stake.mat'];                         % stake input
file

io.stakecompare = 1;                                                    % compare stake
measurements with modelled (1=yes, 0=no)
io.readclimatefromfile = 1;                                             % read climate
data from input files (1=yes, 0=no)
io.out_surface = 1;                                                     % write surface
variables to files (1=yes, 0=no)
io.out_subsurface = 1;                                                  % write subsur-
face variables to files (1=yes, 0=no)
io.freqout = 8;                                                         % frequency of
storing output (every n-th time-step)

io.readbootfile = 1;                                                    % read initial
conditions from file (1=yes, 0=no)
```

```
io.bootfilein = 'boot_file_in.mat';                                    % bootfile to be
read
io.writebootfile = 0;                                                  % write file for
rebooting (1=yes, 0=no)
io.bootfileout = 'boot_file_out.mat';                                  % bootfile to be
written

io.infofile = 'runinfo.mat';                                           % file to store
run information

io.save_to_binary_files = 1;                                           % save output to
binary files (1=yes, 0=no)
io.save_to_netcdf_files = 0;                                           % save output to
netcdf files (1=yes, 0=no)

end
```

func_init_grid.m

```
%%%%%%%%%%%%%%%%%%%%%%%%%%%%%%%%%%%%%%%%%%%%%%%%%%%%%%%%%%%%%%%%%%%%%%%%
%%% Load DEM and glacier outline
%%%%%%%%%%%%%%%%%%%%%%%%%%%%%%%%%%%%%%%%%%%%%%%%%%%%%%%%%%%%%%%%%%%%%%%%

function [grid] = func_init_grid(grid,io)

load(io.gridfile);
gridfile = gridinfo;
grid.Lx = size(gridfile.mask,1);
grid.Ly = size(gridfile.mask,2);

if gridfile.x(1,2)-gridfile.x(1,1)<0
    gridfile.x = fliplr(gridfile.x);
    gridfile.y = fliplr(gridfile.y);
    gridfile.z = fliplr(gridfile.z);
    gridfile.mask = fliplr(gridfile.mask);
    if io.PM==1
        gridfile.gpr = fliplr(gridfile.gpr);                           %gpr PM raster
        gridfile.soviet = fliplr(gridfile.soviet);                     %soviet PM
raster
    end
    if io.PM_slopekorr==1
        gridfile.gpr_slopekorr1555 = fliplr(gridfile.gpr_slopekorr1555);        %gpr PM raster
slopekorr15-55°
        gridfile.soviet_slopekorr1555 = fliplr(gridfile.soviet_slopekorr1555);  %soviet PM
raster slopekorr15-55°
    end
end
if gridfile.y(2,1)-gridfile.y(1,1)<0
    gridfile.x = flipud(gridfile.x);
    gridfile.y = flipud(gridfile.y);
    gridfile.z = flipud(gridfile.z);
    gridfile.mask = flipud(gridfile.mask);
    if io.PM==1
        gridfile.gpr = flipud(gridfile.gpr);                           %gpr PM raster
        gridfile.soviet = flipud(gridfile.soviet);                     %soviet PM
raster
    end
    if io.PM_slopekorr==1
        gridfile.gpr_slopekorr1555 = flipud(gridfile.gpr_slopekorr1555);        %gpr PM raster
slopekorr15-55°
        gridfile.soviet_slopekorr1555 = flipud(gridfile.soviet_slopekorr1555);  %soviet PM
raster slopekorr15-55°
    end
end

grid.x = gridfile.x;
grid.y = gridfile.y;
grid.z = double(gridfile.z);
if io.PM==1
    grid.gpr = double(gridfile.gpr);                                   %gpr PM raster
    grid.soviet = double(gridfile.soviet);                             %soviet PM
raster
end
if io.PM_slopekorr==1
    grid.gpr_slopekorr1555 = double(gridfile.gpr_slopekorr1555);       %gpr PM raster
slopekorr15-55°
    grid.soviet_slopekorr1555 = double(gridfile.soviet_slopekorr1555); %soviet PM
raster slopekorr15-55°
end
```

```
grid.mask_2D = gridfile.mask;
grid.mask = gridfile.mask(:);
grid.mask_short = grid.mask(grid.mask>0);

grid.gpsum = sum(grid.mask>0);

[grid.lat,grid.lon] = utm2ll(gridfile.x,gridfile.y,grid.utmzone);

grid.x_mask = gridfile.x(grid.mask>0);
grid.y_mask = gridfile.y(grid.mask>0);
grid.z_mask = gridfile.z(grid.mask>0);
if io.PM==1
    grid.gpr_mask = gridfile.gpr(grid.mask>0);                                  %gpr PM raster
    grid.soviet_mask = gridfile.soviet(grid.mask>0);                            %soviet PM
raster
end
if io.PM_slopekorr==1
    grid.gpr_slopekorr1555_mask = gridfile.gpr_slopekorr1555(grid.mask>0);      %gpr PM raster
slopekorr15-55°
    grid.soviet_slopekorr1555_mask = gridfile.soviet_slopekorr1555(grid.mask>0);%soviet PM
raster slopekorr15-55°
end
grid.ind = find(grid.mask_2D>0);
grid.maskfull_3d = repmat(grid.mask_2D,1,1,grid.nl);
grid.ind3 = find(grid.maskfull_3d>0);
[grid.xind, grid.yind] = find(grid.mask_2D>0);

end
```

func_loadclimate.m

```
(…)
%% Precipitation [m w.e. ts-1]
%clim.P(:) = A.data_clim(tt,14)/1d3 * 24 * 3600 * time.dt;
% conversion to m w.e. per timestep
if A.data_clim(tt,14) > 0
    if io.PM==0 && io.PM_slopekorr==0
        clim.P(:) = (A.data_clim(tt,14)/1d3*24*3600*time.dt)*C.prec_corr +...
            (A.data_clim(tt,14)/1d3*24*3600*time.dt)*C.prec_grad*(grid.z_mask-
C.metstat_elev);
    elseif io.PM==1 && io.PM_prec_grad==1
% PM raster and new gradient (PM_prec_grad) and prec corr (PM_prec_corr)
        clim.P(:) = (A.data_clim(tt,14)/1d3*24*3600*time.dt)*C.prec_corr +...
            (A.data_clim(tt,14)/1d3*24*3600*time.dt)*grid.gpr_mask*...
% Choose multiplication raster (grid.gpr_mask or grid.soviet_mask)
           C.prec_grad.*(grid.z_mask-C.metstat_elev);
    elseif io.PM==1
% Same settings as Warren's simulation no40, but PM raster
        clim.P(:) = (A.data_clim(tt,14)/1d3*24*3600*time.dt)*C.prec_corr +...
            (A.data_clim(tt,14)/1d3*24*3600*time.dt)*grid.gpr_mask;
% Choose multiplication raster (grid.gpr_mask or grid.soviet_mask)
    elseif io.PM_slopekorr==1 && io.PM_prec_grad==0 % Choose multiplication raster
(grid.gpr_slopekorr2555_mask or soviet and/or 1555)
        clim.P(:) = (A.data_clim(tt,14)/1d3*24*3600*time.dt)*C.prec_corr +...
            (A.data_clim(tt,14)/1d3*24*3600*time.dt)*grid.gpr_slopekorr2555_mask;
    if io.PM_slopekorr==1 && io.PM_prec_grad==0 % Choose multiplication raster
(grid.gpr_slopekorr2555_mask or soviet and/or 1555)
        clim.P(:) = (A.data_clim(tt,14)/1d3*24*3600*time.dt)*C.prec_corr +...
            (A.data_clim(tt,14)/1d3*24*3600*time.dt)*grid.soviet_slopekorr1555_mask;
    else  % Choose multiplication raster (grid.gpr_mask or grid.soviet_mask)
        clim.P(:) = (A.data_clim(tt,14)/1d3*24*3600*time.dt)*C.prec_corr +...
            (A.data_clim(tt,14)/1d3*24*3600*time.dt)*grid.soviet_slopekorr1555_mask*...
           C.prec_grad.*(grid.z_mask-C.metstat_elev);
    end
else
    clim.P(:) = A.data_clim(tt,14)/1d3 * 24 * 3600 * time.dt;
end
(…)
```

func_init_gridpmgpr.m

```
%%%%%%%%%%%%%%%%%%%%%%%%%%%%%%%%%%%%%%%%%%%%%%%%%%%%%%%%%%%%%%%%%%%%%%%%
%%% Load GPR based Precipitation Multiplier raster
%%%%%%%%%%%%%%%%%%%%%%%%%%%%%%%%%%%%%%%%%%%%%%%%%%%%%%%%%%%%%%%%%%%%%%%%

function [gridpmgpr] = func_init_gridpmgpr(gridpmgpr,io)

load(io.gridpmgpr);
gridpmgprfile = gridinfo;
%gridinfo
gridpmgpr.Lx = size(gridpmgprfile.mask,1);
gridpmgpr.Ly = size(gridpmgprfile.mask,2);

if gridpmgprfile.x(1,2)-gridpmgprfile.x(1,1)<0
    gridpmgprfile.x = fliplr(gridpmgprfile.x);
    gridpmgprfile.y = fliplr(gridpmgprfile.y);
    gridpmgprfile.z = fliplr(gridpmgprfile.z);
    gridpmgprfile.mask = fliplr(gridpmgprfile.mask);
end
if gridpmgprfile.y(2,1)-gridpmgprfile.y(1,1)<0
    gridpmgprfile.x = flipud(gridpmgprfile.x);
    gridpmgprfile.y = flipud(gridpmgprfile.y);
    gridpmgprfile.z = flipud(gridpmgprfile.z);
    gridpmgprfile.mask = flipud(gridpmgprfile.mask);
end

gridpmgpr.x = gridpmgprfile.x;
gridpmgpr.y = gridpmgprfile.y;
gridpmgpr.z = double(gridpmgprfile.z);

gridpmgpr.mask_2D = gridpmgprfile.mask;
gridpmgpr.mask = gridpmgprfile.mask(:);
gridpmgpr.mask_short = gridpmgpr.mask(gridpmgpr.mask>0);

gridpmgpr.gpsum = sum(gridpmgpr.mask>0);

[gridpmgpr.lat,gridpmgpr.lon] = utm2ll(gridpmgprfile.x,gridpmgprfile.y,grid.utmzone);
%grid.utmzone

gridpmgpr.x_mask = gridpmgprfile.x(gridpmgpr.mask>0);
gridpmgpr.y_mask = gridpmgprfile.y(gridpmgpr.mask>0);
gridpmgpr.z_mask = gridpmgprfile.z(gridpmgpr.mask>0);
% gridpmgpr.ind = find(gridpmgpr.mask_2D>0);
% gridpmgpr.maskfull_3d = repmat(gridpmgpr.mask_2D,1,1,grid.nl);
%grid.nl
% gridpmgpr.ind3 = find(gridpmgpr.maskfull_3d>0);
% [gridpmgpr.xind, gridpmgpr.yind] = find(gridpmgpr.mask_2D>0);

end
```

func_init_gridpmsoviet.m

```
%%%%%%%%%%%%%%%%%%%%%%%%%%%%%%%%%%%%%%%%%%%%%%%%%%%%%%%%%%%%%%%%%%%%%%%%
%%% Load DEM and glacier outline
%%%%%%%%%%%%%%%%%%%%%%%%%%%%%%%%%%%%%%%%%%%%%%%%%%%%%%%%%%%%%%%%%%%%%%%%

function [gridpmsoviet] = func_init_gridpmsoviet(gridpmsoviet,io)

load(io.gridpmsoviet);
gridpmsovietfile = gridinfo;                                    %gridinfo
gridpmsoviet.Lx = size(gridpmsovietfile.mask,1);
gridpmsoviet.Ly = size(gridpmsovietfile.mask,2);

if gridpmsovietfile.x(1,2)-gridpmsovietfile.x(1,1)<0
    gridpmsovietfile.x = fliplr(gridpmsovietfile.x);
    gridpmsovietfile.y = fliplr(gridpmsovietfile.y);
    gridpmsovietfile.z = fliplr(gridpmsovietfile.z);
    gridpmsovietfile.mask = fliplr(gridpmsovietfile.mask);
end
if gridpmsovietfile.y(2,1)-gridpmsovietfile.y(1,1)<0
    gridpmsovietfile.x = flipud(gridpmsovietfile.x);
    gridpmsovietfile.y = flipud(gridpmsovietfile.y);
    gridpmsovietfile.z = flipud(gridpmsovietfile.z);
    gridpmsovietfile.mask = flipud(gridpmsovietfile.mask);
end
```

```
gridpmsoviet.x = gridpmsovietfile.x;
gridpmsoviet.y = gridpmsovietfile.y;
gridpmsoviet.z = double(gridpmsovietfile.z);

gridpmsoviet.mask_2D = gridpmsovietfile.mask;
gridpmsoviet.mask = gridpmsovietfile.mask(:);
gridpmsoviet.mask_short = gridpmsoviet.mask(gridpmsoviet.mask>0);

gridpmsoviet.gpsum = sum(gridpmsoviet.mask>0);

[gridpmsoviet.lat,gridpmsoviet.lon] =
utm2ll(gridpmsovietfile.x,gridpmsovietfile.y,grid.utmzone); %grid.utmzone

gridpmsoviet.x_mask = gridpmsovietfile.x(gridpmsoviet.mask>0);
gridpmsoviet.y_mask = gridpmsovietfile.y(gridpmsoviet.mask>0);
gridpmsoviet.z_mask = gridpmsovietfile.z(gridpmsoviet.mask>0);
% gridpmsoviet.ind = find(gridpmsoviet.mask_2D>0);
% gridpmsoviet.maskfull_3d = repmat(gridpmsoviet.mask_2D,1,1,grid.nl);
%grid.nl
% gridpmsoviet.ind3 = find(gridpmsoviet.maskfull_3d>0);
% [gridpmsoviet.xind, gridpmsoviet.yind] = find(gridpmsoviet.mask_2D>0);

end
```

Table 29: Changes in model constants and number of simulation.

Date	Run no.	Time start	Time end	Stake measurements	Precipitation gradient	Precipitation correction	Albedo	Rain snow threshold	Lapse rate	BIAS	AME	RMSE	R-squared	Comment
31. Mai	40	01. Nov 13	01. Okt 17	2014-2017	0.00313	2.2	0.25	274.65	-0.005	0.40049	0.610715	0.697149	0.8403	
SW: Runs with settings from Warren Run no. 40 if not indicated otherwise														oNSU = ohne neues Spin-up; mNSU = mit neuem Spin-up
18. Jun	140	01. Nov 13	01. Okt 17	2014-2017		2.2	0.25	274.65	-0.005	-1.02	1.04	1.31	0.67	Soviet raster mNSU
20. Jun	141	01. Nov 13	01. Okt 17	2014-2017		2.2	0.25	274.65	-0.005	-0.86	0.94	1.21	0.69	GPR raster mNSU
21. Jun	142	01. Nov 13	01. Okt 17	2014-2017	0.00131	0.8	0.25	274.65	-0.005	2.19	2.33	2.5	0.73	Soviet raster with PM, PMcorrection and PMgradient
21. Jun	143	01. Nov 13	01. Okt 17	2014-2017	0.0026	0.9	0.25	274.65	-0.005	2.28	2.43	2.62	0.78	Soviet raster with PM, PMcorrection and PMgradient
21. Jun	144	01. Nov 13	01. Okt 17	2014-2017	0.002	0.95	0.25	274.65	-0.005	2.03	2.19	2.35	0.76	Soviet raster with PM, PMcorrection and PMgradient
22. Jun	145	01. Nov 13	01. Okt 17	2014-2017	0.0022	1.2	0.25	274.65	-0.005	1.51	1.69	1.84	0.76	Soviet raster with PM, PMcorrection and PMgradient
25. Jun	146	01. Nov 13	01. Okt 17	2014-2017	0.0026	1.4	0.25	274.65	-0.005	1.22	1.41	1.59	0.77	Soviet raster with PM, PMcorrection and PMgradient
25. Jun	147	01. Nov 13	01. Okt 17	2014-2017	0.003	1.7	0.25	274.65	-0.005	0.81	1.04	1.26	0.77	Soviet raster with PM, PMcorrection and PMgradient
25. Jun	148	01. Nov 13	01. Okt 17	2014-2017	0.004	1.8	0.25	274.65	-0.005	0.75	1.06	1.26	0.78	Soviet raster with PM, PMcorrection and PMgradient
25. Jun	149	01. Nov 13	01. Okt 17	2014-2017	0.004	2.2	0.25	274.65	-0.005	0.12	0.69	0.92	0.77	Soviet raster with PM, PMcorrection and PMgradient
25. Jun	150	01. Nov 13	01. Okt 17	2014-2017	0.0041	2.05	0.25	274.65	-0.005	0.35	0.8	1.01	0.79	Soviet raster with PM, PMcorrection and PMgradient
25. Jun	151	01. Nov 13	01. Okt 17	2014-2017	0.00415	2.05	0.25	274.65	-0.005	0.35	0.81	1.01	0.79	Soviet raster with PM, PMcorrection and PMgradient
25. Jun	152	01. Nov 13	01. Okt 17	2014-2017	0.0044	2	0.25	274.65	-0.005	0.42	0.85	1.06	0.79	Soviet raster with PM, PMcorrection and PMgradient
25. Jun	153	01. Nov 13	01. Okt 17	2014-2017	0.00438	2.04	0.25	274.65	-0.005	0.38	0.83	1.04	0.79	Soviet raster with PM, PMcorrection and PMgradient
25. Jun	154	01. Nov 13	01. Okt 17	2014-2017		2.2	0.2	274.65	-0.005	-0.92	0.98	1.26	0.69	Soviet raster with PM and C.prec_corr
25. Jun	155	01. Nov 13	01. Okt 17	2014-2017		1.7	0.2	274.65	-0.005	-0.21	0.65	0.96	0.66	Soviet raster with PM and C.prec_corr
25. Jun	156	01. Nov 13	01. Okt 17	2014-2017		1.2	0.2	274.65	-0.005	0.37	0.75	1.02	0.7	Soviet raster with PM and C.prec_corr
28. Jun	157	01. Nov 13	01. Okt 17	2014-2017		1.15	0.2	274.65	-0.005	0.43	0.77	1.05	0.71	Soviet raster with PM and C.prec_corr
28. Jun	158	01. Nov 13	01. Okt 17	2014-2017		1.1	0.2	274.65	-0.005	0.49	0.79	1.06	0.73	Soviet raster with PM and C.prec_corr
28. Jun	159	01. Nov 13	01. Okt 17	2014-2017		1.1	0.2	274.65	-0.006	0.58	0.85	1.1	0.77	Soviet raster with PM and C.prec_corr and C.temp_grad
28. Jun	160	01. Nov 13	01. Okt 17	2014-2017		1.1	0.25	274.65	-0.006	0.38	0.68	0.95	0.78	Soviet raster with PM and C.prec_corr and C.temp_grad
28. Jun	161	01. Nov 13	01. Okt 17	2014-2017		1.1	0.25	274.65	-0.008	0.65	0.94	1.14	0.83	Soviet raster with PM and C.prec_corr and C.temp_grad
28. Jun	162	01. Nov 13	01. Okt 17	2014-2017		1.2	0.25	274.65	-0.0078	0.57	0.9	1.11	0.82	Soviet raster with PM and C.prec_corr and C.temp_grad
28. Jun	163	01. Nov 13	01. Okt 17	2014-2017		1.4	0.25	274.65	-0.0075	0.28	0.68	0.96	0.81	Soviet raster with PM and C.prec_corr and C.temp_grad
28. Jun	164	01. Nov 13	01. Okt 17	2014-2017		1.356	0.25	274.65	-0.0075	0.34	0.72	0.98	0.81	Soviet raster with PM and C.prec_corr and C.temp_grad
29. Jun	165	01. Nov 13	01. Okt 17	2014-2017		1.356	0.25	274.65	-0.0075	0.54	0.87	1.08	0.82	GPR raster with PM and C.prec_corr and C.temp_grad
29. Jun	166	01. Nov 13	01. Okt 17	2014-2017		1.45	0.25	274.65	-0.007	0.34	0.69	0.95	0.8	GPR raster with PM and C.prec_corr and C.temp_grad
01. Jul	167	01. Nov 13	01. Okt 17	2014-2017		1.41	0.25	274.65	-0.007	0.34	0.72	0.98	0.81	GPR raster with PM and C.prec_corr and C.temp_grad
02. Jul	168	01. Nov 13	01. Okt 17	2014-2017		1.44	0.25	274.65	-0.0072	0.37	0.72	0.97	0.81	GPR raster with PM and C.prec_corr and C.temp_grad
02. Jul	169	01. Nov 13	01. Okt 17	2014-2017	0.00438	2.04	0.25	274.65	-0.0074	0.34	0.72	0.98	0.81	GPR raster with PM and C.prec_corr and C.temp_grad and PMgradient
02. Jul	170	01. Nov 13	01. Okt 17	2014-2017	0.004	2.3	0.25	274.65	-0.005	-0.14	0.69	0.96	0.71	GPR raster with PM and C.prec_corr and PMgradient
02. Jul	171	01. Nov 13	01. Okt 17	2014-2017	0.0043	2	0.25	274.65	-0.005	0.28	0.75	0.97	0.76	GPR raster with PM and C.prec_corr and PMgradient
New calculations for discassion with slopekorr:														
16. Jul	200	01. Nov 13	01. Okt 17	2014-2017		2.2	0.25	274.65	-0.005	-0.96	1.02	1.28	0.81	GPR PM raster with slopecorr25-55°; oNSU
16. Jul	201	01. Nov 13	01. Okt 17	2014-2017		2.2	0.25	274.65	-0.005	-1.03	1.06	1.31	0.7	GPR PM raster with slopecorr15-55°; mNSU
16. Jul	202	01. Nov 13	01. Okt 17	2014-2017		1.4	0.25	274.65	-0.005	-0.06	0.57	0.85	0.72	GPR PM raster with slopecorr15-55° and C.prec_corr
16. Jul	203	01. Nov 13	01. Okt 17	2014-2017		1.2	0.2	274.65	-0.005	0.41	0.72	0.99	0.74	GPR PM raster with slopecorr15-55° and C.prec_corr and Albedo ice
18. Jul	204	01. Nov 13	01. Okt 17	2014-2017		1.2	0.25	274.65	-0.007	0.5	0.81	1.02	0.81	GPR PM raster with slopecorr15-55° and C.prec_corr and C.temp_grad
18. Jul	205	01. Nov 13	01. Okt 17	2014-2017		1.2	0.25	274.65	-0.005	0.07	0.62	0.9	0.69	Soviet PM raster with slopecorr15-55° and C.prec_corr mNSU
18. Jul	206	01. Nov 13	01. Okt 17	2014-2017		1.1	0.25	274.65	-0.007	0.41	0.72	0.97	0.81	Soviet PM raster with slopecorr15-55° and C.prec_corr and C.temp_grad
18. Jul	207	01. Nov 13	01. Okt 17	2014-2017		1.14	0.25	274.65	-0.0073	0.43	0.75	0.98	0.81	Soviet PM raster with slopecorr15-55° and C.prec_corr and C.temp_grad
18. Jul	208	01. Nov 13	01. Okt 17	2014-2017		1.17	0.25	274.65	-0.0074	0.41	0.75	0.98	0.81	Soviet PM raster with slopecorr15-55° and C.prec_corr and C.temp_grad

Appendix I: Model results

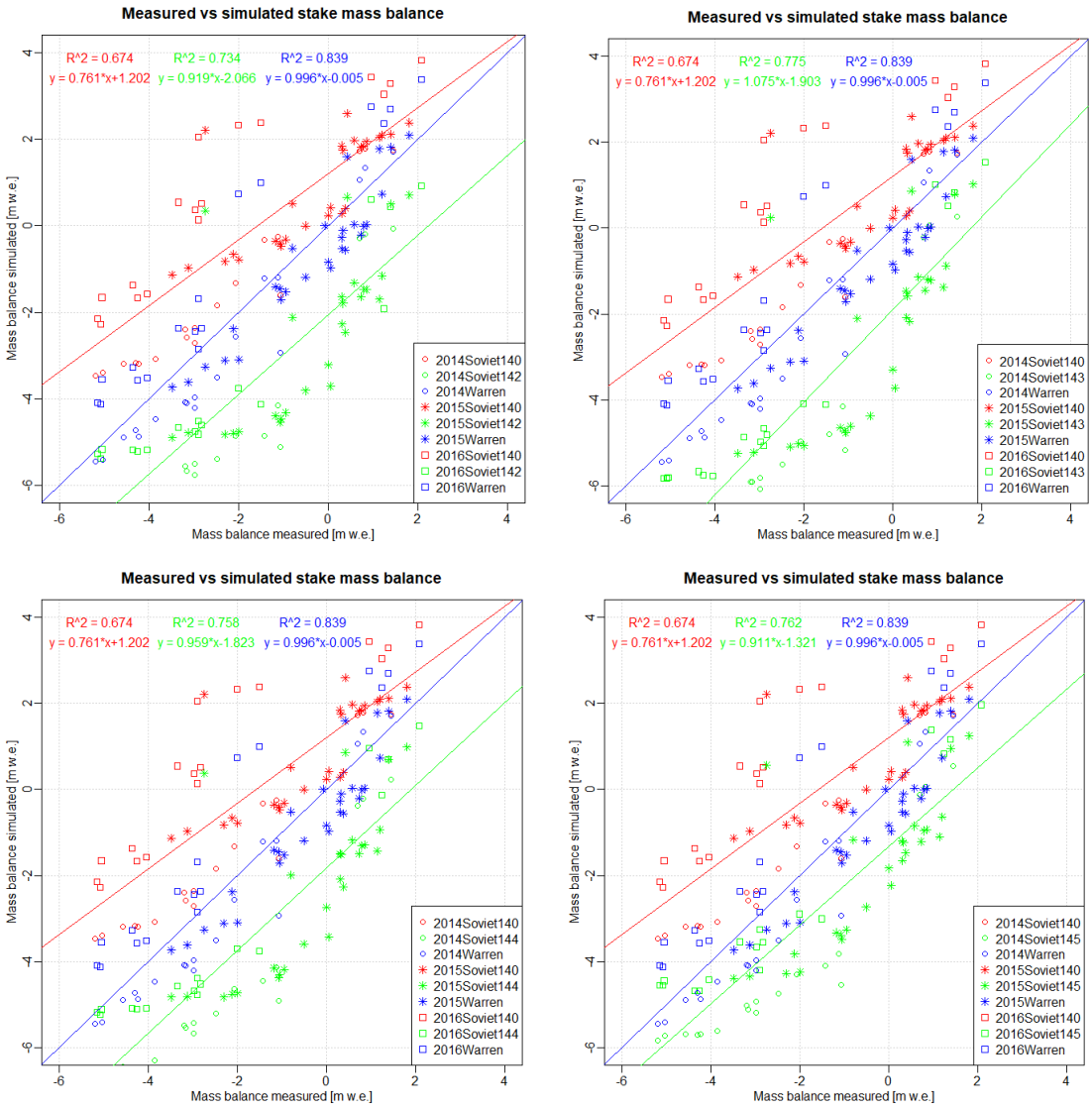


Figure 49: Measured versus simulated mass balance for the period 1 November 2013 02:55 until 1 October 2017 02:55. Warren's best simulation (blue) is compared with the simulations using the Soviet precipitation multiplier and the same settings (red) as well as with improved parameter settings (green). Details about parameter settings: Table 29.

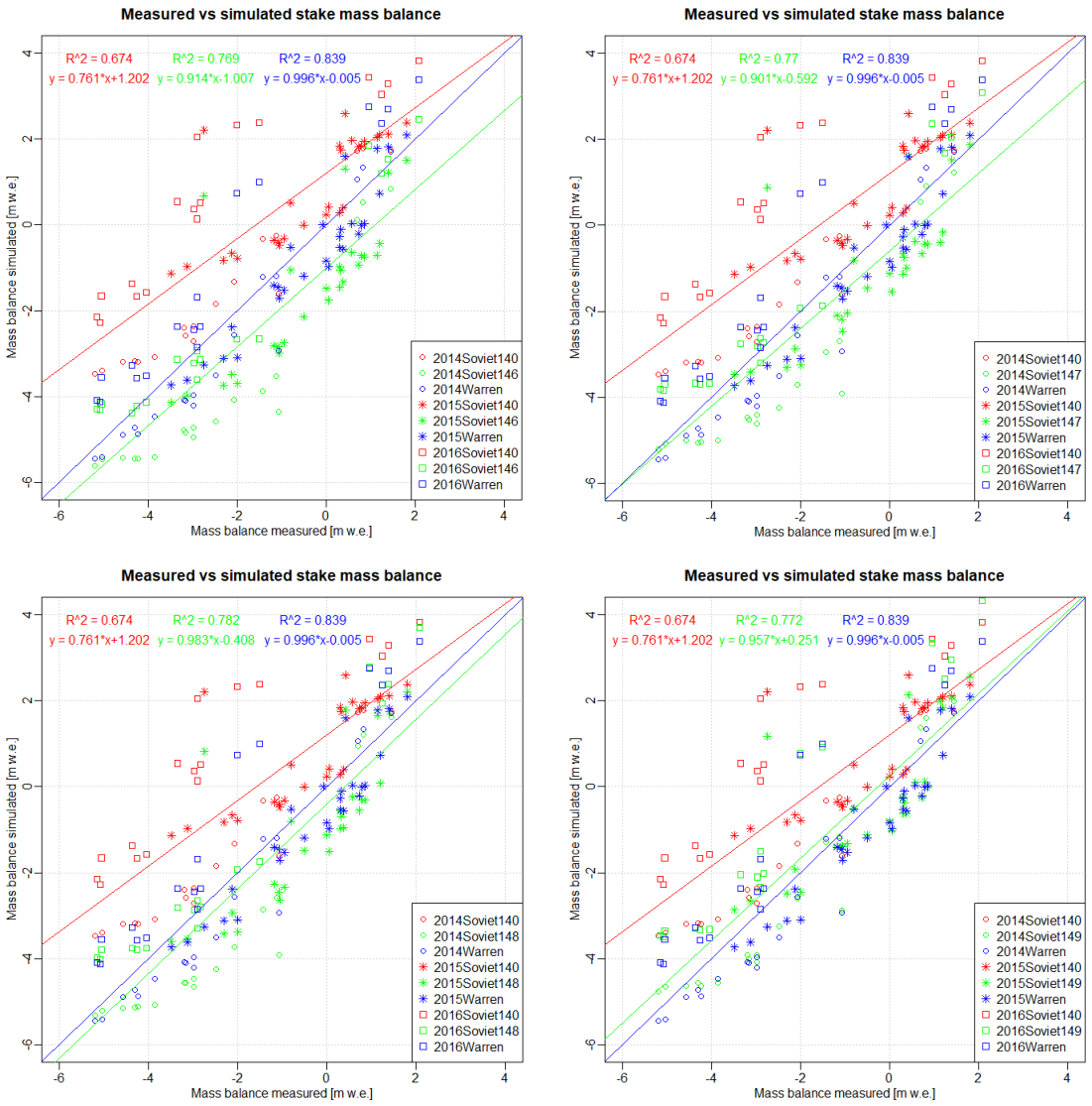


Figure 50: Measured versus simulated mass balance for the period 1 November 2013 02:55 until 1 October 2017 02:55. Warren's best simulation (blue) is compared with the simulations using the Soviet precipitation multiplier and the same settings (red) as well as with improved parameter settings (green). Details about parameter settings: Table 29.

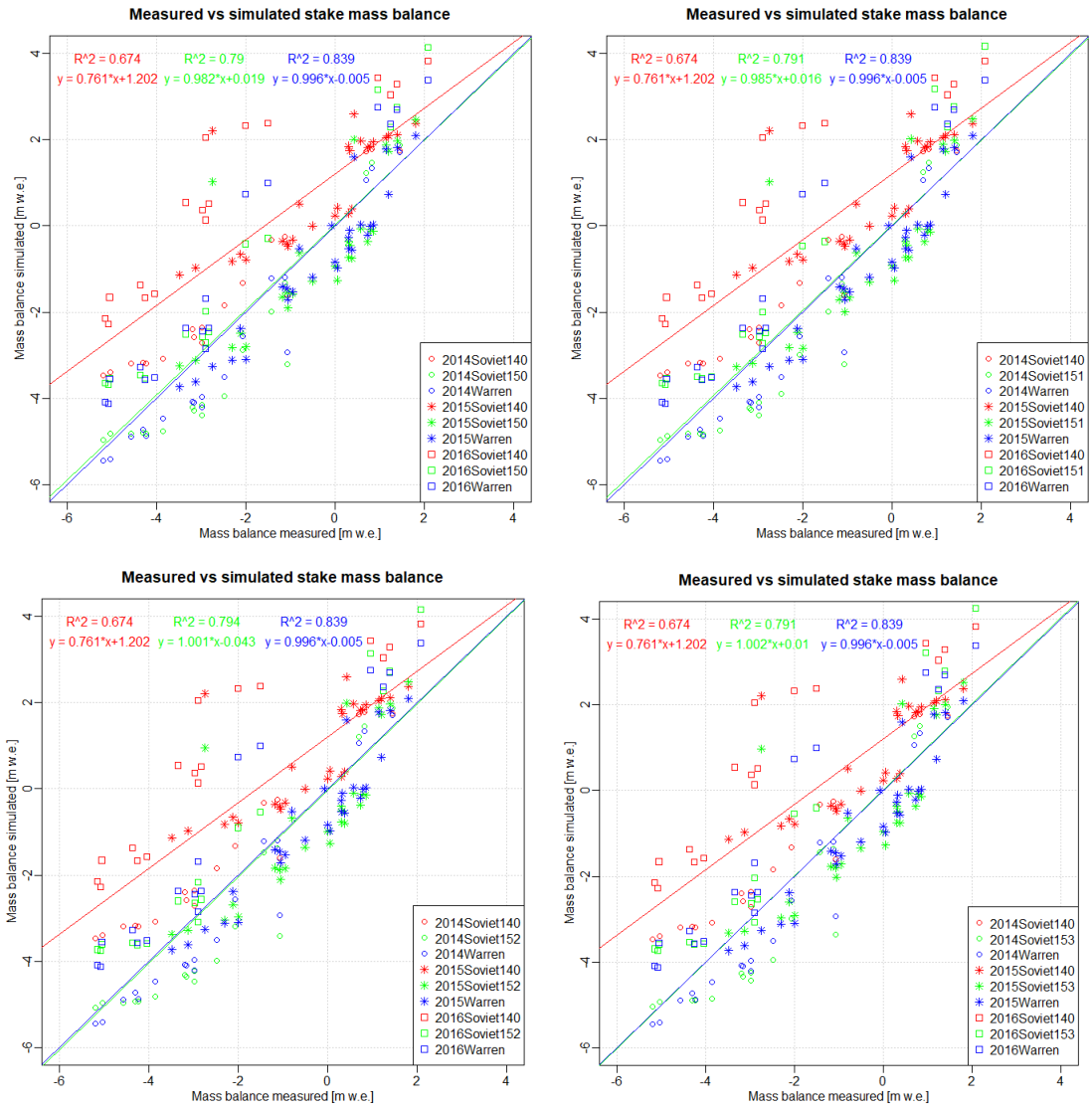


Figure 51: Measured versus simulated mass balance for the period 1 November 2013 02:55 until 1 October 2017 02:55. Warren's best simulation (blue) is compared with the simulations using the Soviet PM and the same settings (red) as well as with improved parameter settings (green). Details about parameter settings: Table 29.

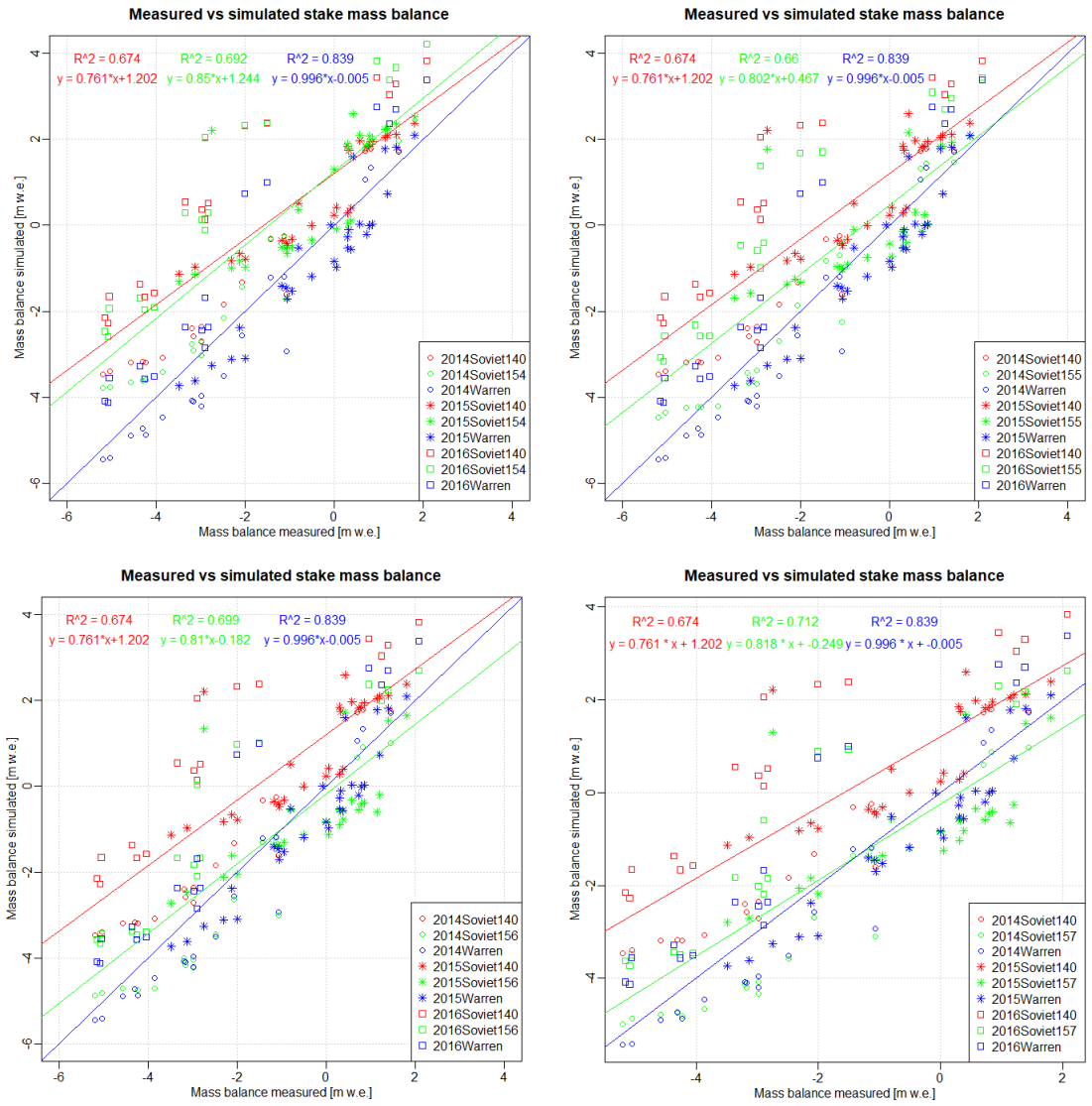


Figure 52: Measured versus simulated mass balance for the period 1 November 2013 02:55 until 1 October 2017 02:55. Warren's best simulation (blue) is compared with the simulations using the Soviet PM and the same settings (red) as well as with improved parameter settings (green). Details about parameter settings: Table 29.

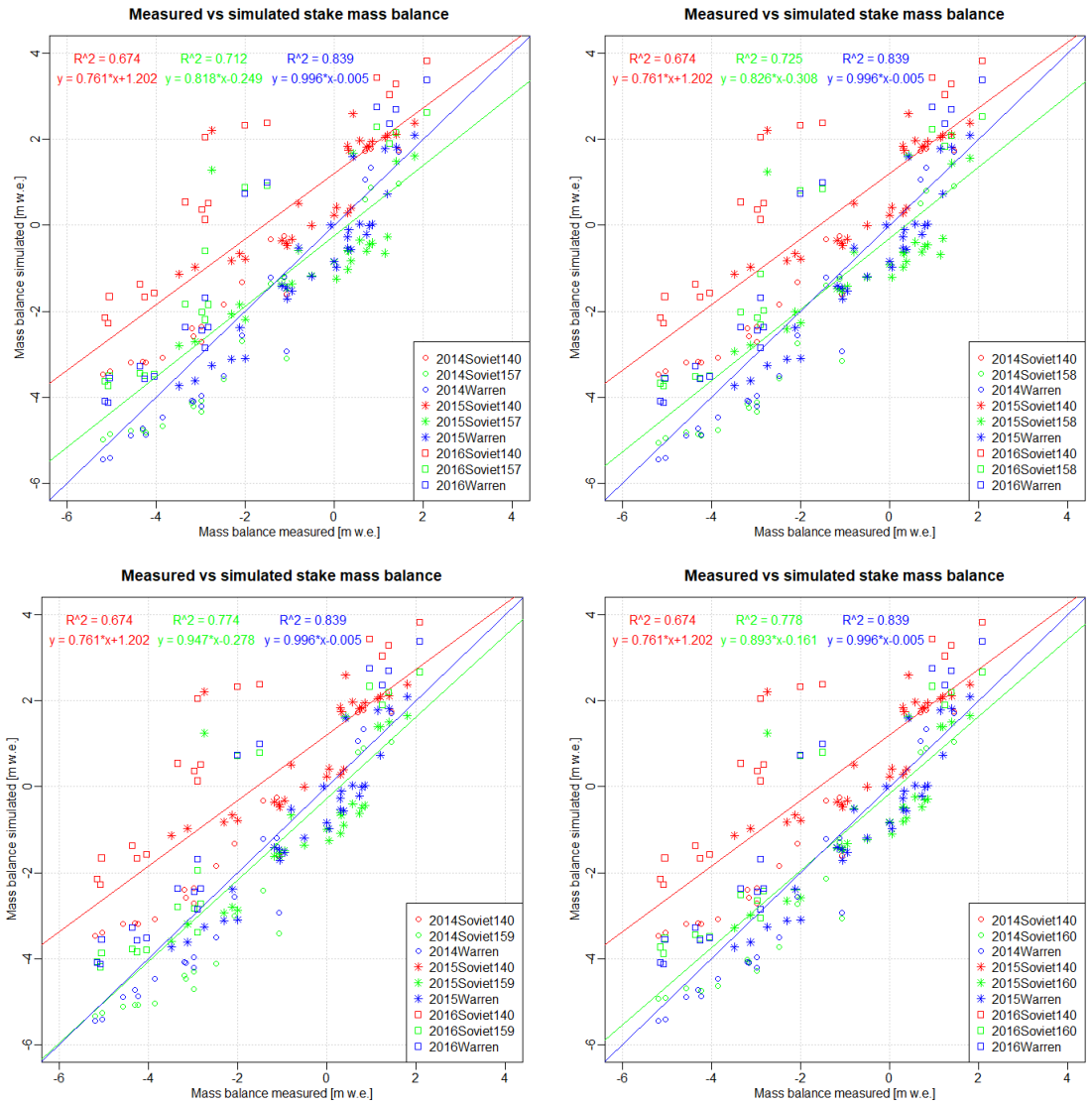


Figure 53: Measured versus simulated mass balance for the period 1 November 2013 02:55 until 1 October 2017 02:55. Warren's best simulation (blue) is compared with the simulations using the Soviet PM and the same settings (red) as well as with improved parameter settings (green). Details about parameter settings: Table 29.

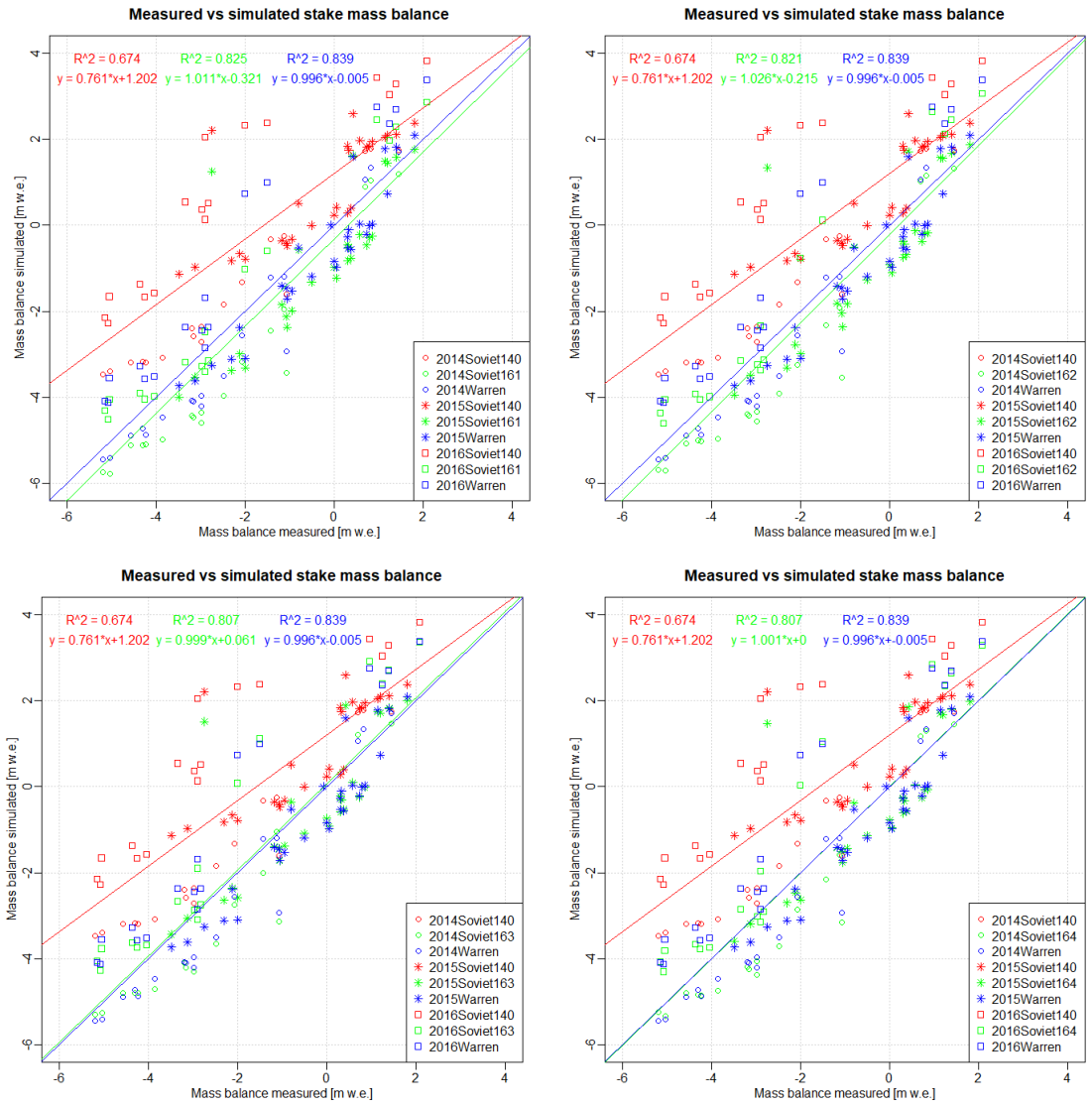


Figure 54: Measured versus simulated mass balance for the period 1 November 2013 02:55 until 1 October 2017 02:55. Warren's best simulation (blue) is compared with the simulations using the Soviet PM and the same settings (red) as well as with improved parameter settings (green). Details about parameter settings: Table 29.

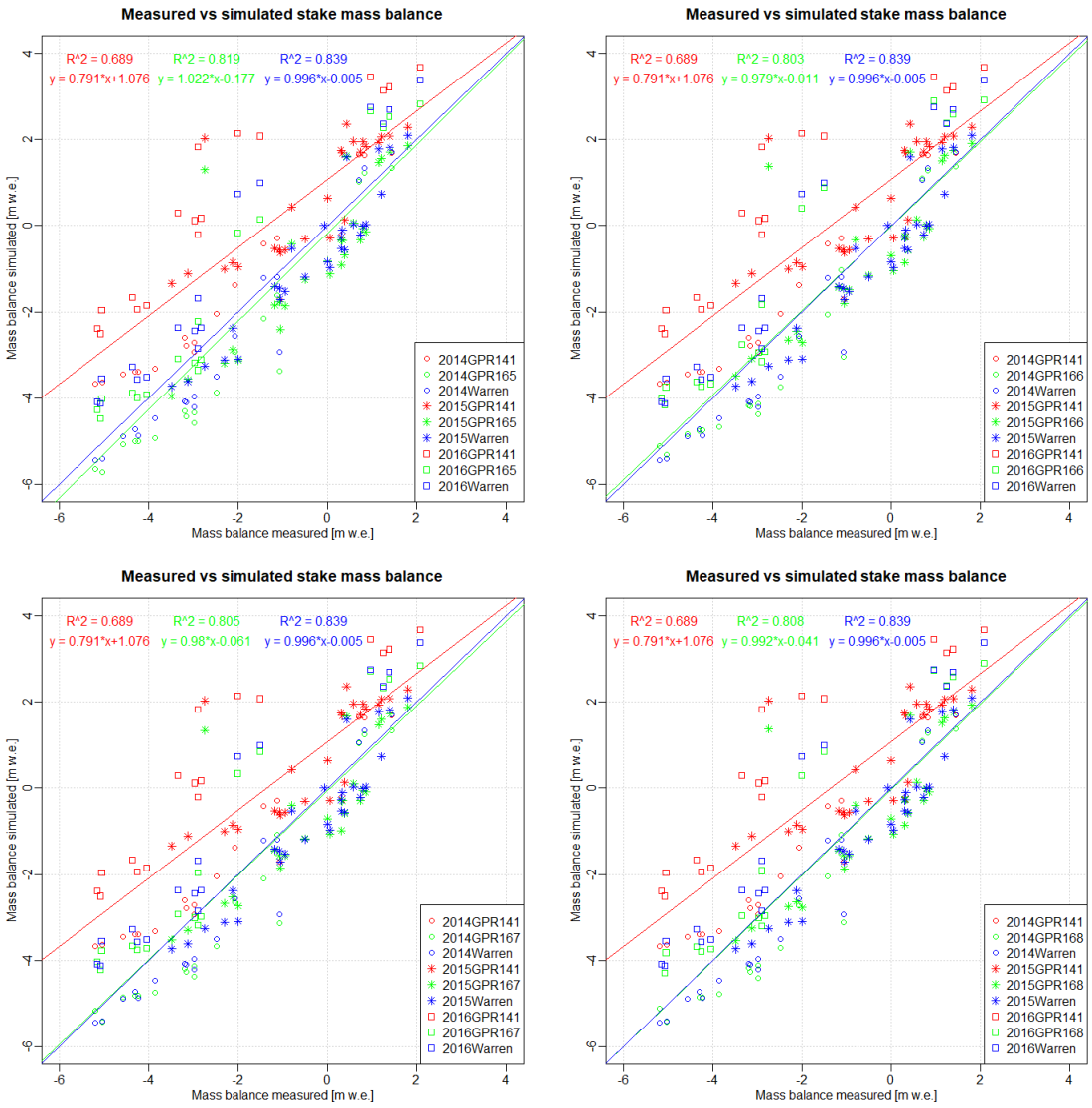


Figure 55: Measured versus simulated mass balance for the period 1 November 2013 02:55 until 1 October 2017 02:55. Warren's best simulation (blue) is compared with the simulations using the GPR PM and the same settings (red) as well as with improved parameter settings (green). Details about parameter settings: Table 29.

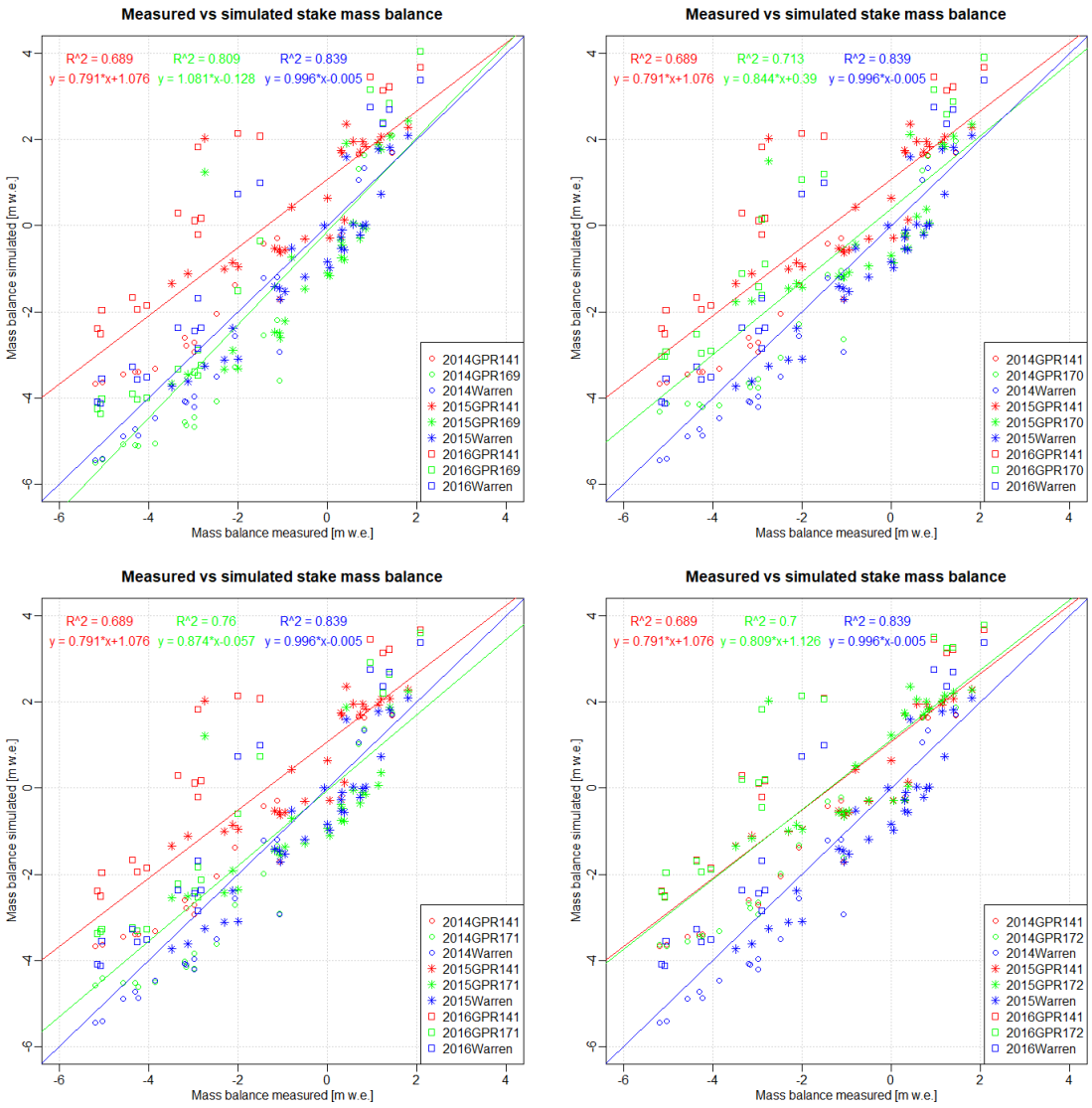


Figure 56: Measured versus simulated mass balance for the period 1 November 2013 02:55 until 1 October 2017 02:55. Warren's best simulation (blue) is compared with the simulations using the GPR PM and the same settings (red) as well as with improved parameter settings (green). Details about parameter settings: Table 29.

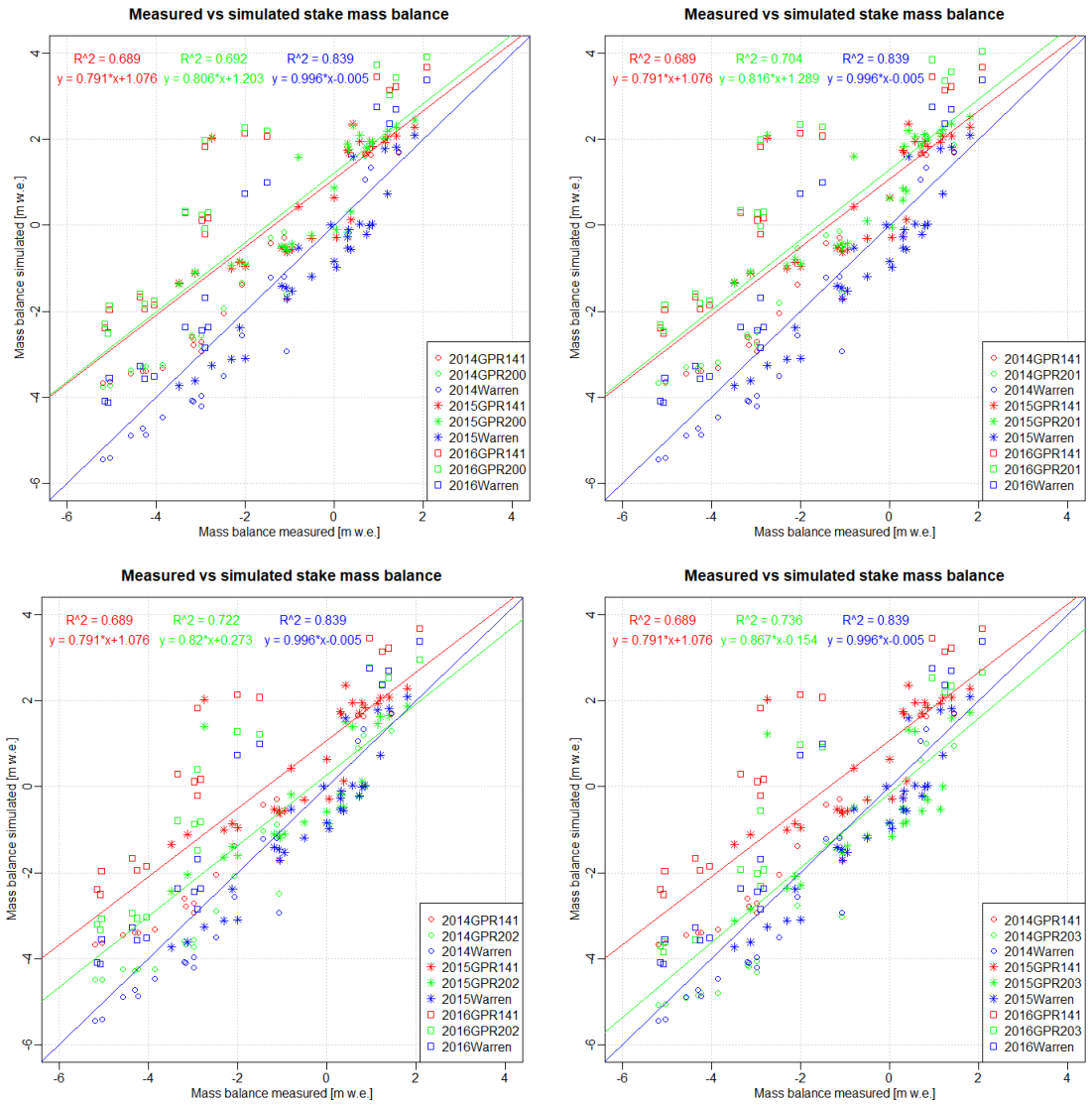


Figure 57: Measured versus simulated mass balance for the period 1 November 2013 02:55 until 1 October 2017 02:55. Warren's best simulation (blue) is compared with the simulations using the GPR PM, corrected for slopes steeper than 15 °, and the same settings (red) as well as with improved parameter settings (green). Details parameter settings: Table 29.

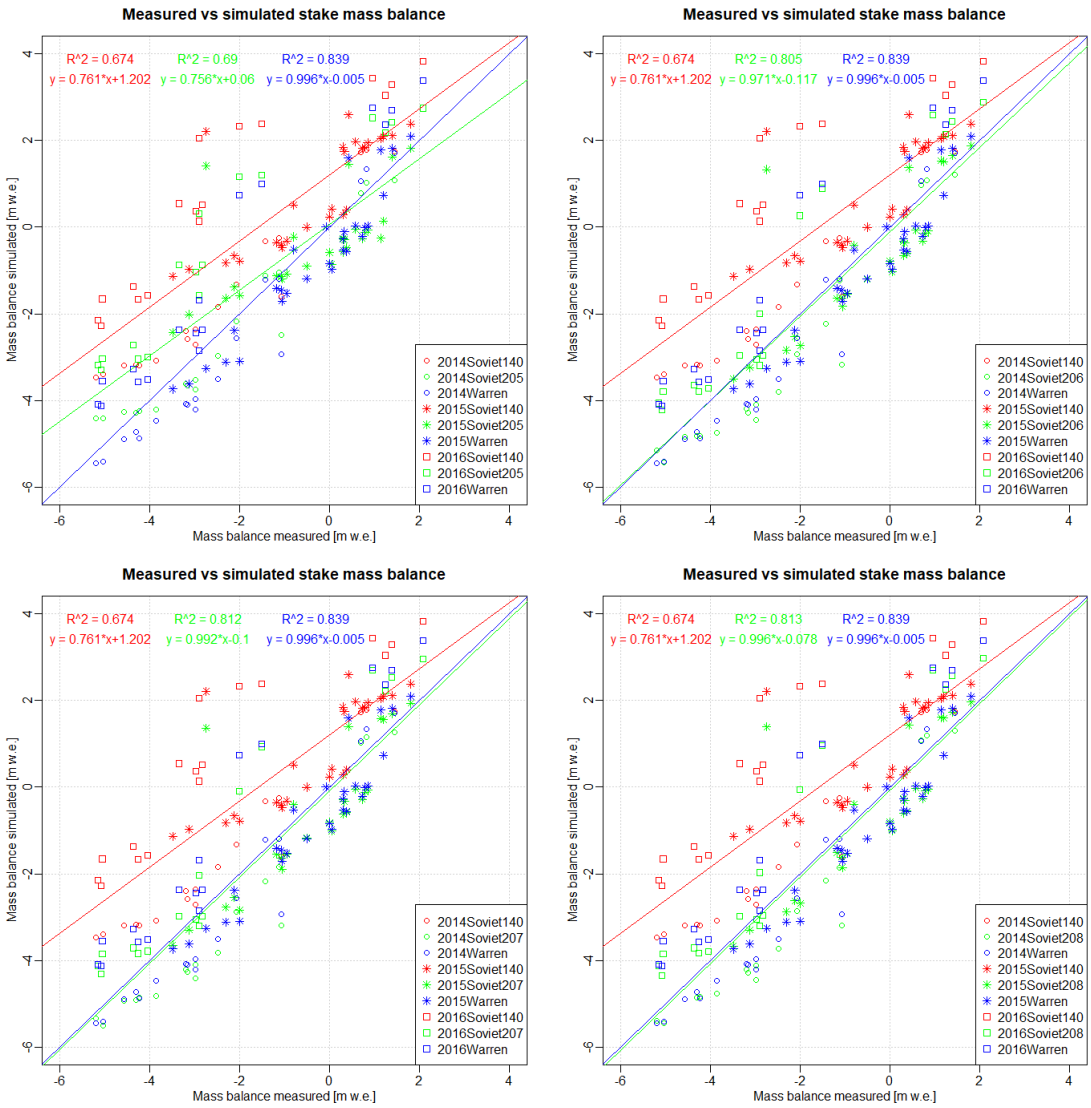


Figure 58: Measured versus simulated mass balance for the period 1 November 2013 02:55 until 1 October 2017 02:55. Warren's best simulation (blue) is compared with the simulations using the Soviet PM, corrected for slopes steeper than 15 °, and the same settings (red) as well as with improved parameter settings (green). Details parameter settings: Table 29.

Appendix J: ERA5 500 hPa

Table 30: ERA5 reanalysis of mean temperature, humidity, wind speeds, calculated wind direction and geopotential at 500 hPa as well as surface precipitation *(ECMWF 2018)*.

year	month	T	hum	u wind	v wind	Wind speed	Wind direction	Geopotential	Precipitation
		°C	%	m s^{-1}	m s^{-1}	m s^{-1}	°	m^2 s^{-2}	mm day^{-1}
2011	10	-16.2	65.3	9.5	4.92	10.7	243	-0.07346	3.101
2011	11	-19.8	81.1	15.1	9.11	17.64	239	-0.18522	5.365
2011	12	-25.8	73	10.1	7.39	12.51	234	-0.07369	1.662
2012	1	-28	69.2	8.78	4.59	9.91	242	-0.04727	1.168
2012	2	-27.4	78.6	8.64	6.81	11	232	-0.07472	2.625
2012	3	-23	70.4	10.54	6.87	12.58	237	-0.08538	3.472
2012	4	-16.4	58.5	3.51	1.18	3.7	251	-0.03677	1.633
2012	10	-17.4	57.6	6.15	1.28	6.29	258	-0.03116	0.791
2012	11	-20.5	52.7	8.39	2.51	8.76	253	-0.0341	1.487
2012	12	-23.1	58.8	10.02	4.75	11.09	245	-0.07695	2.254
2013	1	-25.7	70	9.39	4.92	10.6	242	0.00168	1.495
2013	2	-24.1	73.7	8.86	4.98	10.17	241	-0.07844	2.646
2013	3	-18.7	65	8.56	6.62	10.82	232	-0.00468	2.379
2013	4	-17.6	57.1	5.82	4.57	7.4	232	-0.00824	1.708
2013	10	-14.6	37.9	8.11	3.9	9	244	-0.01842	0.64
2013	11	-20.4	57.4	7.41	2.88	7.95	249	-0.02657	1.117
2013	12	-24.5	72.8	8.47	6.31	10.56	233	-0.00887	1.84
2014	1	-24.9	67.8	10.27	6.74	12.28	237	0.00952	1.681
2014	2	-26.8	72.1	9.67	5.46	11.1	241	-0.07113	2.311
2014	3	-21.2	61.3	6.95	5.78	9.04	230	-0.01764	2.409
2014	4	-18.3	64.5	9.85	4.25	10.73	247	-0.09034	2.787
2014	10	-16.5	58.9	8.8	4.29	9.79	244	-0.03466	1.899
2014	11	-21.4	73.6	11.84	6.56	13.54	241	-0.08512	2.497
2014	12	-23.8	56.4	8.38	4.44	9.49	242	-0.02397	1.782
2015	1	-24.6	75.7	10.85	6.64	12.72	239	-0.06116	2.458
2015	2	-22.2	78	9.69	6.14	11.47	238	-0.08395	3.053
2015	3	-20.8	71.9	10.22	6.17	11.94	239	-0.05774	3.042
2015	4	-17.2	50.1	8.09	2.53	8.48	253	-0.07114	2.298
2015	10	-15	55.2	8.62	3.84	9.44	246	-0.00382	1.643
2015	11	-19.9	70.5	11.3	7.4	13.51	237	-0.03029	2.79
2015	12	-23.7	63.4	11.7	5.36	12.87	245	-0.05531	2.105
2016	1	-23.1	67.3	8.87	3.83	9.67	247	-0.01787	1.656
2016	2	-22.6	48.3	6.61	2.49	7.06	249	0.02162	0.469
2016	3	-18.5	67.2	7.33	5.06	8.91	235	0.00954	2.373
2016	4	-16.6	62.7	6.69	4.33	7.97	237	-0.0215	2.508
2016	10	-16.9	57.8	11.54	4.26	12.3	250	-0.07228	1.882
2016	11	-20.7	66.6	11.46	6.21	13.03	242	-0.10867	2.765
2016	12	-21.1	69.5	15.04	7.7	16.9	243	-0.15782	4.43
2017	1	-26.1	78.3	8.18	6.42	10.4	232	-0.05519	2.704
2017	2	-23.4	71.5	10.97	7.14	13.09	237	-0.09689	4.697

2017	3	-22.9	68.4	11.34	5.91	12.78	242	-0.12232	2.978
2017	4	-17.1	59.1	7.5	2.02	7.76	255	-0.08844	3.369
2017	10	-15.9	47.7	9.5	4.12	10.35	247	-0.02288	1.216
2017	11	-20	59.8	7.88	3.25	8.53	248	-0.01036	0.671
2017	12	-23.9	71.2	9.5	6.65	11.6	235	-0.03795	2.286
2018	1	-24.8	74.7	11.57	5.61	12.86	244	-0.11946	2.12
2018	2	-23.8	70.6	11.45	6.34	13.09	241	-0.08772	2.542
2018	3	-19	68.8	10.68	4.45	11.57	247	-0.07467	3.139
2018	4	-15.9	50.7	7.3	3.76	8.21	243	-0.02357	2.546

Appendix K: R-Scripts

0715_Verortung.R

```
#Diese Datei wird nach den Vorbereitungen in 2 Teile gegliedert:
#1. Teil: Einfüllen der bekannten GPS Punkte in COR
#2. Teil: Füllen der GPS-Daten Lücken der Traces mittels Interpolation der GPS-Daten
#install.packages("chron")
library("chron")
setwd("U:/My Documents/GPR_Auswertung")

#COR <- read.table("COR.cor",header=F,sep="\t")
gps <- read.table("0714_0715_GPS3_KoordOrig.txt",header=F,sep="\t")
#GPR 0714 und 0715 enthalten 18'926 Traces
#Die Frequenz beträgt 2/s
gps[,6:8] <- NA
gps[1,8] <- 0
#Zeitdifferenz und Distanz zwischen zwei GPS-Punkten:
for (i in 2:length(gps[,1])){
  gps[i,6] <- as.POSIXct(strptime(gps[i,5], "%H:%M:%S"))-as.POSIXct(strptime(gps[i-1,5], "%H:%M:%S"))
  gps[i,7] <- ((gps[i,1]-gps[i-1,1])^2+(gps[i,2]-gps[i-1,2])^2)^(1/2)
  gps[i,8] <- gps[i-1,8]+gps[i,7]
}
gps[,5] <- times(gps[,5])
plot(gps[,7])
plot(gps[,8])
gps #Pause von 06:05 bis 06:15 --> Profil nur 300 Traces Pause (=5 min)
#Profil war demnach dort 5 min abgeschaltet, ehe das neue gestartet wurde.
#Laut GPS Camp-Bohrort 2h 43min (9780 s), was mit den
#9463 s (18926/2) + 5*60 s = 9763 s übereinstimmt.

#COR Tabelle vorbereiten:
COR <- matrix(NA,18926,10)
COR <- data.frame(COR)
COR[,1] <- c(1:18926)
COR[,2] <- "2018-01-23"
COR[,5] <- "N"
COR[,7] <- "E"
COR[,9] <- "M"
COR[,10] <- 1
COR[,3] <- times(COR[,3])

#Neue GPS-Tabelle mit nur einem Wert pro Minute (regelmässige Abstände):
plot(gps[,6])
gps2 <- as.data.frame(gps[gps[,6]>50,])


################### 1. Teil: Eindeutige Datenpunkte in COR einfüllen ###################

#Erstes Profil 0715 roh: 3315 Traces = 27.625 min --> 6:05 - 0:27 = 5:38; ab 3992 Stillstand
gps2[gps2[,5]=="05:38:00",] #40
COR[1,c(3,4,6,8)] <- gps2[rownames(gps2)=="40",c(5,2,1,3)]
#Lücke 2 bis 3039 mit gps 44-113 (2. Teil dieser Datei)
#3040 bis 3078 Stillstand:
COR[3040:3078,c(3,4,6,8)] <- gps2[rownames(gps2)=="113",c(5,2,1,3)]
#Lücke 3079 bis 3291 mit gps 113-119: Marsch (2. Teil dieser Datei)
gps2[gps2[,5]=="06:10:01",] #130; Pause 10 min, davon 5 min kein Profil
COR[3292:3589,c(4,6,8)] <- gps2[rownames(gps2)=="130",c(2,1,3)] #Zeiten unten manuell eingefüllt
timeseq <- times((22210*62/60):(22500*62/60)/(86400*62/60))
#timeseq <- times((22210*180/60):(22309*180/60)/(86400*180/60)) #Aktivieren für Test Z165ff.
#timeseq <- times((21908/2):(22500/2)/(86400/2)) #Test 13.3.: Damit keine Zeitlücke
timeseq
tail(timeseq)
length(timeseq)
```

```
COR[3292:3589,3] <- timeseq[1:298] #Länge: 3588-3292+1 = 297
plot(gps[1:120,8])
#Lücke 3590 bis 5517: Marsch (2. Teil dieser Datei)

#Zweites Profil: Snowpitstandort im GPR bei 5518 markiert; 2203/2 = 18 min später passt perfekt mit GPS überein
gps[gps[,5]=="06:33:00",] #192
COR[5518,c(3,4,6,8)] <- gps2[rownames(gps2)=="192",c(5,2,1,3)]
#Lücke 5519 bis 8945: Marsch (2. Teil dieser Datei)
#8946 bis 9226 Stillstand 281 Traces: 140.5 s; 3411/2 = 28 min später - laut GIS besser 7:00
gps[gps[,5]=="07:00:01",] #282
COR[8946:9226,c(4,6,8)] <- gps2[rownames(gps2)=="282",c(2,1,3)]
timeseq <- times((25202*300/118):(25319*300/118)/(86400*300/118))
length(timeseq)
COR[8946:9226,3] <- timeseq
#9227 bis 11043: Marsch (2. Teil dieser Datei)
#11044 bis 11228: Stillstand 2 min 7:17 bis 7:18; wegen Tracestillstand optimiert
gps[gps[,5]=="07:18:00",] #347
which(rownames(gps2)=="347") #116
COR[11044:11229,c(4,6,8)] <- gps2[116,c(2,1,3)] #Zeiten werden unten abgefüllt
#timeseq <- times((26219*3):(26280*3)/(86400*3))
#COR[11044:11229,3] <- timeseq[1:183]
COR[11044:11229,3] <- times("07:17:58")
#11229
gps[gps[,5]=="07:18:00",] #347
#11230 bis 13627: Marsch (2. Teil dieser Datei)
#13628 bis 13910: Stillstand 1 min 7:40 bis 7:41
gps[gps[,5]=="07:40:00",] #422
which(rownames(gps2)=="422") #138
COR[13628:13910,c(4,6,8)] <- gps2[138,c(2,1,3)] #Zeiten werden unten abgefüllt
timeseq <- times((27600*282/60):(27660*282/60)/(86400*282/60))
tail(timeseq)
length(timeseq)
COR[13628:13910,3] <- timeseq
#13911 bis 14145: Marsch (2. Teil dieser Datei)
#14146: Geplanter Bohrpunkt
gps[gps[,5]=="07:43:00",] #428
COR[14146,c(3,4,6,8)] <- gps2[rownames(gps2)=="428",c(5,2,1,3)]
#14147-16059: 1913 Traces = 16 min Marsch (2. Teil dieser Datei)
#16060 bis 16374: Stillstand mit 2 Miniatureschritten; 8:00 bis 8:01
gps[gps[,5]=="08:00:00",] #479
which(rownames(gps2)=="479") #158
COR[16060:16374,c(4,6,8)] <- gps2[158,c(2,1,3)] #Zeiten werden unten abgefüllt
timeseq <- times((28801*6):(28860*6)/(86400*6))
tail(timeseq)
length(timeseq)
COR[16060:16374,3] <- timeseq[1:315]
#16375 bis 16530: Marsch (2. Teil dieser Datei)
#16531 bis 16981: Stillstand 3.8 min -> GPS 2 min 8:05 bis 8:06 damit Distanz zu vor/nach Pause nicht zu gross
gps[gps[,5]=="08:05:01",] #492
which(rownames(gps2)=="492") #163
COR[16531:16981,c(4,6,8)] <- gps2[163,c(2,1,3)] #Zeiten werden unten abgefüllt
timeseq <- times((29101*458/60):(29160*458/60)/(86400*458/60))
tail(timeseq)
length(timeseq)
COR[16531:16981,3] <- timeseq[1:451]
#16982 bis 18926: Marsch (2. Teil dieser Datei)


################### 2. Teil: Datenlücken interpolieren ###################
#Lücke 2 bis 3039: Start laut GPS 5:38 --> 1 3038/2 = 25.3 min
gps[gps[,5]=="06:03:00",] #113
which(rownames(gps2)=="40") #16
which(rownames(gps2)=="113") #41 also 40
(3039-2+1)/(40-16+1)
```

```
122*(40-16+1) #3050 --> Approximation
trace <- 2
traceend <- 3040
tot <- 122
for (gpsmessung in 16:40){
 for (prop in 1:tot){
  verhaeltnis <- gps2[gpsmessung+1,c(5,2,1,3)]-gps2[gpsmessung,c(5,2,1,3)]
  COR[trace,c(3,4,6,8)] <- gps2[gpsmessung,c(5,2,1,3)]+prop/tot*verhaeltnis
  trace = trace + 1
  if (trace==traceend){
   break
  }
 }
}
gps2start <- 16
gps2end <- 40

fillgap <- function(trace, traceend, tot, gps2start, gps2end){
 for (gpsmessung in gps2start:gps2end){
  for (prop in 1:tot){
   verhaeltnis <- gps2[gpsmessung+1,c(5,2,1,3)]-gps2[gpsmessung,c(5,2,1,3)]
   COR[trace,c(3,4,6,8)] <- gps2[gpsmessung,c(5,2,1,3)]+prop/tot*verhaeltnis
   trace = trace + 1
   if (trace==traceend){
    break
   }
  }
 }
}
fillgap(trace1, traceend1, tot1, gps2start1, gps2end1)

#Lücke 3079 bis 3291 mit gps 113-119
which(rownames(gps2)=="113") #41
which(rownames(gps2)=="119") #119 ist 43, also 42
(3291-3079+1)/(42-41+1)
3079+107*(42-41+1) #3293 --> Approximation
trace <- 3079
traceend <- 3292
tot <- 107
for (gpsmessung in 41:42){
 for (prop in 1:tot){
  verhaeltnis <- gps2[gpsmessung+1,c(5,2,1,3)]-gps2[gpsmessung,c(5,2,1,3)]
  COR[trace,c(3,4,6,8)] <- gps2[gpsmessung,c(5,2,1,3)]+prop/tot*verhaeltnis
  trace = trace + 1
  if (trace==traceend){
   break
  }
 }
}

#Lücke 3590 bis 5517
which(rownames(gps2)=="133") #53 #Ev. testen: Bei 133 statt 139 starten (Zeile 61 sowie 167-172 anpassen)
which(rownames(gps2)=="192") #71 also 70
(5517-3590+1)/(70-53+1)
3590+108*(70-53+1) #5534
trace <- 3590
traceend <- 5518
tot <- 108
for (gpsmessung in 53:70){
 for (prop in 1:tot){
  verhaeltnis <- gps2[gpsmessung+1,c(5,2,1,3)]-gps2[gpsmessung,c(5,2,1,3)]
  COR[trace,c(3,4,6,8)] <- gps2[gpsmessung,c(5,2,1,3)]+prop/tot*verhaeltnis
  trace = trace + 1
  if (trace==traceend){
```

```
    break
   }
  }
}

#Lücke 5519 bis 8945
which(rownames(gps2)=="192") #71
which(rownames(gps2)=="282") #98 also 97
(8945-5519+1)/27
5519+127*27 #8948
trace <- 5519
traceend <- 8946
tot <- 127
for (gpsmessung in 71:97){
  for (prop in 1:tot){
    verhaeltnis <- gps2[gpsmessung+1,c(5,2,1,3)]-gps2[gpsmessung,c(5,2,1,3)]
    COR[trace,c(3,4,6,8)] <- gps2[gpsmessung,c(5,2,1,3)]+prop/tot*verhaeltnis
    trace = trace + 1
    if (trace==traceend){
      break
    }
  }
}

#9227 bis 11043
which(rownames(gps2)=="291") #100
which(rownames(gps2)=="347") #116 also 115
(11043-9227+1)/16
9227+114*16 #11051
trace <- 9227
traceend <- 11044
tot <- 114
for (gpsmessung in 100:115){
  for (prop in 1:tot){
    verhaeltnis <- gps2[gpsmessung+1,c(5,2,1,3)]-gps2[gpsmessung,c(5,2,1,3)]
    COR[trace,c(3,4,6,8)] <- gps2[gpsmessung,c(5,2,1,3)]+prop/tot*verhaeltnis
    trace = trace + 1
    if (trace==traceend){
      break
    }
  }
}
COR[9290:9337,c(4,6,8)] <- COR[9310,c(4,6,8)] #kurzer Stillstand im Profil
COR[9949:9965,c(4,6,8)] <- COR[9957,c(4,6,8)] #kurzer Stillstand im Profil

COR[,6] <- as.numeric(COR[,6])
#plot(COR[11100:11500,6]-COR[11099:11499,6])
#plot(COR[13500:14000,6]-COR[13499:13999,6])

#11230 bis 13627
which(rownames(gps2)=="347") #116
gps[gps[,5]=="07:40:00",] #422
which(rownames(gps2)=="422") #138 also 137
(13627-11230+1)/22
11230+109*22 #13628
trace <- 11230
traceend <- 13628
tot <- 109
for (gpsmessung in 116:137){
  for (prop in 1:tot){
    verhaeltnis <- gps2[gpsmessung+1,c(5,2,1,3)]-gps2[gpsmessung,c(5,2,1,3)]
    COR[trace,c(3,4,6,8)] <- gps2[gpsmessung,c(5,2,1,3)]+prop/tot*verhaeltnis
    trace = trace + 1
    if (trace==traceend){
```

```
    break
   }
  }
}

#13911 bis 14145
gps[gps[,5]=="07:41:02",] #424
which(rownames(gps2)=="424") #139
which(rownames(gps2)=="428") #141 also 140
(14145-13911+1)/2
13911+118*2 #14147
trace <- 13911
traceend <- 14146
tot <- 118
for (gpsmessung in 139:140){
 for (prop in 1:tot){
  verhaeltnis <- gps2[gpsmessung+1,c(5,2,1,3)]-gps2[gpsmessung,c(5,2,1,3)]
  COR[trace,c(3,4,6,8)] <- gps2[gpsmessung,c(5,2,1,3)]+prop/tot*verhaeltnis
  trace = trace + 1
  if (trace==traceend){
   break
  }
 }
}

#14147 bis 16059
gps[gps[,5]=="08:00:00",] #479
which(rownames(gps2)=="428") #141
which(rownames(gps2)=="479") #158 also 157
(16059-14147+1)/17
14147+113*17 #16068
trace <- 14147
traceend <- 16060
tot <- 113
for (gpsmessung in 141:157){
 for (prop in 1:tot){
  verhaeltnis <- gps2[gpsmessung+1,c(5,2,1,3)]-gps2[gpsmessung,c(5,2,1,3)]
  COR[trace,c(3,4,6,8)] <- gps2[gpsmessung,c(5,2,1,3)]+prop/tot*verhaeltnis
  trace = trace + 1
  if (trace==traceend){
   break
  }
 }
}

#16375 bis 16530
gps[gps[,5]=="08:01:01",] #482
gps[gps[,5]=="08:05:01",] #492
which(rownames(gps2)=="482") #159
which(rownames(gps2)=="492") #163 also 162
(16530-16375+1)/4
16375+39*4 #16531
trace <- 16375
traceend <- 16531
tot <- 39
for (gpsmessung in 159:162){
 for (prop in 1:tot){
  verhaeltnis <- gps2[gpsmessung+1,c(5,2,1,3)]-gps2[gpsmessung,c(5,2,1,3)]
  COR[trace,c(3,4,6,8)] <- gps2[gpsmessung,c(5,2,1,3)]+prop/tot*verhaeltnis
  trace = trace + 1
  if (trace==traceend){
   break
  }
 }
```

```
}

#16982 bis 18926
gps[gps[,5]=="08:06:00",] #494
gps[gps[,5]=="08:22:01",] #548
which(rownames(gps2)=="494") #164
which(rownames(gps2)=="548") #180 also 179
(18926-16982+1)/16
16982+122*16 #18934
trace <- 16982
traceend <- 18927
tot <- 122
for (gpsmessung in 164:179){
 for (prop in 1:tot){
  verhaeltnis <- gps2[gpsmessung+1,c(5,2,1,3)]-gps2[gpsmessung,c(5,2,1,3)]
  COR[trace,c(3,4,6,8)] <- gps2[gpsmessung,c(5,2,1,3)]+prop/tot*verhaeltnis
  trace = trace + 1
  if (trace==traceend){
   break
  }
 }
}
COR[18882:18926,c(4,6,8)] <- COR[18882,c(4,6,8)] #kurzer Stillstand im Profil

plot(COR[,3])
plot(COR[,4])
plot(COR[8800:9000,4])

summary(COR)

head(COR)
tail(COR)
COR[,4] <- format(round(COR[,4],11),nsmall=11)
COR[,6] <- format(round(COR[,6],11),nsmall=11)
COR[,8] <- format(round(COR[,8],1),nsmall=1)

#File 0715: 3315 Traces
#File 0716: 15611 Traces
COR0715 <- COR[1:3315,]
COR0715[,1] <- c(1:3315)
COR0716 <- COR[3316:18926,]
COR0716[,1] <- c(1:15611)

write.table(COR, file="COR.cor", sep="\t", quote=F, row.names=F, col.names=F)
write.table(COR0715, file="DAT_0715_A1.cor", sep="\t", quote=F, row.names=F, col.names=F)
write.table(COR0716, file="DAT_0716_A1.cor", sep="\t", quote=F, row.names=F, col.names=F)
```

Pick_korrektur.R

```
#Dieses Programmli korrigiert Mehrfacheinträge und fehlende Einträge der gepickten Horizonte

#setwd("U:/My Documents/GPR_Auswertung")
setwd("D:/Studium/Master/MA/Daten_Abramov_GPR/GPR_Auswertung")

list <- list.files("Abramov/ASCII", ".PCK", full.names=T)
for (file in list){
 PCK <- read.table(file,header=F,sep="")
 PCK <- PCK[,-c(3,8,9)]
 PCKsort <- PCK[order(PCK[,1]),]
 # a <- c(1,10,"test",15)
 # b <- c(2,10,"test",15)
 # c <- c(3,10,"test",15)
 # d <- c(1,1000,"test",15)
```

```
 # e <- c(4,10,"test",15)
 # f <- c(1,500,"test",15)
 # g <- c(6,10,"test",15)
 # x <- rbind(a,b,c,d,e,f,g)
 # x[order(x[,1]),]
 # #Gut, wird nach Zeitpunkt des Auftretens sortiert.

 i <- 2                    #Start
 i_end <- length(PCK[,1])    #End Trace

 while (i<i_end) {
  if (PCKsort[i,1]==PCKsort[i-1,1]){
   PCKsort <- PCKsort[-i,]
   i_end <- i_end-1
  }
  else if (PCKsort[i,1]!=PCKsort[i-1,1]+1){
   PCKsort <- rbind(PCKsort[1:(i-1),], PCKsort[i-1,],PCKsort[i:i_end,])
   PCKsort[i,1] <- PCKsort[i-1,1]+1
   PCKsort[i,2] <- PCKsort[i-1,2]+0.5
   i = i+1
  }
  else {
   i = i+1
  }
 }
 PCKsort[,c(2,5)] <- format(round(PCKsort[,c(2,5)],1),nsmall=1)
 PCKsort[,c(3,4,6)] <- format(round(PCKsort[,c(3,4,6)],6),nsmall=6)

 write.table(PCKsort, file=paste0("Abramov/Picked_Layers_korr/", unlist(strsplit(file, "ASCII/"))[2]),
          quote=F, sep="\t", row.names=F, col.names=F)
 message("File ",file," beendet.")
}
```

Pick_Ungenauigkeit.R

```
#Pick Fehler - Statistik der Abweichungen von drei Picks desselben Horizonts

#setwd("U:/My Documents/GPR_Auswertung")
setwd("D:/Studium/Master/MA/Daten_Abramov_GPR/GPR_Auswertung")

list <- list.files("Abramov/Picked_Layers_korr", "0726_layer[1-9_]+", full.names=T)
list <- list.files("Abramov/Picked_Layers_korr", "0728_layer[0_]+", full.names=T)
list <- list.files("Abramov/Picked_Layers_korr", "0736_layer[0_]+", full.names=T)
list <- list[1:3]
a <- read.table(list[1])
b <- read.table(list[2])
c <- read.table(list[3])
length(a[,1])
length(b[,1])
length(c[,1])
hist(c[,6]-a[,6])
hist(c[,6])
mean(c(a[,6], b[,6], c[,6])) #Layer 1: 48.63 #Layer 0 0728: 20.35
mean(c(sd(a[,6]-b[,6]), sd(a[,6]-c[,6]), sd(c[,6]-b[,6])))
sd(c[,6]-b[,6]) #Nur diese weil a vor 2 Monaten leicht anders gepickt wurde

#Layer 1: SD beträgt 0.53 ns bei einer TWT von 48.63 ns --> ± 1,09 % Genauigkeit
#Layer 0 0728: SD beträgt 0.59 ns bie einer TWT von 20.35 ns --> ± 2,9 % Genauigkeit

# #Konfidenzintervalle: Mittelwert ± t * se
# stichprobe <- c(a[,6]-b[,6], a[,6]-c[,6], c[,6]-b[,6])
# #Standardfehler:
# se <- sqrt(var(stichprobe)/length(stichprobe))
# #t-Wert:
```

```
# # t.test(stichprobe, conf.level=0.95) #Besser nicht weil Abw. hier nicht normalverteilt
# # t <- t.test(stichprobe, conf.level=0.95)[1] # dito
# t <- qt(0.025, df=2630, lower.tail=F)
# #Konfidenzintervall:
# up <- mean(stichprobe)+t*se
# low <- mean(stichprobe)-t*se
# up
# low
# (up-mean(stichprobe))/mean(c(a[,6], b[,6], c[,6])) #± 0.04 %
```

WGS84_geodetic_to_projUTM.R

```
#install.packages("sp")
#install.packages("rgdal")
library("sp")
library("rgdal")

setwd()
koordrow <- read.table("koord.txt",header=F,sep="\t")
koord <- SpatialPoints(koordrow, proj4string=CRS("+proj=longlat +datum=WGS84 +ellps=WGS84 +towgs84=0,0,0"))
koord_new <- spTransform(koord, CRS("+proj=utm +zone=42 +datum=WGS84 +units=m +no_defs"))
write.table(koord_new, file="koord_new.txt", sep="\t", row.names=F)
```

dem_total.R

```
library(raster)

setwd("D:/Studium/Master/MA/Daten_Abramov_NurIntern/raster/dem_total")
liste = list.files(pattern=".tif$")[1:3]
DEM1 = raster(liste[1])
DEM2 = raster(liste[2])
DEM3 = raster(liste[3])
crs = crs(DEM1)

DEM_total = merge(DEM1, DEM2, DEM3, overlap=TRUE)

writeRaster(DEM_total, "dem_total.tif", format="GTiff", overwrite=T, dataType="INT2U")
```

dem_total_filled.R

```
library(raster)
library(rgdal)
library(progress)

setwd("D:/Studium/Master/MA/Daten_Abramov_NurIntern/raster/dem_total")
DEM_srtm <- raster("../../../Daten_Kirgistan_DEM/srtm_51_05_zugeschnitten.tif") #im WGS84
DEM_total <- raster("dem_total.tif")

#Reprojiziert Raster ins UTM42N und ändert Zellgrösse auf 20 m:
DEM_srtm_epsg_20m <- projectRaster(DEM_srtm, res=20, crs="+proj=utm +zone=42 +datum=WGS84 +units=m
+no_defs", method="bilinear")

#Ausschneiden des gewünschten Ausschnitts:
vorlage <- ras-
ter(nrows=444,ncols=550,crs=crs(DEM_srtm_epsg_20m),xmn=714000,xmx=725000,ymn=4384820,ymx=4393700)
DEM_srtm_epsg_20m_crop <- resample(DEM_srtm_epsg_20m,vorlage,method="bilinear")

#Aggregiert hochaufgelöstetes 4 m - DEM auf 20 m Auflösung:
DEM_total_20m <- resample(DEM_total, DEM_srtm_epsg_20m_crop, method="bilinear")

#Extents und Auflösung stimmen überein:
DEM_srtm_epsg_20m_crop
```

```
plot(DEM_srtm_epsg_20m_crop)
DEM_total_20m
plot(DEM_total_20m)

summary(DEM_srtm_epsg_20m_crop)
summary(DEM_total_20m)
cellStats(DEM_srtm_epsg_20m_crop, stat="mean")
cellStats(DEM_total_20m, stat="mean")
plot(DEM_total_20m-DEM_srtm_epsg_20m_crop)
#Mittelwertsdifferenz von 1 m basiert v.a. auf Steilhängen sowie dem Ablationsgebiet.
#Weil Lücken im DEM_total_20 m nur im Akkumulationsgebiet --> keine Massnahmen nötig.

#Lücken in DEM_total_20m mit SRTM füllen:
pb <- progress_bar$new(total=ncell(DEM_total_20m))
for (i in 1:ncell(DEM_total_20m)){
  if (is.na(DEM_total_20m[i])){
    DEM_total_20m[i] <- DEM_srtm_epsg_20m_crop[i]
  }
  pb$tick()
}


writeRaster(DEM_srtm_epsg_20m_crop, "DEM_srtm_epsg_20m_crop2.tif", format="GTiff", overwrite=T)
writeRaster(DEM_total_20m, "DEM_total_20m_filled2.tif", format="GTiff", overwrite=T)
#writeRaster(DEM_total_20m-DEM_srtm_epsg_20m_crop, "DEM_total-DEM_srtm.tif", format="GTiff", overwrite=T)
```

FOPDdyNS_100m_major.R

```
library(raster)

setwd("D:/Studium/Master/MA/Daten_Abramov_NurIntern/raster/dem_total")

FOPD <- raster("dem_total_20m_filled_FOPDdyNS2.tif")
FOPD <- round(FOPD,5)

cells <- focalWeight(FOPD, 100, type="circle")

for (i in 1:length(cells)){
  if (cells[i]==0){
    cells[i] <- NA
  }
}
cells

FOPD_100m <- focal(FOPD, w=cells, fun=modal, na.rm=T)
FOPD_100m
plot(FOPD_100m)

writeRaster(FOPD_100m, "dem_total_20m_filled_FOPDdyNS2_100mMajor_round5_weights.tif", format="GTiff", overwrite=T)
```

ProfCurv_100m_median.R

```
library(raster)

setwd("D:/Studium/Master/MA/Daten_Abramov_NurIntern/raster/dem_total")

ProfCurv <- raster("dem_total_20m_filled_ProfCurv2.tif")

cells <- focalWeight(ProfCurv, 100, type="circle")

for (i in 1:length(cells)){
  if (cells[i]==0){
```

```
   cells[i] <- NA
  }
  else {
   cells[i] <- 1 #Nötig, sonst Gewichtung falsch (0.012)
  }
}
cells

ProfCurv_100m <- focal(ProfCurv, w=cells, fun=median, na.rm=T)
ProfCurv_100m
plot(ProfCurv_100m)

writeRaster(ProfCurv_100m, "dem_total_20m_filled_ProfCurv2_100mMedian.tif", format="GTiff", overwrite=T)
```

SOPDdxx_100m_major.R

```
library(raster)

setwd("D:/Studium/Master/MA/Daten_Abramov_NurIntern/raster/dem_total")

SOPD <- raster("dem_total_20m_filled_SOPDdxx2.tif")
SOPD <- round(SOPD,5)

cells <- focalWeight(SOPD, 100, type="circle")

for (i in 1:length(cells)){
  if (cells[i]==0){
    cells[i] <- NA
  }
}
cells

SOPD_100m <- focal(SOPD, w=cells, fun=modal, na.rm=T)
SOPD_100m
plot(SOPD_100m)

writeRaster(SOPD_100m, "dem_total_20m_filled_SOPDdxx2_100mMajor_round5_weights.tif", format="GTiff", over-
write=T)
```

SOPDdxy_100m_sum.R

```
library(raster)

setwd("D:/Studium/Master/MA/Daten_Abramov_NurIntern/raster/dem_total")

SOPD <- raster("dem_total_20m_filled_SOPDdxy2.tif")

cells <- focalWeight(SOPD, 100, type="circle")
# Gewichtung nötig, daher untenstehenden Block nicht ausführen!
# for (i in 1:length(cells)){
#   if (cells[i]!=0){
#     cells[i] <- 1
#   }
#   else{
#     cells[i] <- 0
#   }
# }
cells

SOPD_100m <- focal(SOPD, w=cells, fun=sum, na.rm=T)
SOPD_100m
plot(SOPD_100m)
```

```
writeRaster(SOPD_100m, "dem_total_20m_filled_SOPDdxy2_100mSum_weights.tif", format="GTiff", overwrite=T)
```

dem.R

```
setwd("E:/Eigene Dateien/Studium/Master/MA/Literatur/DEM")
library(ncdf4)
library(raster)
library(rgdal)
library(sp)
#library(RColorBrewer)
library(shape)
library(stringr)
library(maptools)
library(hydroGOF)
library(gdalUtils)

#Settings
wgs <- "+proj=longlat +datum=WGS84 +ellps=WGS84 +towgs84=0,0,0"
#ch1903p <-  "+proj=somerc +lat_0=46.95240555555556 +lon_0=7.439583333333333 +k_0=1 +x_0=2600000 +y_0=1200000
+ellps=bessel +towgs84=674.374,15.056,405.346,0,0,0,0 +units=m +no_defs"
list <- dir(path="alle",pattern=".tif", full.names=TRUE)
list(raster(list[1:12]))
r1 <- raster(list[1])
r2 <- raster(list[2])
r3 <- raster(list[3])
r4 <- raster(list[4])
r5 <- raster(list[5])
r6 <- raster(list[6])
r7 <- raster(list[7])
r8 <- raster(list[8])
r9 <- raster(list[9])
r10 <- raster(list[10])
r11 <- raster(list[11])
r12 <- raster(list[12])
rnew <- merge(r1,r2,r3,r4,r5,r6,r7,r8,r9,r10,r11,r12)

#Raster ausgeben
writeRaster(rnew, "merged.tif", format="GTiff")
#rnew <- raster("merged.tif")

#Shapefile mit Rasterumfang
extent <- extent(rnew)
poly <- as(extent, "SpatialPolygons")
poly$outlier <- 1
crs(poly) <- crs(rnew)
writeOGR(poly, "dem_merged_outliers.shp", layer="test", driver="ESRI Shapefile")

#Raster aggregieren für River Auswertung:
rnew_agg <- aggregate(rnew,fact=100,fun=mean)
rnew_agg10 <- aggregate(rnew,fact=10,fun=mean)
writeRaster(rnew_agg, "merged_agg.tif", format="GTiff")
writeRaster(rnew_agg10, "merged_agg10.tif", format="GTiff")
```

ncdf_files_20CRV2C.R

```
library(raster)
library(ncdf4)

setwd("D:/Studium/Master/MA/Daten_Klima")

list <- dir(pattern=".nc$")
list
```

```
dat <- nc_open(list[1])
u <- ncvar_get(dat)
time <- ncvar_get(dat, varid="time") #units hours since 1800-1-1 00:00:0.0; range 447048 to 1883904
nc_close(dat) #Wichtig!

dat <- nc_open(list[2])
v <- ncvar_get(dat)
nc_close(dat)

dat <- nc_open(list[3])
hum <- ncvar_get(dat)
nc_close(dat)

#Daten
timedays <- time/24
dates <- as.Date(timedays, origin="1800-01-01")
year <- as.numeric(substr(dates,1,4))
month <- as.numeric(substr(dates,6,7))

tot <- data.frame("date"=dates,"year"=year,"month"=month,"u"=u,"v"=v,"wind"=NA,"dir"=NA,"hum"=hum)

#Winde
for (i in 1:length(tot$u)){
 if (tot$u[i]>0){
  tot$dir[i] <- 270-atan(tot$v[i]/tot$u[i])*180/pi
 }
 else if (tot$u[i]<0){
  tot$dir[i] <- 90-atan(tot$v[i]/tot$u[i])*180/pi
 }
 else {
  if (tot$v[i]>0){
   tot$dir[i] <- 180
  }
  else {
   tot$dir[i] <- 0
  }
 }
}
tot$wind <- (tot$u^2+tot$v^2)^(1/2)

write.table(format(tot, digits=4), "20CRV2c.csv", sep="\t", row.names=F, quote=F)
```

ncdf_files_ERA5.R

```
library(raster)
library(ncdf4)

setwd("D:/Studium/Master/MA/Daten_Klima")

list <- dir(pattern="era5")
list

dat <- nc_open(list[1])
hum <- ncvar_get(dat)
nc_close(dat)

dat <- nc_open(list[2])
t <- ncvar_get(dat)
nc_close(dat)

dat <- nc_open(list[3])
p <- ncvar_get(dat) #Einheit mm/d
nc_close(dat)
```

```
dat <- nc_open(list[4])
u <- ncvar_get(dat)
time <- ncvar_get(dat, varid="time") #units: months since Jan 2008; Jan 2008=0
nc_close(dat) #Wichtig!

dat <- nc_open(list[5])
v <- ncvar_get(dat)
nc_close(dat)

dat <- nc_open(list[6])
w <- ncvar_get(dat)
nc_close(dat)


#Daten
timedays <- time
year_part <- seq(2008,2018)
year <- rep(year_part,each=12)
month <- rep(1:12,11)

tottot <- data.frame("year"=year,"month"=month,"T"=t,"hum"=hum,"u"=u,"v"=v,"wind"=NA,"dir"=NA,"w"=w, "p"=p)
#Letzt 6 Monate leer
tot <- tottot[c(1:126),]
tail(tot)

#Winde
for (i in 1:length(tot$u)){
 if (tot$u[i]>0){
   tot$dir[i] <- 270-atan(tot$v[i]/tot$u[i])*180/pi
 }
 else if (tot$u[i]<0){
   tot$dir[i] <- 90-atan(tot$v[i]/tot$u[i])*180/pi
 }
 else {
   if (tot$v[i]>0){
     tot$dir[i] <- 180
   }
   else {
     tot$dir[i] <- 0
   }
 }
}
tot$wind <- (tot$u^2+tot$v^2)^(1/2)
totwahl <- tot[tot$year%in%2011:2018&tot$month%in%c(10,11,12,1,2,3,4),]
totwahl <- totwahl[5:length(totwahl[,1]),]
totwahl$year <- rep(2011:2017,each=7)

totwahlmean <- aggregate(totwahl[,3:length(totwahl[1,])], list(totwahl$year), FUN=mean)

write.table(format(totwahl,digits=3), "ERA5_tottable.csv", sep="\t", row.names=F, quote=F)
write.table(format(totwahlmean, digits=3),"ERA5_mean_Oct_Apr.csv", sep="\t", row.names=F, quote=F)

#Für Oct-Jan:
totwahl <- totwahl[totwahl$month%in%c(10,11,12,1),]
totwahl
totwahlmean <- aggregate(totwahl[,3:length(totwahl[1,])], list(totwahl$year), FUN=mean)
write.table(format(totwahlmean, digits=3),"ERA5_mean_Oct_Jan.csv", sep="\t", row.names=F, quote=F)
```

Meteodaten.R

```
#D:\Studium\Master\MA\Daten_Abramov_Meteo
pfad <- gsub("\\","/",readClipboard())
setwd(pfad)
files <- dir(pattern=".txt")
```

```
files

#Daten einlesen
T <- read.table(files[1],sep=",")
head(T)
T <- T[-1,]
T$V2 <- as.numeric(as.character(T$V2))
# T$year <- as.numeric(substr(T[1,1],1,4))
# T$month <- as.numeric(substr(T[1,1],6,7))
head(T)
P <- read.table(files[3],sep=",")
head(P)
P<- P[-1,]
P$V2 <- as.numeric(as.character(P$V2))
W <- read.table(files[4],sep=",")
head(W)
W <- W[-1,]
W$V2 <- as.numeric(as.character(W$V2))

#Daten sichten
plot(T[,2])
T[which(max(T[,2])==T[,2]),]
T[224400:224800,]
plot(P[,2])
plot(W[,2])

#Tabelle vorbereiten
y <- c(2011:2017)
df <- data.frame(y,NA,NA,NA,NA,NA,NA)
colnames(df)[2:7] <- c("T_OctJan","T_OctApr","P_OctJan","P_OctApr","W_OctJan","W_OctApr")

#Zeiträume definieren T
j <- data.frame(2011:2017,NA,NA,NA)
colnames(j) <- c("jahr","start","endJan","endApr")
for (jahr in j[1,1]:j[7,1]) {
  j[j$jahr==jahr,2] <- which(substr(as.character(T[,1]),1,10)==paste0(jahr,"-10-01"))[1] #8593
  j[j$jahr==jahr,3] <- which(substr(as.character(T[,1]),1,10)==paste0(jahr+1,"-02-01"))[1]-1
  j[j$jahr==jahr,4] <- which(substr(as.character(T[,1]),1,10)==paste0(jahr+1,"-04-01"))[1]-1
}

#Tabelle füllen T
for(y in c(2011:2012,2014:2017)){
  df$T_OctJan[df$y==y] <- mean(T$V2[j$start[j$jahr==y]:j$endJan[j$jahr==y]])
  df$T_OctApr[df$y==y] <- mean(T$V2[j$start[j$jahr==y]:j$endApr[j$jahr==y]])
}

#Zeiträume definieren P
j <- data.frame(2011:2017,NA,NA,NA)
colnames(j) <- c("jahr","start","endJan","endApr")
for (jahr in j[1,1]:j[7,1]) {
  j[j$jahr==jahr,2] <- which(substr(as.character(P[,1]),1,10)==paste0(jahr,"-10-01"))[1]
  j[j$jahr==jahr,3] <- which(substr(as.character(P[,1]),1,10)==paste0(jahr+1,"-02-01"))[1]-1
  j[j$jahr==jahr,4] <- which(substr(as.character(P[,1]),1,10)==paste0(jahr+1,"-04-01"))[1]-1
}

#Tabelle füllen P
for(y in c(2011:2012,2014:2017)){
  df$P_OctJan[df$y==y] <- sum(P$V2[j$start[j$jahr==y]:j$endJan[j$jahr==y]])
  df$P_OctApr[df$y==y] <- sum(P$V2[j$start[j$jahr==y]:j$endApr[j$jahr==y]])
}

#Zeiträume definieren W
j <- data.frame(2011:2017,NA,NA,NA)
colnames(j) <- c("jahr","start","endJan","endApr")
```

```
for (jahr in j[1,1]:j[7,1]) {
  j[j$jahr==jahr,2] <- which(substr(as.character(W[,1]),1,10)==paste0(jahr,"-10-01"))[1]
  j[j$jahr==jahr,3] <- which(substr(as.character(W[,1]),1,10)==paste0(jahr+1,"-02-01"))[1]-1
  j[j$jahr==jahr,4] <- which(substr(as.character(W[,1]),1,10)==paste0(jahr+1,"-04-01"))[1]-1
}

#Tabelle füllen P
for(y in c(2011:2012,2014:2017)){
  df$W_OctJan[df$y==y] <- mean(W$V2[j$start[j$jahr==y]:j$endJan[j$jahr==y]])
  df$W_OctApr[df$y==y] <- mean(W$V2[j$start[j$jahr==y]:j$endApr[j$jahr==y]])
}

write.table(df,"df.csv",row.names=F)
```

MultiRegr_SDD_we.R

```
setwd("D:/Studium/Master/MA/Auswertung_TWT_zu_we")
# library("glmulti") #Problem auf meinem PC mit mitgeliefertem rJava Package
# library("GGally")
# library("mctest")
# library("ppcor")
library("progress")

#Teil 1: Regression Stakes -> Tiefe
#Teil 2: Regression Pits -> we, Durchchecken aller Möglichkeiten (ohne Einbezug von Tiefe)
#Teil 3: Versuch Check Multikollinearität


#############################################################################################################
#####################
#Teil1
#############################################################################################################
#####################
#Stakes Topographical-Tiefe Relation
tabstakes <- read.table("Tiefe_Stakes_Sovjet2.txt",header=T,sep="\t")
winterPS <- read.table("../Daten_Abramov_alt/Climate_Winter_PS.csv",header=T,sep="\t")
klima <- read.table("../Daten_Klima/20CRV2c.csv",header=T,sep="\t")
head(tabstakes)

#Monat wählen
tab <- tabstakes[tabstakes$Monat%in%c(12,1,2,3,4)&tabstakes$Jahr<=1998,] #Monat anpassen; Nur Feb, 1999 nicht mehr
(wegen fehlenden Meteodaten)
tab <- cbind(tab,rep(NA,length(tab[,1])))
colnames(tab)[length(tab[1,])] <- "WinterNS_Apr" #Monat anpassen
for (jahr in c(1968:1997)){
  tab$WinterNS_Dez[tab$Jahr==jahr] <- winterPS$WinterNS_Dez[winterPS$Winter==(jahr+1)] #Monat anpassen #Ach-
tung wenn Dez: Winter==(jahr+1), aber nur bis 1997
}
for (jahr in c(1968:1998)){
  tab$WinterNS_Jan[tab$Jahr==jahr] <- winterPS$WinterNS_Jan[winterPS$Winter==jahr] #Monat anpassen #Achtung
wenn Dez: Winter==(jahr+1), aber nur bis 1997
}
for (jahr in c(1968:1998)){
  tab$WinterNS_Feb[tab$Jahr==jahr] <- winterPS$WinterNS_Feb[winterPS$Winter==jahr] #Monat anpassen #Achtung
wenn Dez: Winter==(jahr+1), aber nur bis 1997
}
for (jahr in c(1968:1998)){
  tab$WinterNS_Mrz[tab$Jahr==jahr] <- winterPS$WinterNS_Mrz[winterPS$Winter==jahr] #Monat anpassen #Achtung
wenn Dez: Winter==(jahr+1), aber nur bis 1997
}
for (jahr in c(1968:1998)){
  tab$WinterNS_Apr[tab$Jahr==jahr] <- winterPS$WinterNS_Apr[winterPS$Winter==jahr] #Monat anpassen #Achtung
wenn Dez: Winter==(jahr+1), aber nur bis 1997
}
```

```
#Klimadaten 20CRV2c an tabtot anfügen
tab <- cbind(tab,matrix(nrow=length(tab[,1]),ncol=3))
colnames(tab)[(length(tab[1,])-2):length(tab[1,])] <- c("wind","dir","hum")
for (jahr in c(1968:1998)){
  for (monat in c(1:4,12)){
    tab[tab$Jahr==jahr&tab$Monat==monat,(length(tab[1,])-2):length(tab[1,])] <- kli-
ma[klima$year==jahr&klima$month==monat,6:8]
  }
}
tab[tab$Jahr==1967,(length(tab[1,])-2):length(tab[1,])] <- klima[klima$year==1967&klima$month==12,6:8]

write.table(tab, "Tiefe_Stakes_Sovjet2_complete.txt", sep="\t", row.names=F, quote=F)


###Manuelle Multiple lineare Regression, nur Topographicalparameter direkt an Pit-Standort###
fit <- lm(Tiefe ~ Z_m + Slope + Aspect + TangCurv + ProfCurv + FOPDdyNS + FOPDdxEW +
        SOPDdyy + SOPDdxy + SOPDdxx, data=tab)
summary(fit) #R^2 0.52
plot(fit)
#Tiefe primär abhängig von: Höhe, Ausrichtung und FOPDdyNS und WinterNS!
fit <- lm(Tiefe ~ Z_m + Aspect + FOPDdyNS, data=tab)
summary(fit) #R2 0.34
tab2 <- tab[tab$Monat==1,]
fit <- lm(Tiefe ~ Z_m + Aspect + WinterNS_Jan, data=tab2)
summary(fit) #R^2 0.68

#Nur fünf Jahre mit maximalen Messungen
aggregate(tab$Tiefe, by=list(tab$Jahr))
ftable(tab$Jahr)
#1987, 1988, 1993, 1994, 1995
tab <- tabstakes[tabstakes$Monat%in%c(2)&tabstakes$Jahr%in%c(1987,1988,1993,1994,1995),]
fit <- lm(Tiefe ~ Z_m + Slope + Aspect + TangCurv + ProfCurv + FOPDdyNS + FOPDdxEW +
        SOPDdyy + SOPDdxy + SOPDdxx, data=tab)
summary(fit) #R^2 0.65
fit <- lm(Tiefe ~ Z_m + Aspect + FOPDdyNS, data=tab)
summary(fit) #R^2 0.65
#--> Stets dieselben drei Einflussgrössen Höhe, Ausrichtung und FOPDdyNS entscheidend! Regression würde natürlich
viel genauer,
#wenn noch der Niederschlag berücksichtigt würde. Dies ist hier vorderhand aber nicht das Ziel, weil nicht das einzel-
ne Jahr,
#sondern das Akkumulationsmuster beschrieben werden soll. Dieses wird als konstant betrachtet, egal wie viel Nieder-
schlag fällt.


###Manuelle Multiple lineare Regression, Topographicalparameter 100 m Radius###
colnames(tab)
#Gewünschten Teil der cat Zeile manuell kopieren
cat(paste(colnames(tab),collapse=" + "))
fit <- lm(Tiefe ~ Z_m + TangCurv + Slope + ProfCurv + Aspect + SOPDdyy + SOPDdxy + SOPDdxx + FOPDdyNS +
        FOPDdxEW + aspect_sum + aspect_mea + aspect_med + aspect_maj + FOPDdxEW_s + FOPDdxEW_m +
        FOPDdxEW_1 + FOPDdxEW_2 + FOPDdyNW_s + FOPDdyNW_m + FOPDdyNW_1 + FOPDdyNW_2 +
ProfCurv_s +
        ProfCurv_m + ProfCurv_1 + ProfCurv_2 + SOPDdxx_su + SOPDdxx_me + SOPDdxx__1 + SOPDdxx_ma +
        SOPDdxy_su + SOPDdxy_me + SOPDdxy__1 + SOPDdxy_ma + SOPDdyy_su + SOPDdyy_me + SOPDdyy__1 +
        SOPDdyy_ma + slope_sum + slope_mean + slope_medi + slope_majo + TangCurv_s + TangCurv_m +
TangCurv_1 + TangCurv_2, data=tab)
summary(fit) #R^2 0.53
#Mind. 95 % sign. Level erklärende Parameter
fit <- lm(Tiefe ~ Z_m + slope_majo + TangCurv_1 + slope_sum + slope_mean + SOPDdxy_ma + SOPDdxy_me +
SOPDdxy_su +
        FOPDdxEW_s + FOPDdxEW_m + aspect_sum + aspect_mea + FOPDdxEW_2 + FOPDdyNW_1, data=tab)
summary(fit) #R^2 0.52
#Mind. 95 % sign. Level erklärende Parameter
```

```
fit <- lm(Tiefe ~ Z_m + slope_majo + TangCurv_1 + slope_sum + slope_mean +
        FOPDdxEW_s + FOPDdxEW_m + aspect_sum + aspect_mea + FOPDdxEW_2 + FOPDdyNW_1, data=tab)
summary(fit) #R^2 0.52
#Mind. 99 % sign. Level erklärende Parameter
fit <- lm(Tiefe ~ Z_m + slope_majo + TangCurv_1 + slope_sum + slope_mean + aspect_sum + aspect_mea +
FOPDdxEW_2, data=tab)
summary(fit) #R^2 0.52
#Mind. 95 % sign. Level erklärende Parameter
fit <- lm(Tiefe ~ Z_m + slope_majo + TangCurv_1 + FOPDdxEW_2, data=tab)
summary(fit) #R^2 0.52
#Mind. 95 % sign. Level erklärende Parameter
fit <- lm(Tiefe ~ Z_m + slope_majo + TangCurv_1, data=tab)
summary(fit) #R^2 0.52
#Fast gleich gutes Modell mit nur 3 der 46 Parametern!
#HÖHE, 100 m Puffer NEIGUNG MODUS (majo, Mehrheit) sowie 100 m Puffer TANGENTIAL CURVATURE MEDI-
AN entscheidende Parameter
#Aber: Modell unwesentlich besser als wenn nur Stakestandorte selber verwendet werden (R^2 0.5157 gegen 0.5119;
#im April gar nur 0.0031 schlechter)
#Fazit: Verwende nur 3 Parameter Höhe, Neigung und FOPDdyNS an Stakestandorten


#Automatisierte Regressionen Stakes 3 Parameter
#Zeilen 16 bis und mit 52 einlesen oder hier:
tabstakes <- read.table("Tiefe_Stakes_Sovjet2_complete.txt",header=T,sep="\t")
tab <- tabstakes[tabstakes$Monat%in%c(2),]

results_auto <- matrix(nrow=600000,ncol=6)
colnames(results_auto) <- c("R^2","Topographicalparameterchoice","Intercept","a_V1","b_V2","c_V3")
colnames(tab)
start <- 10
end <- length(tab[1,])
j <- 1
pb <- progress_bar$new(total=length(start:(end-2)))
for (V1 in start:(end-2)){
  for (V2 in (V1+1):(end-1)){
    for (V3 in (V2+1):end){
      reg <- lm(tab$Tiefe ~ tab[,V1] + tab[,V2] + tab[,V3])
      results_auto[j,] <- c(summary(reg)$r.squared, paste("Tiefe ~", paste(colnames(tab)[V1],
      colnames(tab)[V2], colnames(tab)[V3], sep=" + "),", data=tab"),summary(reg)$coeff[,1])
      j <- j+1
    }
  }
  pb$tick() #Läuft gegen Ende immer schneller
}
tail(results_auto)
results_auto <- results_auto[!is.na(results_auto[,1]),]
#plot(results_auto[,1])
str(results_auto)
#Nachfolgend stets Monat anpassen
write.table(results_auto,"../Auswertung_SDD_Raster_Sovjet/results_auto2_SDD_NS_Klima_Feb.csv",sep="\t")
results_auto <- read.table("../Auswertung_SDD_Raster_Sovjet/results_auto2_SDD_NS_Klima_Feb.csv",sep="\t") #Nach
Neueinlesen: results_auto[,c(1,3:6)] sind Numeric
str(results_auto)
summary(results_auto[,1]) #Bestes R^2 = 0.516 #Mit NS_Dec 0.672, NS_Jan 0.692, NS_Feb 0.687, NS_Mrz 0.705, NS_Apr
0.621
best <- results_auto[results_auto[,1]>=0.68,] #Z_m, TangCurv_s, TangCurv_1
write.table(best,"../Auswertung_SDD_Raster_Sovjet/results_auto2_BestRegressionsSDD_NS_Klima_Feb.csv",sep="\t")


#Automatisierte Regressionen Stakes, 4 Parameter
results_auto <- matrix(nrow=6000000,ncol=7)
colnames(results_auto) <- c("R^2","Topographicalparameterchoice","Intercept","a_V1","b_V2","c_V3","d_V4")
colnames(tab)
start <- 10
```

```
end <- length(tab[1,])
j <- 1
pb <- progress_bar$new(total=length(start:(end-4)))
for (V1 in start:(end-3)){
 for (V2 in (V1+1):(end-2)){
  for (V3 in (V2+1):(end-1)){
   for (V4 in (V3+1):end){
    reg <- lm(tab$Tiefe ~ tab[,V1] + tab[,V2] + tab[,V3] + tab[,V4])
    results_auto[j,] <- c(summary(reg)$r.squared, paste("Tiefe ~", paste(colnames(tab)[V1],
    colnames(tab)[V2], colnames(tab)[V3], colnames(tab)[V4], sep=" + "),", data=tab"),summary(reg)$coeff[,1])
    j <- j+1
   }
  }
 }
 pb$tick() #Läuft gegen Ende immer schneller
}
tail(results_auto)
results_auto <- results_auto[!is.na(results_auto[,1]),]
#plot(results_auto[,1])
str(results_auto)
write.table(results_auto,"../Auswertung_SDD_Raster_Sovjet/results_auto2_SDD_4Param_NS_Feb.csv",sep="\t")
results_auto <- read.table("../Auswertung_SDD_Raster_Sovjet/results_auto2_SDD_4Param_NS_Feb.csv",sep="\t")
#Nach Neueinlesen: results_auto[,c(1,3:6)] sind Numeric
str(results_auto)
summary(results_auto[,1]) #Bestes R^2 = 0.518 = unwesentlich besser als mit zwei Parametern #Mit NS_Dec 0.676,
NS_Jan 0.696, NS_Feb 0.691, NS_Mrz 0.708, NS_Apr 0.624
best <- results_auto[results_auto[,1]>=0.685,]
write.table(best,"../Auswertung_SDD_Raster_Sovjet/results_auto2_BestRegressionsSDD4Param_NS_Feb.csv",sep="\t")

#Automatisierte Regressionen Stakes, 2 Parameter
results_auto <- matrix(nrow=60000,ncol=5)
colnames(results_auto) <- c("R^2","Topographicalparameterchoice","Intercept","a_V1","b_V2")
colnames(tab)
start <- 10
end <- length(tab[1,])
j <- 1
pb <- progress_bar$new(total=length(start:(end-2)))
for (V1 in start:(end-1)){
 for (V2 in (V1+1):(end)){
  reg <- lm(tab$Tiefe ~ tab[,V1] + tab[,V2])
  results_auto[j,] <- c(summary(reg)$r.squared, paste("Tiefe ~", paste(colnames(tab)[V1],
  colnames(tab)[V2], sep=" + "),", data=tab"),summary(reg)$coeff[,1])
  j <- j+1
 }
 pb$tick() #Läuft gegen Ende immer schneller
}
tail(results_auto)
results_auto <- results_auto[!is.na(results_auto[,1]),]
#plot(results_auto[,1])
str(results_auto)
write.table(results_auto,"../Auswertung_SDD_Raster_Sovjet/results_auto_SDD_2Param.csv",sep="\t")
results_auto <- read.table("../Auswertung_SDD_Raster_Sovjet/results_auto_SDD_2Param.csv",sep="\t") #Nach
Neueinlesen: results_auto[,c(1,3:6)] sind Numeric
str(results_auto)
summary(results_auto[,1]) #Bestes R^2 = 0.513
best <- results_auto[results_auto[,1]>=0.513,] #Z_m, TangCurv_1
write.table(best,"../Auswertung_SDD_Raster_Sovjet/results_auto_BestRegressionsSDD2Param.csv",sep="\t")


#########################################################################################################
######################
#Teil2
#########################################################################################################
######################
```

```
#Strukturierte Multiple lineare Regressionen

#glmulti kann auf meinem PC leider nicht installiert werden...
# glmulti(we, colnames(tab)[-c(1:5)], data=tab, name="glmulti.analysis", minsize=3, maxsize=5,
#         plotty=T, fitfunction="lm")
#Andere Möglichkeiten:
#PC Analyse
#liste, lapply, napply,...

taborig <- read.table("Tiefe_zu_we_Pits_Sovjet2.txt",header=T,sep="\t")
SDD <- read.table("../Auswertung_SDD_Raster_Sovjet/SDD_norm_Pits2.csv",header=T,sep=",")
winterPS <- read.table("../Daten_Abramov_alt/Climate_Winter_PS.csv",header=T,sep="\t")
klima <- read.table("../Daten_Klima/20CRV2c.csv",header=T,sep="\t")

colnames(taborig)
colnames(taborig)[c(1:3,7:19)] <-
c(colnames(taborig)[1:3],"Tiefe_m","we",colnames(taborig)[9:14],"Hoehe","TangCurv","Neigung","ProfCurv","Ausrichtu
ng")
#tabtot <- taborig[,-c(4,5,6)]
#Auswahl der Spalten
#ohne SOPD, nur sum, mean, median und major; Einzeiler, sonst wird erster Ausdruck nicht gefiltert!
#wahl <-
grep("Pit|Jahr|Monat|Tiefe_m|we|SDD_extrapolated|Hoehe|TangCurv|Neigung|ProfCurv|Ausrichtung|FOPDdyN
S|FOPDdxEW|aspect_sum|aspect_mea|aspect_med|aspect_maj|FOPDdxEW_s|FOPDdxEW_m|FOPDdxEW_1|FOP
DdxEW_5|FOPDdyNS_s|FOPDdyNS_m|FOPDdyNS_1|FOPDdyNS_5|ProfCurv_s|ProfCurv_m|ProfCurv_1|ProfCur
v_5|TangCurv_s|TangCurv_m|TangCurv_1|TangCurv_5|Slope_sum|Slope_mean|Slope_medi|Slope_majo",colname
s(taborig))
# wahl <-
c(1:3,7:19,20:22,26:29,33:36,40:43,47:50,54:57,61:64,68:71,75:78,82:85,89:92,96:99,103:106,110:113,117:120,124:127,131:134,13
8:141,145:148,152:155,159:162,166:169,
# paste(wahl2, collapse=",")
#
173:176,180:183,187:190,194:197,201:204,208:211,215:218,222:225,229:232,236:239,243:246,250:253,257:260,264:267,271)
# wahl <-
c(1:3,7:24,25,26,27,31,32,33,34,38,39,40,41,45,46,47,48,52,53,54,55,59,60,61,62,66,67,68,69,73,74,75,76,80,81,82,83,87,88,89,90,
94,95,96,97,101,102,103,104,108,109,110,111,115,116,117,118,122,123,124,125,129,130,131,132,136,137,138,139,143,144,145,1
46,150,151,152,153,157,158,159,160,164,165,166,167,171,172,173,174,178,179,180,181,185,186,187,188,192,193,194,195,199,20
0,201,202,206,207,208,209,213,214,215,216,220,221,222,223,227,228,229,230,234,235,236,237,241,242,243,244,248,249,250,251
,255,256,257,258,262,263,264,265,269,270,271,272,276)
# tabtot <- taborig[wahl]

tabtot <- taborig[,-c(4:6)]
colnames(tabtot)

#SDD Spalten auffüllen
head(SDD)
for (i in c(1,3:9)){
  tabtot[tabtot$Pit==i,c(6:10)] <- SDD[i,c(1:5)]
  tabtot[tabtot$Pit==i,11] <- mean(as.numeric(SDD[i,c(1:5)]))
}

#NSdaten an tabtot anfügen
tabtot <- tabtot[tabtot$Monat%in%c(12,1,2,3,4)&tabtot$Jahr<=1998&tabtot$Pit!=2,] #Pit 2 entfernen weil ausserhalb
Gletscher; bei SDD_extrapolated nicht vorhanden
tabtot <- cbind(tabtot,matrix(nrow=length(tabtot[,1]),ncol=5))
colnames(tabtot)[(length(tabtot[1,])-4):length(tabtot[1,])] <-
c("WinterNS_Dez","WinterNS_Jan","WinterNS_Feb","WinterNS_Mrz","WinterNS_Apr")
for (jahr in c(1968:1998)){
  tabtot$WinterNS_Jan[tabtot$Jahr==jahr] <- winterPS$WinterNS_Jan[winterPS$Winter==jahr]
  tabtot$WinterNS_Feb[tabtot$Jahr==jahr] <- winterPS$WinterNS_Feb[winterPS$Winter==jahr]
  tabtot$WinterNS_Mrz[tabtot$Jahr==jahr] <- winterPS$WinterNS_Mrz[winterPS$Winter==jahr]
  tabtot$WinterNS_Apr[tabtot$Jahr==jahr] <- winterPS$WinterNS_Apr[winterPS$Winter==jahr]
}
for (jahr in c(1967:1997)){
```

```
  tabtot$WinterNS_Dez[tabtot$Jahr==jahr] <- winterPS$WinterNS_Dez[winterPS$Winter==(jahr+1)]
}
tabtot$WinterNS_Dez[tabtot$Jahr==1998] <- 125.9 #Oktober bis Dezember 1998
tail(tabtot[c(1:3,165:170)])

#Klimadaten 20CRV2c an tabtot anfügen
tabtot <- cbind(tabtot,matrix(nrow=length(tabtot[,1]),ncol=3))
colnames(tabtot)[(length(tabtot[1,])-2):length(tabtot[1,])] <- c("wind","dir","hum")
for (jahr in c(1968:1998)){
  for (monat in c(1:4,12)){
    tabtot[tabtot$Jahr==jahr&tabtot$Monat==monat,(length(tabtot[1,])-2):length(tabtot[1,])] <- kli-
ma[klima$year==jahr&klima$month==monat,6:8]
  }
}
tabtot[tabtot$Jahr==1967,(length(tabtot[1,])-2):length(tabtot[1,])] <- klima[klima$year==1967&klima$month==12,6:8]

# #Wegen anderer Methode in R (100 m Major Berechnung gibt grosse Stufen) Modus entfernen und Regressionen neu
durchlaufen:
# colnames(tabtot)
# abwahl <- seq(25, 165, by=4)
# tabtot <- tabtot[,-abwahl]
write.table(tabtot, "Tiefe_zu_we_Pits_Sovjet2_complete.txt", row.names=F, sep="\t")

#Monat wählen
tabtot <- read.table("Tiefe_zu_we_Pits_Sovjet2_complete.txt",header=T,sep="\t")
tab <- tabtot[tabtot$Monat%in%c(12),]
tab <- tab[,-c(58:165)] #Nur noch <= 100 m Radius
colnames(tab)
#Weiter ab Zeile 464


#Manuelle Multiple lineare Regression
fit <- lm(we ~ SDD_Dec + X100m_slope_medi + X100m_SOPDdyy_su + WinterNS_Dez, data=tab)
summary(fit) #Dez Best: 0.70; dyy_su oder me 0.696
fit <- lm(we ~ SDD_Mrz + X100m_slope_medi + X100m_SOPDdyy_su + WinterNS_Mrz, data=tab)
summary(fit) #Mrz 6. best: 0.80; dyy_su oder me 0.798; Hoehe statt SDD: 0.803
fit <- lm(we ~ SDD_Apr + X100m_slope_medi + X100m_SOPDdyy_su + WinterNS_Apr, data=tab)
summary(fit) #Apr 6. best: 0.82; dyy_su oder me 0.818
fit <- lm(we ~ SDD_Feb + X100m_slope_sum + X100m_SOPDdyy_su + WinterNS_Feb, data=tab)
summary(fit)
fit <- lm(we ~ SDD_Dec + X100m_SOPDdxx_ma + X100m_SOPDdxy_su + WinterNS_Dez, data=tab)
summary(fit)


# #(Visualisierung w.e. nach Snowpit)
# mon <- 2 #Monat
# par(mfrow=c(3,3))
# for (pit in c(2,1,3,4,6,9,7,5,8)){
#   hoehe <- tabtot[tabtot[,1]==pit&tabtot[,3]==mon,6]
#   plot(tabtot[tabtot[,1]==pit&tabtot[,3]==mon,5], ylab="m w.e.", main=paste(hoehe[1],"m","snowpit",pit,"month",mon))
#   legend("topright",legend=round(mean(tabtot[tabtot[,1]==pit&tabtot[,3]==mon,5]),3),bg="",bty="n") #Mittelwert
# }

# #Auswahl der Hauptkomponenten mittels PCA
# #https://tgmstat.wordpress.com/2013/11/28/computing-and-visualizing-pca-in-r/
# PCA <- prcomp(tab[,6:length(tab[1,])], retx=T, center=T, scale.=T) #Unbedingt Scale!
# plot(PCA, type="l")
# #Bedeutung jeder PCA:
# summary(PCA)

###Manuelle Analyse###

#Output der cat-Zeile kopieren und ins lm einfügen
colnames(tab)
```

```
results <- data.frame(nrow=1,ncol=3)
colnames(results) <- c("Topographicalparameterchoice","Constant","R^2")
k <- 1

cat(paste(colnames(tab)[grep("Ausrichtung|aspect_sum|aspect_mea|aspect_med|aspect_maj",
colnames(tab))],collapse=" + "))
fit_aspect_1_1 <- lm(we ~ Ausrichtung + X100m_aspect_sum + X100m_aspect_mea + X100m_aspect_med +
X100m_aspect_maj, data=tab)
fit_aspect_1_2 <- lm(we ~ Ausrichtung + X200m_aspect_sum + X200m_aspect_mea + X200m_aspect_med +
X200m_aspect_maj, data=tab)
fit_aspect_1_3 <- lm(we ~ Ausrichtung + X300m_aspect_sum + X300m_aspect_mea + X300m_aspect_med +
X300m_aspect_maj, data=tab)
fit_aspect_1_4 <- lm(we ~ Ausrichtung + X400m_aspect_sum + X400m_aspect_mea + X400m_aspect_med +
X400m_aspect_maj, data=tab)
fit_aspect_2_1 <- lm(we ~ Ausrichtung + X100m_aspect_sum + X200m_aspect_sum + X300m_aspect_sum +
X400m_aspect_sum, data=tab)
fit_aspect_2_2 <- lm(we ~ Ausrichtung + X100m_aspect_mea + X200m_aspect_mea + X300m_aspect_mea +
X400m_aspect_mea, data=tab)
fit_aspect_2_3 <- lm(we ~ Ausrichtung + X100m_aspect_med + X200m_aspect_med + X300m_aspect_med +
X400m_aspect_med, data=tab)
fit_aspect_2_4 <- lm(we ~ Ausrichtung + X100m_aspect_maj + X200m_aspect_maj + X300m_aspect_maj +
X400m_aspect_maj, data=tab)
for(j in 1:2){
 for(i in 1:4){
  dat <- summary(get(paste0("fit_aspect_",j,"_",i)))$r.squared
  print(dat)
  print(summary(get(paste0("fit_aspect_",j,"_",i))))
  results[k,1] <- paste0("fit_aspect_",j,"_",i)
  results[k,3] <- dat
  k <- k+1
 }
}

cat(paste(colnames(tab)[grep("FOPDdxEW_s|FOPDdxEW_m|FOPDdxEW_1|FOPDdxEW_5", colna-
mes(tab))],collapse=" + "))
fit_aspect_3_1 <- lm(we ~ FOPDdxEW + X100m_FOPDdxEW_s + X100m_FOPDdxEW_m + X100m_FOPDdxEW_1 +
X100m_FOPDdxEW_5, data=tab)
fit_aspect_3_2 <- lm(we ~ FOPDdxEW + X200m_FOPDdxEW_s + X200m_FOPDdxEW_m + X200m_FOPDdxEW_1 +
X200m_FOPDdxEW_5, data=tab)
fit_aspect_3_3 <- lm(we ~ FOPDdxEW + X300m_FOPDdxEW_s + X300m_FOPDdxEW_m + X300m_FOPDdxEW_1 +
X300m_FOPDdxEW_5, data=tab)
fit_aspect_3_4 <- lm(we ~ FOPDdxEW + X400m_FOPDdxEW_s + X400m_FOPDdxEW_m + X400m_FOPDdxEW_1 +
X400m_FOPDdxEW_5, data=tab)
fit_aspect_4_1 <- lm(we ~ FOPDdxEW + X100m_FOPDdxEW_s + X200m_FOPDdxEW_s + X300m_FOPDdxEW_s +
X400m_FOPDdxEW_s, data=tab)
fit_aspect_4_2 <- lm(we ~ FOPDdxEW + X100m_FOPDdxEW_m + X200m_FOPDdxEW_m + X300m_FOPDdxEW_m +
X400m_FOPDdxEW_m, data=tab)
fit_aspect_4_3 <- lm(we ~ FOPDdxEW + X100m_FOPDdxEW_1 + X200m_FOPDdxEW_1 + X300m_FOPDdxEW_1 +
X400m_FOPDdxEW_1, data=tab)
fit_aspect_4_4 <- lm(we ~ FOPDdxEW + X100m_FOPDdxEW_5 + X200m_FOPDdxEW_5 + X300m_FOPDdxEW_5 +
X400m_FOPDdxEW_5, data=tab)
for(j in 3:4){
 for(i in 1:4){
  dat <- summary(get(paste0("fit_aspect_",j,"_",i)))$r.squared
  print(dat)
  results[k,1] <- paste0("fit_FOPDdxEW_",j,"_",i)
  results[k,3] <- dat
  k <- k+1
 }
}

cat(paste(colnames(tab)[grep("FOPDdyNS_s|FOPDdyNS_m|FOPDdyNS_1|FOPDdyNS_5", colnames(tab))],collapse="
+ "))
```

```
fit_aspect_5_1 <- lm(we ~ FOPDdyNS + X100m_FOPDdyNS_s + X100m_FOPDdyNS_m + X100m_FOPDdyNS_1 +
X100m_FOPDdyNS_5, data=tab)
fit_aspect_5_2 <- lm(we ~ FOPDdyNS + X200m_FOPDdyNS_s + X200m_FOPDdyNS_m + X200m_FOPDdyNS_1 +
X200m_FOPDdyNS_5, data=tab)
fit_aspect_5_3 <- lm(we ~ FOPDdyNS + X300m_FOPDdyNS_s + X300m_FOPDdyNS_m + X300m_FOPDdyNS_1 +
X300m_FOPDdyNS_5, data=tab)
fit_aspect_5_4 <- lm(we ~ FOPDdyNS + X400m_FOPDdyNS_s + X400m_FOPDdyNS_m + X400m_FOPDdyNS_1 +
X400m_FOPDdyNS_5, data=tab)
fit_aspect_6_1 <- lm(we ~ FOPDdyNS + X100m_FOPDdyNS_s + X200m_FOPDdyNS_s + X300m_FOPDdyNS_s +
X400m_FOPDdyNS_s, data=tab)
fit_aspect_6_2 <- lm(we ~ FOPDdyNS + X100m_FOPDdyNS_m + X200m_FOPDdyNS_m + X300m_FOPDdyNS_m +
X400m_FOPDdyNS_m, data=tab)
fit_aspect_6_3 <- lm(we ~ FOPDdyNS + X100m_FOPDdyNS_1 + X200m_FOPDdyNS_1 + X300m_FOPDdyNS_1 +
X400m_FOPDdyNS_1, data=tab)
fit_aspect_6_4 <- lm(we ~ FOPDdyNS + X100m_FOPDdyNS_5 + X200m_FOPDdyNS_5 + X300m_FOPDdyNS_5 +
X400m_FOPDdyNS_5, data=tab)
for(j in 5:6){
 for(i in 1:4){
  dat <- summary(get(paste0("fit_aspect_",j,"_",i)))$r.squared
  print(dat)
  results[k,1] <- paste0("fit_FOPDdyNS_",j,"_",i)
  results[k,3] <- dat
  k <- k+1
 }
}

cat(paste(colnames(tab)[grep("ProfCurv_s|ProfCurv_m|ProfCurv_1|ProfCurv_5", colnames(tab))],collapse=" + "))
fit_aspect_7_1 <- lm(we ~ ProfCurv + X100m_ProfCurv_s + X100m_ProfCurv_m + X100m_ProfCurv_1 +
X100m_ProfCurv_5, data=tab)
fit_aspect_7_2 <- lm(we ~ ProfCurv + X200m_ProfCurv_s + X200m_ProfCurv_m + X200m_ProfCurv_1 +
X200m_ProfCurv_5, data=tab)
fit_aspect_7_3 <- lm(we ~ ProfCurv + X300m_ProfCurv_s + X300m_ProfCurv_m + X300m_ProfCurv_1 +
X300m_ProfCurv_5, data=tab)
fit_aspect_7_4 <- lm(we ~ ProfCurv + X400m_ProfCurv_s + X400m_ProfCurv_m + X400m_ProfCurv_1 +
X400m_ProfCurv_5, data=tab)
fit_aspect_8_1 <- lm(we ~ ProfCurv + X100m_ProfCurv_s + X200m_ProfCurv_s + X300m_ProfCurv_s +
X400m_ProfCurv_s, data=tab)
fit_aspect_8_2 <- lm(we ~ ProfCurv + X100m_ProfCurv_m + X200m_ProfCurv_m + X300m_ProfCurv_m +
X400m_ProfCurv_m, data=tab)
fit_aspect_8_3 <- lm(we ~ ProfCurv + X100m_ProfCurv_1 + X200m_ProfCurv_1 + X300m_ProfCurv_1 +
X400m_ProfCurv_1, data=tab)
fit_aspect_8_4 <- lm(we ~ ProfCurv + X100m_ProfCurv_5 + X200m_ProfCurv_5 + X300m_ProfCurv_5 +
X400m_ProfCurv_5, data=tab)
for(j in 7:8){
 for(i in 1:4){
  dat <- summary(get(paste0("fit_aspect_",j,"_",i)))$r.squared
  print(dat)
  results[k,1] <- paste0("fit_ProfCurv_",j,"_",i)
  results[k,3] <- dat
  k <- k+1
 }
}

cat(paste(colnames(tab)[grep("TangCurv_s|TangCurv_m|TangCurv_1|TangCurv_5", colnames(tab))],collapse=" + "))
fit_aspect_9_1 <- lm(we ~ TangCurv + X100m_TangCurv_s + X100m_TangCurv_m + X100m_TangCurv_1 +
X100m_TangCurv_5, data=tab)
fit_aspect_9_2 <- lm(we ~ TangCurv + X200m_TangCurv_s + X200m_TangCurv_m + X200m_TangCurv_1 +
X200m_TangCurv_5, data=tab)
fit_aspect_9_3 <- lm(we ~ TangCurv + X300m_TangCurv_s + X300m_TangCurv_m + X300m_TangCurv_1 +
X300m_TangCurv_5, data=tab)
fit_aspect_9_4 <- lm(we ~ TangCurv + X400m_TangCurv_s + X400m_TangCurv_m + X400m_TangCurv_1 +
X400m_TangCurv_5, data=tab)
fit_aspect_10_1 <- lm(we ~ TangCurv + X100m_TangCurv_s + X200m_TangCurv_s + X300m_TangCurv_s +
X400m_TangCurv_s, data=tab)
```

```
fit_aspect_10_2 <- lm(we ~ TangCurv + X100m_TangCurv_m + X200m_TangCurv_m + X300m_TangCurv_m +
X400m_TangCurv_m, data=tab)
fit_aspect_10_3 <- lm(we ~ TangCurv + X100m_TangCurv_1 + X200m_TangCurv_1 + X300m_TangCurv_1 +
X400m_TangCurv_1, data=tab)
fit_aspect_10_4 <- lm(we ~ TangCurv + X100m_TangCurv_5 + X200m_TangCurv_5 + X300m_TangCurv_5 +
X400m_TangCurv_5, data=tab)
for(j in 9:10){
 for(i in 1:4){
  dat <- summary(get(paste0("fit_aspect_",j,"_",i)))$r.squared
  print(dat)
  results[k,1] <- paste0("fit_TangCurv_",j,"_",i)
  results[k,3] <- dat
  k <- k+1
 }
}

cat(paste(colnames(tab)[grep("Slope_sum|Slope_mean|Slope_medi|Slope_majo", colnames(tab))],collapse=" + "))
fit_aspect_11_1 <- lm(we ~ Neigung + X100m_Slope_sum + X100m_Slope_mean + X100m_Slope_medi +
X100m_Slope_majo, data=tab)
fit_aspect_11_2 <- lm(we ~ Neigung + X200m_Slope_sum + X200m_Slope_mean + X200m_Slope_medi +
X200m_Slope_majo, data=tab)
fit_aspect_11_3 <- lm(we ~ Neigung + X300m_Slope_sum + X300m_Slope_mean + X300m_Slope_medi +
X300m_Slope_majo, data=tab)
fit_aspect_11_4 <- lm(we ~ Neigung + X400m_Slope_sum + X400m_Slope_mean + X400m_Slope_medi +
X400m_Slope_majo, data=tab)
fit_aspect_12_1 <- lm(we ~ Neigung + X100m_Slope_sum + X200m_Slope_sum + X300m_Slope_sum +
X400m_Slope_sum, data=tab)
fit_aspect_12_2 <- lm(we ~ Neigung + X100m_Slope_mean + X200m_Slope_mean + X300m_Slope_mean +
X400m_Slope_mean, data=tab)
fit_aspect_12_3 <- lm(we ~ Neigung + X100m_Slope_medi + X200m_Slope_medi + X300m_Slope_medi +
X400m_Slope_medi, data=tab)
fit_aspect_12_4 <- lm(we ~ Neigung + X100m_Slope_majo + X200m_Slope_majo + X300m_Slope_majo +
X400m_Slope_majo, data=tab)
for(j in 11:12){
 for(i in 1:4){
  dat <- summary(get(paste0("fit_aspect_",j,"_",i)))$r.squared
  print(dat)
  results[k,1] <- paste0("fit_Slope_",j,"_",i)
  results[k,3] <- dat
  k <- k+1
 }
}

results[1:(12*4),2] <- rep(c("100m","200m","300m","400m","sum","mean","median","major"),12*4/8)
results
plot(results[,3])
write.table(results,"results_R2.csv",sep="\t")
#Fazit aspect: 400 m am bedeutendsten R^2 0.46; darunter Sum und Median am wichtigsten
#Fazit FOPDdxEW: 100 m und Mean am bedeutendsten R^2 0.54 und 0.55; darunter nur Median und Major wichtig
#Fazit FOPDdyNS: 400 m ähnlich bedeutend wie 100 m R^2 0.56 und 0.54; darunter Mean besonders wichtig
#Fazit ProfCurv: 400 m am bedeutendsten R^2 0.6; darunter Sum, Mean und Median wichtig
#Fazit TangCurv: Median am bedeutendsten R^2 0.55; darunter 200 m am bedeutendsten sowie TangCurv an Pit
#Fazit Slope: 100 m sowie Sum und Mean am bedeutendsten R^2 0.60, 0,61 und 0,60; darunter Mjaor und Slope, Pit
Standort und 100 m resp. Pit Standort und 100 m am bedeutendsten
#Detailbetrachtung der guten Variablen mit summary(fit_aspect_...)

colnames(tab)
fit <- lm(we ~ X400m_aspect_med + X100m_FOPDdxEW_1 + TangCurv, data=tab)
summary(fit)
fit <- lm(we ~ X400m_FOPDdyNS_m + X400m_ProfCurv_s + Neigung, data=tab)
summary(fit)

###Funktioniert absolut nicht - automatischer Ansatz nötig! (Oder Package glmulti auf 32 Bit Rechner)###
```

```
###Automatisierte Regressionen###
#Einlesen:
tabtot <- read.table("Tiefe_zu_we_Pits_Sovjet2_complete.txt",header=T,sep="\t")
colnames(tabtot)
tabtot <- tabtot[,-c(58:165)] #Nur noch <= 100 m Radius
#tabtot <- tabtot[,-c(49:129)] #Nur noch <= 100 m Radius, wenn Major abgewählt (siehe Zeile 276ff.)

#Die meisten der folgenden Analysen werden aus Zeitgründen nur für die Umgebungen <=100 m um die Pits gemacht.
#!!!!!!!!!Achtung: Vermeinde rbind in Schleife, dauert sonst ca. 10 Stunden!!!!!!!!!
#Wesentlich schnellere Variante ohne Rbind (ca. 15 min, Fortschrittsbalken erscheint nach 1 min)

tab <- tabtot[tabtot$Monat%in%c(2)&tabtot$Jahr%in%c(1968:1998),]

results_auto <- matrix(nrow=600000,ncol=6)
colnames(results_auto) <- c("R^2","Topographicalparameterchoice","Intercept","a_V1","b_V2","c_V3")
colnames(tab)
start <- 6
end <- length(tab[1,])
j <- 1
pb <- progress_bar$new(total=length(start:(end-2)))
for (V1 in start:(end-2)){
  for (V2 in (V1+1):(end-1)){
    for (V3 in (V2+1):end){
      reg <- lm(tab$we ~ tab[,V1] + tab[,V2] + tab[,V3])
      results_auto[j,] <- c(summary(reg)$r.squared, paste("we ~", paste(colnames(tab)[V1],
      colnames(tab)[V2], colnames(tab)[V3], sep=" + "),", data=tab"),summary(reg)$coeff[,1])
      j <- j+1
    }
  }
  pb$tick() #Läuft gegen Ende immer schneller
}
tail(results_auto)
tail(results_auto[!is.na(results_auto[,1]),])
results_auto <- results_auto[!is.na(results_auto[,1]),]
#plot(results_auto[,1])
write.table(results_auto,"../Auswertung_PM_Raster_Sovjet/results_auto2_R2_Dez_ohneMaj.csv",sep="\t")
results_auto <- read.table("../Auswertung_PM_Raster_Sovjet/results_auto2_R2_Dez_ohneMaj.csv",sep="\t") #Nach
Neueinlesen: results_auto[,c(1,3:6)] sind Numeric
summary(results_auto[,1])
best <- results_auto[results_auto[,1]>=0.66,]
best
write.table(best,"../Auswertung_PM_Raster_Sovjet/results_auto2_BestRegressions_Dez_ohneMaj.csv",sep="\t")

#Beste Wahl mit 4 Parametern Feb
tab <- tabtot[tabtot$Monat%in%c(2)&tabtot$Jahr%in%c(1968:1998),]
results_auto <- matrix(nrow=60000000,ncol=7)
colnames(results_auto) <- c("R^2","Topographicalparameterchoice","Intercept","a_V1","b_V2","c_V3","d_V4")
colnames(tab)
start <- 6
end <- length(tab[1,])
j <- 1
pb <- progress_bar$new(total=length(start:(end-4)))
for (V1 in start:(end-3)){
  for (V2 in (V1+1):(end-2)){
    for (V3 in (V2+1):(end-1)){
      for (V4 in (V3+1):end){
        reg <- lm(tab$we ~ tab[,V1] + tab[,V2] + tab[,V3] + tab[,V4])
        results_auto[j,] <- c(summary(reg)$r.squared, paste("we ~", paste(colnames(tab)[V1],
        colnames(tab)[V2], colnames(tab)[V3], colnames(tab)[V4], sep=" + "),", data=tab"),summary(reg)$coeff[,1])
        j <- j+1
      }
    }
  }
```

```
  pb$tick() #Läuft gegen Ende immer schneller
}
tail(results_auto)
results_auto <- results_auto[!is.na(results_auto[,1]),]
#plot(results_auto[,1])
str(results_auto)
write.table(results_auto,"../Auswertung_PM_Raster_Sovjet/results_auto2_R2_4Param_Feb.csv",sep="\t")
results_auto <- read.table("../Auswertung_PM_Raster_Sovjet/results_auto2_R2_4Param_Feb.csv",sep="\t") #Nach
Neueinlesen: results_auto[,c(1,3:6)] sind Numeric
str(results_auto)
summary(results_auto[,1])
best <- results_auto[results_auto[,1]>=0.79,] #NS_Dez dabei: 0.794
write.table(best,"../Auswertung_PM_Raster_Sovjet/results_auto2_BestRegressions4Param_Feb.csv",sep="\t")

# #Versuch: Beste Wahl mit 5 Parametern Feb
# tab <- tabtot[tabtot$Monat%in%c(2),]
# tab <- tab[,-c(58:165)] #Nur noch <= 100 m Radius
# #tab <- tab[,-c(22:57)] #Nur noch an Pit Standorten
# results_auto <- matrix(nrow=60000000,ncol=8)
# colnames(results_auto) <-
c("R^2","Topographicalparameterchoice","Intercept","a_V1","b_V2","c_V3","d_V4","e_V5","f_V6")
# colnames(tab)
# start <- 6
# end <- length(tab[1,])
# j <- 1
# pb <- progress_bar$new(total=length(start:(end-5)))
# for (V1 in start:(end-4)){
#   for (V2 in (V1+1):(end-3)){
#     for (V3 in (V2+1):(end-2)){
#       for (V4 in (V3+1):(end-1)){
#         for (V5 in (V4+1):(end)){
#           reg <- lm(tab$Tiefe ~ tab[,V1] + tab[,V2] + tab[,V3] + tab[,V4]+ tab[,V5])
#           results_auto[j,] <- c(summary(reg)$r.squared, paste("we ~", paste(colnames(tab)[V1],
#           colnames(tab)[V2], colnames(tab)[V3], colnames(tab)[V4], colnames(tab)[V5], sep=" + "),", da-
ta=tab"),summary(reg)$coeff[,1])
#           j <- j+1
#         }
#       }
#     }
#   }
#   pb$tick() #Läuft gegen Ende immer schneller
# }
# tail(results_auto)
# results_auto <- results_auto[!is.na(results_auto[,1]),]
# #plot(results_auto[,1])
# str(results_auto)
#
write.table(results_auto,"../Auswertung_PM_Raster_Sovjet/results_auto_R2_5Param_Feb_NurPitStandorte.csv",sep="\t
")
# results_auto <-
read.table("../Auswertung_PM_Raster_Sovjet/results_auto_R2_5Param_Feb_NurPitStandorte.csv",sep="\t") #Nach
Neueinlesen: results_auto[,c(1,3:6)] sind Numeric
# str(results_auto)
# summary(results_auto[,1])
# best <- results_auto[results_auto[,1]>=0.8,]
# wri-
te.table(best,"../Auswertung_PM_Raster_Sovjet/results_auto_BestRegressions5Param_Feb_NurPitStandorte.csv",sep="\t
")

#Beste Wahl mit 4 Parametern Dez
tab <- tabtot[tabtot$Monat%in%c(12)&tabtot$Jahr%in%c(1968:1998),]
results_auto <- matrix(nrow=6000000,ncol=7)
colnames(results_auto) <- c("R^2","Topographicalparameterchoice","Intercept","a_V1","b_V2","c_V3","d_V4")
colnames(tab)
```

```
start <- 6
end <- length(tab[1,])
j <- 1
pb <- progress_bar$new(total=length(start:(end-4)))
for (V1 in start:(end-3)){
  for (V2 in (V1+1):(end-2)){
    for (V3 in (V2+1):(end-1)){
      for (V4 in (V3+1):end){
        reg <- lm(tab$we ~ tab[,V1] + tab[,V2] + tab[,V3] + tab[,V4])
        results_auto[j,] <- c(summary(reg)$r.squared, paste("we ~", paste(colnames(tab)[V1],
        colnames(tab)[V2], colnames(tab)[V3], colnames(tab)[V4], sep=" + "),", data=tab"),summary(reg)$coeff[,1])
        j <- j+1
      }
    }
  }
  pb$tick() #Läuft gegen Ende immer schneller
}
tail(results_auto)
results_auto <- results_auto[!is.na(results_auto[,1]),]
#plot(results_auto[,1])
str(results_auto)
write.table(results_auto,"../Auswertung_PM_Raster_Sovjet/results_auto2_R2_4Param_Dez.csv",sep="\t")
results_auto <- read.table("../Auswertung_PM_Raster_Sovjet/results_auto2_R2_4Param_Dez.csv",sep="\t") #Nach
Neueinlesen: results_auto[,c(1,3:6)] sind Numeric
str(results_auto)
summary(results_auto[,1]) #wenn NS_Dez dabei: 0.702
best <- results_auto[results_auto[,1]>=0.71,]
write.table(best,"../Auswertung_PM_Raster_Sovjet/results_auto2_BestRegressions4Param_Dez.csv",sep="\t")
fit <- lm(we ~ SDD_Dec + X100m_SOPDdxx_ma + X100m_SOPDdxy__1 + WinterNS_Dez , data=tab); summary(fit)

#Beste Wahl mit 4 Parametern Jan
tab <- tabtot[tabtot$Monat%in%c(1)&tabtot$Jahr%in%c(1968:1998),]
results_auto <- matrix(nrow=6000000,ncol=7)
colnames(results_auto) <- c("R^2","Topographicalparameterchoice","Intercept","a_V1","b_V2","c_V3","d_V4")
colnames(tab)
start <- 6
end <- length(tab[1,])
j <- 1
pb <- progress_bar$new(total=length(start:(end-4)))
for (V1 in start:(end-3)){
  for (V2 in (V1+1):(end-2)){
    for (V3 in (V2+1):(end-1)){
      for (V4 in (V3+1):end){
        reg <- lm(tab$we ~ tab[,V1] + tab[,V2] + tab[,V3] + tab[,V4])
        results_auto[j,] <- c(summary(reg)$r.squared, paste("we ~", paste(colnames(tab)[V1],
        colnames(tab)[V2], colnames(tab)[V3], colnames(tab)[V4], sep=" + "),", data=tab"),summary(reg)$coeff[,1])
        j <- j+1
      }
    }
  }
  pb$tick() #Läuft gegen Ende immer schneller
}
tail(results_auto)
results_auto <- results_auto[!is.na(results_auto[,1]),]
#plot(results_auto[,1])
str(results_auto)
write.table(results_auto,"../Auswertung_PM_Raster_Sovjet/results_auto2_R2_4Param_Jan.csv",sep="\t")
results_auto <- read.table("../Auswertung_PM_Raster_Sovjet/results_auto2_R2_4Param_Jan.csv",sep="\t") #Nach
Neueinlesen: results_auto[,c(1,3:6)] sind Numeric
str(results_auto)
summary(results_auto[,1]) #wenn NS_Jan dabei: 0.797
best <- results_auto[results_auto[,1]>=0.797,]
write.table(best,"../Auswertung_PM_Raster_Sovjet/results_auto2_BestRegressions4Param_Jan.csv",sep="\t")
```

```
#Beste Wahl mit 4 Parametern Mrz
tab <- tabtot[tabtot$Monat%in%c(3)&tabtot$Jahr%in%c(1968:1998),]
results_auto <- matrix(nrow=6000000,ncol=7)
colnames(results_auto) <- c("R^2","Topographicalparameterchoice","Intercept","a_V1","b_V2","c_V3","d_V4")
colnames(tab)
start <- 6
end <- length(tab[1,])
j <- 1
pb <- progress_bar$new(total=length(start:(end-4)))
for (V1 in start:(end-3)){
 for (V2 in (V1+1):(end-2)){
  for (V3 in (V2+1):(end-1)){
   for (V4 in (V3+1):end){
    reg <- lm(tab$we ~ tab[,V1] + tab[,V2] + tab[,V3] + tab[,V4])
    results_auto[j,] <- c(summary(reg)$r.squared, paste("we ~", paste(colnames(tab)[V1],
    colnames(tab)[V2], colnames(tab)[V3], colnames(tab)[V4], sep=" + "),", data=tab"),summary(reg)$coeff[,1])
    j <- j+1
   }
  }
 }
 pb$tick() #Läuft gegen Ende immer schneller
}
tail(results_auto)
results_auto <- results_auto[!is.na(results_auto[,1]),]
#plot(results_auto[,1])
str(results_auto)
write.table(results_auto,"../Auswertung_PM_Raster_Sovjet/results_auto2_R2_4Param_Mrz.csv",sep="\t")
results_auto <- read.table("../Auswertung_PM_Raster_Sovjet/results_auto2_R2_4Param_Mrz.csv",sep="\t") #Nach
Neueinlesen: results_auto[,c(1,3:6)] sind Numeric
str(results_auto)
summary(results_auto[,1]) #wenn NS_Mrz dabei: 0.822
best <- results_auto[results_auto[,1]>=0.822,]
write.table(best,"../Auswertung_PM_Raster_Sovjet/results_auto2_BestRegressions4Param_Mrz.csv",sep="\t")
fit <- lm(we ~ SDD_Mrz + X100m_SOPDdxx_ma + X100m_SOPDdxy_su + WinterNS_Mrz , data=tab); summary(fit)

#Beste Wahl mit 4 Parametern Apr
tab <- tabtot[tabtot$Monat%in%c(4)&tabtot$Jahr%in%c(1968:1998),]
results_auto <- matrix(nrow=6000000,ncol=7)
colnames(results_auto) <- c("R^2","Topographicalparameterchoice","Intercept","a_V1","b_V2","c_V3","d_V4")
colnames(tab)
start <- 6
end <- length(tab[1,])
j <- 1
pb <- progress_bar$new(total=length(start:(end-4)))
for (V1 in start:(end-3)){
 for (V2 in (V1+1):(end-2)){
  for (V3 in (V2+1):(end-1)){
   for (V4 in (V3+1):end){
    reg <- lm(tab$we ~ tab[,V1] + tab[,V2] + tab[,V3] + tab[,V4])
    results_auto[j,] <- c(summary(reg)$r.squared, paste("we ~", paste(colnames(tab)[V1],
    colnames(tab)[V2], colnames(tab)[V3], colnames(tab)[V4], sep=" + "),", data=tab"),summary(reg)$coeff[,1])
    j <- j+1
   }
  }
 }
 pb$tick() #Läuft gegen Ende immer schneller
}
tail(results_auto)
results_auto <- results_auto[!is.na(results_auto[,1]),]
#plot(results_auto[,1])
str(results_auto)
write.table(results_auto,"../Auswertung_PM_Raster_Sovjet/results_auto2_R2_4Param_Apr.csv",sep="\t")
results_auto <- read.table("../Auswertung_PM_Raster_Sovjet/results_auto2_R2_4Param_Apr.csv",sep="\t") #Nach
Neueinlesen: results_auto[,c(1,3:6)] sind Numeric
```

```
str(results_auto)
summary(results_auto[,1]) #wenn NS_Apr: 0.836
best <- results_auto[results_auto[,1]>=0.837,]
write.table(best,"../Auswertung_PM_Raster_Sovjet/results_auto2_BestRegressions4Param_Apr.csv",sep="\t")


#Versuch: Beste Wahl mit nur 2 Parametern
tab <- tabtot[tabtot$Monat%in%c(2)&tabtot$Jahr%in%c(1968:1998),]
tab <- tab[,-c(49:134)] #Nur noch <= 100 m Radius
results_auto <- matrix(nrow=200000,ncol=5)
colnames(results_auto) <- c("R^2","Topographicalparameterchoice","Intercept","a_V1","b_V2")
colnames(tab)
start <- 6
end <- length(tab[1,])
j <- 1
pb <- progress_bar$new(total=length(start:(end-2)))
for (V1 in start:(end-2)){
 for (V2 in (V1+1):(end-1)){
  reg <- lm(tab$we ~ tab[,V1] + tab[,V2])
  results_auto[j,] <- c(summary(reg)$r.squared, paste("we ~", paste(colnames(tab)[V1],
  colnames(tab)[V2], sep=" + "),", data=tab"),summary(reg)$coeff[,1])
  j <- j+1
 }
 pb$tick() #Läuft gegen Ende immer schneller
}
tail(results_auto)
results_auto <- results_auto[!is.na(results_auto[,1]),]
write.table(results_auto,"../Auswertung_PM_Raster_Sovjet/results_auto2_R2_2ParamOhneMaj.csv",sep="\t")
results_auto <- read.table("../Auswertung_PM_Raster_Sovjet/results_auto2_R2_2ParamOhneMaj.csv",sep="\t") #Nach
Neueinlesen: results_auto[,c(1,3:6)] sind Numeric
summary(results_auto[,1]) #Bestes R^2 = 0.528
best <- results_auto[results_auto[,1]>=0.685,]
write.table(best,"../Auswertung_PM_Raster_Sovjet/results_auto2_BestRegressions_2ParamOhneMaj.csv",sep="\t")


#########################################################################################################
#####################
#Teil3
#########################################################################################################
#####################

#Check nach Multikollinearität:
#1) Korrelation zwischen jedem Paar erklärender Variablen (--> stark korreliert --> wahrsch. multikollinear)
#2) Farrar-Glauber Test (F-G Test)
#Angelehnt an: https://www.r-bloggers.com/multicollinearity-in-r/
#1)
ggpairs(tab[,6:13]) #Wenn grosse Korrelation zwischen einem Paar --> Multikollineare erklärende Variablen
#2)
omcdiag(tab[,6:13],tab$we) #Chi^2 sehr hoch --> Multikorr. wahrsch.
imcdiag(tab[,6:13],tab$we) #VIF > 100 Multikollinearität sicher...
#Demnach ProfKruemmung einziger nicht sicher multikollinearer Faktor
pcor(tab[,6:13],method="pearson") #wenn p.wert bei mehreren 0 --> diese Variablen multikollinear

sel <- tab[,c("Hoehe","Neigung","Ausrichtung","TangKruemmung","ProfKruemmung","FirstOPD_NS",
           "FirstOPD_EW")]
#sel <- tab[,c("Hoehe","ProfKruemmung","FirstOPD_NS")]
ggpairs(sel)
omcdiag(sel,tab$we)
imcdiag(sel,tab$we)
#Hoehe, TangKruemmung und ProfKruemmung enthalten bedeutende Info
summary(fit)
summary(lm(we ~ Hoehe + Neigung + Ausrichtung + TangKruemmung + ProfKruemmung + FirstOPD_NS +
         FirstOPD_EW, data=tab))
summary(lm(we ~ Hoehe + TangKruemmung + ProfKruemmung, data=tab))
```

```
summary(lm(we ~ Hoehe + FirstOPD_NS + ProfKruemmung, data=tab)) #Beste Auswahl (Jan-Feb), R^2: 0.52; Jan: 0.66
#0 Nutzen: TangKruemmung
```

Tiefe_zu_we_Scatterplot2d.R

```
setwd("D:/Studium/Master/MA/Auswertung_TWT_zu_we")

taborig <- read.table("Tiefe_zu_we_Pits_Sovjet2_complete.txt",header=T,sep="\t")
head(taborig)
tabtot <- taborig
colnames(tabtot)

#Monate wählen - !!!Zeile 30 anpassen!!!
tab <- tabtot[tabtot$Monat%in%c(1,2,3),]

###Scatterplot 2d Tiefe vs we nach Höhe###
summary(as.factor(tab[,1]))
#colors0 <- sample(colors(),length(unique(tab[,6])))
colors0 <- rainbow(length(unique(tab$Hoehe)))
colors <- colors0[as.factor(tab$Hoehe)]

par()$mgp
par(mgp=c(1.5,0.5,0), mar=c(3,3,3,2))
plot(tab[,4], tab[,5], pch=16, col=colors,
    xlab=colnames(tab)[4],
    ylab=colnames(tab)[5],
    xlim=c(.3,6),
    ylim=c(0.05,2),
    main="Soviet snow pits MRZ") #Monate anpassen
legend("bottomright", legend=levels(as.factor(tab$Hoehe)),
     pch=16, col=colors0, horiz=F)

#Überprüfen
tab[1:12,]
colors[1:12]
```

TWT_zu_we_Scatterplot3d.R

```
library(scatterplot3d)

#setwd("U:/My Documents/Daten_Abramov_GPR/GPR_Extrapolation_TWT_we")
setwd("D:/Studium/Master/MA/Auswertung_TWT_zu_we")


#Ursprüngliche Versuche: Messwerte 2018
taborig <- read.table("TWT_zu_we.txt",header=T,sep="\t")
tab <- taborig[taborig[,4]<=3,]
head(tab)
colors0 <- c("darkred","red","orange","lightblue","blue")
colors <- colors0[as.factor(tab[,3])]

###TWT zu we - Scatterplot 3d###
s3d <- scatterplot3d(tab[,3],tab[,1],tab[,2],
          xlab=colnames(tab)[3],
          ylab=colnames(tab)[1],
          zlab=colnames(tab)[2],
          pch=16, color=colors, grid=T, type="h",
          angle=30)

# #Grid hinzufügen
# source("addgrids3d.R")
# addgrids3d(tab[,3],tab[,1],tab[,2],grid=c("xy","xz","yz"),col.grid="grey",lty.grid=par("lty"))
```

```
#Regressionsebene
reg <- lm(tab[,2]~tab[,3]+tab[,1])
s3d$plane3d(reg)

#Hilfe: http://www.sthda.com/english/wiki/scatterplot3d-3d-graphics-r-software-and-data-visualization

# ###Scatterplot 2d###
plot(tab[,1], tab[,2], pch=16, col=colors,
    xlab=colnames(tab)[1],
    ylab=colnames(tab)[2])
legend("bottomright", legend=levels(as.factor(tab[,3])),
      pch=16, col=colors0, horiz=F)


#Neue Versuche: Ev. Anpassen sobald Multi. Regr. Modell mit extrapolierten TWTs ergänzt; nur ein Jahr wählen
taborig <- read.table("Tiefe_zu_we_Sovjet.txt",header=T,sep="\t")
head(taborig)
tabtot <- taborig[,-c(4,5,6)]
colnames(tabtot)
#OPD = OrderPartialDerivative
colnames(tabtot) <- c(colnames(tabtot)[1:3],"Tiefe","we","Hoehe","Neigung","Ausrichtung","TangKruemmung",
                      "ProfKruemmung","FirstOPD_NS","SecondOPD_dxx",
                      "FirstOPD_EW","SecondOPD_dxy","SecondOPD_dyy")
#Monate wählen - !!!Zeile 30 anpassen!!!
tab <- tabtot[tabtot$Monat%in%c(1,2),]

colors0 <- rainbow(9)
colors <- colors0[as.factor(tab$Hoehe)]

###TWT zu we - Scatterplot 3d###
s3d <- scatterplot3d(tab$Hoehe, tab$FirstOPD_NS, tab$we,
                     xlab="Höhe",
                     ylab="First Order Partial Derivative N-S",
                     zlab="m w.e.",
                     pch=16, color=colors, grid=T, type="h",
                     angle=30)

# #Grid hinzufügen
# source("sonstiges/addgrids3d.R")
# addgrids3d(tab$we,tab$ProfKruemmung,tab$FirstOPD_NS,grid=c("xy","xz","yz"),col.grid="grey",lty.grid=par("lty"))

#Regressionsebene
reg <- lm(tab$we~tab$ProfKruemmung+tab$FirstOPD_NS)
s3d$plane3d(reg)
```

Topographicalparameter_Stakes_combine.R

```
#Fügt die Topographicalparameter allen Stakemessungen an
setwd("D:/Studium/Master/MA/Auswertung_TWT_zu_we/Topographicalparameter_Stakes")
temp <- read.table("Tiefe_Stakes_Sovjet_temp.txt",sep="\t",header=T)
topographical <- read.csv("Topographicalparameter_Stakes_Joined2.csv",sep=",")
topographical_puff100 <- read.csv("Topographicalparameter_Stakes2_Puffer100.csv",sep=",")

#Beide Topographicals zusammenfügen
topographicaltot <- cbind(topographical,topographical_puff100)
topographicaltot[,1]==topographicaltot[,16] #ID's alle gleich
topographicaldef <- topographicaltot[,-c(16:21)] #Überflussspalten löschen

#In Temp mehr ID's als in Topographicaldef! Zuerst korrigieren:
temp <- temp[temp[,1]%in%topographicaldef[,1],]
sort(unique(temp[,1]))==sort(unique(topographicaldef[,1])) #gut

#temp vorbereiten
a <- length(temp[,6:c(length(temp[1,]))]) #12
```

```
b <- length(topographicaldef[,2:length(topographicaldef[1,])]) #50
temp <- cbind(temp, matrix(NA,length(temp[,1]),b-a))

#Dann aus Topographicaldef die Parameter hinzufügen:
colnames(temp)[6:length(colnames(temp))] <- colnames(topographicaldef)[2:length(colnames(topographicaldef))]
ID <- sort(unique(topographicaldef[,1]))
for (i in ID){
  temp[temp[,1]==i,c(6:length(temp[1,]))] <- topographicaldef[topographicaldef[,1]==i,c(2:length(topographicaldef[1,]))]
}

colnames(temp)[4] <- "Tiefe_cm"
temp$Tiefe_cm <- temp$Tiefe_cm/100
colnames(temp)[4] <- "Tiefe"

write.table(temp, "../Tiefe_Stakes_Sovjet2.txt", sep="\t", row.names=F, quote=F)
```

addgrids3d.R

```
#Quelle Funktion: http://www.sthda.com/sthda/RDoc/functions/addgrids3d.r

#' Add grids to a scatterplot3d
#'
#' @description The goal of this function is to add grids on an existing
#'  plot created using the package scatterplot3d
#' @param x,y,z numeric vectors specifying the x, y, z coordinates of points.
#'  x can be a matrix or a data frame containing 3 columns corresponding to
#'  the x, y and z coordinates. In this case the arguments y and z are optional
#' @param grid specifies the facet(s) of the plot on which grids should be drawn.
#'  Possible values are the combination of "xy", "xz" or "yz".
#'  Example: grid = c("xy", "yz"). The default value is TRUE to add grids only on xy facet.
#' @param col.grid,lty.grid color and line type to be used for grids
#' @param lab a numerical vector of the form c(x, y, len).
#'  The values of x and y give the (approximate) number of tickmarks on the x and y axes.
#' @param lab.z the same as lab, but for z axis
#' @param scale.y of y axis related to x- and z axis
#' @param angle angle between x and y axis
#' @param "xlim, ylim, zlim" the x, y and z limits (min, max) of the plot.
#'
#' @note
#' Users who want to extend an existing scatterplot3d graphic with the
#'  function addgrids3d, should consider to set the arguments scale.y, angle, ...,
#'  to the value used in scatterplot3d.
#'
#' @author Alboukadel Kassambara \email{alboukadel.kassambara@@gmail.com}
#' @references http://www.sthda.com
#'
#' @example
#' library(scatterplot3d)
#' data(iris)
#' scatterplot3d(iris[, 1:3], pch = 16, grid=T, box=F)
#' addgrids3d(iris[, 1:3], grid = c("xy", "xz", "yz"))
addgrids3d <- function(x, y=NULL, z=NULL, grid = TRUE,
                       col.grid = "grey", lty.grid = par("lty"),
                       lab = par("lab"), lab.z = mean(lab[1:2]),
                       scale.y = 1, angle = 40,
                       xlim=NULL, ylim=NULL, zlim=NULL){


  if(inherits(x, c("matrix", "data.frame"))){
    x <- as.data.frame(x)
    y <- unlist(x[,2])
    z <- unlist(x[,3])
    x <- unlist(x[,1])
  }
```

```
p.lab <- par("lab")

angle <- (angle%%360)/90
yz.f <- scale.y * abs(if (angle < 1) angle else if (angle >3) angle - 4 else 2 - angle)
yx.f <- scale.y * (if (angle < 2) 1 - angle else angle - 3)


# x axis range
x.range <- range(x[is.finite(x)], xlim)
x.prty <- pretty(x.range, n = lab[1], min.n = max(1, min(0.5 *lab[1], p.lab[1])))
x.scal <- round(diff(x.prty[1:2]), digits = 12)
x <- x/x.scal
x.range <- range(x.prty)/x.scal
x.max <- ceiling(x.range[2])
x.min <- floor(x.range[1])
if (!is.null(xlim)) {
  x.max <- max(x.max, ceiling(xlim[2]/x.scal))
  x.min <- min(x.min, floor(xlim[1]/x.scal))
}
x.range <- range(x.min, x.max)

# y axis range
y.range <- range(y[is.finite(y)], ylim)
y.prty <- pretty(y.range, n = lab[2], min.n = max(1, min(0.5 *lab[2], p.lab[2])))
y.scal <- round(diff(y.prty[1:2]), digits = 12)
y.add <- min(y.prty)
y <- (y - y.add)/y.scal
y.max <- (max(y.prty) - y.add)/y.scal
if (!is.null(ylim))
  y.max <- max(y.max, ceiling((ylim[2] - y.add)/y.scal))

# Z axis range
z.range <- range(z[is.finite(z)], zlim)
z.prty <- pretty(z.range, n = lab.z, min.n = max(1, min(0.5 *lab.z, p.lab[2])))
z.scal <- round(diff(z.prty[1:2]), digits = 12)
z <- z/z.scal
z.range <- range(z.prty)/z.scal
z.max <- ceiling(z.range[2])
z.min <- floor(z.range[1])
if (!is.null(zlim)) {
  z.max <- max(z.max, ceiling(zlim[2]/z.scal))
  z.min <- min(z.min, floor(zlim[1]/z.scal))
}
z.range <- range(z.min, z.max)

# Add grid
if ("xy" %in% grid || grid == TRUE) {
  i <- x.min:x.max
  segments(i, z.min, i + (yx.f * y.max), yz.f * y.max +
           z.min, col = col.grid, lty = lty.grid)
  i <- 0:y.max
  segments(x.min + (i * yx.f), i * yz.f + z.min, x.max +
           (i * yx.f), i * yz.f + z.min, col = col.grid, lty = lty.grid)
}

if ("xz" %in% grid) {
  i <- x.min:x.max
  segments(i + (yx.f * y.max), yz.f * y.max + z.min,
           i + (yx.f * y.max), yz.f * y.max + z.max,
           col = col.grid, lty = lty.grid)
  temp <- yx.f * y.max
  temp1 <- yz.f * y.max
  i <- z.min:z.max
```

```
   segments(x.min + temp,temp1 + i,
         x.max + temp,temp1 + i , col = col.grid, lty = lty.grid)

 }

 if ("yz" %in% grid) {
  i <- 0:y.max
  segments(x.min + (i * yx.f), i * yz.f + z.min,
         x.min + (i * yx.f) ,i * yz.f + z.max,
         col = col.grid, lty = lty.grid)
  temp <- yx.f * y.max
  temp1 <- yz.f * y.max
  i <- z.min:z.max
  segments(x.min + temp,temp1 + i,
         x.min, i , col = col.grid, lty = lty.grid)
 }

}
```

Normalisierung.R (SDD)

```
library(raster)

setwd("D:/Studium/Master/MA/Auswertung_SDD_Raster_Sovjet")
#list <- dir(pattern="SDD_[a-zA-Z0-9]{3}.tif")
list <- dir(pattern="^SDD_[a-zA-Z0-9]{3}2.tif$")
list

for (file in 1:length(list)){
 dat <- raster(list[file])
 mean <- cellStats(dat, stat="mean")
 datnorm <- dat/mean
 writeRaster(datnorm, sub(".tif","_norm.tif",list[file]), overwrite=T)
}
```

Genauigkeit_SDD.R

```
setwd("D:/Studium/Master/MA/Auswertung_SDD_Raster_Sovjet")

SDD <- read.table("sonstiges/SDD_Stakes.csv", header=T, sep=",") #Unnormalisierte Datei
data <- read.table("../Auswertung_TWT_zu_we/Tiefe_Stakes_Sovjet.txt", header=T, sep="\t")

#Nur berücksichtigte Jahre
data <- data[data$Jahr%in%c(1968:1998),]
SDD <- SDD[!is.na(SDD$SDD_Dec),]
cbind(SDD, "mean_Dez", "mean_Jan", "mean_Feb", "mean_Mrz", "mean_Apr")

for (stake in SDD$ID){
 SDD$mean_Dez[SDD$ID==stake] <- mean(data$Tiefe[data$Stake==stake&data$Monat==12])
 SDD$mean_Jan[SDD$ID==stake] <- mean(data$Tiefe[data$Stake==stake&data$Monat==1])
 SDD$mean_Feb[SDD$ID==stake] <- mean(data$Tiefe[data$Stake==stake&data$Monat==2])
 SDD$mean_Mrz[SDD$ID==stake] <- mean(data$Tiefe[data$Stake==stake&data$Monat==3])
 SDD$mean_Apr[SDD$ID==stake] <- mean(data$Tiefe[data$Stake==stake&data$Monat==4])
}


a <- length(colnames(SDD))

SDD[,(a+1):(a+5)] <- SDD[,2:(2+4)]-SDD[,7:(7+4)] #Berechnet - gemessen
colnames(SDD)[12:16] <- c("abw_Dez", "abw_Jan", "abw_Feb", "abw_Mrz", "abw_Apr")
for (i in 1:length(SDD[,1])){
 SDD$abw_mean[i] <- mean(as.numeric(SDD[i,12:16]))
}
```

```
write.table(SDD, "sonstiges/Genauigkeit_SDD.txt", row.names=F, quote=F, sep="\t")

summary(SDD)
plot(SDD$abw_mean)
SDD[,c(1,17)]
#Negativ v.a. Stakes 409 bis 511, 1306-1313
#Positiv v.a. Stakes 601 bis 615, 1124, 1125
```

PM_slopekorr.R (Soviet)

```
library(raster)

setwd("D:/Studium/Master/MA/Auswertung_PM_Raster_Sovjet")
neigung <- raster("../Daten_Abramov_NurIntern/raster/dem_total/dem_total_20m_filled_slope2maske2.tif")
list <- dir(pattern="2.tif$")
list
#list <- dir(pattern="^PM_[a-zA-Z]{3}(2|3).tif$")
treshold_min <- 25 #Neigung, ab der lineare Abnahme startet
treshold_max <- 55 #Neigung, bei der 0 % des ursprünglichen PM's erreicht werden
tdiff <- treshold_max-treshold_min

Fun <- function(dat,neigung){
 ifelse(!is.na(neigung)&neigung>=treshold_min&neigung<treshold_max,
   datkorr <- dat*(tdiff-(neigung-treshold_min))/(tdiff),ifelse(!is.na(neigung)&
   neigung>=treshold_max,datkorr<-0,datkorr <- dat))
}

for (file in 1:length(list)){
 dat <- raster(list[file])
 test <- overlay(dat, neigung, fun=Fun)
 # s <- stack(neigung,dat)
#   for (i in 1:ncell(dat)){
#     if (!is.na(dat[i])){
#       if (neigung[i]>=treshold_min&neigung[i]<treshold_max){
#                   dat[i] <- dat[i]*(tdiff-(neigung[i]-treshold_min))/(tdiff)
#                 }
#                 else if (neigung[i]>=treshold_max){
#                   dat[i] <- 0
#                 }
#     }
#     print(i)
#             }
 writeRaster(test, sub(".tif",paste0("_slopekorr",treshold_min,"-",treshold_max,".tif"),list[file]),overwrite=T)
 message("Datei ",list[file]," beendet")
}
```

Jan2018_Validierung.R

```
setwd("D:/Studium/Master/MA/Auswertung_PM_Raster_Sovjet")

dat <- read.table("PM_Jan2018_extr.csv",sep=",",header=T)
dat$we_GPR <- 0.0274*dat$field_6^1.1352
dat$diff <- dat$PM_Jan2018-dat$we_GPR #Negativ --> GPR zu viel w.e.
head(dat)
summary(dat$diff)
sd(dat$PM_Jan2018)
sd(dat$we_GPR)
sd(dat$diff)
var(dat$diff)

for(i in 1:3){
 dat[,i] <- round(dat[,i],digits=0)
```

```
}
for(i in 4:7){
  dat[,i] <- round(dat[,i],digits=3)
}
head(dat)

write.table(dat,"PM_Jan2018_extr_completed.csv",sep="\t",row.names=F)
```

Normalisierung.R (PM)

```
library(raster)

setwd("D:/Studium/Master/MA/Auswertung_PM_Raster_Sovjet")
#list <- dir(pattern="SDD_[a-zA-Z0-9]{3}.tif")
list <- dir(pattern="^PM_[a-zA-Z]{3}(2|3).tif$")
list <- dir(pattern="slopekorr25-55.tif$")
list

for (file in 1:length(list)){
  dat <- raster(list[file])
  # min <- cellStats(dat, stat="min")
  # dat <- dat-min #Sofern min <0
  mean <- cellStats(dat, stat="mean")
  datnorm <- dat/mean
#   for (i in 1:ncell(dat)){
#                 if (dat[i]<0&!is.na(dat[i])){
#                   dat[i] <- 0 #Minimaler Multiplikator für Niederschläge (damit nicht negative PM Werte)
#                 }
#               }
  writeRaster(datnorm, sub(".tif","_norm.tif",list[file]),overwrite=T)
}
```

Korrektur.R

```
library(raster)

setwd("D:/Studium/Master/MA/Auswertung_PM_Raster_GPR")
#list <- dir(pattern="SDD_[a-zA-Z0-9]{3}.tif")
list <- dir(pattern="extr.tif$")
list
dat <- raster(list)
dat[dat<0] <- 0
plot(dat)

writeRaster(dat, sub(".tif","_korr.tif",list),overwrite=T)
```

PM_slopekorr.R (GPR)

```
library(raster)

setwd("D:/Studium/Master/MA/Auswertung_PM_Raster_GPR")
neigung <- raster("../Daten_Abramov_NurIntern/raster/dem_total/dem_total_20m_filled_slope2maske2.tif")
treshold_min <- 15 #Neigung, ab der lineare Abnahme startet
treshold_max <- 55 #Neigung, bei der 0 % des ursprünglichen PM's erreicht werden
tdiff <- treshold_max-treshold_min

Fun <- function(dat,neigung){
  ifelse(!is.na(neigung)&neigung>=treshold_min&neigung<treshold_max,
     datkorr <- dat*(tdiff-(neigung-treshold_min))/(tdiff),ifelse(!is.na(neigung)&
     neigung>=treshold_max,datkorr<-0,datkorr <- dat))
}
```

```
dat <- raster("PM_GPR_extr_korr.tif")
test <- overlay(dat, neigung, fun=Fun)

writeRaster(test, paste0("PM_GPR_extr_korr","_slopekorr",treshold_min,"-",treshold_max,".tif"),overwrite=T)
```

Normalisierung.R (GPR)

```
library(raster)

setwd("D:/Studium/Master/MA/Auswertung_PM_Raster_GPR")
list <- dir(pattern="korr.tif$")
list

#Ursprüngliches Raster:
dat <- raster(list)
mean <- cellStats(dat, stat="mean")
datnorm <- dat/mean
writeRaster(datnorm, sub(".tif","_norm.tif",list),overwrite=T)

#Slopekorr Raster:
dat <- raster("PM_GPR_extr_korr_slopekorr25-55.tif")
mean <- cellStats(dat, stat="mean")
datnorm <- dat/mean
writeRaster(datnorm, "PM_GPR_extr_korr_slopekorr25-55_norm.tif",overwrite=T)
```

MultiRegr_we_GPR.R

```
setwd("D:/Studium/Master/MA/Auswertung_PM_Raster_GPR")
library("progress")

#1 Vorarbeiten
#1.1 Vorarbeiten in QGis:
#Punktauswahl einlesen und Topographicalparameter anfügen
#Dasselbe mit 100 m Radius
#Details siehe readme.txt

#1.2 Vorbeiten Tabellen zusammenfügen
tabpoints <- read.table("Topographicalparameter_GPR/Topographicalparameter_GPR.csv",header=T,sep=",")
tab100 <- read.table("Topographicalparameter_GPR/Topographicalparameter_GPR_puff.csv",header=T,sep=",")
#SDD wird explizit nicht angefügt, damit unabhängige Validierung möglich!
head(tabpoints)
head(tab100)
tot <- cbind(tab100[,c(1,2,4,5,6,7,3)],tabpoints,tab100[,c(8:length(tab100[1,]))])
head(tot)
colnames(tot)[1:7] <- c("x_m","y_m","TWT_ns","PM_Jan2018_we","we_GPR","GPR-PM","z_m")
write.table(tot,"Topographicalparameter_GPR/Topographicalparameter_tot.csv",sep="\t",row.names=F,quote=F)


#2 Automatisierte Regressionen
#2.1 Einlesen und Parameterwahl
tot <- read.table("Topographicalparameter_GPR/Topographicalparameter_tot.csv",header=T,sep="\t")

#2.2 Beste Regression 3 Parameter
results_auto <- matrix(nrow=600000,ncol=6)
colnames(results_auto) <- c("R^2","Topographicalparameterchoice","Intercept","a_V1","b_V2","c_V3")
colnames(tot)
start <- 7
end <- length(tot[1,])
j <- 1
pb <- progress_bar$new(total=length(start:(end-2)))
for (V1 in start:(end-2)){
  for (V2 in (V1+1):(end-1)){
    for (V3 in (V2+1):end){
```

```
    reg <- lm(tot$we ~ tot[,V1] + tot[,V2] + tot[,V3])
    results_auto[j,] <- c(summary(reg)$r.squared, paste("we_GPR ~", paste(colnames(tot)[V1],
    colnames(tot)[V2], colnames(tot)[V3], sep=" + "),", data=tot"),summary(reg)$coeff[,1])
    j <- j+1
   }
  }
  pb$tick() #Läuft gegen Ende immer schneller
}
tail(results_auto)
tail(results_auto[!is.na(results_auto[,1]),])
results_auto <- results_auto[!is.na(results_auto[,1]),]
write.table(results_auto,"results_auto_3Param.csv",sep="\t")
results_auto <- read.table("results_auto_3Param.csv",sep="\t")
#Nach Neueinlesen: results_auto[,c(1,3:6)] sind Numeric
str(results_auto)
summary(results_auto[,1])
best <- results_auto[results_auto[,1]>=0.736,] #0.74
write.table(best,"results_auto_3Param_BestRegressions.csv",sep="\t")

#2.3 Beste Regression 4 Parameter
results_auto <- matrix(nrow=6000000,ncol=7)
colnames(results_auto) <- c("R^2","Topographicalparameterchoice","Intercept","a_V1","b_V2","c_V3","d_V4")
colnames(tot)
start <- 7
end <- length(tot[1,])
j <- 1
pb <- progress_bar$new(total=length(start:(end-4)))
for (V1 in start:(end-3)){
  for (V2 in (V1+1):(end-2)){
    for (V3 in (V2+1):(end-1)){
      for (V4 in (V3+1):end){
        reg <- lm(tot$we ~ tot[,V1] + tot[,V2] + tot[,V3] + tot[,V4])
        results_auto[j,] <- c(summary(reg)$r.squared, paste("we_GPR ~", paste(colnames(tot)[V1],
        colnames(tot)[V2], colnames(tot)[V3], colnames(tot)[V4], sep=" + "),", data=tot"),summary(reg)$coeff[,1])
        j <- j+1
      }
    }
  }
  pb$tick() #Läuft gegen Ende immer schneller
}
tail(results_auto)
results_auto <- results_auto[!is.na(results_auto[,1]),]
#plot(results_auto[,1])
str(results_auto)
write.table(results_auto,"results_auto_4Param.csv",sep="\t")
results_auto <- read.table("results_auto_4Param.csv",sep="\t")
#Nach Neueinlesen: results_auto[,c(1,3:6)] sind Numeric
str(results_auto)
summary(results_auto[,1])
best <- results_auto[results_auto[,1]>=0.748,] #0.75
write.table(best,"results_auto_4Param_BestRegressions.csv",sep="\t")

#2.4 Beste Regression 3 Parameter mit einer Auswahl an GPR-Punkten
length(tot[,1]) #50521 Punkte vorhanden
gap <- 100 #jeder ... Punkt wird verwendet (Variante (2.4a))
n_points <- 1000 #Anzahl Punkte werden verwendet (Variante 2.4b)

#Variante 2.4a
index <- seq(1,length(tot[,1]),gap)
results_auto <- matrix(nrow=600000,ncol=6)
colnames(results_auto) <- c("R^2","Topographicalparameterchoice","Intercept","a_V1","b_V2","c_V3")
colnames(tot)
totind <- tot[index,]
start <- 7
```

```
end <- length(tot[1,])
j <- 1
pb <- progress_bar$new(total=length(start:(end-2)))
for (V1 in start:(end-2)){
 for (V2 in (V1+1):(end-1)){
  for (V3 in (V2+1):end){
   reg <- lm(totind$we ~ totind[,V1] + totind[,V2] + totind[,V3])
   results_auto[j,] <- c(summary(reg)$r.squared, paste("we_GPR ~", paste(colnames(totind)[V1],
   colnames(totind)[V2], colnames(totind)[V3], sep=" + "),", data=tot"),summary(reg)$coeff[,1])
   j <- j+1
  }
 }
 pb$tick() #Läuft gegen Ende immer schneller
}
tail(results_auto)
tail(results_auto[!is.na(results_auto[,1]),])
results_auto <- results_auto[!is.na(results_auto[,1]),]
write.table(results_auto,paste0("results_auto_3Param_gap",gap,".csv"),sep="\t")
results_auto <- read.table(paste0("results_auto_3Param_gap",gap,".csv"),sep="\t")
#Nach Neueinlesen: results_auto[,c(1,3:6)] sind Numeric
summary(results_auto[,1])
best <- results_auto[results_auto[,1]>=0.74,] #0.749
write.table(best,paste0("results_auto_3Param_gap",gap,"_BestRegressions.csv"),sep="\t")

#Variante 2.4b
#floor(runif(n_points,min=1,max=length(tot[,1])+1)) #Zufallseinträge
index <- sample(1:length(tot[,1]),n_points,replace=F)
results_auto <- matrix(nrow=600000,ncol=6)
colnames(results_auto) <- c("R^2","Topographicalparameterchoice","Intercept","a_V1","b_V2","c_V3")
colnames(tot)
totind <- tot[index,]
start <- 7
end <- length(tot[1,])
j <- 1
pb <- progress_bar$new(total=length(start:(end-2)))
for (V1 in start:(end-2)){
 for (V2 in (V1+1):(end-1)){
  for (V3 in (V2+1):end){
   reg <- lm(totind$we ~ totind[,V1] + totind[,V2] + totind[,V3])
   results_auto[j,] <- c(summary(reg)$r.squared, paste("we_GPR ~", paste(colnames(totind)[V1],
   colnames(totind)[V2], colnames(totind)[V3], sep=" + "),", data=tot"),summary(reg)$coeff[,1])
   j <- j+1
  }
 }
 pb$tick() #Läuft gegen Ende immer schneller
}
tail(results_auto)
tail(results_auto[!is.na(results_auto[,1]),])
results_auto <- results_auto[!is.na(results_auto[,1]),]
write.table(results_auto,paste0("results_auto_3Param_npoints",n_points,".csv"),sep="\t")
results_auto <- read.table(paste0("results_auto_3Param_npoints",n_points,".csv"),sep="\t")
#Nach Neueinlesen: results_auto[,c(1,3:6)] sind Numeric
summary(results_auto[,1])
best <- results_auto[results_auto[,1]>=0.75,] #0.755
write.table(best,paste0("results_auto_3Param_npoints",n_points,"_BestRegressions.csv"),sep="\t")

#Bei allen 3 Varianten stets folgende drei Parameter am besten:
#we_GPR ~ z_m + FOPDdyNS + ProfCurv_1
#R^2 bei Variante mit allen GPR-Punkten und 3 Parametern nur 0.004 kleiner als mit 4 Parametern
#bei Auswahl an Punkten sogar höher
```

RasterResampeln.R

```
library(raster)
```

```
setwd("D:/Studium/Master/MA")

vorlage <- raster("Auswertung_Modell_WardVanPelt/GIS/Raster/abra_dem_mask_50m.asc")
#soviet <- raster("Auswertung_PM_Raster_Sovjet/PM_norm_mean.tif")
soviet <- raster("Auswertung_PM_Raster_Sovjet/PM_norm_slopekorr25-55_mean.tif")
#GPR <- raster("Auswertung_PM_Raster_GPR/PM_GPR_extr_korr_norm.tif")
GPR <- raster("Auswertung_PM_Raster_GPR/PM_GPR_extr_korr_slopekorr25-55_norm.tif")
# #DEM probehalber:
#DEM <- raster("Daten_Abramov_NurIntern/raster/dem_total/DEM_total_20m_filled2.tif")
DEM <- raster("Auswertung_Modell_WardVanPelt/GIS/Raster/abra_dem_50m_WarrenGanz.asc")
crs(DEM) <- crs(vorlage)

soviet_res <- resample(soviet, vorlage, method="ngb")
GPR_res <- resample(GPR, vorlage, method="ngb")
DEM_res <- resample(DEM, vorlage, mehtod="ngb")

#Damit exakte Pixelkongruenz mit vorlage:
soviet_res[vorlage==0] <- NA
GPR_res[vorlage==0] <- NA
DEM_res[vorlage==0] <- NA

#writeRaster(soviet_res, "Auswertung_Modell_WardVanPelt/GIS/Raster/PM_norm_mean50m.asc", format="ascii",
overwrite=T)
writeRaster(soviet_res, "Auswertung_Modell_WardVanPelt/GIS/Raster/PM_Soviet_slopekorr25-
55_norm_mean50m.asc", format="ascii", overwrite=T)
#writeRaster(GPR_res, "Auswertung_Modell_WardVanPelt/GIS/Raster/PM_GPR_extr_korr_norm50m.asc", for-
mat="ascii", overwrite=T)
writeRaster(GPR_res, "Auswertung_Modell_WardVanPelt/GIS/Raster/PM_GPR_extr_korr_slopekorr25-
55_norm50m.asc", format="ascii", overwrite=T)
#Vorlage existiert bereits in 50m Auflösung
writeRaster(DEM_res, "Auswertung_Modell_WardVanPelt/GIS/Raster/abra_dem_50m.asc", format="ascii", overwri-
te=T)


vorlageNA <- vorlage
vorlageNA[vorlageNA==0] <- NA #damit aggregierbar
vorlage100 <- aggregate(vorlageNA,fact=2, na.rm=T)
vorlage100[is.na(vorlage100)] <- 0
plot(vorlageNA)
plot(vorlage100)

soviet_res100 <- resample(soviet, vorlage100, method="ngb")
GPR_res100 <- resample(GPR, vorlage100, method="ngb")
DEM_res100 <- resample(DEM, vorlage100, method="ngb")

soviet_res100[vorlage100==0] <- NA
GPR_res100[vorlage100==0] <- NA
DEM_res100[vorlage100==0] <- NA

#writeRaster(soviet_res100, "Auswertung_Modell_WardVanPelt/GIS/Raster/PM_norm_mean100m.asc", format="ascii",
overwrite=T)
writeRaster(soviet_res100, "Auswertung_Modell_WardVanPelt/GIS/Raster/PM_Soviet_slopekorr25-
55_norm_mean100m.asc", format="ascii", overwrite=T)
#writeRaster(GPR_res100, "Auswertung_Modell_WardVanPelt/GIS/Raster/PM_GPR_extr_korr_norm100m.asc", for-
mat="ascii", overwrite=T)
writeRaster(GPR_res100, "Auswertung_Modell_WardVanPelt/GIS/Raster/PM_GPR_extr_korr_slopekorr25-
55_norm100m.asc", format="ascii", overwrite=T)
writeRaster(vorlage100, "Auswertung_Modell_WardVanPelt/GIS/Raster/abra_dem_mask_100m.asc", format="ascii",
overwrite=T)
writeRaster(DEM_res100, "Auswertung_Modell_WardVanPelt/GIS/Raster/abra_dem_100m.asc", format="ascii",
overwrite=T)
```

Diagramme.R

```
#Zuerst Pfad kopieren
#D:\Studium\Master\MA\Auswertung_Modell_WardVanPelt\MATLAB\output_copied
pfad <- gsub("\\\\","/",readClipboard())
setwd(pfad)
files <- dir(pattern=".txt")
files

#Einlesen und Einstellungen
# GPR <- read.table("OUT_stake_PM_GPR_mNSU_141.txt", head=T)
Soviet140 <- read.table("OUT_stake_PM_Soviet_mNSU_140.txt", head=T)
# Soviet156 <- read.table("OUT_stake_PM_Soviet_mNSU_156.txt", head=T)
#GPR141 <- read.table("OUT_stake_PM_GPR_mNSU_141.txt", head=T)
Soviet208 <- read.table("OUT_stake_PM_Soviet_208_slopekorr1555.txt", head=T)
Warren <- read.table("OUT_stake_SimulationWarren.txt", head=T)
objectnames <- c("Soviet140","Soviet208","Warren") #Namen anpassen
#xlim und ylim bei Zeilen 92f. eintragen

jahre <- "GPR" #Datenquelle für Darstellung nach Jahren (Soviet, GPR oder Warren)
pm <- 2014 #Jahr für PM-Vergleich
pch <- c(1,8,0) #Punktart wählen


#Die Datei besteht nachfolgend aus drei Teilen:
#1) Vergleich beider Varianten gleichzeitig mit Farbe und Symbol
#2) Vergleich der 3 PM Varianten
#3) Vergleich der Jahre für in Zeile 13 ausgewählte Variante


#Tabellen Vorbereiten
analyze <- function(object){
 object[,length(object[1,])+1] <- rep(NA,length(object[,1]))
 object[,length(object[1,])] <- substr(object$timets,8,11)
 colnames(object)[length(object[1,])] <- "jahr"
 object[,length(object[1,])+1] <- rep(NA,length(object[,1]))
 object[,length(object[1,])] <- objectnames[i]
 colnames(object)[length(object[1,])] <- "pm"
 return(object)
}
for (i in 1:length(objectnames)){
 if (length(get(objectnames[i])$pm)==0){
  assign(objectnames[i],analyze(eval(parse(text=objectnames[i]))))
 }
}

#allfällige Kalibrationsjahre entfernen
dat <- get(objectnames[2])
if (which(dat$timets=="18-Aug-2014")[1]!=1){
 dat <- dat[-c(1:(which(dat$timets=="18-Aug-2014")[1]-1)),]
 write.table(format(dat, nsmall=6), paste0("OUT_stake_PM_",substr(objectnames[2],1,nchar(objectnames[1])-
3),"_mNSU_",
          sub("[a-zA-Z]+","",objectnames[2]),".txt"), row.names=F, sep=" ", quote=F)
 assign(objectnames[2],dat)
}


#1) Variante mit Farbe und Form (3 Jahre und 3 PM-Raster gleichzeitig)
#Daten vorbereiten
for (h in 1:length(objectnames)){
 temp <- get(objectnames[h])
 l <- length(temp[,1])
 if (h==1){
  df <- matrix(NA,nrow=length(temp[,1])*length(objectnames),ncol=6)
  df <- as.data.frame(df)
```

```
   colnames(df) <- c("jahr","pm","meas","sim","color","pch")
   df$jahr[1:l] <- temp$jahr
   df$pm[1:l] <- temp$pm
   df$meas[1:l] <- temp$meas
   df$sim[1:l] <- temp$sim
  }
  else{
   df$jahr[((h-1)*l+1):(h*l)] <- temp$jahr
   df$pm[((h-1)*l+1):(h*l)] <- as.character(temp$pm)
   df$meas[((h-1)*l+1):(h*l)] <- temp$meas
   df$sim[((h-1)*l+1):(h*l)] <- temp$sim
  }
}
#Plotten
colors0 <- rainbow(length(objectnames)) #Jedes PM-Raster / Warren's Gradient eine Farbe
for (i in 1:length(objectnames)){
 df$color[objectnames[i]==df$pm] <- colors0[i]
}
#Nachfolende 3 Zeilen ist der einzige nicht-automatisierte Teil dieses Skripts. Anpassen wenn Jahre geändert werden
df$pch[df$jahr==2014] <- pch[1]
df$pch[df$jahr==2015] <- pch[2]
df$pch[df$jahr==2016] <- pch[3]
par()$mgp
par(mgp=c(1.5,0.5,0), mar=c(3,3,3,2))
# plot(get(objectnames[i])$meas, get(objectnames[i])$sim)
# grid()
plot(df$meas, df$sim, pch=df$pch, col=df$color, panel.first=grid(),
  xlab="Mass balance measured [m w.e.]",
  ylab="Mass balance simulated [m w.e.]",
  xlim=c(-6,4),
  ylim=c(-6,4),
  main="Measured vs simulated stake mass balance")
lev <- unique(paste0(df$jahr,df$pm))
legend("bottomright", legend=levels(as.factor(lev)),
  pch=c(rep(pch[1],length(unique(df$jahr))),rep(pch[2],length(unique(df$jahr))),rep(pch[3],length(unique(df$jahr)))),
col=colors0, horiz=F)
xmin <- par()$usr[1]+1.3
xmax <- par()$usr[2]-2.3
ymin <- par()$usr[3]+1
ymax <- par()$usr[4]-0.5
for (i in 1:length(objectnames)){
 mod <- lm(df$sim[df$pm==objectnames[i]]~df$meas[df$pm==objectnames[i]])
 assign(paste0("reg",i),mod)
 abline(get(paste0("reg",i)),col=colors0[i])
 text(xmin+(xmax-xmin)/length(objectnames)*(i-1), ymax, labels=paste0("R^2 =
",format(summary(mod)$r.squared,digits=3)), col=colors0[i])
 coeff <- round(as.numeric(mod$coefficients),3)
 text(xmin+(xmax-xmin)/length(objectnames)*(i-1), ymax-0.5, labels=paste0("y = ",coeff[2],
   "*x",if(sign(coeff[1])==1){"+"}else{""},coeff[1]), col=colors0[i])
}


# #2) 3 PM Varianten plotten
# for (i in 1:length(objectnames)){
#   #colors0 <- sample(colors(),length(unique(tab[,6])))
#   colors0 <- rainbow(length(objectnames))
#   colors <- colors0[as.factor(get(objectnames[i])$jahr)]
#   par()$mgp
#   par(mgp=c(1.5,0.5,0), mar=c(3,3,3,2))
#   if (i==1){
#     plot(get(objectnames[i])$meas, get(objectnames[i])$sim) #, usr=c(par()$usr[1],par()$usr[2],-6,4)
#     grid()
#     plot(get(objectnames[i])$meas, get(objectnames[i])$sim, pch=16, col=colors,
#       panel.first=grid(),
```

```
#       xlab="Mass balance measured [m w.e.]",
#       ylab="Mass balance simulated [m w.e.]",
#       # xlim=c(.3,6),
#       # ylim=c(0.05,2),
#       main="Measured vs simulated stake mass balances")
#   }
#   else{
#     points(get(objectnames[i])$meas, get(objectnames[i])$sim, pch=16, col=colors0[i])
#   }
# }
# legend("bottomright", legend=levels(as.factor(objectnames)),
#       pch=16, col=colors0, horiz=F)
#
#
# #3) Jahre plotten 2d modelliertes vs gemessenes we (einzeln nach PM Variante)
# #jahre in den Einstellungen anpassen (Soviet, GPR oder Warren)
# colors0 <- rainbow(length(unique(get(jahre)$jahr)))
# colors <- colors0[as.factor(get(jahre)$jahr)]
# par()$mgp
# par(mgp=c(1.5,0.5,0), mar=c(3,3,3,2))
# plot(get(jahre)$meas, get(jahre)$sim)
# grid()
# plot(get(jahre)$meas, get(jahre)$sim, pch=16, col=colors,
#     panel.first=grid(),
#     xlab="Mass balance measured [m w.e.]",
#     ylab="Mass balance simulated [m w.e.]",
#     # xlim=c(.3,6),
#     # ylim=c(0.05,2),
#     main="Measured vs simulated stake mass balances")
# legend("bottomright", legend=levels(as.factor(get(jahre)$jahr)),
#     pch=16, col=colors0, horiz=F)
```